

https://dspace.org/

Iron and cobalt catalysts supported on carbon nanotubes for use in the Fischer-Tropsch synthesis

Motchelaho, Anne Myriam Megne

2012-01-31
http://hdl.handle.net/10539/11208

Downloaded from a DSpace repository. https://dspace.org/

IRON AND COBALT CATALYSTS SUPPORTED ON CARBON NANOTUBES FOR USE IN THE FISCHER-TROPSCH SYNTHESIS

Anne Myriam Megne Motchelaho

A thesis submitted to the Faculty of Engineering and the Built Environment, University of the Witwatersrand, Johannesburg, in fulfillment of the requirements for the degree of Doctor of Philosophy.

Johannesburg, 2011

DECLARATION

I declare that the work presented in this thesis was carried out by myself under the supervision of Professor Linda L. Jewell and Professor Neil. J. Coville. It is being submitted for the degree of Doctor of Philosophy at the University of the Witwatersrand, Johannesburg. It has not been submitted before for any degree or examination to any other University.

.....

Anne Myriam Megne Motchelaho

On this…….day of ……2011

ABSTRACT

Fischer-Tropsch (FT) synthesis is the catalytic conversion of syngas (a mixture of carbon monoxide and hydrogen derived from coal, natural gas or biomass) into hydrocarbons and oxygenates. At the heart of the FT process is the catalyst, since it provides a surface where the various reactions can take place. In this study, iron or cobalt catalysts, and alkali (Li, Na and K) promoted iron catalysts supported on carbon nanotubes and nitrogen-doped carbon nanotubes were synthesized and tested for their performance in the Fischer-Tropsch process.

The carbon nanotubes (CNTs), used as a support material for the iron and cobalt based FT catalysts, were obtained through the catalytic decomposition of acetylene at 700^{o}C over a 10% Fe-Co supported on calcium carbonate ($CaCO_3$). High quality carbon nanotubes in high yields were obtained under optimum conditions (synthesis time: 1h, temperature: 700^{o}C, acetylene to nitrogen flowrate ratio of 1: 2.67). TEM analysis of the CNTs revealed that they are multiwalled, with outer diameters ranging from 20 to 35 nm and inner diameters ranging from 8 to18 nm. The synthesized CNTs were refluxed at 120^{o}C in 30% $HN0_3$ for 2 and 6 h or in 55% HNO_3 for 2 and 6 h in order to remove residual growth reagents, to introduce surface functional groups and to render the CNTs less hydrophobic. After characterization using TEM, FTIR, TGA, Raman spectroscopy and zeta potential measurements, it was found that the CNT surface roughness, together with the degree of surface functionalization correlated with the harshness of the acid treatment.

Nitrogen-doped carbon nanotubes (N-CNTs) were synthesized by a post-doping method using acetonitrile as the nitrogen source at temperatures ranging from 700 to 900^{o}C. There was no significant change in the morphology of the N-CNTs up to 850^{o}C.The nitrogen content and the % mass increase of the N-CNTs increased almost linearly with increasing reaction temperature whereas the surface area was found to

decrease. The Raman data showed that the graphite layers of the N-doped CNT are more ordered than the purified CNTs as reflected by the decrease in the I_D/I_G ratio.

Iron or cobalt catalysts and alkali (Li, Na and K) promoted iron catalysts supported on CNTs and N-CNTs were synthesized by the deposition precipitation method using urea as the precipitating agent. The catalysts were characterized using TEM, N_2-physisorption, TPR, XRD and TGA. The catalytic testing was carried out in a fixed-bed micro reactor at 220^{o}C (cobalt based catalysts) or 275^{o}C (iron based catalysts), 8 bar, 2400 h^{-1} and at a H_2 : CO ratio of 2.

The FT data of iron metal deposited on differently functionalized carbon nanotubes revealed that the activity correlates with the degree of acid functionalisation of the carbon support. The effect of the catalyst precursor source ($Fe(C_5H_8O_2)_3$, $Fe(OOCCH_3)_2$, $Fe(NO_3)_3 \cdot 9H_2O$ and $Fe(C_2O_4) \cdot 2H_2O$) and solvent (water or acetone) used in the preparation of iron supported on CNTs catalysts has been investigated. Results showed that the precursor and solvent used in the catalyst preparation have an influence on the metal dispersion and the catalyst reducibility and this affects their performance during Fischer-Tropsch.

The effect of alkali (Li, Na, K) promoted Fe/CNT catalysts on the particle size, surface area, catalyst reducibility, activity and selectivity during FTS was studied. It was observed that adding the alkali promoter increased the Fe crystallite size and as a result the catalyst surface area decreased relative to the unpromoted catalyst. This study revealed that Na is an effective promoter for Fe/CNT catalysts, followed by K and lastly Li.

Fe catalysts supported on post-doped N-CNTs revealed that the CNT containing 1.7 % nitrogen is not a suitable support for Fe-based catalysts. However, functionalizing this N-CNT support using 55% HNO_3 resulted in a better catalyst support.

DEDICATION

I dedicate this to the following people:

- My husband Christophe Foka and children, Stessy and Nathan Foka

- My father papa Motchelaho Samuel, my mother maman Motchelaho Elisabeth and the Buh Tamtseu family especially Tonouo Zacharie, Tamwouo Jean Bernard, Tamo Pierre, Tatchum Emmanuel and Claude Nzudie for years of support and motivation

- My brothers (Sylvain, Jerome and Arnold Motchelaho), sisters (Laurence and Ariane Motchelaho) and my nephew Aaron Tayou Motchelaho

- To the memory of my uncles, papa Fohouo Michel, papa Nemogne Paul, Papa Koguem Joseph and my cousins Talla Ernest and Talla Sando Yves. May your soul rest in peace.

ACKNOWLEDGEMENTS

I would like to acknowledge the following people for their contribution to this work:

- Firstly, my supervisors, Professor Linda L. Jewell and Professor Neil J. Coville for their guidance, support and ideas during this research.

- My friends and colleagues in the catalysis-materials-organometallics group (CATOMAT).

- The electron microscopy unit personel: Professor Michael Witcomb, Abe Seema and Caroline Lalkhan for teaching me how to use the TEM and SEM.

- The School of Chemical and Metallurgical Engineering and the Molecular Sciences Institute, school of Chemistry for giving me the grounds to conduct my research.

- Many thanks are due to Mr Basil Chassoulas for all the technical assistance.

- Mr Rudolf M. Erasmus for doing the Raman analysis on my carbon nanotube samples.

- Mr Mike Philpott from the Institute for Soil, Climate and Water, Pertorial for CNS analysis.

- Ahmed Shaikjee for proofreading my work, Natsayi and Matthew for helping me with XRD.

- The University of the Witwatersrand Postgraduate Merit Award, The Bradlow scholarship and the Andrew W. Mellon Postgraduate Mentoring Program for financial assistance.

- The Gordon Research Conference (GRC), The Catalysis Society of South Africa (CATSA), and WITS for travel grants.

- My Friends, Mrs L. Ngeukeng, S. Kamga, S. Wambo, N. Louzolo, M. Feugeu, C. Djonon, E. Nya, R. Dassi, J.M. Moualeu, Bertine, Smart Lions family, Y. Fongang, L. Dacnou, M. Nzoufack, D. Sakang, Aline, Nadine Tayem.

- Thanks are also due to my extended family members: Prisca Tatiekam, Christelle Kappe, Mr. & Mrs Talla Paul, Mr. & Mrs Kamdem Jean Bernard, Eugenie Tayou and Gwladys Tamtseu.

- Many thanks to Mariam for taking good care of my children when I was busy with my studies.

- Thanks to God almighty for the strength and perseverance over the years.

PUBLICATIONS AND PRESENTATIONS

Publications

- Myriam A.M Motchelaho, Haifeng Xiong, M. Moyo, L. L. Jewell and N. J. Coville, "Effect of acid treatment on the surface of mutiwalled carbon nanotubes prepared from Fe-Co supported on $CaCO_3$: Correlation with Fischer-Tropsch catalyst activity", **Journal of Molecular Catalysis A: Chemical, 2011**, 335, 189-198.

- Haifeng Xiong, Myriam A.M Motchelaho, M. Moyo, L. L. Jewell and N. J. Coville, "Correlating the preparation and performance of cobalt catalysts supported on carbon nanotubes and carbon spheres in the Fischer-Tropsch synthesis", **Journal of Catalysis, 2010,** accepted.

- Haifeng Xiong, M. Moyo, Myriam A.M. Motchelaho, L. L. Jewell and N. J. Coville, "Fischer-Tropsch synthesis over model iron catalysts supported on carbon spheres: the effect of iron precursor, support pretreatment, catalyst preparation method and promoters" **Applied Catalysis A., 2010**, 388, 168-178.

- Myriam A.M Motchelaho, L. L. Jewell and N. J. Coville "Iron-based Fischer-Tropsch catalysts supported on post-doped nitrogen-containing carbon nanotubes" to be submitted.

- Myriam A.M Motchelaho, L. L. Jewell and N. J. Coville "Fe/CNT catalyzed Fischer-Tropsch synthesis: effect of group 1 alkali promoters" to be submitted.

Presentations

- Myriam A.M. Motchelaho "Effect of acid treatment on carbon nanotubes: correlation with iron Fischer-Tropsch activity", Catsa, Bloemfontein, November 7-10, 2010. Oral presentation

- Myriam A.M. Motchelaho, "Fischer-Tropsch synthesis over carbon nanoubes supported Fe catalysts: Effect of iron precursors" GRC, Colby Sawyer College, New London, USA, June 27, to July 2, 2010. Poster presentation

- Myriam A.M. Motchelaho, "Carbon nanotubes supported iron catalysts for use in the Fischer-Tropsch synthesis" SANI Conference, 7 May 2010, University of Johannesburg. Oral presentation

- Myriam A.M. Motchelaho, "Multiwalled carbon nanotubes supported Fe catalyst: effect of acid treatment" Wits 2nd cross faculty symposium, 25-27 october 2009. Oral presentation

CONTENTS

DECLARATION…… i

ABSTRACT…… ii

DEDICATION…… iv

ACKNOWLEDGEMENTS…… v

PUBLICATIONS AND PRESENTATIONS……...vii

LIST OF FIGURES……..xvi

LIST OF TABLES……..xxiii

LIST OF SYMBOLS……..xxv

Chapter One: Introduction 1

1.1 Aims and objectives of the study 4

1.2 Thesis outline 5

1.3 References 6

Chapter Two: Literature Review..... 9

2.1 Introduction 9

2.2 Brief history of the FT process..... 12

2.3 Fischer-Tropsch reactors 14

2.4 Fischer-Tropsch Chemistry..... 16

2.5 Fischer-Trospch mechanism 19

2.5.1 The carbide/alkyl mechanism..... 20

2.5.2 The enolic mechanism..... 21

2.5.3 The vinyl/ alkenyl mechanism 21

2.5.4 The CO insertion mechanism 23
2.6 Fischer-Tropsch catalysts 24
2.6.1 Effect of metal dispersion/ particle size 25
2.6.2 Promoters for Fischer-Trospch catalysts 27
2.6.3 Catalyst supports 29
2.7 CNT synthesis methods 36
2.7.1 Chemical vapour deposition (CVD) 37
2.7.2 Carbon nanotube growth mechanism on supported catalysts 38
2.7.3 Purification of carbon nanotubes 39
2.7.4 Functionalisation of carbon nanotubes 40
2.8 Nitrogen doping of CNTs 42
2.9 Synthesis of Fischer-Trospch catalysts 43
2.9.1 Incipient wetness impregnation method 44
2.9.2 Deposition-precipitation method 46
2.10 Catalyst deactivation 46
2.11 References 47

Chapter Three: Equipment description 66
3.1 The horizontal CVD reactor 66
3.2 The Fischer-Tropsch single micro reactor system 68
3.2.1 The Fixed-bed micro reactor 71
3.2.2 Sampling and composition analysis 73
3.3 References 75

Chapter Four: Experimental Procedure 76
4.1 Materials and chemicals used 77

4.1.1 Chemicals 77
4.1.2 Gases 77
4.2 Carbon nanotubes, a support for the Fischer-Tropsch catalysts 78
4.2.1 Preparation of 10%Fe-Co/$CaCO_3$ catalyst 78
4.2.2 Synthesis of multiwalled carbon nanotubes 78
4.2.3 Carbon nanotubes purification/functionalisation 79
4.2.4 Synthesis of nitrogen-doped multiwalled carbon nanotubes 79
4.3 Synthesis of catalysts supported on carbon nanotubes 80
4.3.1 Deposition Precipitation Method 80
4.3.2 Incipient wetness impregnation method [5] 81
4.3.3 Synthesis of promoted catalysts supported on carbon nanotubes 81
4.4 Characterization techniques 81
4.4.1 Transmission Electron Microscopy (TEM) 81
4.4.2 Zeta potential measurements 82
4.4.3 N_2 Physisorption (BET surface area) 82
4.4.4 Thermogravimetric analysis (TGA) 82
4.4.5 Raman spectroscopy 83
4.4.6 Fourier Transform Infra-red (FTIR) Spectroscopy 83
4.4.7 Temperature programmed reduction 84
4.4.8 H_2 chemisorption and O_2 titration 84
4.4.9 Elemental analysis 85
4.5 Fischer-Tropsch studies 85
4.5.1 Gas Chromatograph (GC) calibration 85
4.5.2 Pressure testing/ leak detection and elimination 88
4.5.3 Catalyst evaluation 89
4.5.4 Data analysis and calculations 89
4.6 References 95

Chapter Five: Effect of acid treatment on the surface of multiwalled carbon nanotubes prepared from Fe-Co supported in CaCO3: correlation with FT catalyst activity 97

5.1 Introduction 97

5.2 Experimental section 101

5.2.1 Catalyst preparation 101

5.2.2 Carbon nanotube synthesis 101

5.2.3 Carbon nanotube purification/functionalisation 102

5.2.4 Characterisation techniques 102

5.2.5 Fischer-Tropsch 104

5.3 Results and Discussion 106

5.3.1 Electron microscopy 106

5.3.2 Zeta potential measurements 110

5.3.3 Surface Area and Pore volume measurements 111

5.3.4 Thermogravimetric analysis (TGA) 112

5.3.5 Raman analysis 120

5.3.6 FTIR analysis 122

5.3.7 Fischer-Tropsch data 123

5.4 Conclusion 131

5.5 References 132

Chapter Six: Fe/CNT catalyzed Fischer Tropsch Synthesis: the effect of iron precursor and solvent 137

6.1 Introduction 137

6.2 Experimental Section 139

6.2.1 Carbon nanotube synthesis 139

6.2.2 Carbon nanotube purification/functionalisation 139

6.2.3 Catalyst preparation 140
6.2.4 Carbon nanotubes and iron catalyst characterization 141
6.2.5 Catalyst evaluation and data analysis 142
6.3 Results and discussion 143
6.3.1 X-ray diffraction analysis (XRD) 143
6.3.2 TEM analysis 145
6.3.3 Thermogravimetric analysis (TGA) 152
6.3.4 Surface area and pore volume analysis 154
6.3.5 Temperature programmed reduction (TPR) 155
6.4 Fischer-Tropsch synthesis 159
6.5 Catalyst characterization after FTS 164
6.6 Conclusion 166
6.7 References 167

Chapter Seven: Fe/CNT catalyzed Fischer-Tropsch Synthesis: effect of group 1 alkali promoters 170

7.1 Introduction 170
7.2 Experimental section 172
7.3 Results and discussion 174
7.3.1 Effect of alkali promotion (Li, Na, K) 174
7.3.2 Effect of varying the sodium loading 190
7.5 Conclusion 197
7.5 References 197

Chapter Eight: Iron-based FT catalysts supported on post-doped nitrogen-containing carbon nanotubes 201

8.1 Introduction 201

8.2 Experimetal 203

8.2.1 Synthesis of the N-CNTs by the post-doping technique using acetonitrile as the nitrogen source. 203

8.2.2 Synthesis of Fe supported on N-CNTs catalysts 205

8.3 Characterization techniques 206

8.3.1 Transmission electron microscopy (TEM) analysis 206

8.3.2 Elemental (CNS) analysis 206

8.3.3 BET surface area measurements 206

8.3.4 Thermogravimetric analysis (TGA) 207

8.3.5 Raman spectroscopy 207

8.3.6 Temperature programmed reduction (TPR) 207

8.3.7 X-ray diffraction 208

8.3.8 Catalytic testing 208

8.4 Results and discussion 209

8.4.1 Purified carbon nanotubes and nitrogen doped carbon nanotubes 209

8.4.2 Fe catalyst supported on nitrogen-doped carbon nanotubes 220

8.4.3 Catalytic evaluation 227

8.5 Conclusion 230

8.7 References 231

Chapter Nine: The effect of Co(nitrate) and Co(acetate) catalysts supported on CNT for use in the FTS……..234

9.1 Introduction 234

9.2 Experimental 236

9.2.1 Carbon nanotube synthesis 236

9.2.2 Catalyst preparation 236

9.2.3 Catalyst characterization 237
9.2.4 Catalyst testing 238
9.3 Results and discussion 239
9.3.1 Surface Area and pore volume measurements 239
9.3.2 TEM analysis of carbon nanotubes 240
9.3.3 TEM analysis of Co/CNT catalysts 242
9.3.4 XRD analysis 244
9.3.5 Temperature programmed reduction (TPR) 246
9.3.6 Thermogravimetric analysis (TGA) 249
9.4 Catalytic results for the FTS process 251
9.5 Conclusion 254
9.6 References 255

Chapter Ten: General Conclusions 259

LIST OF FIGURES

Figure 2.1: Fischer-Tropsch process overview after [3] 10
Figure 2.2: Variation of the price of crude oil [1]. 11
Figure 2.3: Theoretical product distribution as a function of the chain growth probability assuming ideal ASF kinetics [3]. 18
Figure 2.4: an Alkyl FT reaction mechanism for initiation and propagation of hydrocarbon chain: (a) methylene formation, (b) initiation, (c) initiated chain growth, (d) propagation [51] 20
Figure 2.5: Enol mechanism [52]. 21
Figure 2.6: Alkenyl mechanism: (a) chain initiation, (b) chain growth including insertion of methylene and isomerization, (c) chain propagation [51]. ... 22
Figure 2.7: CO insertion mechanism [47]. 23
Figure 2.8: Carbon allotropes [128]. 31
Figure 2.9: Different types of carbon nanotubes [139]. 34
Figure 2.10: Possible carbon nanotube growth mechanism [128, 188]. 39
Figure 2.11: Different oxygen-containing surface groups on carbon. a) carboxyl groups, b) carboxylic anhydride groups, c) lactone groups, d) phenol groups, e) carbonyl groups, f) quinone groups, g) xanthene or ether groups [238]. 41
Figure 2.12: Schematic representation of experimental set up for incipient wetness impregnation method [63]. 45
Figure 3.1: The horizontal CVD set up for the synthesis of carbon nanotubes 67
Figure 3.2: Schematic diagram of the Fischer-Tropsch single fixed-bed micro reactor system set up (not to scale) 69
Figure 3.3: Photograph of the FT single micro reactor system set up 70
Figure 3.4: Schematic diagram of the fixed-bed micro reactor 72
Figure 3.5: Photograph of the assembled fixed-bed micro reactor 73

Figure 3.6: A schematic diagram of the valves viewed from the preload end (VICI Valco Instruments Co. Inc. Technical Note 203) 74
Figure 4.1: A trace for the calibration gas using the TCD GC and argon as a carrier gas 86
Figure 4.2: A trace for the calibration gas using the FID GC and nitrogen as a carrier gas 87
Figure 4.3: A trace for the syngas calibration using the TCD GC and argon as a carrier gas 87
Figure 5.1: a) TEM image of as-grown CNTs and b) TEM image of as-grown CNTs showing some encapsulated metal particles indicated by arrow. 106
Figure 5.2: Diameter size distribution before and after acid treatment. a) Comparison of inner diameters; b) comparison of outer diameters. 107
Figure 5.3: Effect of acid treatment on the texture and morphologies of CCVD synthesized CNTs: a) CNTs-30R2; b) CNT-30R6; c) CNT-55R2; d) CNT-55R6.....108
Figure 5.4: EDX spectrum of: (a) as grown CNT showing the presence of residual metal and (b) acid treated, CNT-55R6 showing that most of the residual metal particles are removed. 109
Figure 5.5: Zeta potential measurements of as-grown and acid treated CNTs as a function of pH. 111
Figure 5.6: TGA and DTG profiles of as-grown CNTs under air atmosphere. 113
Figure 5.7: a) TGA and b) DTG profiles of as-grown CNTs as well as purified CNTs in 30%HNO_3 under air atmosphere. 115
Figure 5.8: a) TGA and b) DTG profiles of as-grown CNTs as well as purified CNTs in 55%HNO_3 under air atmosphere. 116
Figure 5.9: a) TGA and b) DTG profiles of as-grown and acid treated CNTs under N_2 atmosphere. 118
Figure 5.10: Evolution of oxygen as CO_2 versus reflux time. 119
Figure 5.11: Raman spectra of CNTs: a) as-grown CNTs, b) CNT-55R2, C) CNT-30R6, d) CNT-55R6.....121

Figure 5.12: FTIR spectra of untreated (CNT-as grown) and oxidized carbon nanotubes. 123
Figure 5.13: a) and b) TEM images of 10%Fe/CNT-as grown with arrow indicating large Fe clusters (iron cluster size ~ 35 nm); c) and d) TEM images of 10%Fe/CNT-55R6 with arrow indicating small Fe particle (iron particle size ~ 6 nm); 124
Figure 5.14: TPR profiles of a) CNT-55R2 support, b) 10%Fe/CNT-55R2 catalyst and c) 10%Fe/CNT-55R6 catalyst. 127
Figure 5.15: CO conversion with time on stream showing reproducibility of results 128
Figure 5.16: CO conversion with time on stream. 130
Figure 6.1: XRD data of Fe/CNT catalysts prepared using different iron precursors and either a) water or b) acetone as solvents: * = graphite; O = Fe_3O_4; # = Fe_2O_3; ◘ = Fe_2O_3 and Fe_3O_4; ● = Co-Fe, Fe_3C, Co_3C or Co_2C [13, 27] 144
Figure 6.2: CNT-as grown: a) TEM, b) HRTEM with ovals representing amorphous carbon 146
Figure 6.3: TEM image of CNTs after reflux in 55%HNO_3 for 2 h 146
Figure 6.4: TEM image with arrows indicating the Fe particles, and Fe particle size histogram for the Fe-acet catalyst. 148
Figure 6-5: TEM image with arrows indicating the Fe particles, and Fe particle size histogram for the Fe-nitr catalyst. 149
Figure 6.6: TEM image with arrows indicating the Fe particles, and Fe particle size histogram for the Fe-oxal catalyst. 149
Figure 6.7: TEM image with arrows indicating the Fe particles, and Fe particle size histogram for the Fe-acet-1 catalyst 150
Figure 6.8: TEM image with arrows indicating the Fe particles, and Fe particle size histogram for the Fe-nitr-1 catalyst 150
Figure 6.9: TEM image with arrows indicating the Fe particles, and Fe particle size histogram for the Fe-acac catalyst 151
Figure 6.10: TEM image with arrows indicating the Fe particles, and Fe particle size histogram for the Fe-acac-350 catalyst. 151

Figure 6.11: TGA profile in air atmosphere for the Fe-acac catalyst: a) before heat treatment together with the derivative plot and b) before heat treatment and after heat treatment (250^{o}C, 150 min). 153
Figure 6.12: TGA profile for the Fe-oxal catalyst in air atmosphere; a) before heat treatment together with the derivative plot and b) before heat treatment and after heat treatment (350^{o}C, 150 min). 153
Figure 6.13: a)-TGA and b)-DTA of Fe-acac, Fe-acet, Fe-nitr and Fe-oxal. 154
Figure 6.14: TPR profiles of the support and the Fe/CNT catalysts prepared using water as the solvent 157
Figure 6.15: TPR profiles of Fe/CNT catalysts prepared using acetone as the solvent. 158
Figure 6.16: CO conversion as a function of time on stream 160
Figure 6.16: CO conversion with time on stream for catalysts prepared using acetone as solvent. 162
Figure 6.17: TEM image with arrows indicating the Fe particles, and Fe particle size histogram for the Fe-nitr-1 after 12 h time on stream (particle size: 5-10 nm) 164
Figure 6.18: TEM image with arrows indicating the Fe particles, and Fe particle size histogram for the Fe-nitr-1 after 120 h time on stream (particle size: 7-14 nm) 165
Figure 6.19: TEM image with arrows indicating the Fe particles, and Fe particle size histogram for the Fe-acet after 120 h time on stream (particle size: 5-12 nm) 165
Figure 7.1: CNTs as-grown - a) TEM, b) HRTEM with red oval representing amorphous carbon. 175
Figure 7.2: Purified CNTs a) TEM, b) SEM 175
Figure 7.3: a) TEM image and b) EDX spectrum of unpromoted Fe/CNT catalyst with arrows indicating the Fe particles 177
Figure 7.4: a) and b) TEM images of Li promoted Fe/CNT catalysts (100Fe-3.38K/CNT) with arrows indicating the Fe particles 178

Figure 7.5: a) and b) TEM images of Na promoted Fe/CNT catalysts (100Fe-3.35K/CNT) with arrows indicating the Fe particles 178

Figure 7.6: Potassium promoted Fe/CNT catalyst (100Fe-3.31K/CNT): a) TEM image with arrow indicating an Fe particle and b) EDX spectrum.....179

Figure 7.7: a) TGA and b) DTA of CNTs, and promoted and unpromoted Fe catalysts 181

Figure 7.8: TPR profiles of the CNT, unpromoted and alkali-promoted Fe-catalysts: a) CNT support, b) 100Fe/CNT, c) 100Fe-3.38Li/CNT, d) 100Fe-3.35Na/CNT, e) 100Fe-3.31K/CNT. 183

Figure 7.9: XRD patterns of CNTs, unpromoted and alkali promoted Fe/CNT catalysts: a) CNT support, b) 100Fe/CNT, c) 100Fe-3.38Li/CNT, d) 100Fe-3.35Na/CNT, e) 100Fe-3.31K/CNT; * = graphite; O = Fe_3O_4 ; # = Fe_2O_3; ◘ = Fe_2O_3 and Fe_3O_4; ● = Co-Fe, Fe_3C, Co_3C or Co_2C [19, 27]. 185

Figure 7.10: % CO conversion versus time on stream for unpromoted and alkali promoted Fe/CNT catalysts. 189

Figure 7.11: XRD patterns of unpromoted and Na promoted Fe/CNT catalysts: a) 100Fe/CNT, b) 100Fe-3.35Na/CNT, c) 100Fe-12Na/CNT, d) 100Fe-24Na/CNT; * = graphite; O = Fe_3O_4 ; # = Fe_2O_3; ◘ = Fe_2O_3 and Fe_3O_4; ● = Co-Fe, Fe_3C, Co_3C or Co_2C ; 192

Figure 7.12: TPR profiles of the unpromoted and Na-promoted Fe-catalysts supported on CNTs: a) 100Fe/CNT, b) 100Fe-3.35Na/CNT, C) 100Fe-12Na/CNT; d) 100Fe-24Na/CNT. 193

Figure 8.1: Dependence of the % mass increase and nitrogen content in N-CNTs on reaction temperature.....211

Figure 8.2: Dependence of the % mass increase and surface area in N-CNTs on reaction temperature.....211

Figure 8.3: TEM images of CNTs and N-CNTs (prepared by post-doping at different temperatures): a) purified CNTs; b) N-CNT-700^{o}C; c) N-CNT-750^{o}C;

d) N-CNT-800^{o}C; e) N-CNT-850^{o}C; f) N-CNT-900^{o}C (duration of deposition in all cases is 2 h) 213

Figure 8.4: TGA and DTA profiles of the purified CNTs and N-CNTs (obtained at different post treatment temperatures): a) purified CNT; b) N-CNT-700^{o}C; c) N-CNT-750^{o}C; d) N-CNT-800^{o}C; e) N-CNT-850^{o}C; f) N-CNT-900^{o}C. 215

Figure 8.5: Raman spectra of CNTs and N-CNTs (obtained at different post treatment temperatures): a- purified CNT; b- N-CNT-700^{o}C; c- N-CNT-750^{o}C; d- N-CNT-800^{o}C; e- N-CNT-850^{o}C; f- N-CNT-900^{o}C. 218

Figure 8.6: I_D/I_G ratio as function of (a) nitrogen content and (b) reaction temperature 219

Figure 8.7: (a) and (b) TEM images and (c) Fe particle size histogram of the Fe/N-CNT-750 catalyst, (arrows on the TEM images show iron particles) ...222

Figure 8.8: (a) and (b) TEM images and (c) Fe particle size histogram of the Fe/N-CNT-750-55R2 catalyst, (arrows on the TEM images show iron particles).....223

Figure 8.9: XRD patterns of the purified CNTs and Fe supported on N-CNTs: * = graphite; O = Fe_3O_4; # = Fe_2O_3; ◘ = Fe_2O_3 and Fe_3O_4; ● = Co-Fe, Fe_3C, Co_3C or Co_2C [33, 34]. 225

Figure 8.10: H_2-TPR profiles of Fe/N-CNT-750-55R2 and Fe/N-CNT-750 catalysts. 227

Figure 8.11: CO conversion versus time on stream. 228

Figure 9.1: (a) TEM image of as-grown CNTs; (b) HRTEM of CNTs showing multi-walls and (c) TEM image of purified CNTs 241

Figure 9.2: TEM image and cobalt particle size histogram for Co-N/CNT (average cobalt particle size = 12 nm): some Fe particles are indicated by the circles 243

Figure 9.3: TEM image and cobalt particle size histogram for Co-A/CNT (average cobalt particle size = 8.9 nm): some Fe particles are indicated by the circles 243

Figure 9.4: XRD patterns of the CNT support and Co/CNT catalysts: * = CNT; ◘ = Co_3O_4; ● = Co-Fe, Co_3C, Co_2C or Fe_3C.....245

Figure 9.5: TPR profiles of (a) $Co(NO_3)_2 \cdot 6H_2O$ calcined at 250°C for 2 h and (b) 10 wt% Co/CNT prepared using cobalt nitrate and cobalt acetate precursors. 248

Figure 9.6: TGA curves of as-grown and purified carbon nanotubes and cobalt catalysts under air: (a) As-grown CNTs; (b) purified CNTs; (c) Co-N/CNT; and (d) Co-A/CNT. 250

Figure 9.7: CO conversion versus time on stream (reaction conditions: T = 220°C, P = 8 bar, H_2 : CO = 2, GHSV = 2400 h^{-1}) 253

LIST OF TABLES

Table 2.1: Overview of the current commercial reactor types for FT synthesis [15] ... 14
Table 2.2: Relative price of catalytically active Fischer-Tropsch metals (2007). ... 24
Table 2.3: A comparison of the methods commonly used to produce CNTs [183] ... 36
Table 4.1: Operating conditions of the GCs used in this work ... 88
Table 4.2: Molar response factors for hydrocarbon products [10, 11]. ... 91
Table 5.1: Point of zero charge (PZC) obtained from zeta potential measurements ... 110
Table 5.2: Surface area and pore volume of as-grown and acid-treated CNTs. ... 112
Table 5.3: Weight loss of CNTs due to the formation of CO/CO_2 on heating in N_2 . 119
Table 5.4: Raman data for as-grown and acid-treated CNTs ... 122
Table 5.5: Surface area and pore volume of Fe catalysts supported on differently functionalised CNTs ... 125
Table 5.6: Fe dispersion and degree of reduction for Fe catalysts ... 126
Table 5.7: Activity and selectivity of iron catalyst supported on differently functionalized CNTs in Fischer-Tropsch synthesis ... 130
Table 6.1: Overview of the prepared catalysts[a] ... 140
Table 6.2: d-space values and corresponding reflection planes for all the phases identified in the XRD figures ... 148
Table 6.3: Particle size comparison ... 148
Table 6.4: BET surface area and pore volume and of the support (CNT) and Fe/CNT catalysts. ... 155
Table 6.5: Temperature at which each reduction steps occur during the H_2-TPR ... 157
Table 6.6: Activity and selectivity of iron catalysts supported on CNTs (prepared using water as solvent) in FTS[a] ... 161
Table 6.7: FTS[a] activity and selectivity of iron catalysts supported on CNTs prepared using acetone as a solvent. ... 163
Table 6.8: Particle size comparison ... 166
Table 7.1: Summary data of the catalysts prepared ... 174

Table 7.2: Temperature at which each reduction step occurred during the H_2-TPR..183
Table 7.3: Iron particle size measured using XRD and for comparison TEM data are added. 185
Table 7.4: BET surface area and pore volume of the CNT, unpromoted and promoted catalysts. 186
Table 7.5: Activity and selectivity of unpromoted and alkali promoted iron catalysts supported on CNTs during FTS[a]. 190
Table 7.6: Temperature at which each reduction steps occur during the H2-TPR..... 193
Table 7.7: BET surface area and pore volume of the unpromoted and Na promoted catalysts. 194
Table 7.8: Activity and selectivity of sodium promoted iron catalysts supported on CNTs with different sodium loading 196
Table 8.1: Overview of the N-CNTs synthesized 205
Table 8.2: % mass increase, C/N ratio, surface area and pore volume of purified and N-CNTs as a function of reaction temperature. 210
Table 8.3: Decomposition temperature and peak breadth of purified and N-CNT as a function of reaction temperature. 216
Table 8.4: Raman data for the purified and nitrogen-doped CNTs 219
Table 8.5: Nitrogen content, surface area and pore volume measurements 220
Table 8.6: Metal loading and average particle size of the N-CNT supported Fe catalyst 225
Table 8.7: Activity and selectivity of Fe/N-CNT catalysts in FTS. 230
Table 9.1: Metal loading, BET surface area and pore volume results of CNT and Co/CNT 240
Table 9.2: Metal loading and particle size for Co-N/CNT and Co-A/CNT 245
Table 9.3: TPR peak position for cobalt catalysts 248
Table 9.4: TGA peak position of weight loss/gain for different samples 251
Table 9.5 FTS catalytic performance of Co/CNT catalysts 254

LIST OF SYMBOLS

ASF	Anderson-Schulz-Flory
BET	Brunauer-Emmett-Teller
C_2H_2	Acetylene
$CaCO_3$	Calcium carbonate
CaO	Calcium oxide
CCVD	Catalytic chemical vapour deposition
CVD	Chemical vapour deposition
CNFs	Carbon nanofibers
CNS	Carbon nitrogen sulfur analysis
CNTs	Carbon nanotubes
CO_2	Carbon dioxide
CSs	Carbon sphere
DWCNTs	Double walled carbon nanotubes
EDX	Energy dispersive X-ray spectroscopy
EM	Electron micscopy
Fe	Iron
FT	Fischer-Tropsch
FTS	Fischer-Tropsch synthesis
GC	Gas chromatography
GHSV	Gas hourly space velocity
h	Hour
H_2	Hydrogen
HNO_3	Nitric acid
mL/min	Millilitre per minute
N_2	Nitrogen
nm	Nanometre
SBA	Mesoporous silica template
SWCNTs	Single walled carbon nanotubes
t	Time
TCD	Thermal conductivity detector
TEM	Transmission electron microscopy
TGA	Thermogravimetric analysis
TPR	Temperature programmed reduction
WGS	Water gas shift
wt. %	Weight percentage
α	Alpha value

1

Chapter One

Introduction

A reliable supply of hydrocarbons is of vital importance to the industrialized world. Worldwide, chemicals and fuels have been mainly produced from crude oil [1]. Nowadays, with the rising cost of crude oil, the depleting oil reserves, the drive to supply environmentally friendly automotive fuels, the diversification of sources of fossil fuels and the commercialization of otherwise unmarketable natural gas [2, 3], there is a global renewal of interest in the Fischer-Tropsch (FT) technology. This technology was discovered in 1922 by Fischer and Tropsch and used by Germany to produce fuels from its coal reserves. Sasol I, II and III plants in South Africa are based on the FT technology and it is used to produce synthetic fuels and chemicals.

Fischer-Tropsch synthesis (FTS) provides an alternative and most promising route for the production of clean fuels and chemicals from non-petroleum based feedstock such as coal biomass and natural gas [2, 4]. Fischer-Tropsch synthesis is the catalytic conversion of syngas (a mixture of CO and H_2 derived from coal, natural gas or

biomass) into hydrocarbons of various chain lengths [5]. At the heart of the FT process is the catalyst. Catalysts are used to activate the reactants and to provide a surface where the various reactions can take place. Several metals have been found active for CO hydrogenation, namely Ni, Fe, Co and Ru [6-9]. However, only Fe and Co have been intensively used industrially. Fe and Co both have their advantages and disadvantages (see Chapter 2 for more details) and the choice of the active FT metal to be used is based on various parameters [2, 4, 10, 11] such as: the price of the active element, the desired product and the source of carbon used to make syngas. For example Fe is the preferred catalyst when the syngas is produced from coal or biomass as Fe is an active catalyst for the water-gas-shift reaction.

Industrial catalysts (Fe or Co) are generally supported on an appropriate support and suitably promoted in order to achieve a well dispersed active metal with enhanced catalytic performance. Previous work on Fe-based FTS catalysts used industrially has focused on precipitated iron catalysts [12-16]. Unlike precipitated iron catalysts, supported iron catalysts have many advantages, such as improved metal dispersion, enhanced catalyst stability and decreased deactivation rate [17-19]. Traditionally used FTS support materials include Al_2O_3, SiO_2, TiO_2, and MgO [17, 20-24]. The major drawback of these metal oxide supports is that they form strong metal-support interactions and often lead to the formation of mixed compounds such as $CoTiO_4$ [25] or FeO-MgO [17, 20] and hence they are only reducible at very high temperatures [3]. One way to overcome this problem is to use a weakly interacting support (but not so weak as to allow metal sintering) such as carbon materials [26-28]. Carbon materials, for example, activated carbon and carbon nanomaterials (carbon nanotubes (CNTs), carbon nanofibers (CNFs), carbon spheres (CSs), nitrogen-doped carbon spheres (N-CSs)), have been used as FTS catalyst supports because they are stable at high temperatures, resistant to acidic or basic media, have a relatively high surface area and precious metals can easily be recovered upon oxidizing the support from the spent catalyst [29]. Studies [30, 31] comparing the catalytic activity of metal catalysts supported on various oxides, amorphous carbon, and CNTs have shown that catalytic

performance was generally the best on CNTs [32]. Previous studies on iron supported on carbon nanotubes for FTS concluded that the catalyst exhibits high catalytic activity with high olefin selectivity, high selectivity toward C_2-C_4 and C_{5+} fractions [32] and that the catalyst is stable under FTS conditions [19, 33]. It was also found that iron nanoparticles encapsulated in the CNT channels are easily reduced and showed higher FTS activity than iron nanoparticles dispersed on the outer walls of the CNTs [34, 35].

The catalytic behavior of FTS catalysts is influenced by many factors such as the type of support [23, 24], metal loading [36], particle size [26, 37], type of metal precursor used [24, 38], catalyst preparation method [19, 38, 39], types of promoters [14, 38, 40] and catalyst pre-treatment conditions. Modifying any of these variables results in a catalyst with different catalytic properties. For example K-promoted Fe/CNT catalyst is known to inhibit the reduction of the Fe species [19, 38] whereas Cu-promoted Fe/CNT enhances the reducibility of Fe species [19, 38]. This difference in catalyst characteristics affects their catalytic performance during FTS [38]. Also, the source of Fe used to make a catalyst can affect its activity. Thus, the iron catalyst prepared from iron acetate was shown to give a higher CO conversion that a catalyst prepared from iron nitrate [38].

In terms of Fe-based FTS catalysts supported on carbon nanotubes, many issues still need to be explored such as the effect of acid treatment on the surface of multiwalled carbon nanotubes prepared from Fe-Co supported on $CaCO_3$, the use of N-doped CNTs as a catalyst support, the catalyst preparation using different solvents and iron precursors and the use of group 1 alkali promoter (Li, Na, K) on Fe/CNT catalysts.

1.1 Aims and objectives of the study

The aims of this research work are to synthesize carbon nanotube supported Fe and Co-based Fischer-Tropsch catalysts and test their catalytic performance in the FT reaction. These aims will be achieved through the following objectives:

i. To synthesize multiwalled carbon nanotubes (MWCNTs) using a catalytic chemical vapor deposition method (CCVD) with acetylene as the carbon source, and bimetallic Fe-Co supported on $CaCO_3$ as catalyst.

ii. To prepare N-doped MWCNTs using a post-doping technique.

iii. To purify / functionalize the synthesized MWCNTs using nitric acid (HNO_3).

iv. To characterize the synthesized and purified MWCNTs using Transmission Electron Microscopy (TEM), Scanning Electron Microscopy (SEM) for their morphology and structure, N_2 physisorption for surface area and pore volume, Zeta potential (Zp) for the surface charge, Thermogravimetric analysis (TGA) for purity, composition, thermal stability, Fourier Transform Infra-Red (FTIR) spectroscopy for the qualitative evaluation of oxygen surface groups and Raman spectroscopy for the extent of graphitization.

v. To load iron (Fe) and cobalt (Co) metal on the purified multiwalled carbon nanotubes and N-MWCNTs using the deposition precipitation method with urea as the precipitating agent, and characterize (i.e. measure those physical and chemical properties assumed to be responsible for its performance in a given reaction) the catalysts using TEM, XRD, N_2 physisorption, TGA, Temperature Programmed Reduction (TPR) and H_2-Chemisorption.

vi. To promote Fe/CNT catalysts using promoters such as Li, Na and K.

vii. To evaluate the catalysts in terms of their Fischer-Tropsch activity and selectivity in a fixed-bed micro reactor.

viii. To explore issues such as support pre-treatment, catalyst precursor salts, effect of promoters on the activity and selectivity of the catalyst during the Fischer-Tropsch reaction.

1.2 Thesis outline

Following this introductory chapter, a general literature review is presented in Chapter 2. The review is followed by Chapter 3 which gives a description of the equipment used for this study. The experimental procedures are detailed in Chapter 4. Chapter 5 presents the results and discussion of work done on "Effect of acid treatment on the surface of multiwalled carbon nanotubes prepared from Fe-Co supported on $CaCO_3$: Correlation with Fischer-Tropsch catalyst activity". In Chapter 6, work done on "The effect of iron precursor on Fe/CNT catalyzed Fischer-Tropsch synthesis" is presented. Chapter 7 presents the results and discussion of work done on "Fe/CNT catalyzed Fischer-Tropsch synthesis: effect group 1 alkali promoters". Chapter 8 contains work done on "Fe-based Fischer-Tropsch catalysts supported on N-doped CNT". In Chapter 9 the results for "Co-based catalysts supported on CNT for use in the Fischer-Tropsch synthesis" are presented. Chapter 10 gives the conclusions that emanate from the analyses of the results obtained whilst conducting the research and recommendations for further studies.

Aspects of the study have been presented at numerous conferences and workshops and publications have started emanating from the study for example: Chapter 5 was published in the Journal of Molecular Catalysis A: Chemical 335 (2011) 189. More will follow in late 2011.

1.3 References

[1] M.E. Dry, in: G. Ertl, H. Knozinger, F. Schuth and J. Weitkamp (Eds.), Handbook of Heterogeneous Catalysis, Wiley-CVH-Weinheim, 2008, p. 2965.

[2] F. Morales, B.M. Weckhuysen, ChemInform 38 (2007) 1.

[3] A.Y. Khodakov, W. Chu, P. Fongarland, Chemical Review 107 (2007) 1692.

[4] M.J. Gradassi, Studies in Surface Science and Catalysis 119 (1998) 35.

[5] A. Guerrero-Ruiz, I. Rodriguez-Ramos, in: J.A. Anderson and M.F. Garcia (Eds.), Supported Metals in Catalysis, Imperial College Press, London, 2005, p. 155.

[6] M.E. Dry, Catalysis Letters 7 (1990) 241.

[7] M.E. Dry, Catalysis Today 71 (2002) 227.

[8] P. Sabatier, J.B. Senderens, Compte rendu 134 (1902) 514.

[9] M.A. Vannice, Journal of Catalysis 37 (1975) 449.

[10] M.E. Dry, Studies in Surface Science and Catalysis 152 (2004) 533.

[11] M.E. Dry, Applied Catalysis A: General 276 (2004) 1.

[12] A.N. Pour, S.M.K. Shahri, H.R. Bozorgzadeh, Y. Zamani, A. Tavasoli, M.A. Marvast, Applied Catalysis A: General 348 (2008) 201.

[13] C.H. Zhang, Y. Yang, B.T. Teng, T.Z. Li, H.Y. Zheng, H.W. Xiang, Y.W. Li, Journal of Catalysis 237 (2006) 405.

[14] W. Ngantsoue-Hoc, Y. Zhang, R.J. O'Brien, M. Luo, B.H. Davis, Applied Catalysis A: General 236 (2002) 77.

[15] Y. Yang, H.W. Xiang, Y.Y. Xu, L. Bai, Y.W. Li, Applied Catalysis A: General 266 (2004) 181.

[16] D.B. Bukur, D. Mukesh, S.A. Patel, Industrial & Engineering Chemistry Research 29 (1990) 194.

[17] Y.M. Jin, A.K. Datye, Journal of Catalysis 196 (2000) 8.

[18] E. van Steen, F.F. Prinsloo, Catalysis Today 71 (2002) 327.

[19] M.C. Bahome, L.L. Jewell, D. Hildebrandt, D. Glasser, N.J. Coville, Applied Catalysis A, General 287 (2005) 60.

[20] M. Boudart, A. Delbouille, J.A. Dumesic, S. Khammouma, H. Topsře, Journal of Catalysis 37 (1975) 486.

[21] B. Jongsomjit, J. Panpranot, J.G. Goodwin, Journal of Catalysis 215 (2003) 66.

[22] H. Xiong, Y. Zhang, K. Liew, J. Li, Journal of Molecular Catalysis A: Chemical 295 (2008) 68.

[23] J.A.L. Lodya, T. Seda, A.M. Strydom, S.S. Manzini, in: Anonymous , Characterization of Fe/C catalysts supported on Al2O3, SiO2 and TiO2, Journal of Physics: Conference Series, IOP Publishing, 2010, p. 082016.

[24] M. Kraum, M. Baerns, Applied Catalysis A: General 186 (1999) 189.

[25] K. Jalama, N.J. Coville, D. Hildebrandt, D. Glasser, L.L. Jewell, Fuel 86 (2007) 73.

[26] R.C. Reuel, C.H. Bartholomew, Journal of Catalysis 85 (1984) 78.

[27] P. Serp, M. Corrias, P. Kalck, Applied Catalysis A, General 253 (2003) 337.

[28] G.L. Bezemer, A. Van Laak, A.J. Van Dillen, K.P. De Jong, Studies in Surface Science and Catalysis 147 (2004) 259.

[29] A. Tavasoli, R.M.M. Abbaslou, M. Trepanier, A.K. Dalai, Applied Catalysis A: General 345 (2008) 134.

[30] S.F. Yin, Q.H. Zhang, B.Q. Xu, W.X. Zhu, C.F. Ng, C.T. Au, Journal of Catalysis 224 (2004) 384.

[31] J. García, H.T. Gomes, P. Serp, P. Kalck, J.L. Figueiredo, J.L. Faria, Catalysis Today 102 (2005) 101.

[32] L. Guczi, G. Stefler, O. Geszti, Z. Koppány, Z. Kónya, É. Molnár, M. Urbán, I. Kiricsi, Journal of Catalysis 244 (2006) 24.

[33] U.M. Graham, A. Dozier, R.A. Khatri, M.C. Bahome, L.L. Jewell, S.D. Mhlanga, N.J. Coville, B.H. Davis, Catalysis Letters 129 (2009) 39.

[34] W. Chen, Z. Fan, X. Pan, X. Bao, Journal of the American Chemical Society 130 (2008) 9414.

[35] R.M.M. Abbaslou, A. Tavassoli, J. Soltan, A.K. Dalai, Applied Catalysis A: General 367 (2009) 47.

[36] M. Trépanier, A. Tavasoli, A.K. Dalai, N. Abatzoglou, Applied Catalysis A: General 353 (2009) 193.

[37] G.L. Bezemer, J.H. Bitter, H. Kuipers, H. Oosterbeek, J.E. Holewijn, X. Xu, F. Kapteijn, A.J. van Dillen, K.P. de Jong, Journal of the American Chemical Society 128 (2006) 3956.

[38] H. Xiong, M. Moyo, M.A.M. Motchelaho, L.L. Jewell, N.J. Coville, Applied Catalysis A: General (2010) Accepted.

[39] E. van Steen, F.F. Prinsloo, Catalysis Today 71 (2002) 327.

[40] X. An, B. Wu, H.J. Wan, T.Z. Li, Z.C. Tao, H.W. Xiang, Y.W. Li, Catalysis Communications 8 (2007) 1957.

2

Chapter Two

Literature Review

2.1 Introduction

An increasing demand for clean fuels and chemicals is expected to lead to an important shift from crude oil to natural gas as feedstock for the chemical industries. It has also been predicted that the crude oil supplies may only last for about 50 more years [1]. Therefore there is a need to find alternative energy sources which are secure and stable [2]; for example, natural gas which is more widely distributed over the world than are the crude oil deposits [1]. One of the approaches to the production of substitutes for the dwindling crude petroleum reserves is Fischer-Tropsch (FT) synthesis which involves the conversion of organic material (natural gas, coal or biomass) into a mixture of hydrogen and carbon monoxide (syngas). This syngas is subsequently converted to hydrocarbons by reaction over suitable catalysts. The syngas required for the FT process is produced by the gasification of either coal or

methane. The efficiency of syngas production is very important since syngas production can account for up to 70% of the capital cost of the overall process [1]. Therefore, for the process to be economically sustainable, natural gas and coal must be available at low cost. A typical FT process is given in Figure 2.1.

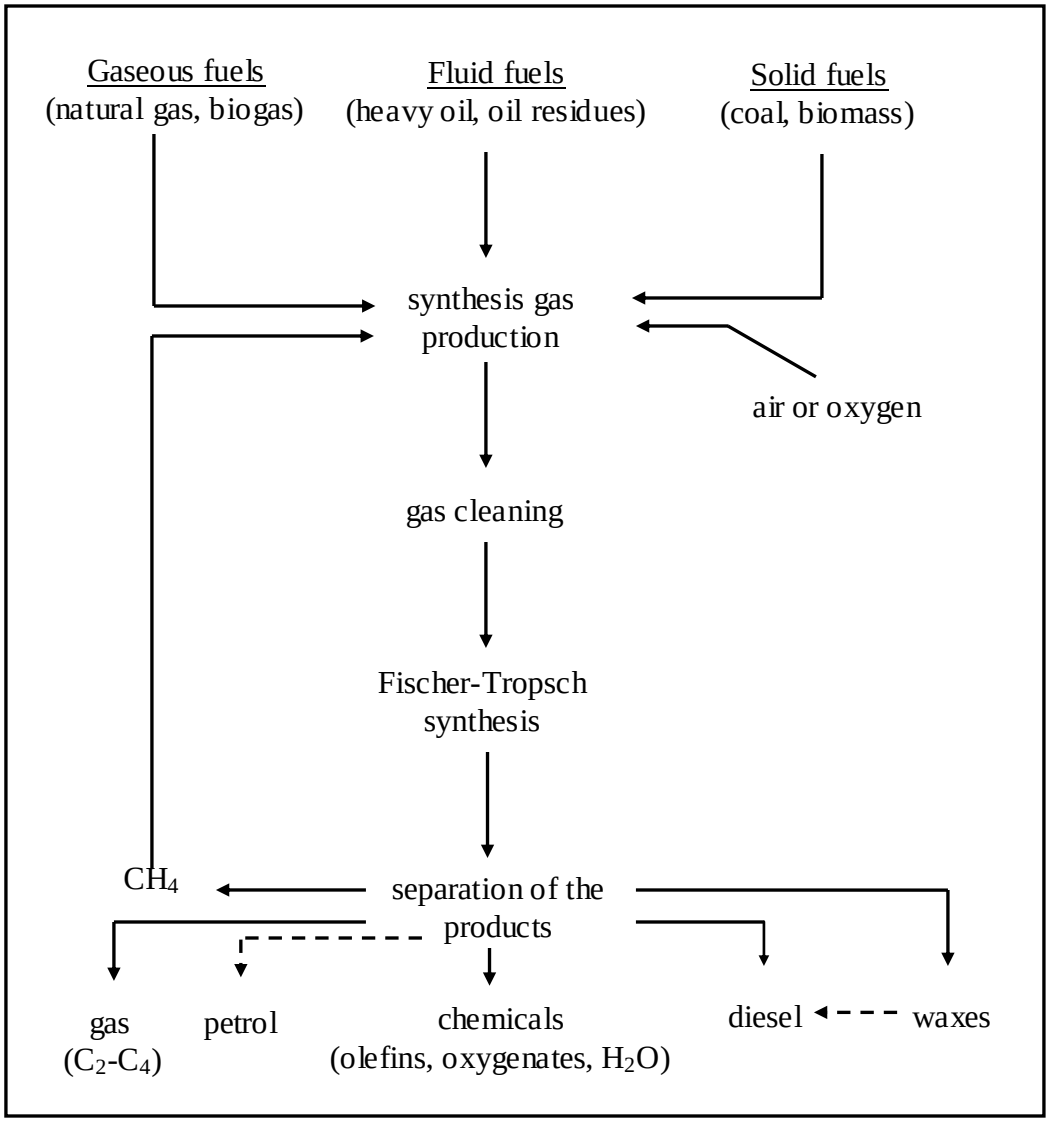


Figure 2.1: Fischer-Tropsch process overview after [3]

Since the FT process has to compete directly with a crude oil refinery process, the price of crude oil is very important and would determine the viability of the FT process. Figure 2.2 presents the variation in the price of crude oil since 1940 [1]. It has been estimated that the FT gas-to-liquid technology would be economically viable when the price of crude oil is about US$ 20 per barrel [4]. The price of crude oil has been well above US$ 50 per barrel for some time [5] making the FT process an option for those countries having huge reserves of natural gas and coal.

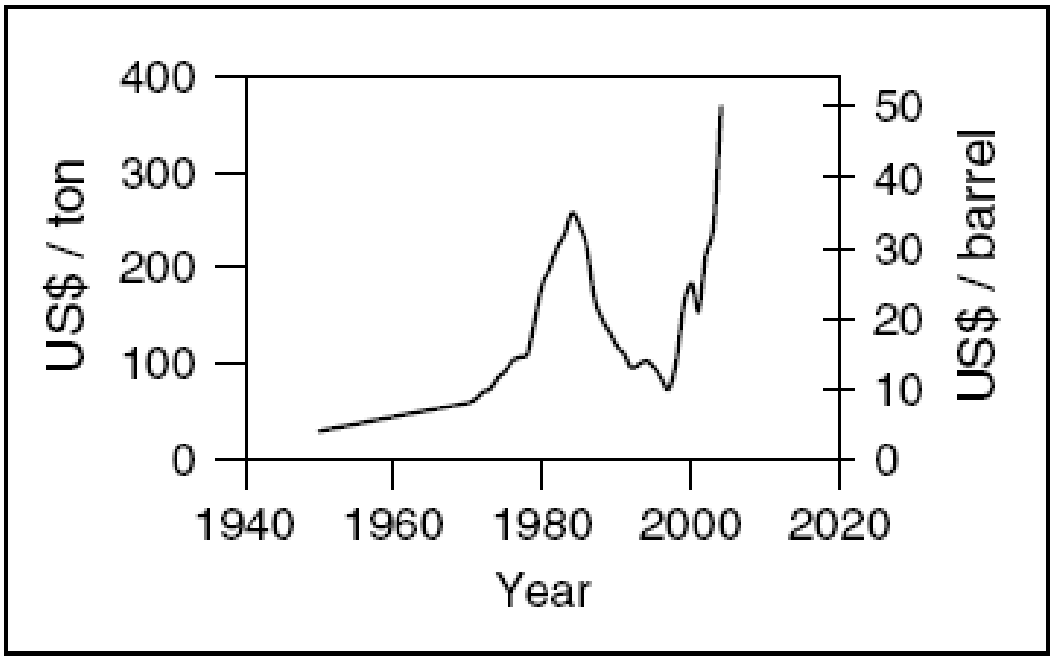


Figure 2.2: Variation of the price of crude oil [1].

The FT fuels have some advantages compared to the crude oil-derived fuels. For example, crude oils are highly aromatic and as a result are not suitable for the production of either linear alkenes, or high-quality diesel fuel [1], whereas both of these products are readily produced via the FT synthesis. The FT fuels are sulfur and nitrogen free and FT gasoline contains less that 1% benzene (a carcinogenic compound) which has a much lower concentration than in crude oil-derived gasoline. FT derived fuels have low NOx and CO emissions and low particulate formation

values (environmentally friendlier) [5]. Moreover the FT diesel is readily biodegradable [1]. The FT gas-to-liquid technology (GTL) is now very attractive and competitive when compared with the current crude oil refinery industry processes.

2.2 Brief history of the FT process

The catalytic synthesis of hydrocarbons from H_2 and CO has a long history [3]. There are numerous articles, including review papers by Storch et al. [6], Pichler [7] and Dry [8] that adequately describe the history of the Fischer-Tropsch process. In this thesis, no attempt is made to give a comprehensive literature review on the FT process and for more detailed information on the history of FT, research and development and early FT patents, interested readers are referred to the reviews mentioned above. A few highlights are mentioned below:

- In 1902, Sabatier and Senderens [9] produced methane from H_2 and CO mixtures over a nickel catalyst at atmospheric pressure.
- In 1913, the German firm 'Badische Anilin und Soda Fabrik' (BASF) was awarded a patent for their work on the catalytic synthesis of heavier hydrocarbons and oxygenated compounds from synthesis gas using alkali promoted osmium and cobalt catalysts when operating at higher pressures [10].
- In 1920, Fischer and Tropsch pioneered the technology for the production of longer chain hydrocarbons from H_2 and CO using metal catalysts at high pressure of up to 300 bar [11] and at relatively low pressure (1-5 bar) with the use of a precipitated cobalt catalyst [12].
- In 1936, the first four production plants were commissioned in Germany (total capacity of 200,000 tons of hydrocarbons per year).

- In the 1950's, a Bureau of Mines plant (Fe catalyst) came into production in Louisiana, Missouri, and a hydrocol plant (based on fixed fluid bed reactor, Fe-K catalyst, syngas from methane) operated briefly in Brownsville, Texas.
- In the mid 1950's, German plants were shut down. Interest in the FT synthesis declined worldwide with the discovery of large oil deposits in the Middle East. In South Africa, despite the oil discovery, Sasol I was commissioned (based on Fe catalyst, using ARGE fixed bed and circulating fluid bed reactors to produce high yields of wax and diesel fuel) in 1955.
- In the 1970's and 1980's, there was a renewed interest in the Fischer-Tropsch synthesis due to the increasing oil price and fear of oil shortages. Sasol II and Sasol III were commissioned based on Synthol circulating fluid bed technology.
- In 1992, the Mossgas plant (now known as PetroSA, Mossel Bay, South Africa) was commissioned using Sasol technology and syngas from natural gas. The Shell middle distillate plant in Malaysia (based on Co catalyst and fixed bed reactor) started operating in 1992-1993. Other companies that took advantages of FT technology in the 1990's era included BP (British Petroleum), ConocoPhillips, Energy International and Exxon (now known as Exxon Mobil).
- More recently in 2007, an FT complex came on line in the Ras Laffan industrial city complex in Qatar. This region, situated in the North of Qatar was chosen because it is close to large natural gas reserves. The planned capacity is about one million tons of products per year. The technologies utilized are Haldor-Topsoe for gas reforming, Sasol for slurry phase FT synthesis using a cobalt catalyst and ChevronTexaco for hydroprocessing [13].
- Towards the end of 2007, a pilot FT plant was commissioned in China using a fixed bed reactor and supported Co and precipitated Fe catalysts. Syngas from coal is used for the production of a cheaper and cleaner liquid fuel. Production started in April 2008 [14].

- An FT complex is being constructed at Escravos in the Niger delta, Nigeria. This plant will use the natural gas which is associated with the recovery of crude oil in that region. The capacity and technologies are the same to those in Qatar [13].

2.3 Fischer-Tropsch reactors

The Fischer-Tropsch synthesis is a highly exothermic reaction with an enthalpy change of about 165-180 kJ mol^{-1} CO converted, depending on the precise product composition [15]. All FT reactors are therefore designed in such a way as to maximize heat removal because inadequate heat removal would lead to an increase in the catalyst deactivation, decreased selectivity towards the preferred products, excessive methane yields, particle fragmentation and reactor runaway [15-17]. An overview of the current commercially used reactor designs for the Fischer-Tropsch synthesis is presented in Table 2.1.

Table 2.1: Overview of the current commercial reactor types for FT synthesis [15]**.**

Process type	FT reaction	Catalyst	Technology
Multitubular Fixed-Bed	LTFT	Co and Fe	ARGE
	LTFT	Co	Shell GTL
Slurry bubble column	LTFT	Co	Sasol's slurry phase distillate, ExxonMobil's AGC-21
Fixed fluidized bed	HTFT	Fe	Sasol's advanced Synthol
Entrained fluidized bed	HTFT	Fe	Sasol's Synthol (also used by PetroSA)

There are two modes of operation of the FTS [17]:

- The high temperature process (300-350^{o}C), where Fe-based catalysts are used for the production of gasoline and linear low molecular mass olefins.
- The low temperature process (200-240^{o}C), where either Fe or Co-based catalysts are used for the production of high molecular mass linear waxes.

The reactors designed for FT synthesis are mostly one of the three types:

- The fixed bed reactors which are used by Sasol to produce high value linear waxes at low temperatures (225^{o}C). Heat removal is achieved by water, circulating outside of the tubes [18];
- The fluidised bed reactors with either a fixed or circulating bed. The major difference between these two types of reactor is that the catalyst bed in the fixed fluidised bed reactor remains stationary and the gases pass upward through the bed while the catalyst in the circulating fluidised bed reactor is entrained in a fast moving stream of gases. The main advantages of the fixed fluidised bed over the circulating fluidised bed reactors include:

    - Low construction cost;
    - Increase in cooling capacity;
    - Low overall catalyst consumption.

- The slurry bed reactors in which gas is bubbled through a suspension of finely devided catalyst in a liquid which has a low vapour pressure at the temperature of operation. The use of slurry bed reactors for FTS was studied by several researchers in the 1950's [17]. The advantages of slurry over multitubular reactors are:

    - The low cost of the reactor train;
    - The lower gas compression costs;
    - The lower catalyst consumption per tonne of product;

- The ability to operate at a higher average temperature resulting in higher conversions and on-line removal or addition of catalyst to allow for longer runs.

The major drawback of this type of reactor is that of catalyst poisoning; all the catalyst is deactivated whereas in the case of a fixed bed reactor for example, the poisoning substance is adsorbed on the top layers of the catalyst, leaving the rest of the catalyst bed unaffected [17].

In this PhD study, a fixed-bed reactor was chosen to conduct experiments because despite its disadvantages (poor heat transfer, tedious catalyst loading and unloading), it had a good operational flexibility, did not required a facility for the separation of catalyst and liquid products, no catalyst attrition was experienced and it was easy to operate [8, 17, 19, 20].

2.4 Fischer-Tropsch Chemistry

The FT reaction converts syngas (a mixture of carbon monoxide and hydrogen) derived from coal, natural gas or biomass to liquid fuels [21]. The chemistry taking place in the Fischer-Tropsch reactor is complex [22]; it involves a variety of competing chemical reactions [23] but can be divided into three groups of reactions [2]:

1- Product forming reactions

Methanation:	$3H_2 + CO \leftrightarrow CH_4 + H_2O$
Paraffins:	$(2n+1)H_2 + nCO \rightarrow C_nH_{2n+2} + nH_2O$
Olefins:	$2nH_2 + nCO \rightarrow C_nH_{2n} + nH_2O$
Methanol:	$2H_2 + CO \rightarrow CH_3OH$
Higher alcholols:	$2nH_2 + nCO \rightarrow C_nH_{2n+1}OH + (n-1)H_2O$

2- Non-product forming reactions

Boudouard reaction:	$2CO \rightarrow C + CO_2$
Carbide formation:	$xM + 2CO \rightarrow M_xC + CO_2$
	$xM + CO + H_2 \rightarrow M_xC + H_2O$
Catalyst oxidation:	$xM + yH_2O \rightarrow M_xO_y + yH_2$
Catalyst reduction:	$M_xO_y + yCO \leftrightarrow xM + yCO_2$

3- Secondary reactions

Water gas shift reaction:	$CO + H_2O \leftrightarrow CO_2 + H_2$

All the reactions mentioned above account for almost all the possible products observed during the Fischer-Tropsch reaction, ranging from fuels to chemicals, including paraffins, olefins and oxygenates.

The Fischer-Tropsch reaction is considered to be a chain polymerization reaction and hence the product spectrum can be described by a chain polymerization kinetic model [24]. Anderson, Schulz and Flory proposed a model (ASF model) to explain the product spectrum and the relevant equation proposed to model the reaction is shown below:

$$W_n / n = (1-\alpha)^2 \alpha^{n-1} \qquad [2.1]$$

where n is the carbon number, W_n is the weight fraction of product containing n atoms and α is the chain growth probability. The Anderson-Schulz-Flory (ASF) model is usually linearised into the following equation:

$$\log(W_n / n) = n\log(\alpha) + \log((1-\alpha)^2 / \alpha) \qquad [2.2]$$

This equation is used to determine the α value from experimental data by plotting $\log(W_n / n)$ versus carbon number (n). This plot is linear and the chain growth probability is obtained from its slope as log (α).

Alpha (α) can also be defined in terms of the rate of chain propagation (r_p) and chain termination (r_t) as:

$$\alpha = \frac{r_p}{r_t + r_p} \qquad [2.3]$$

The value of α typically lies between 0 and 1 with a higher value indicating a greater selectivity towards waxy products. The theoretical limits of the various product cuts for various values of α are shown in Figure 2.3.

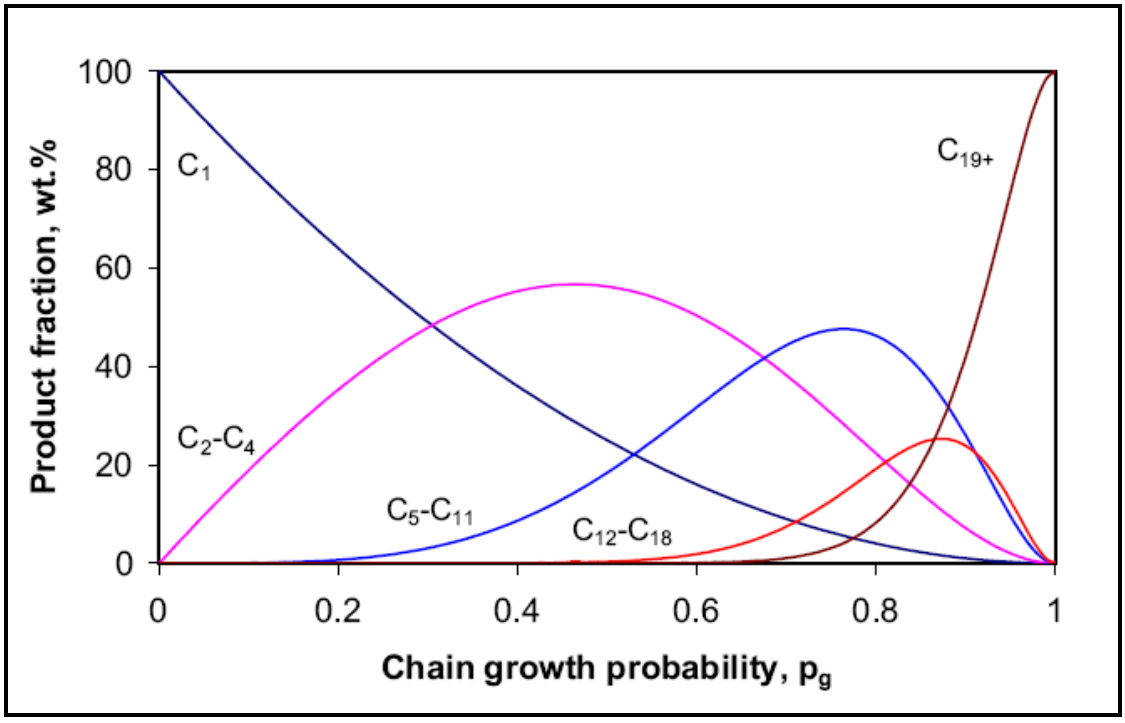


Figure 2.3: Theoretical product distribution as a function of the chain growth probability assuming ideal ASF kinetics [3].

Deviations from the ASF model are often observed in distributions of real FTS products [25-27]:

- Relatively high molar methane content: two phenomena have been proposed to explain this observation. 1) Additional sites responsible for only methane production [28] and 2) methane formation by more than one pathway [29].
- A lower than expected C_2 selectivity: the relatively lower than expected amounts of C_2 in the Fischer-Tropsch product distributions is believed to be due to the much higher reactivity of ethylene compared to the other α-olefins [30] and their re-insertion into the growing chain.
- Positive [31-38] and negative [32, 39] deviations from the ASF plot have been reported; especially when the carbon number is greater than 8. Various theories accounting for chain-length related phenomena, including a vapour-liquid equilibrium, diffusion-enhanced olefin readsorption model, different physisorption strength of the olefins and the two-active-site model, have been proposed [40].

2.5 Fischer-Trospch mechanism

The Fischer-Tropsch synthesis provides an alternative route for obtaining liquid fuels from natural gas, coal and biomass [41]. It is a chain polymerization reaction which produces various products and the product spectrum is described by a chain polymerization kinetic model [42]. An understanding of this reaction at molecular scale is very important. There is still debate about the Fischer-Tropsch reaction mechanism [43] although several mechanisms and variations thereof have been proposed and reviewed in the literature [6, 8, 20, 31, 44-47]. The carbide/alkyl, the enolic, the vinyl/alkenyl, and the CO insertion mechanisms are the most common mechanisms proposed [45, 48-50]. These mechanisms are briefly discussed in the next sections.

2.5.1 The carbide/alkyl mechanism

In this mechanism CO and H_2 adsorb dissociatively onto the surface of the catalyst in such a way that the carbon monoxide forms surface carbide. The surface carbide is hydrogenated by the dissociated hydrogen to form surface carbene species. This species then react further with hydrogen to form methyl species on the surface. The surface methyl species is either desorbed by the addition of hydrogen to form methane or it combines with another carbene to initiate a chain reaction. Larger molecules are then formed in this stepwise manner [48, 49]. Because the carbide mechanism does not explain the formation of alcohols, the enol mechanism was proposed [6, 31]. The alkyl or methylene mechanism is an improved version of the original carbide mechanism [1].

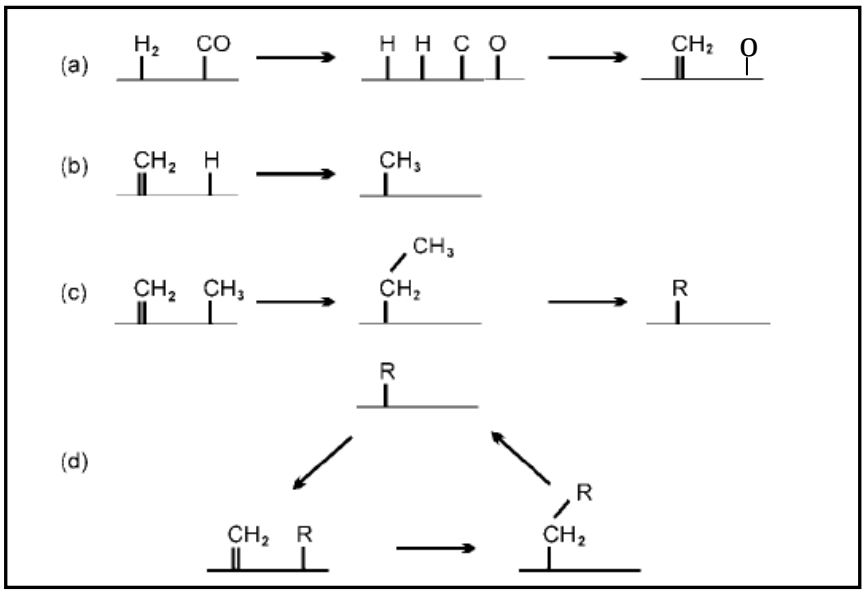


Figure 2.4: an Alkyl FT reaction mechanism for initiation and propagation of hydrocarbon chain: (a) methylene formation, (b) initiation, (c) initiated chain growth, (d) propagation [51]

2.5.2 The enolic mechanism

This mechanism involves the molecular adsorption of CO onto the metal surface (1). The adsorbed CO is then attacked by dissociated surface hydrogen species to form an enolic intermediate surface species (2) which serves as both the chain initiator and monomer [52]. The enolic surface species (2) is further hydrogenated (3) and converted to a methyl surface species (4). Two enol surface species can also undergo a condensation reaction and a water elimination step results in chain growth [53]. Chain termination results in the formation of α-olefins or oxygenated compounds. Hydrogenation of α-olefins yields n-paraffins.

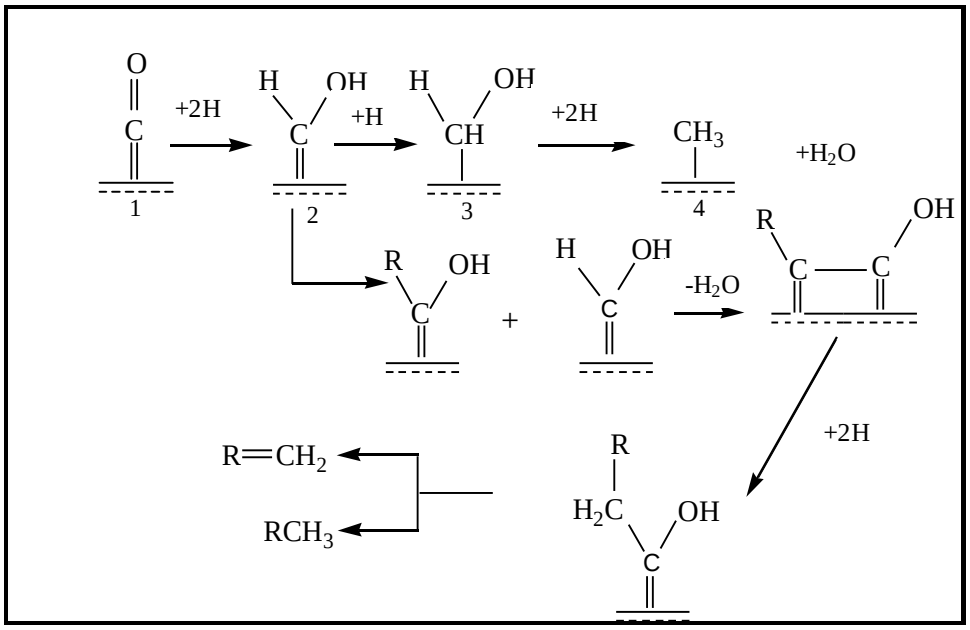


Figure 2.5: Enol mechanism [52].

2.5.3 The vinyl/ alkenyl mechanism

This mechanism involves the surface coupling of a surface methyne (CH) and methylene (CH_2) species to form surface vinyl (-CH=CH_2) [45, 50, 54]. The surface

methyne (CH) and methylene (CH_2) are formed in a manner similar to that described in the carbide mechanism. The vinyl species is considered as the chain initiator and the methylene surface species is the chain propagation monomer. The surface vinyl then undergoes chain growth by reaction with surface methylene to form a surface allyl. The allyl isomerizes to an alkenyl which is turn reacts with more methylene. Chain termination occurs when the surface alkenyl reacts with a surface hydride to give an alkene Figure 2.6 [45, 50, 54] and accounts for α-olefin formation as primary products [55]. This mechanism explains the formation of branched hydrocarbons by allyl isomerisation; however, it does not explain the formation of methane and oxygenated compounds [27].

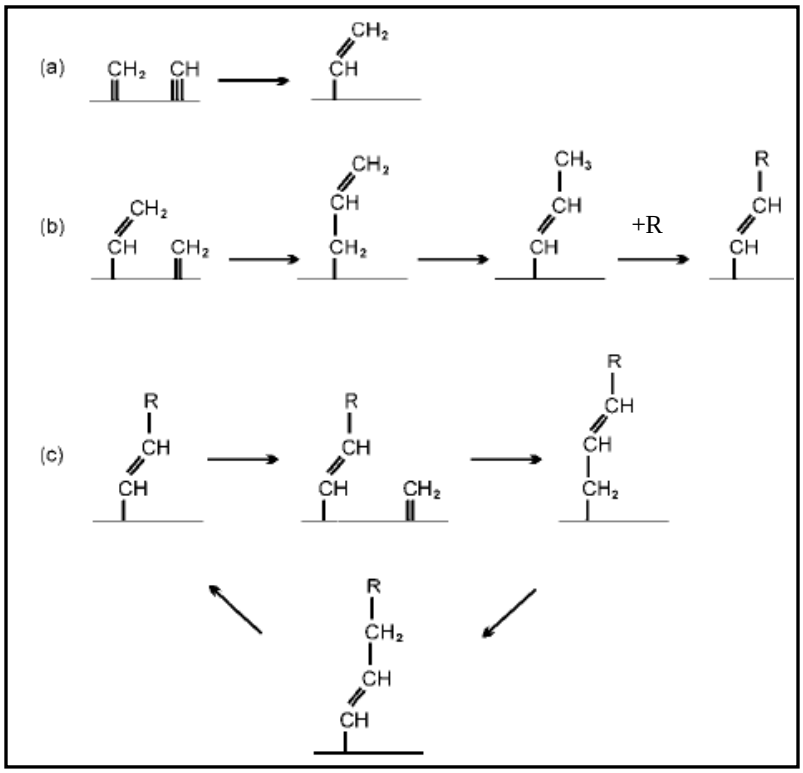


Figure 2.6: Alkenyl mechanism: (a) chain initiation, (b) chain growth including insertion of methylene and isomerization, (c) chain propagation [51].

2.5.4 The CO insertion mechanism

In this mechanism, the surface adsorbed CO is the building unit. This mechanism is believed to be the main reaction pathway which accounts for the formation of oxygenated compounds in the FTS [47]. During the insertion mechanism, the CO inserts into a metal-alkyl (methyl or methylene) carbon bond which is then hydrogenated to produce an alcohol or an alkene.

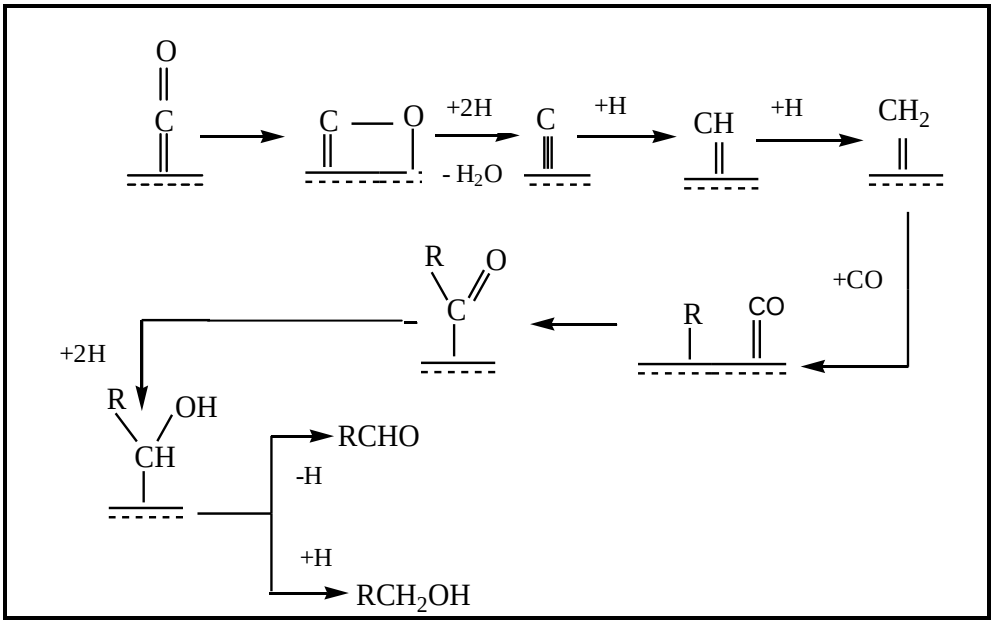


Figure 2.7: CO insertion mechanism [47].

The common features of all the proposed mechanisms are: reactant adsorption, chain initiation, chain growth (propagation), chain termination, product desorption, re-adsorption of reactive products and further reactions [53].

2.6 Fischer-Tropsch catalysts

Elements of group 8 to 10 of the periodic table are most commonly used as active metals for CO hydrogenation reactions since they can dissociatively adsorb CO and H_2 [53]. However, Fe, Ni, Co and Ru are known to be most active for CO hydrogenation to hydrocarbons [9, 17, 56, 57]. Of the four metals Ni is the most active for hydrogenation reactions but under typical FTS reaction conditions, it has a very high selectivity for methane and, at high pressure, volatile nickel carbonyls are formed and so the catalyst is lost from the reactor [58-60]. For these reasons, it is generally agreed that nickel is not a good choice of catalyst for the Fischer-Tropsch reaction [56, 61].

The choice has to be made between Fe, Co and Ru. Factors such as cost, availability, desired product spectrum, require catalyst lifetime and activity are considered when determining the choice of a catalyst [56]. The relative price of catalytically active Fischer-Tropsch metals (at 2007 level) is shown in Table 2.2 [62].

Table 2.2: Relative price of catalytically active Fischer-Tropsch metals (2007).

Metal	Price[1]
Fe	1
Co	235
Ni	140
Ru	76000

[1]Price per kg in 2007 relative to the price of 1 kg of scrap iron.

Ru has been found to have a lower selectivity to methane and more selective to the C_{5+} hydrocarbon fraction than other metals but the very high cost of Ru and its low availability is a great obstacle to its commercial application [56, 57, 61, 63].

However, its use as an additive to Co or Fe catalysts has been intensively investigated [64-68].

This leaves Fe and Co as viable catalysts for FTS [17]. Fe is by far the cheapest metal [56, 61, 62], its specific activity for FTS is high and Fe-based catalysts have high water-gas shift activity. Moreover Fe can convert low H_2/CO ratio syngas (syngas derived from coal and biomass) without an external shift reaction step [61].

Co catalysts offer advantages over Fe catalysts when operating in a LTFT mode. These include: 1- higher activity per active site [69], 2- higher selectivity for longer chain hydrocarbons, 3- lower coke formation, 4- lower olefin selectivity, 5- lower water gas shift activity, 6- lower oxygenate selectivity and 7- higher resistance to oxidation by water [70, 71]. However, under HTFT conditions, Co displays low selectivity generating much methane [17]. In contrast to Co, Fe displays good activity and selectivity in HTFT synthesis. As a result, Fe is the only active metal currently in commercial use for this application [1].

The versatility, availability and cost of Fe have made it the metal of choice for this project. The catalytic behaviour of iron catalysts for FTS is influenced by many factors such as the type of support [72], the source of iron [73], Fe dispersion and particle size [74], catalyst preparation method [73, 75, 76], promoters used [73, 77, 78], catalyst pre-treatment conditions [76], etc. Some of these factors are briefly discussed below.

2.6.1 Effect of metal dispersion/ particle size

The catalytic behaviour of a supported metal catalyst has been reported to be dependent on the degree of dispersion of the metal on the support [79-81]. The metal particle size is inversely proportional to the metal dispersion i.e. the greater the

dispersion, the smaller the metal particles. It is often believed that catalytic activity increases with increasing dispersion, that is, with increasing surface area or decreasing crystallite size [79]. It is observed that small metal particles lead to strong metal support interactions and as a result are more difficult to reduce. Bigger metal particles can be reduced easily due to the weak metal support interaction but are poorly dispersed. Many researchers have shown that there is an optimum particle size required for FTS [82]. For instance, Bezemer et al. [82] have demonstrated that for a Co catalyst with a particle size smaller than 6-8 nm, the turnover frequency (TOF) depends on the particle size and it is independent on the Co particle size for particles > 6-8 nm. In another study, Mabaso et al. [83] have reported that carbon supported Fe catalysts that have smaller particles (< 7-9 nm) exhibit lower TOF and higher selectivity toward methane compared to catalysts with bigger particle size. Park et al. [80] have also shown that Fe/Al_2O_3 catalysts prepared from pre-synthesized iron oxide with an Fe particle size of 6.1 nm were best suited to FTS studies (catalysts with Fe particle < 6.1 nm have lower activity per unit metal site). These results are all in agreement and the slight difference observed in the optimum particle size could be due to the difference in the support or the FTS conditions used. It is important to note that some studies [65, 70, 84-89] did not observe a significant effect of cobalt particle size on specific activity.

We now know that there is an optimum metal particle size required for FTS below which the TOF is low and the selectivity toward methane is high. How can we then control the synthesis of the catalyst to obtain the required particle size? Various studies have attempted to control particle size using several techniques such as: catalyst preparation method [3, 81] (including varying the solvent used to dissolve the metal precursor [67]), different metal precursors [90, 91], catalyst pre-treatment conditions (sintering at various temperatures in a stream of hydrogen [79]), different catalyst support materials etc.

2.6.2 Promoters for Fischer-Trospch catalysts

The Fischer-Tropsch synthesis is a non selective reaction and therefore results in a large variety of products (from methane to waxes) [43, 92]. Attempts to improve the product distribution as well as to increase the CO hydrogenation activity have been made [2]. One way of achieving this is by modifying the supported metal through the addition of promoters. Promoters are a subject of great interest in catalyst research due to their remarkable influence on the activity, selectivity and stability of industrial catalysts [93]. A promoter is regarded as a component of the catalyst that does not take part in the reaction, but changes the catalytic properties of the catalyst [67, 93].

Typical Fe-based catalysts contain varying amounts of structural and chemical promoters known to increase the overall FTS activity or to facilitate the reduction of iron oxide to metallic iron during hydrogen activation [78, 94].
The main function of structural promoters (e.g. SiO_2 [22, 95], TiO_2 [22, 85, 91], CeO_2 [91]) is to influence the metal dispersion by governing the metal-support interaction [96] whereas electronic promoters (e.g. K [97], Na, [78, 98] Cu [8], Ru [64]) are known to affect the local electronic structure of an active metal mostly by adding or withdrawing electron density near the Fermi level in the valence band of the metal [99, 100].

It has been shown that promoting Fe catalysts with group 1 alkali metals has a strong influence on the product selectivity, and that other promoters have a lesser influence [8]. The basicity of the alkali metals is one of the reasons for the significant influence of these metals on the catalyst performance during FTS; it has been shown that, for equivalent amounts of alkali present the basicity of the reduced catalysts increased in the order Li < Na < K< Rb [101] and Anderson [31] demonstrated that the effectiveness of the alkali promoter decreases in the order Rb > K > Na > Li [6]. The more basic the alkali metal, the more readily it can donate its electrons to the metal (Fe) and facilitate CO chemisorption, since CO tends to accept electrons from iron

[102]. The electrons donated to Fe from the alkali metal weaken the strength of the Fe-H bond. Alkali metals strengthen the Fe-C bond and weaken the Fe-H [94, 99, 103]. Alkali promoted Fe catalysts suppress the formation methane and the amount of methane produced during FTS decreases as the surface basicity increases [78, 101].

Modification of FT catalysts by potassium has been investigated for many years [59]. Results showed that potassium can improve FTS activity [8, 103-105], decrease activity [8, 103], and in some cases the activity appears to reach a maximum with increasing potassium loading then decrease with further addition of potassium [8, 104]. Ngantsoue-Hoc et al. [78] studied the impact of the group 1 alkali metals upon the activity and selectivity of a precipitated iron-silica catalyst and they reported that the relative impact of the alkali metal depends upon the conversion level with potassium being the promoter that has the highest impact on the activity at all conversion levels. Their results also showed that Na and K exhibit much higher WGS rates than the other alkali promoted and unpromoted catalysts. A similar study by An et al. [98] compared the effect of K or Na promoted $FeCu/SiO_2$ catalyst and found that the addition of a K or Na can improve the catalytic activity during FTS and shift the product distribution to heavy hydrocarbons to different extents. These two studies show similar trends as far as Na and K are concerned. Moreover it has been shown that sodium plays a positive role as an alkali promoter for Fischer-Tropsch synthesis [101, 106, 107]. The focus of the earlier studies was on precipitated or co-precipitated Fe catalysts [77, 78, 108]. More recently, Bahome et al. [109] investigated the promotion of carbon nanotube-supported iron catalysts by potassium and/or Cu. Fischer-Tropsch synthesis (conditions: 8 bar, 275^{o}C, CO/H_2 ratio of 1:2) results revealed that the potassium promoted catalyst was very active for the water gas shift reaction (higher yields of CO_2), less selective to methane and produced more olefins compared to the unpromoted catalysts. On the other hand, the addition of copper enhanced the reducibility and the catalytic activity of the Fe catalyst but did not have any effect on the product selectivity. Alkali promoters have been shown to be very important but data to document their relative influence during FTS synthesis are not

abundant [78]. There is hence a need to further explore the influence of alkali promoters on carbon nanotube supported Fe catalysts.

2.6.3 Catalyst supports

The chemical composition of a catalyst is one of the parameters which determine its activity [110]. Other factors such as a high surface area and appropriate physical properties can also be important [110]. Industrial catalysts are often made of metal or metal compounds supported on a suitable support. The interest in supports originates from the realization that transition metal-support interfaces influence catalytic activity and generate better catalysts than unsupported transition metals [111, 112]. Supported catalysts are usually preferred in industry for the following reasons [113]:

- Costs - the active phase of a supported catalyst is often an expensive metal. The metal usually represents only a small fraction of the total catalyst mass since it is dispersed on the support in order to achieve a higher activity per unit mass of metal.
- Activity - the high activity leads to fast reaction rates, short reaction times and maximum throughput.
- Selectivity - facilitates maximum yield of the desired products, elimination of side products and lowering of purification costs; it is the most important parameter in catalyst design.
- Regenerability - helps to keep process costs low.

The main function of the catalyst support is to increase the surface area of the active component by providing a surface for the dispersion of the active metals, stabilization of the active metal against loss of surface area through sintering during reaction, to maintain the catalyst's mechanical strength and to facilitate the mass or heat transfer in a diffusion-limited or an exothermic reaction [113-115]. It also increases the

resistance of a catalyst to poisoning [116]. Apart from the physical effects mentioned above, there are chemical interactions between the active phase and the support that can significantly affect the catalytic performance. This includes the choice of the appropriate catalyst support for a particular active metal since the support is not just a carrier [111, 113, 116]. For example, Reuel and Bartholomew [117] studied the effect of the support (titania, alumina, silica, carbon and magnesia) on the CO hydrogenation properties of Co catalysts. Their results showed that the activity and selectivity of Co catalysts was support dependent. It is also crucial to optimize the support and metal interaction strength, so that it is strong enough to obtain a good dispersion but not so strong as to inhibit low temperature reduction [118].

There are many commercially available catalyst supports including: activated carbon, Al_2O_3, TiO_2, SiO_2, CeO_2, MgO [72, 91, 119-122] and more recently, carbon nanostructures (CNTs, CNFs, CSs) [72, 117, 123-125]. Traditionally, Al_2O_3, TiO_2 and SiO_2 were the most widely used supports for FT catalysts because they have a high surface area and favour the preparation of well dispersed metal catalysts [5]. However, the major drawback of these oxidic supports is that they form a strong-metal support interaction and often lead to the formation of mixed compounds. These mixed compounds are only reducible at very high temperatures, leading to catalyst materials with a limited number of accessible surface metal sites [5, 63]. One of the proposed solutions to overcome this problem is to use a weakly interacting support such as a carbon material [123, 124, 126].

Carbon materials as catalyst supports

Carbon is a versatile, fascinating element and it is very abundant [127]. There is a large difference in chemical bonding within the layers and between them in the layered structure of graphite. The σ-bonds connecting each carbon atom with its three neighbours within the layers are created by sp^2 hybridization; they are very strong

chemical bonds. The remaining fourth, delocalized electron in graphite is responsible for the very weak π-bonds acting between layers [127]. The two features which make carbon quite unique are that a carbon atom can bond with another carbon atom by using a range of orbitals, and can also bond with many other elements [128]. Diamond, graphite and amorphous carbon are the well-known allotropes of carbon. However, other structures of carbon are now known (fullerenes, carbon nanotubes, carbon spheres, carbon fibres etc.) that emanate from the unique ability of carbon to achieve various combinations of sp, sp^2 and sp^3 electronic configurations. Different types of carbons possess distinct physical forms and properties (Figure 2.8) and they are widely used in a range of industrial applications such as adsorption and catalytic processes.

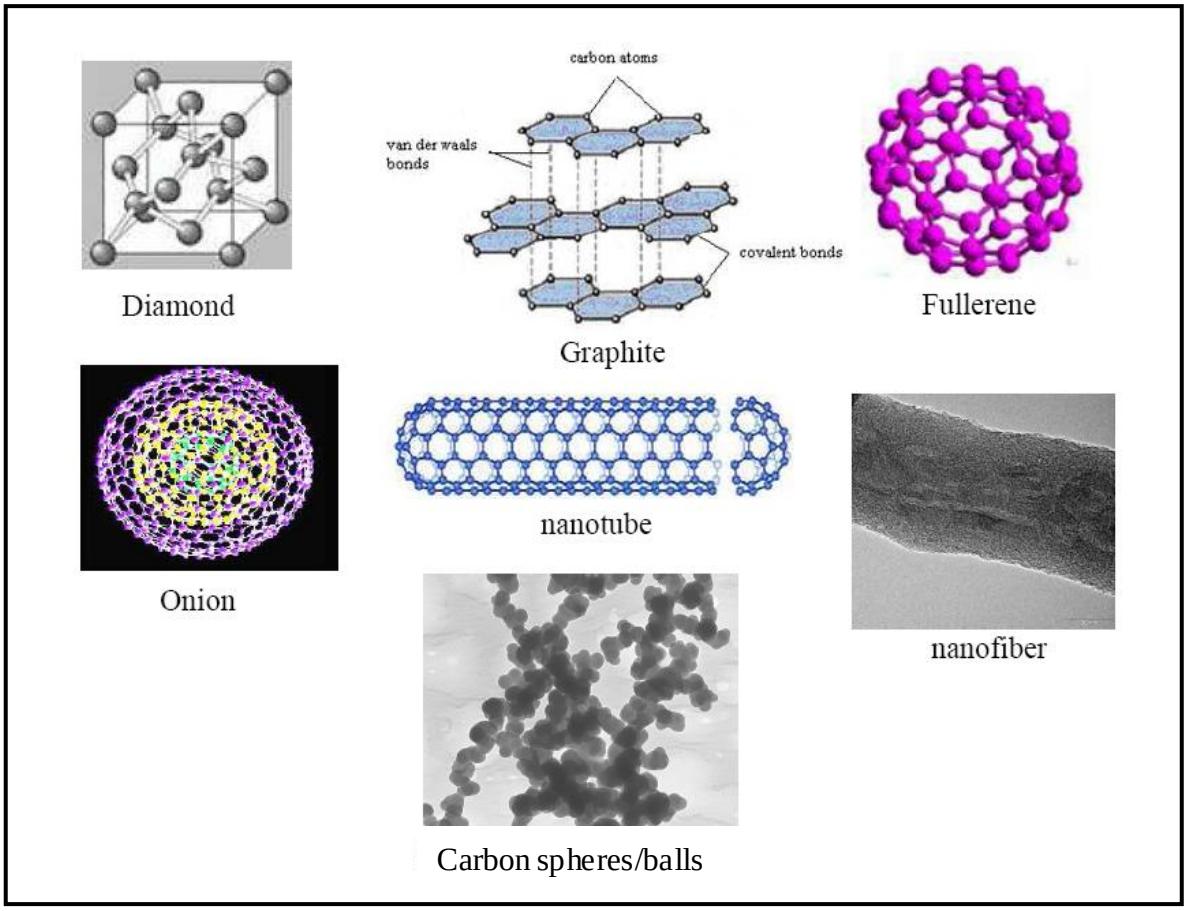


Figure 2.8: Carbon allotropes [128].

A large variety of carbon materials such as granular and powdered activated carbons and carbon blacks have been used as catalyst supports [129]. Recently, there has been an increasing interest in related carbon materials such as carbon fibers, spheres, nanotubes and nanofibers and a comprehensive review published by Serp [124] discusses the use of some of these materials as catalysts and catalyst supports.

Although carbon materials cannot be used as a support in hydrogenation reactions at temperatures greater than 430^{o}C (because they will gasify to form methane) or in the presence of oxygen at temperatures greater than 230^{o}C (because they will gasify to form carbon dioxide), they possess some valuable characteristics that are not attainable with other supports [116]. These unique characteristics/virtues are [116, 124]:

- The carbon surface is resistant to both acidic and basic media.
- The structure is stable at high temperatures.
- The pore structure can be tailored to obtain the pore size distribution needed for a given application.
- The chemical properties of the surface can be modified to control polarity and hydrophobicity.
- The active phase can be recovered easily from spent catalysts by a controlled combustion of the carbon support (very important when the active phase is a precious metal).
- Carbon supports are usually cheaper than other conventional catalyst supports.

These properties of carbon can be exploited in various catalytic reactions such as hydrogenation [130-132], oxidation [133, 134] and Fischer-Tropsch [135] reactions. Some early studies reported on the use of activated carbons as a catalyst support but the reproducibility as well as the microporosity of activated carbon has often hampered catalyst development (activated carbon is a support with chemical properties that are difficult to control) [136]. As a result of this, more recent studies

have analyzed the possibilities of using other carbon materials, such as nanofibers, nanotubes and nanospheres. Our discussion is limited to carbon nanotubes since it is the support material that was used to conduct our investigations.

Carbon nanotubes

Elemental carbon with sp^2 hybridization can form a variety of amazing structures, such as graphite (3D), graphene (2D), carbon nanotubes (CNTs, 1D) and fullerene (OD) [137]. Carbon nanotubes are composed entirely of carbon-carbon bonds with the carbon having sp^2 bonds, similar to graphite. This bonding structure provides nanotubes with their unique strength and flexibility.

Carbon nanotubes are divided into two major classes: single-walled carbon nanotubes (SWCNTs), and multiwalled carbon nanotubes (MWCNTs) [128]. A single walled carbon nanotube is a sheet of graphite that is one atom thick and is rolled up into a seamless cylinder. A double walled carbon nanotube is formed when an additional sheet of graphite exists around the central SWCNT. A MWCNT is made of a multiple-shell structure of cylindrical tubes arranged coaxially along the tube axis [138]. The separation between the neighboring tubes is about 0.34 nm [137, 138] (Figure 2.9). These carbon materials are called nanotubes because they possess diameters in the order of the nanometer range. They are usually a few microns to several millimeters in length.

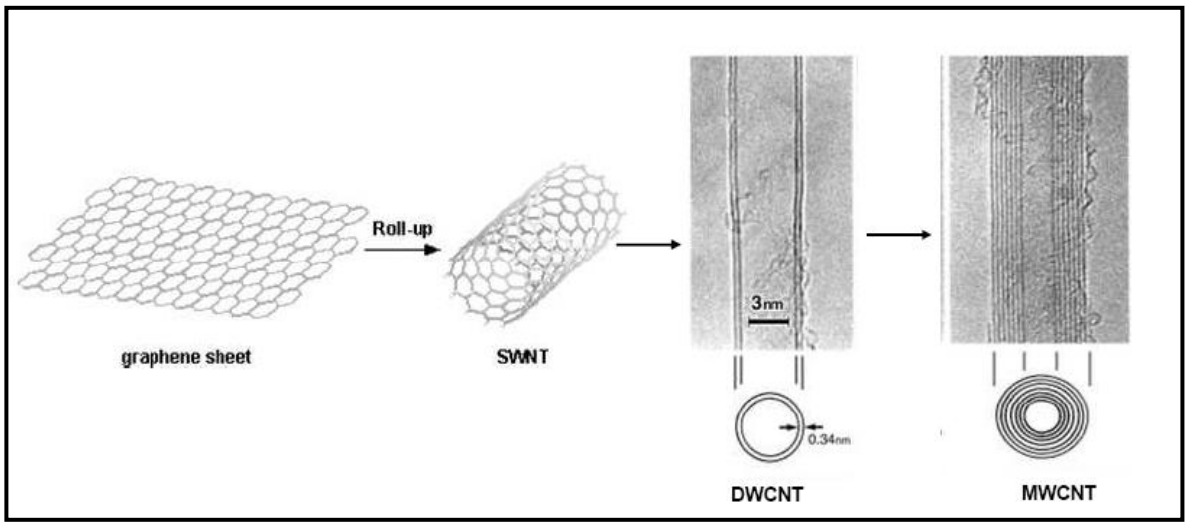


Figure 2.9: Different types of carbon nanotubes [139].

Carbon nanotubes are very useful in nanotechnology applications because of their unique and novel properties (a Young's modulus of over 1 Tera Pascal [140, 141], high aspect ratio of about 1000:1 and high tensile strength). The outstanding properties of CNTs find potential applications in various fields including catalyst supports, in hydrogen storage, lithium batteries, biosensors, electronics, polymer composites, energy storage, pharmaceuticals, biomedical applications, field emission devices, fuel cell membranes and in water purification [124, 142-150].

Increasingly, carbon nanotubes are at the forefront of today's research and heterogeneous catalysis is among the potential applications of these fascinating nanostructures [124, 151]. Apart from the properties already mentioned above, carbon nanotubes are also high in purity (which eliminates self-poisoning), mechanical strength, electrical conductivity, accessibility of the active phase and they have no microporosity (thus eliminating diffusion and intraparticle mass transfer in the reactions medium), the possibility of tuning the specific metal-support interactions which is known to directly affect their catalytic activity and selectivity, and the possibility of confinement effects in their inner cavity [152]. In addition carbon nanotubes have a high flexibility for the dispersion of the active phase since it is

possible to easily chemically functionalize their surfaces [153], deposit the active metal either on their external surface or in their inner cavity [154, 155] and change their chemical composition by doping (nitrogen or boron). Various chemical reactions have been successfully conducted using carbon nanotube supported catalysts. For instance Kang et al. [156] used Ru nanoparticles supported on CNT to catalyze the conversion of syngas and the catalyst was found to be highly selective for the formation of C_{10}-C_{20} hydrocarbons. Yin et al. [157] found that Ru/CNT catalysts are highly active for ammonia decomposition. A study by Bambagioni et al. [158] showed that carbon nanotube supported Pd or Pt nanoparticles are effective catalysts for the electro-oxidation of methanol. Fe and Co catalysts supported on CNT have been shown to be active and stable catalysts for the conversion of syngas to hydrocarbons [109, 159].

Given all these virtues associated with CNTs, a focus of our research group is to synthesize and manipulate carbon nanotubes for application as metal catalyst supports for various reactions including the Fischer-Tropsch synthesis.

Carbon nanotubes as supports for FT catalysts

The use of carbon nanotubes as a FT catalyst support dates back to 2002 when van Steen and Prinsloo [75] first used CNTs as a support for Fe-based FT catalysts to investigate the effect of catalyst preparation method and promoters on the catalyst performance during FTS. Since then, a number of publications have appeared in the literature on the use of CNTs as a support for Fe and Co-based Fischer-Tropsch catalysts [64, 109, 123, 155, 160-167]. However, it is sometimes difficult to directly compare the results reported in the literature. Different authors, although using carbon nanotubes as catalyst support, have used carbon nanotubes from different sources, CNTs pre-treated differently (purification and functionalisation), different catalyst preparation methods, various metal loadings, different location of the active metal on the CNT (ie. Inside the tube versus outside), the use of various promoter metals etc.

In this thesis, an attempt will be made whenever possible to relate the data obtained to the literature data.

2.7 CNT synthesis methods

Several methods are currently being employed to synthesize carbon nanotubes. These methods are: arc discharge [139, 168], laser ablation [169, 170], chemical vapor deposition (CVD) [138, 171-178] and more recently autoclave processes [179-182]. While all techniques used to produce CNTs have their own advantages in terms of purity and cost, the CVD process is the method that is used most widely to produce CNTs. High space-time yields can only be achieved by CVD processes [183]. Table 2.3 gives a comparison of the methods commonly used to produce CNTs in terms of the space-time yield, purity and amorphous content of the CNTs.

Table 2.3: A comparison of the methods commonly used to produce CNTs [183]

Method	Space-time yield	Amorphous carbon	Carbon purity
Arc discharge	low	high	high
Laser ablation	low	high	high
CVD and CCVD[a]	high	low	medium - high[b]

[a]CCVD- Catalytic Chemical Vapour Deposition
[b]High purity carbon can be attained after purification [183]

In this thesis, no attempt is made to describe all the different methods used to prepare CNTs. Interested readers are referred to the above-cited references. Because the CVD method was used in this project to synthesize CNTs, a brief discussion of this technique is given below.

2.7.1 Chemical vapour deposition (CVD)

The chemical vapour deposition (CVD) method for the production of carbon nanotubes is a very promising method since it gives a large quantity, and good quality single wall carbon nanotubes (SWCNTs) or multi-wall carbon nanotubes (MWCNTs) at relatively low cost [175, 184-186]. By employing a specific catalyst material, pyrolysis temperature and carbon sources it is possible to control the structural characteristics of CNTs when the CVD method is used [177].

The CVD synthesis of CNTs involves two main steps; the catalyst preparation in the first step and the synthesis of the CNTs as the second step. The choice of the catalyst ingredients and the catalyst preparation step is crucial since it determines the quality, quantity and properties of the resultant CNTs. The chemical vapour deposition synthesis of CNTs is achieved by decomposing a carbon source such as methane, acetylene, ethylene, carbon monoxide, benzene, short alcohols and toluene [128, 136, 187] over a supported transition metal catalyst at high temperature. The reaction temperature for the synthesis of nanotubes by CVD is generally within the 600^{o}C-900^{o}C range [128, 188]. The transition metals most frequently used as catalysts are Ni, Fe, Co, as well as alloys of these nanoparticles [189, 190]. It has been observed that mixtures of transition metals (alloys) are more efficient for CNT production than one metal alone [188]. These metals are usually loaded on support materials that are stable at high temperature. Conventional, high surface area catalyst supports such as silica, alumina, titania and zeolites have successfully been used in the catalytic production of CNTs [187, 191-200] but purification of the product has proven to be difficult due to the nature of these support materials. Support removal usually requires several oxidation steps or very harsh acid treatment that results in damage to the CNT graphitic structures and as a result, CNTs with lower thermal stability are obtained. To overcome these problems the use of readily removable support has been investigated [174, 175, 186, 201-203]. A detailed study by Magrez et al. [186] showed that $CaCO_3$ is an excellent support for CNT synthesis because of the good

match between the calcium carbonate decomposition temperature and the nanotube growth (700 ^{o}C). The CO_2 originating from the carbonate reacts with acetylene to produce carbon for the CNT production. After CNT synthesis, the residual CaO support can be easily removed by a one step acid treatment [202, 204]. Earlier studies [185, 205, 206] revealed the order of calcium carbonate supported catalyst activity in the CVD synthesis of CNTs is Fe-Co/$CaCO_3$ >> Co/$CaCO_3$ > Fe/$CaCO_3$. Because of the high activity exhibited by the bimetallic Fe-Co/$CaCO_3$ catalyst in the synthesis of CNTs, this catalyst was used for the CNTs produced in this project.

2.7.2 Carbon nanotube growth mechanism on supported catalysts

Many studies have reported on the growth mechanism of CNTs synthesized on supported catalysts [188, 207-217]. Although, there is still some controversy surrounding the growth mechanism, all studies agree that the mechanism can occur in two ways depending on the type of interaction existing between the metal and the support. The metal-support interactions play a determining role in the carbon nanotube growth mechanism [173, 210]. Weak interactions between the metal and the support yield tip-growth mode (confirmed by the presence of the metal particles at the tips of carbon nanotubes) whereas strong interactions lead to a base/root-growth mechanism (the metal particles remain attached to the support). Both growth mechanisms are shown in Figure 2.10. Since both interactions can exist within the same catalyst, it is believed that these mechanisms can occur simultaneously [128]. Since there is an analogy between CNTs and carbon filaments grown by CVD on a supported catalyst [188], it is proposed that the CNT growth mechanism is based on the concepts of vapour-liquid-solid (VLS) theory developed by Wagner and Ellis [209]. In brief, the hydrocarbon molecule dissociates into molecular hydrogen and carbon atoms on the free-metal surface. The carbon dissolves in and diffuses through the bulk of metal. Diffusion through the support cannot be excluded. Finally precipitation of the graphite on the other side of the metal particle occurs [218-221].

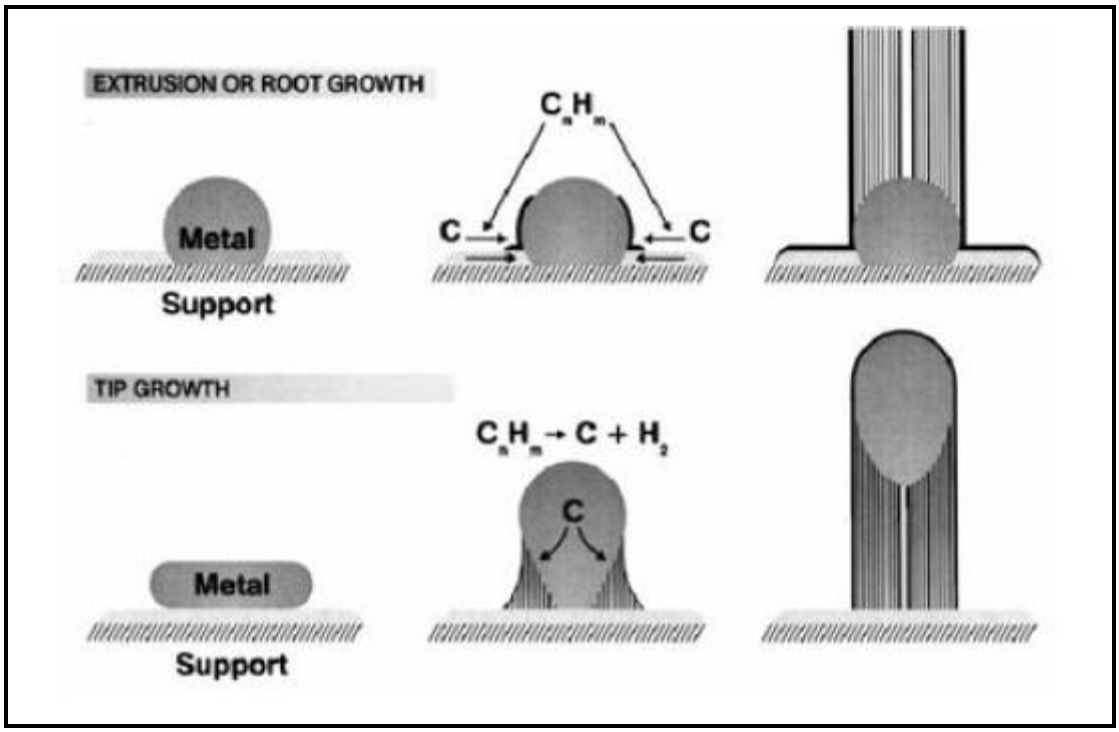


Figure 2.10: Possible carbon nanotube growth mechanism [128, 188].

2.7.3 Purification of carbon nanotubes

Regardless of the method used to produce CNTs, there is always a significant amount of impurity present in the final product [222] and the nature of this impurity depends on the synthesis method, type of catalyst, catalyst support and carbon source employed. The impurities usually present are: graphitic debris, residual catalyst particles and support materials. Since these impurities often influence the desired properties of the CNTs, purification is an essential issue to be addressed [137]. In an effort to obtain CNTs with the desired purity, a number of purification methods have been developed. These include: chemical oxidation (gas phase oxidation, liquid phase oxidation and electrochemical oxidation), physical separation (filtration, centrifugation, high temperature annealing) and combinations of chemical and physical techniques [137]. The choice of the purification technique employed is

largely driven by the intended use of the materials as some purification methods might add secondary impurities to the CNT (for example purifying the CNTs with HNO_3 + H_2SO_4 would certainly dissolve the residual metal and support but sulphur, which is known as a poison for FT catalysts might be left behind). Discussion here is limited to the chemical liquid-phase oxidation of CNTs and interested readers are referred to a comprehensive review on other purification procedures by Hou et al. [137].

The commonly used oxidants for the liquid phase oxidation include: HNO_3 [223-226], H_2O_2 or a mixture of H_2O_2 and HCl [227-229], a mixture of H_2SO_4, HNO_3, $KMnO_4$ and NaOH [176, 230-232], and $KMnO_4$ [231, 233]. The disadvantages of these methods are that they often open the ends of CNTs, cut CNTs, and damage the surface structure of the CNTs. During acid treatment (surface oxidation), a wide range of oxygen containing groups are formed which can be acidic or basic in nature. The amount of oxygen surface groups present depends on the oxidizing agent used, its concentration and the treatment time [226].

2.7.4 Functionalisation of carbon nanotubes

Carbon nanotubes are hydrophobic and inert in nature [234] and to employ them as catalyst supports, it is important to be able to modify their surface. For example, the introduction of oxygen-containing surface groups via acid treatment of the carbon nanotubes renders the tubes less hydrophobic, decreases the pH of the point of zero charge and improves their wetting properties [235, 236]. These effects are very important in catalyst preparation because the dispersion of an active metal phase increases with an increasing amount of surface oxygen groups [237, 238]. The presence of carboxy groups on a CNT surface gives rise to cation exchange sites [236] which can act as anchor sites for metal particles. Figure 2.11 presents the

different oxygen-containing functionalities that can be present on the surface of carbon materials after acid treatment [238].

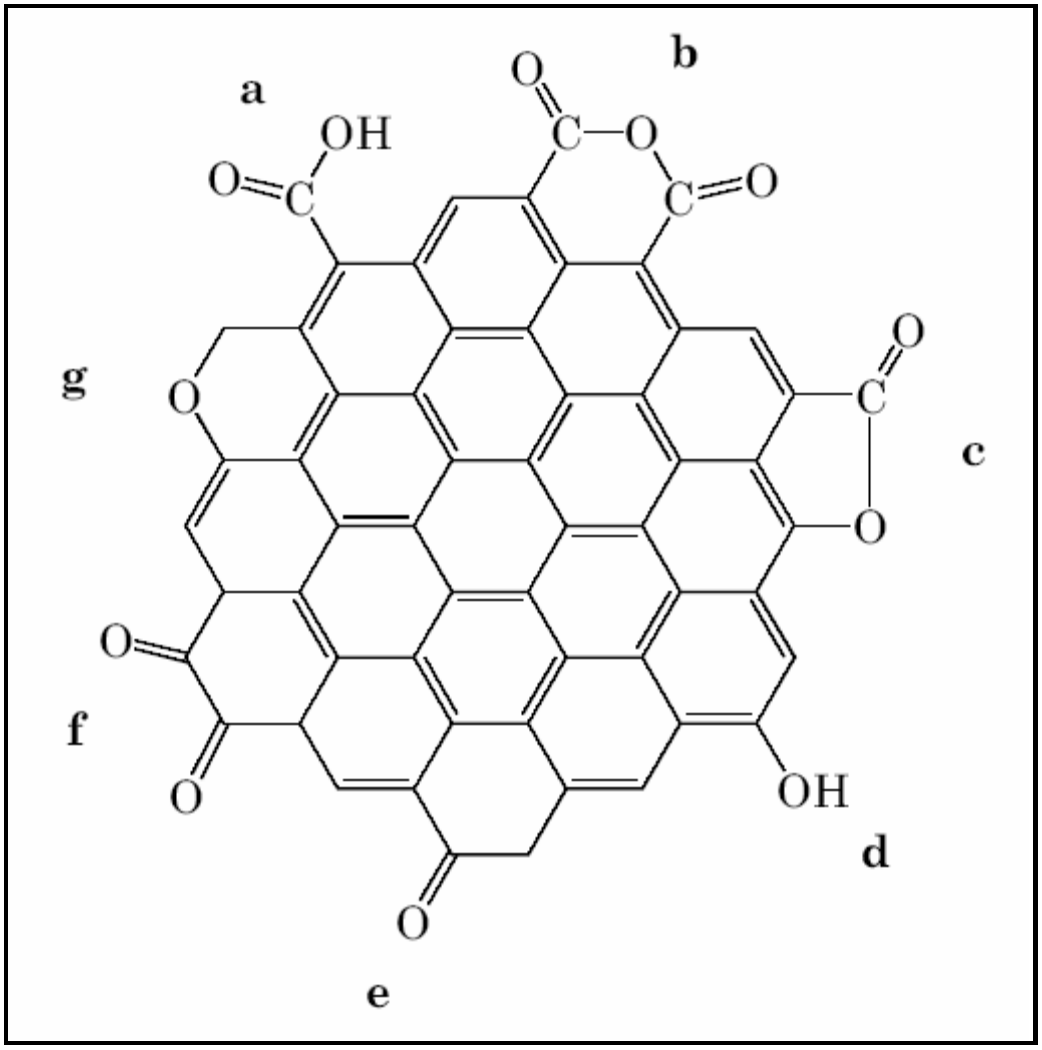


Figure 2.11: Different oxygen-containing surface groups on carbon. a) carboxyl groups, b) carboxylic anhydride groups, c) lactone groups, d) phenol groups, e) carbonyl groups, f) quinone groups, g) xanthene or ether groups [238].

Detailed knowledge of the nature and amount of oxygen functional groups on CNT surfaces is of great interest, especially when using a CNT as a catalyst support [234]. A critical survey of the methods most frequently used for the determination of

surface-oxygen groups and the use of nitric acid treatment to oxidize carbon surfaces has been given by Boehm [239]. Although the precise nature of the carbon-oxygen structures is not well established, results from many studies demonstrate that several types of surface oxygen-groups can be identified and quantified using titration methods [236, 239], FTIR spectroscopy and thermogravimetric-mass spectroscopy (TG-MS) [136, 238], [240], temperature programmed desorption [241] and high resolution XPS [234, 241, 242].

2.8 Nitrogen doping of CNTs

CNTs are chemically inert in nature and functionalization or surface modification is crucial to make them chemically active [243]. Doping the CNT with nitrogen provides an alternative to surface oxidation. It is a way of chemically modifying the surface of CNTs. The presence of embedded N gives rise to a CNT with unique bulk and surface properties [244]. Properties such as pH, catalytic activity, conductivity and nanostructure can be affected due to the doping of carbon [245].
Carbon nanomaterials doped with nitrogen can be used as chemical and biological sensors [246, 247], lithium storage materials [248], catalyst supports [249-251] etc. The use of nitrogen-doped carbon as catalyst support is expected to improve the durability of the resultant catalysts owing to enhanced π bonding [252, 253] and the enhanced surface basic property due to the strong electron donor behaviour of nitrogen [254-256].

Nitrogen can be introduced into the carbon matrix by treatment with nitrogen containing reagents such as ammonia, acetonitrile, urea, HCN, etc. The type of nitrogen functional groups present on the carbon surface depend on the treatment applied (nitrogen source, chemical activity of the carbon surface and the temperature).
Methods to synthesize N-doped CNTs can be grouped into two categories [257]:

1. Doping directly during the synthesis of the carbon nanotubes (in-situ doping).
2. Post-treatment of pre-synthesized carbon nanotube materials with nitrogen containing precursor (N_2, NH_3, acetonitrile etc.). This method is called post-doping.

The in-situ doping method is often used in the synthesis of N-doped carbon nanotubes (N-CNTs) and N-doped carbon nanofibers (N-CNFs) [245]. However, post-doping can also be employed to synthesize N-CNTs and N-CNFs. The post-doping reaction is carried out in a nitrogen containing atmosphere (NH_3, acetonitrile etc.) at high temperatures (600-900^oC) [258-260].

N-doped carbon materials are hydrophilic due to the presence of basic nitrogen containing groups such as amines on the CNT [259]. They possess sites that are chemically active and allow for anchoring of metal precursors onto the carbon surface. It has been reported that N-CNTs exhibit enhanced electrocatalytic activity toward oxygen reduction [258]. Pt has been supported on N-CNTs for use in proton exchange membrane fuel cell (PEMFC) electrodes and this catalyst showed superior fuel cell performance and high stability over commercial fuel cell electrodes [250, 251]. The use of nitrogen-doped carbon nanomaterials as a support for FT catalysts has not yet been extensively explored. Xiong et al. demonstrated that a Co-based FT catalyst supported on nitrogen-doped carbon spheres (N-CSs) can be autoreduced to produce a stable Co/N-CS. In Chapter 8, we explore the use of N-CNTs as supports for Fe-based FTS catalysts.

2.9 Synthesis of Fischer-Trospch catalysts

Catalyst preparation has a strong influence on the catalytic performance of FT catalysts [63]. For example van Steen and Prinsloo [75] prepared carbon nanotube-

supported iron catalysts by incipient wetnesss impregnation, deposition-precipitation with K_2CO_3 and deposition-precipitation with urea as the precipitating agent. The results showed that, although the three catalysts showed similar metal dispersions after the reduction step, their catalytic activities in the Fischer-Tropsch synthesis differed significantly, with the catalyst prepared by wetness impregnation being the most active. However, the selectivity was found to be independent of the preparation method.

Several steps are involved in the preparation of the FT catalysts and these include: the selection of the appropriate catalyst support, choice of the method of deposition of the active phase on the support, choice of the appropriate promoter and pre-treatment conditions. The goal in catalyst preparation is to achieve a homogenous, well dispersed active metal catalyst that is stable.

Several methods exist for the preparation of supported FT catalysts and these include: incipient wetness impregnation [75, 109, 189], deposition-precipitation [75, 109, 261], reverse micelle impregnation [202], sol-gel procedures [262], preparation of eggshell structures [263], monolithic catalyst preparation [264], use of microemulsion [265], as well as chemical vapor deposition [266] and plasma methods [267].
The incipient wetness impregnation and deposition-precipitation methods are the only two methods that were used in this project and as a result only these methods are discussed further.

2.9.1 Incipient wetness impregnation method

In the chemical industry, impregnation is usually employed for practical and economical reasons [268]. The method is relatively simple; catalyst preparation is rapid and high metal loadings can be achieved [268]. However, a disadvantage of this

method is that sometimes the active metal is nonuniformly deposited inside the pores of the catalyst support.

Briefly, in this method, the precursor salt is dissolved in a volume of solvent equal to the catalyst pore volume, and this solution is added dropwise to the support (Figure 2.12). Addition of the solution continues until the pores of the support are filled [268]. Afterward, the catalyst is dried and calcined. The precise amount of the active metal is present in the carrier/ support when this method is used. Large metal catalyst particles are obtained when the concentration of the metal salt is high. Small metal particles are obtained if a diluted solution of the metal salt is used [269]. Incipient wetness impregnation is the most common method used to prepare cobalt-supported catalysts [63]. Tavasoli et al. [163] used this technique to prepare supported mono- and bimetallic Co and Fe catalysts on carbon nanotubes.

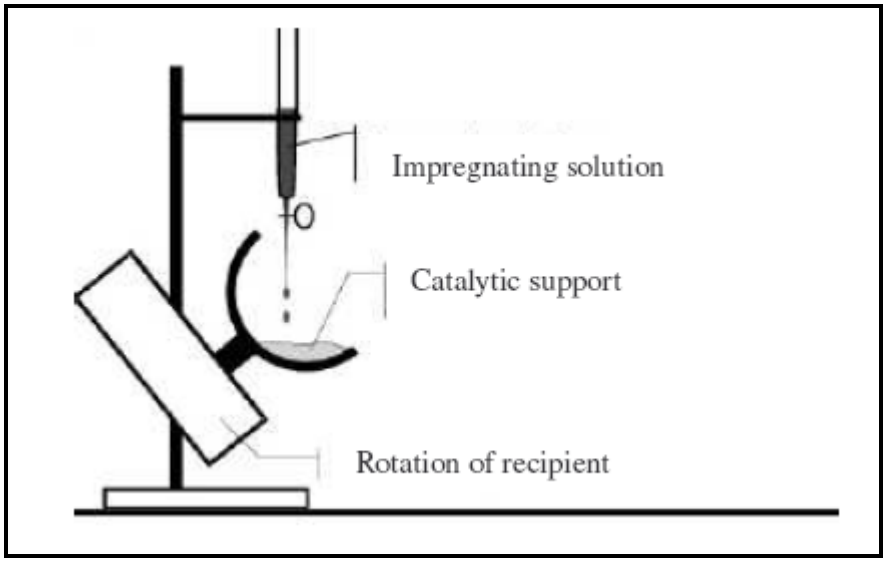


Figure 2.12: Schematic representation of experimental set up for incipient wetness impregnation method [63].

2.9.2 Deposition-precipitation method

This method is based on the use of precipitation combined with deposition from a liquid medium [270]. The method combines all the advantages of the precipitation method related to size control and size distribution of precipitated particles but reduces the risk of the formation of bulk mixed compounds of the support and active phase [271, 272]. A most important feature of this method of catalyst preparation is to prevent precipitation far from the support surface [270].

The deposition-precipitation method, using urea as the precipitating agent [268, 273], makes it possible to avoid local pH rises and metal hydroxide precipitation in the bulk solution. A solution of the precursor salt and urea is added to the support and under slow heating, the OH^- ions precipitate slowly throughout the bulk solution due to the hydrolysis of urea that occurs at 90^oC:

$$CO(NH_2)_2 + 3H_2O \longrightarrow 2NH_4^+ + CO_2 + 2OH^-$$

After precipitation, the precursor-support is generally washed to remove undesirable, soluble ions, dried, and finally pre-treated to decompose the catalyst precursor. This method has been used, for example by Bahome et al. [64, 109] and van Steen and Prinsloo [75] to prepare high loadings (10 wt.%), of well-dispersed metal particles on supports with narrow size distributions suitable for Fischer-Tropsch synthesis.

2.10 Catalyst deactivation

Catalyst deactivation is the decrease of catalyst activity with time. Catalysts have a limited lifetime with some losing their activity after a short period, while others can last for more than ten years [274]. The decline or loss of activity by a catalyst during a reaction can be the result of various physical and chemical factors such as [274]:

- Blocking of the catalytically active sites;
- Loss of catalytically active sites due to chemical, thermal or mechanical processes.

Great efforts are usually made to avoid catalyst deactivation in industrial processes.

2.11 References

[1] M.E. Dry, in: G. Ertl, H. Knozinger, F. Schuth and J. Weitkamp (Eds.), Handbook of Heterogeneous Catalysis, Wiley-CVH-Weinheim, 2008, p. 2965.

[2] D.J. Duvenhage, "The preparation, characterisation and evaluation of titania supported iron:cobalt bimetallic catalysts for the hydrogenation of carbon monoxide" PhD thesis, University of the Witwatersrand, Johannesburg, (1993).

[3] E.I. Mabaso, "Nanosized iron crystallites for Fischer-Tropsch synthesis" PhD. thesis, University of Cape Town, Rondebosch, Cape Town, (2005).

[4] A.C. Vosloo, Fuel Process Technol 71 (2001) 149.

[5] F. Morales, B.M. Weckhuysen, ChemInform 38 (2007) 1.

[6] H.H. Storch, N. Golumbic, R.B. Anderson, The Fischer-Tropsch and Related Syntheses, John Wiley & Sons, Inc., New York, 1951.

[7] H. Pichler, Advances in catalysis and related subjects 302 (1952) 271.

[8] M.E. Dry, In: Anderson J.R., Boudart M (Eds.) Catalysis Science and Technology, Vol. 1 Berlin: Springer-Verlag (1981) 159.

[9] P. Sabatier, J.B. Senderens, Compte Rendu 134 (1902) 514.

[10] Badische Anilin und Soda Fabrik: German Pat. 293, (1913) 787.

[11] F. Fischer, H. Tropsch, D. Dilthes, Brennstoff-Chemie 6 (1925) 265.

[12] F. Fischer, H. Tropsch, Brennstoff-Chemie 7 (1926) 97.

[13] Fundamentals of gas to liquid, Petroleum economist, ISBN 1 86186 1583, (Jan 2003).

[14] X. Lu, School of Chemical and Metallurgical Engineering, University of the Witwatersrand, Johannesburg, South Africa. Personal communications (2011).

[15] T.J. Remans, G. Jenzer, A. Hoek, in: G. Ertl, H. Knozinger, F. Schuth and J. Weitkamp (Eds.), Handbook of Heterogeneous catalysis, Wiley-CVH, Weinheim, 2008, p. 2994.

[16] A.A. Adesina, Applied Catalysis A, General 138 (1996) 345.

[17] M.E. Dry, Catalysis Today 71 (2002) 227.

[18] M.E. Dry, Applied Industrial Catalysis (B.E. Leach, Ed.), Vol. 2 Academic Press, New York (1983).

[19] C.H. Bartholomew, Studies in Surface Science and Catalysis 64 (1991) 158.

[20] M.E. Dry, Applied Catalysis A: General 138 (1996) 319.

[21] P.M. Maitlis, V. Zanotti, Chemical Communications 2009 (2009) 1619.

[22] M.E. Dry, Studies in Surface Science and Catalysis 152 (2004) 196.

[23] W.M. Hexana, "A systematic study of the effect of chemical promoters on the precipitated Fe-based Fischer-Tropsch synthesis catalyst" PhD. thesis, University of the Witwatersrand, Johannesburg, (2009).

[24] H.G. Stenger Jr, C.F. Askonas, Industrial & Engineering Chemistry Fundamentals 25 (1986) 410.

[25] E. Iglesia, S.C. Reyes, R.J. Madon, S.L. Soled, Advances in catalysis 39 (1993) 221.

[26] H. Schulz, M. Claeys, Applied Catalysis A: General 186 (1999) 71.

[27] M. Claeys, E. Van Steen, in: A. Steynberg and M. Dry (Eds.), Elsevier, 2004, p. 601.

[28] H. Schulz, E. van Steen, M. Claeys, Topics in Catalysis 2 (1995) 223.

[29] V. Ponec, In: Coal Science, Academic Press, New York, 1984, p. 1.

[30] H. Schulz, Applied Catalysis A, General 186 (1999) 3.

[31] R.B. Anderson (Ed.), Catalysts for Fischer-Tropsch synthesis, in: P.H. Emmett (Ed.), Catalysis, Van Nostrand-Reinhold, New York, 1956.

[32] R.A. Dictor, A.T. Bell, Industrial & Engineering Chemistry Process Design and Development 22 (1983) 678.

[33] R.J. Madon, W.F. Taylor, Journal of Catalysis 69 (1981) 32.

[34] L. König, J. Gaube, Chemie Ingenieur Technik-CIT 55 (1983) 14.

[35] E.W. Kuipers, C. Scheper, J.H. Wilson, I.H. Vinkenburg, H.J. Oosterbeek, Journal of Catalysis 158 (1996) 288.

[36] G.A. Huff, C.N. Satterfield, Journal of Catalysis 85 (1984) 370.

[37] E. Iglesia, S.C. Reyes, R.J. Madon, Journal of Catalysis 129 (1991) 238.

[38] H.E. Atwood, C.O. Bennett, Industrial & Engineering Chemistry Process Design and Development 18 (1979) 163.

[39] C.N. Satterfield, G.A. Huff, Journal of Catalysis 73 (1982) 187.

[40] K. Jalama, "Fischer-Tropsch synthesis over supported cobalt catalysts: effect of ethanol addition, precursors and gold doping" PhD thesis, University of the Witwatersrand, Johannesburg (2008).

[41] A. Tavasoli, M. Trepanier, A.K. Dalai, N. Abatzoglou, Journal of Chemical Engineering Data 55 (2010) 2757.

[42] R.B. Anderson, R.A. Friedel, H.H. Storch, Journal of Chemistry and Physics 19 (1951) 313.

[43] Y. Traa, Chemical Communications 46 (2010) 2175.

[44] A.P. Steynberg, in: A. Steynberg and M.E. Dry (Eds.), Studies in Surface Science and Catalysis, Elsevier, 2004, p. 1.

[45] P.M. Maitlis, R. Quyoum, H.C. Long, M.L. Turner, Applied Catalysis A: General 186 (1999) 363.

[46] P. Biloen, W.M.H. Sachtler, Advances in Catalysis 30 (1981) 165.

[47] J.P. Hindermann, G.J. Hutchings, A. Kiennemann, Catalysis Reviews-Science and Engineering 35 (1993) 1.

[48] B.W. Wojciechowski, Catalysis Reviews 30 (1988) 629.

[49] H. Chen, A.A. Adesina, Journal of Chemical Technology & Biotechnology 60 (1994) 103.

[50] H.C. Long, M.L. Turner, P. Fornasiero, J. Kapar, M. Graziani, P.M. Maitlis, Journal of Catalysis 167 (1997) 172.

[51] F.A.N. Fernandes, Chem. Eng. Technol. 28 (2005) 930.

[52] H.H. Storch, N. Golumbic, R.B. Anderson, The Fischer-Tropsch and Related Syntheses, Wiley New York, 1951.

[53] L.Z. Linganiso, "Microwave induced solid-state interactions for the synthesis of Fischer-Tropsch catalysts" PhD. thesis, University of the Witwatersrand, Johannesburg, (2009).

[54] M.L. Turner, P.K. Byers, H.C. Long, P.M. Maitlis, Journal of the American Chemical Society 115 (1993) 4417.

[55] A. Guerrero-Ruiz, I. Rodriguez-Ramos, in: J.A. Anderson and M.F. Garcia (Eds.), Supported Metals in Catalysis, Imperial College Press, London, 2005, p. 155.

[56] M.E. Dry, Catalysis Letters 7 (1990) 241.

[57] M.A. Vannice, Journal of Catalysis 37 (1975) 449.

[58] M.E. Dry, Studies in Surface Science and Catalysis 152 (2004) 533.

[59] R.B. Anderson, The Fischer-Tropsch Synthesis, Academic Press Inc., New York, 1984, p. 295.

[60] F. Morales, B.M. Weckhuysen, ChemInform 38 (2007).

[61] V.U.S. Rao, G.J. Stiegel, G.J. Cinquegrane, R.D. Srivastava, Fuel Processing Technology 30 (1992) 83.

[62] E. van Steen, M. Claeys, Chemical Engineering and Technology 31 (2008) 655.

[63] A.Y. Khodakov, W. Chu, P. Fongarland, Chemical Reviews 107 (2007) 1692.

[64] M.C. Bahome, L.L. Jewell, K. Padayachy, D. Hildebrandt, D. Glasser, A.K. Datye, N.J. Coville, Applied Catalysis A: General 328 (2007) 243.

[65] E. Iglesia, Applied Catalysis A: General 161 (1997) 59.

[66] E. Iglesia, S.L. Soled, R.A. Fiato, G.H. Via, Journal of Catalysis 143 (1993) 345.

[67] T. Chronis, (1999) .

[68] A.R. Belambe, R. Oukaci, J.G. Goodwin, Journal of Catalysis 166 (1997) 8.

[69] M.E. Dry, Applied Catalysis A: General 276 (2004) 1.

[70] A. Martínez, C. López, F. Marquez, I. Diaz, Journal of Catalysis 220 (2003) 486.

[71] C.A. Chanenchuk, I.C. Yates, C.N. Satterfield, Energy Fuels 5 (1991) 847.

[72] J.A.L. Lodya, T. Seda, A.M. Strydom, S.S. Manzini, in: Anonymous, Characterization of Fe/C catalysts supported on Al2O3, SiO2 and TiO2, Journal of Physics: Conference Series, IOP Publishing, 2010, p. 082016.

[73] H. Xiong, M. Moyo, M.A.M. Motchelaho, L.L. Jewell, N.J. Coville, Applied Catalysis A: General (2010).

[74] H.J. Jung, P.L. Walker Jr, M.A. Vannice, Journal of Catalysis 75 (1982) 416.

[75] E. van Steen, F.F. Prinsloo, Catalysis Today 71 (2002) 327.

[76] L. Guczi, G. Stefler, O. Geszti, Z. Koppány, Z. Kónya, É. Molnár, M. Urbán, I. Kiricsi, Journal of Catalysis 244 (2006) 24.

[77] X. An, B. Wu, H. Wan, T. Li, Z. Tao, H. Xiang, Y. Li, Catalysis Communications 8 (2007) 1957.

[78] W. Ngantsoue-Hoc, Y. Zhang, R.J. O'Brien, M. Luo, B.H. Davis, Applied Catalysis A: General 236 (2002) 77.

[79] J.L. Carter, J.A. Cusumano, J.H. Sinfelt, Journal of Physical Chemistry 70 (1966) 2257.

[80] J.Y. Park, Y.J. Lee, P.K. Khanna, K.W. Jun, J.W. Bae, Y.H. Kim, Journal of Molecular Catalysis A: Chemical 323 (2010) 84.

[81] D. Barkhuizen, I. Mabaso, E. Viljoen, C. Welker, M. Claeys, E. van Steen, J.C.Q. Fletcher, Pure and applied chemistry 78 (2006) 1759.

[82] G.L. Bezemer, J.H. Bitter, H. Kuipers, H. Oosterbeek, J.E. Holewijn, X. Xu, F. Kapteijn, A.J. van Dillen, K.P. de Jong, Journal of the American Chemical Society 128 (2006) 3956.

[83] E.I. Mabaso, E. van Steen, M. Claeys, DGMK Tagungsbericht 4 (2006) 93.

[84] A.Y. Khodakov, A. Griboval-Constant, R. Bechara, V.L. Zholobenko, Journal of Catalysis 206 (2002) 230.

[85] E. Iglesia, S.L. Soled, R.A. Fiato, Journal of Catalysis 137 (1992) 212.

[86] S.W. Ho, M. Houalla, D.M. Hercules, Journal of Physical Chemistry 94 (1990) 6396.

[87] B.G. Johnson, C.H. Bartholomew, D.W. Goodman, Journal of Catalysis 128 (1991) 231.

[88] W.P. Ma, Y.J. Ding, L.W. Lin, Industrial & Engineering Chemistry Research 43 (2004) 2391.

[89] B. Ernst, L. Hilaire, A. Kiennemann, Catalysis Today 50 (1999) 413.

[90] J. Zwart, R. Snel, Journal of Molecular Catalysis 30 (1985) 305.

[91] M. Kraum, M. Baerns, Applied Catalysis A: General 186 (1999) 189.

[92] T. Kaneko, F. Derbyshire, E. Makino, D. Gray, M. Tamura, in: Anonymous, Wiley Online Library, 2005.

[93] R.A. van Santen, Surface Science 251 (1991) 6.

[94] D.B. Bukur, D. Mukesh, S.A. Patel, Industrial & Engineering Chemistry Research 29 (1990) 194.

[95] G.J. Haddad, B. Chen, J.G. Goodwin, Journal of Catalysis 160 (1996) 43.

[96] B. Cornils, W.A. Herrmann, R. Schlögl, C.H. Wong, Catalysis from A to Z , A concise encyclopedia, Wiley-VCH, Weinheim, 2000.

[97] M. Luo, R.J. O'Brien, S. Bao, B.H. Davis, Applied Catalysis A: General 239 (2003) 111.

[98] X. An, B. Wu, H.J. Wan, T.Z. Li, Z.C. Tao, H.W. Xiang, Y.W. Li, Catalysis Communications 8 (2007) 1957.

[99] M.E. Dry, T. Shingles, L.J. Boshoff, G.J. Oosthuizen, Journal of Catalysis 15 (1969) 190.

[100] M.E. Dry, T. Shingles, Journal of Catalysis 17 (1970) 341.

[101] M.E. Dry, G.J. Oosthuizen, Journal of Catalysis 11 (1968) 18.

[102] Y. Yang, H.W. Xiang, Y.Y. Xu, L. Bai, Y.W. Li, Applied Catalysis A: General 266 (2004) 181.

[103] H. Arakawa, A.T. Bell, Industrial & Engineering Chemistry Process Design and Development 22 (1983) 97.

[104] R.B. Anderson, B. Seligman, J.F. Shultz, R. Kelly, M.A. Elliott, Industrial & Engineering Chemistry 44 (1952) 391.

[105] D.B. Bukur, X. Lang, D. Mukesh, W.H. Zimmerman, M.P. Rosynek, C. Li, Industrial & Engineering Chemistry Research 29 (1990) 1588.

[106] J. Abbott, N.J. Clark, B.G. Baker, Applied Catalysis 26 (1986) 141.

[107] R.A. Diffenbach, D.J. Fauth, Journal of Catalysis 100 (1986) 466.

[108] Y. Yang, H.W. Xiang, Y.Y. Xu, L. Bai, Y.W. Li, Applied Catalysis A: General 266 (2004) 181.

[109] M.C. Bahome, L.L. Jewell, D. Hildebrandt, D. Glasser, N.J. Coville, Applied Catalysis A, General 287 (2005) 60.

[110] H. Jüntgen, Fuel 65 (1986) 1436.

[111] S. Maity, Current Science 80 (2001) 628.

[112] S.J. Tauster, S.C. Fung, Journal of Catalysis 55 (1978) 29.

[113] J. Hagen, Industrial catalysis: a practical approach, Wiley-VCH Verlag GmbH & Co. KGaA, 2006.

[114] Q. Zhang, J. Kang, Y. Wang, ChemCatChem 2 (2010) 1030.

[115] R. Burch, A.R. Flambard, Journal of Catalysis 85 (1984) 16.

[116] F. Rodríguez-reinoso, Carbon 36 (1998) 159.

[117] R.C. Reuel, C.H. Bartholomew, Journal of Catalysis 85 (1984) 78.

[118] S.L. Soled, E. Iglesia, R.A. Fiato, J.E. Baumgartner, H. Vroman, S. Miseo, Topics in Catalysis 26 (2003) 101.

[119] Y.M. Jin, A.K. Datye, Journal of Catalysis 196 (2000) 8.

[120] B. Jongsomjit, J. Panpranot, J.G. Goodwin, Journal of Catalysis 215 (2003) 66.

[121] H. Xiong, Y. Zhang, K. Liew, J. Li, Journal of Molecular Catalysis A: Chemical 295 (2008) 68.

[122] M. Boudart, A. Delbouille, J.A. Dumesic, S. Khammouma, H. Topsře, Journal of Catalysis 37 (1975) 486.

[123] G.L. Bezemer, A. Van Laak, A.J. Van Dillen, K.P. De Jong, Studies in Surface Science and Catalysis 147 (2004) 259.

[124] P. Serp, M. Corrias, P. Kalck, Applied Catalysis A, General 253 (2003) 337.

[125] M. Carmo, V.A. Paganin, J.M. Rosolen, E.R. Gonzalez, Journal of Power Sources 142 (2005) 169.

[126] R.C. Reuel, C.H. Bartholomew, Journal of Catalysis 85 (1984) 63.

[127] S.N. Marinkovic, Journal of the Serbian Chemical Society 73 (2008) 891.

[128] S.D. Mhlanga, "Synthesis and study of carbon nanotubes and carbon spheres" PhD. thesis, University of the Witwatersrand, Johannesburg, (2009).

[129] F. Rodriguez-Reinoso, A. Sepúlveda-Escribano, in: P. Serp and J.L. Figueiredo (Eds.), Carbon materials for catalysis, Wiley Online Library, 2009, p. 131.

[130] C. Park, M.A. Keane, Journal of Colloid Interface Science, 266 (2003) 183.

[131] F. Coloma, A. Sepúlveda-Escribano, J.L.G. Fierro, F. Rodríguez-Reinoso, Applied Catalysis A: General 150 (1997) 165.

[132] A. Nieto-Márquez, D. Toledano, J.C. Lazo, A. Romero, J.L. Valverde, Applied Catalysis A: General 373 (2010) 192.

[133] S. Demirel-Gülen, M. Lucas, P. Claus, Catalysis Today 102 (2005) 166.

[134] J. Bedia, J.M. Rosas, J. Rodríguez-Mirasol, T. Cordero, Applied Catalysis B: Environmental 94 (2010) 8.

[135] A. Guerrero-Ruiz, A. Sepúlveda-Escribano, I. Rodríguez-Ramos, Applied Catalysis A: General 81 (1992) 101.

[136] K.P. De Jong, J.W. Geus, Catalysis Reviews-Science and Engineering 42 (2000) 481.

[137] P.X. Hou, C. Liu, H.M. Cheng, Carbon 46 (2008) 2003.

[138] M.J. Ledoux, C. Pham-Huu, Cattech 5 (2001) 226.

[139] S. Iijima, Nature 354 (1991) 56.

[140] Y.Q. Zhang, G.R. Liu, X. Han, Physics Letters A 349 (2006) 370.

[141] R.B. Pipes, P. Hubert, Compos. Sci. Technol 62 (2002) 419.

[142] P. Ajayan, O. Zhou, Carbon nanotubes: Topics in Applied Physics 80 (2001) 391.

[143] M. Terrones, A. Jorio, M. Endo, A.M. Rao, Y.A. Kim, T. Hayashi, H. Terrones, J.C. Charlier, G. Dresselhaus, M.S. Dresselhaus, Materials Today 7 (2004) 30.

[144] M. Trojanowicz, TrAC Trends in Analytical Chemistry 25 (2006) 480.

[145] M.S. Dresselhaus, G. Dresselhaus, A. Jorio, Annual Review of Material Research 34 (2004) 247.

[146] M.S. Dresselhaus, G. Dresselhaus, P. Avouris, Carbon nanotubes : synthesis, structure, properties, and applications, Springer, Berlin, 2001, p. 447.

[147] L. Dai, Carbon nanotechnology: recent developments in chemistry, physics, materials science and device applications, Elsevier Science Ltd, Dayton, Ohio 45489-0240, USA, 2006.

[148] J. Robertson, Materials Today 10 (2007) 36.

[149] M. Paradise, T. Goswami, Mater. Des. 28 (2007) 1477.

[150] K.L. Salipira, B.B. Mamba, R.W. Krause, T.J. Malefetse, S.H. Durbach, Environmental Chemistry Letters 5 (2007) 13.

[151] M. Monthioux, P. Serp, E. Flahaut, C. Laurent, A. Peigney, M. Razafinimanana, W. Bacsa, J.-. Broto, in Springer Handbook of Nanotechnology,

2nd revised and extended edition (Ed.B. Bhushan), Springer-Verlag, Heidelberg, Germany, 2007, p. 43–112.

[152] P. Serp, E. Castillejos, ChemCatChem 2 (2010) 41-47.

[153] D. Tasis, N. Tagmatarchis, A. Bianco, M. Prato, Chemical Reviews 106 (2006) 1105.

[154] E. Castillejos, P.J. Debouttière, L. Roiban, A. Solhy, V. Martinez, Y. Kihn, O. Ersen, K. Philippot, B. Chaudret, P. Serp, Angewandte Chemie International Edition 48 (2009) 2529.

[155] W. Chen, Z. Fan, X. Pan, X. Bao, Journal of the American Chemical Society 130 (2008) 9414.

[156] J. Kang, S. Zhang, Q. Zhang, Y. Wang, Angewandte Chemie International Edition English 48 (2009) 2565.

[157] S.F. Yin, B.Q. Xu, W.X. Zhu, C.F. Ng, X.P. Zhou, C.T. Au, Catalysis Today 93 (2004) 27.

[158] V. Bambagioni, C. Bianchini, A. Marchionni, J. Filippi, F. Vizza, J. Teddy, P. Serp, M. Zhiani, J. Power Sources 190 (2009) 241.

[159] M.C. Bahome, "Synthesis and use of carbon nanotubes as a support for the Fischer-Tropsch synthesis" PhD thesis, University of the Witwatersrand, Johannesburg (2008).

[160] R.M.M. Abbaslou, A. Tavassoli, J. Soltan, A.K. Dalai, Applied Catalysis A: General 367 (2009) 47.

[161] U.M. Graham, A. Dozier, R.A. Khatri, M.C. Bahome, L.L. Jewell, S.D. Mhlanga, N.J. Coville, B.H. Davis, Catalysis Letters 129 (2009) 39.

[162] L. Guczi, G. Stefler, O. Geszti, Z. Koppány, Z. Kónya, É. Molnár, M. Urbán, I. Kiricsi, Journal of Catalysis 244 (2006) 24.

[163] A. Tavasoli, M. Trépanier, R.M.M. Abbaslou, A.K. Dalai, N. Abatzoglou, Fuel Processing Technology 90 (2009) 1486.

[164] M. Trépanier, A. Tavasoli, A.K. Dalai, N. Abatzoglou, Fuel Processing Technology 90 (2009) 367.

[165] M. Trépanier, A. Tavasoli, A.K. Dalai, N. Abatzoglou, Applied Catalysis A: General 353 (2009) 193.

[166] H. Xiong, M.A.M. Motchelaho, M. Moyo, L.L. Jewell, N.J. Coville, Journal of Catalysis Accepted (2010).

[167] A. Tavasoli, R.M.M. Abbaslou, M. Trepanier, A.K. Dalai, Applied Catalysis A: General 345 (2008) 134.

[168] H. Zeng, L. Zhu, G. Hao, R.S. Sheng, Carbon 36 (1998) 259.

[169] T. Guo, P. Nikolaev, A. Thess, D.T. Colbert, R.E. Smalley, Chemical Physics Letters 243 (1995) 49.

[170] A. Thess, R. Lee, P. Nikolaev, H. Dai, P. Petit, J. Robert, C.H. Xu, Y.H. Lee, S.G. Kim, A.G. Rinzler, D.T. Colbert, G.E. Scuseria, D. Tomanek, J.E. Fischer, R.E. Smalley, Science 273 (1996) 483.

[171] C.T. Hsieh, Y.T. Lin, J.Y. Lin, J.L. Wei, Materials Chemistry and Physics 114 (2009) 702.

[172] K. Hernadi, Z. Konya, A. Siska, J. Kiss, A. Oszko, J. Nagy, I. Kiricsi, Materials Chemistry & Physics 77 (2003) 536.

[173] A.M. Cassell, J.A. Raymakers, J. Kong, H. Dai, Journal of Physical Chemistry B 103 (1999) 6484.

[174] J. Cheng, X. Zhang, Z. Luo, F. Liu, Y. Ye, W. Yin, W. Liu, Y. Han, Materials Chemistry and Physics 95 (2006) 5.

[175] E. Couteau, K. Hernadi, J.W. Seo, L. Thiên-Nga, C. Mikó, R. Gaál, L. Forró, Chemical Physics Letters 378 (2003) 9.

[176] Y. Li, X. Zhang, J. Luo, W. Huang, J. Cheng, Z. Luo, T. Li, F. Liu, G. Xu, X. Ke, Nanotechnology 15 (2004) 1645.

[177] S. Porro, S. Musso, M. Giorcelli, A. Chiodoni, A. Tagliaferro, Physica E: Low-dimensional Systems and Nanostructures 37 (2007) 16.

[178] M. Su, B. Zheng, J. Liu, Chemical physics letters 322 (2000) 321.

[179] V.O. Nyamori, N.J. Coville, Organometallics 26 (2007) 4083.

[180] J. Liu, M. Shao, Q. Xie, L. Kong, W. Yu, Y. Qian, Carbon 41 (2003) 2101.

[181] M. Laskoski, W. Steffen, J.G.M. Morton, M.D. Smith, U.H.F. Bunz, Journal of the American Chemical Society 124 (2002) 13814.

[182] P.I. Dosa, C. Erben, V.S. Iyer, K.P.C. Vollhardt, I.M. Wasser, Journal of the American Chemical Society 121 (1999) 10430.

[183] M. Bierdel, S. Buchholz, V. Michele, L. Mleczko, R. Rudolf, M. Voetz, A. Wolf, physica status solidi (b) 244 (2007) 3939.

[184] K. Hernadi, Z. Konya, A. Siska, J. Kiss, A. Oszko, J.B. Nagy, I. Kiricsi, Materials Chemistry and Physics 77 (2002) 536.

[185] Z. Li, E. Dervishi, Y. Xu, X. Ma, V. Saini, A.S. Biris, R. Little, A.R. Biris, D. Lupu, Journal of Chemisty and Physics 129 (2008) 074712.

[186] A. Magrez, J.W. Seo, C. Miko, K. Hernadi, L. Forro, Journal of Physical Chemistry B 109 (2005) 10087.

[187] S. Inoue, T. Nakajima, Y. Kikuchi, Chemical Physics Letters 406 (2005) 184.

[188] A.C. Dupuis, Progress in Materials Science 50 (2005) 929.

[189] S.D. Mhlanga, K.C. Mondal, R. Carter, M.J. Witcomb, N.J. Coville, South African Journal of Chemistry 62 (2009) 67.

[190] M. Kumar, Y. Ando, Journal of Nanoscience and Nanotechnology 10 (2010) 3739.

[191] C.J. Lee, J. Park, Carbon 39 (2001) 1891.

[192] C.J. Lee, J. Park, J.A. Yu, Chemical Physics Letters 360 (2002) 250.

[193] J.E. Herrera, D.E. Resasco, Journal of catalysis 221 (2004) 354.

[194] W. Qian, F. Wei, T. Liu, Z.W. Wang, Solid State Commun. 126 (2003) 365.

[195] R.L. Vander Wal, T.M. Ticich, V.E. Curtis, Carbon 39 (2001) 2277.

[196] S. Inoue, Y. Kikuchi, Chemical Physics Letters 410 (2005) 209.

[197] K. Hernadi, A. Fonseca, J.B. Nagy, D. Bernaerts, A. Fudala, A.A. Lucas, Zeolites 17 (1996) 416.

[198] K. Hernadi, A. Fonseca, J.B. Nagy, D. Bernaerts, A.A. Lucas, Carbon 34 (1996) 1249.

[199] F. Pinna, Catalysis Today 41 (1998) 129.

[200] A.L. Balch, M.M. Olmstead, Chemical Reviews 98 (1998) 2123.

[201] A.R. Harutyunyan, B.K. Pradhan, J. Chang, G. Chen, P.C. Eklund, Journal of Physical Chemistry B 106 (2002) 8671.

[202] S.D. Mhlanga, N.J. Coville, Diamond & Related Materials 17 (2008) 1489.

[203] W.Z. Li, J.G. Wen, M. Sennett, Z.F. Ren, Chemical Physics Letters 368 (2003) 299.

[204] Z. Li, E. Dervishi, Y. Xu, X. Ma, V. Saini, A.S. Biris, R. Little, A.R. Biris, D. Lupu, Journal of Chemical Physics 129 (2008) 074712.

[205] H. Kathyayini, N. Nagaraju, A. Fonseca, J.B. Nagy, Journal of Molecular Catalysis A: Chemical 223 (2004) 129.

[206] S.D. Mhlanga, N.J. Coville, Diamond and Related Materials 17 (2008) 1489.

[207] H. Liu, D. Takagi, H. Ohno, S. Chiashi, T. Chokan, Y. Homma, Applied physics express 1 (2008) 14001.

[208] M. Endo, T. Hayashi, Y. Ahm Kim, M. Terrones, M.S. Dresselhaus, Philosophical Transactions A 362 (2004) 2223.

[209] R.S. Wagner, W.C. Ellis, Trans. Metall. Soc. AIME 233 (1965) 1053–1064.

[210] R.T.K. Baker, Carbon 27 (1989) 315.

[211] H. Kanzow, A. Ding, Physical review B 60 (1999) 11180.

[212] A. Yasuda, N. Kawase, W. Mizutani, Journal of Physical Chemistry B 106 (2002) 13294.

[213] S.B. Sinnott, R. Andrews, D. Qian, A.M. Rao, Z. Mao, E.C. Dickey, F. Derbyshire, Chemical Physics Letters 315 (1999) 25.

[214] K. Liu, K. Jiang, C. Feng, Z. Chen, S. Fan, Carbon 43 (2005) 2850.

[215] R. Seidel, G.S. Duesberg, E. Unger, A.P. Graham, M. Liebau, F. Kreupl, Journal of Physical Chemistry B 108 (2004) 1888.

[216] C. Jin, K. Suenaga, S. Iijima, ACS nano 2 (2008) 1275.

[217] Y. Homma, Y. Kobayashi, T. Ogino, D. Takagi, R. Ito, Y.J. Jung, P.M. Ajayan, Journal of Physical Chemistry B 107 (2003) 12161.

[218] R.T.K. Baker, M.A. Barber, P.S. Harris, F.S. Feates, R.J. Waite, Journal of catalysis 26 (1972) 51.

[219] J. Rostrup-Nielsen, D.L. Trimm, Journal of Catalysis 48 (1977) 155.

[220] A. Kock, P.K. De Bokx, E. Boellaard, W. Klop, J.W. Geus, Journal of catalysis 96 (1985) 468.

[221] I. Alstrup, Journal of Catalysis 109 (1988) 241.

[222] D. Vairavapandian, P. Vichchulada, M.D. Lay, Analytica Chimica Acta 626 (2008) 119.

[223] E. Dujardin, T.W. Ebbesen, A. Krishnan, M.M.J. Treacy, Advanced Materials 10 (1998) 611.

[224] H. Hu, B. Zhao, M.E. Itkis, R.C. Haddon, Journal of Physical Chemistry B 107 (2003) 13838.

[225] A.G. Rinzler, J. Liu, H. Dai, P. Nikolaev, C.B. Huffman, F.J. Rodriguez-Macias, P.J. Boul, A.H. Lu, D. Heymann, D.T. Colbert, Applied Physics A 67 (1998) 29.

[226] M.A.M. Motchelaho, H. Xiong, M. Moyo, L.L. Jewell, N.J. Coville, Journal of Molecular Catalysis A: Chemical 335 (2011) 189.

[227] X. Zhao, M. Ohkohchi, S. Inoue, T. Suzuki, T. Kadoya, Y. Ando, Diamond and Related Materials 15 (2006) 1098.

[228] T. Suzuki, K. Suhama, X. Zhao, S. Inoue, N. Nishikawa, Y. Ando, Diamond and Related Materials 16 (2007) 1116.

[229] Y. Wang, H. Shan, R.H. Hauge, M. Pasquali, R.E. Smalley, Journal of Physical Chemisty B 111 (2007) 1249.

[230] J. Liu, A.G. Rinzler, H. Dai, J.H. Hafner, R.K. Bradley, P.J. Boul, A. Lu, T. Iverson, K. Shelimov, C.B. Huffman, Science 280 (1998) 1253.

[231] J. Zhang, H. Zou, Q. Qing, Y. Yang, Q. Li, Z. Liu, X. Guo, Z. Du, Journal of Physical Chemistry B 107 (2003) 3712.

[232] J.G. Wiltshire, A.N. Khlobystov, L.J. Li, S.G. Lyapin, G.A.D. Briggs, R.J. Nicholas, Chemical Physics Letters 386 (2004) 239.

[233] K. Hernadi, A. Siska, L. Thien-Nga, L. Forro, I. Kiricsi, Solid State Ionics 141 (2001) 203.

[234] S. Kundu, Y. Wang, W. Xia, M. Muhler, Journal of Physical Chemistry C 112 (2008) 16869.

[235] C. Moreno-Castilla, M.A. Ferro-Garcia, J.P. Joly, I. Bautista-Toledo, F. Carrasco-Marin, J. Rivera-Utrilla, Langmuir 11 (1995) 4386.

[236] H.P. Boehm, Carbon 32 (1994) 759.

[237] C. Prado-Burguete, A. Linares-Solano, F. Rodriguez-Reinoso, C. de Lecea, Journal of Catalysis 115 (1989) 98.

[238] T.G. Ros, A.J. Van Dillen, J.W. Geus, D.C. Koningsberger, Chemistry European Journal 8 (2002) 1151.

[239] H.P. Boehm, Carbon 40 (2002) 145.

[240] H.P. Boehm, Advanced Catalysis and Related Subjects 16 (1966) 179.

[241] M.L. Toebes, J.M.P. van Heeswijk, J.H. Bitter, A. Jos van Dillen, K.P. de Jong, Carbon 42 (2004) 307.

[242] T.I.T. Okpalugo, P. Papakonstantinou, H. Murphy, J. Mclaughlin, N.M.D. Brown, Carbon 43 (2005) 2951.

[243] P. Ayala, R. Arenal, M. Rümmeli, A. Rubio, T. Pichler, Carbon 48 (2010) 575.

[244] A.E. Shalagina, Z.R. Ismagilov, O.Y. Podyacheva, R.I. Kvon, V.A. Ushakov, Carbon 45 (2007) 1808.

[245] Y. Shao, J. Sui, G. Yin, Y. Gao, Applied Catalysis B: Environmental 79 (2008) 89.

[246] S. Peng, K.J. Cho, Nano Letters 3 (2003) 513.

[247] H.J. Hamnett, S.A. Contera, K. Voitchovsky, N. Grobert, J.F. Ryan, in: Anonymous , Nitrogen-doped nanotubes as biosensor, 6th International conference on the science and application of nanotubes, Gothenburg (Sweden), 2005, Gothenburg, Sweden, 2005, p. 190.

[248] D.Y. Zhong, G.Y. Zhang, S. Liu, E.G. Wang, Q. Wang, H. Li, X.J. Huang, Applied Physics Letters 79 (2001) 3500.

[249] H. Xiong, M. Moyo, M.K. Rayner, L.L. Jewell, D.G. Billing, N.J. Coville, ChemCatChem 2 (2010) 514.

[250] Y. Chen, J. Wang, H. Liu, R. Li, X. Sun, S. Ye, S. Knights, Electrochemistry Communications 11 (2009) 2071.

[251] M.S. Saha, R. Li, X. Sun, S. Ye, Electrochemistry Communications 11 (2009) 438.

[252] S. Maldonado, K.J. Stevenson, Journal of Physical Chemistry B 109 (2005) 4707.

[253] F. Coloma, A. Sepulveda-escribano, F. Rodriguez-Reinoso, Journal of Catalysis 154 (1995) 299.

[254] S. Dommele, K.P. Jong, J.H. Bitter, Chemical Communications 2006 (2006) 4859.

[255] R. Czerw, M. Terrones, J.C. Charlier, X. Blase, B. Foley, R. Kamalakaran, N. Grobert, H. Terrones, D. Tekleab, P.M. Ajayan, Nano Letters 1 (2001) 457.

[256] V.V. Strelko, N.T. Kartel, I.N. Dukhno, V.S. Kuts, R.B. Clarkson, B.M. Odintsov, Surface Science 548 (2004) 281.

[257] C.P. Ewels, M. Glerup, Journal of Nanoscience and Nanotechnology 5 (2005) 1345.

[258] R.A. Sidik, A.B. Anderson, N.P. Subramanian, S.P. Kumaraguru, B.N. Popov, Journal of Physical Chemistry B 110 (2006) 1787.

[259] L.Q. Jiang, L. Gao, Carbon 41 (2003) 2923.

[260] S.C. Roy, A.W. Harding, A.E. Russell, K.M. Thomas, Journal of the Electrochemical Society 144 (1997) 2323.

[261] J.H. Bitter, M.K. Van der Lee, A.G.T. Slotboom, A.J. Van Dillen, K.P. De Jong, Catalysis Letters 89 (2003) 139.

[262] K. Okabe, X. Li, M. Wei, H. Arakawa, Catalysis Today 89 (2004) 431.

[263] R. Baratti, V. Feckova, M. Morbidelli, A. Varma, Industrial & Engineering Chemistry Research 36 (1997) 3416.

[264] A.F. Pérez-Cadenas, M.M.P. Zieverink, F. Kapteijn, J.A. Moulijn, Catalysis Today 105 (2005) 623.

[265] I. Capek, Advances in Colloid and Interface Science 110 (2004) 49.

[266] M. Kurhinen, T.A. Pakkanen, Langmuir 16 (2000) 2658.

[267] A. Rautiainen, M. Lindblad, L.B. Backman, R.L. Puurunen, Physical Chemistry Chemical Physics 4 (2002) 2466.

[268] R.J. Farrauto, C.H. Bartholomew, Fundamentals of industrial catalytic processes, Blackie Academic & Professional New York, 1997.

[269] G.C. Bond, P.W. in: Atkins, J.C.E. Holker, A.K., Holliday, Heterogeneous catalysis: Principles and applications, Oxford University Press, New York, 1990.

[270] N.A. Pakhomov, R.A. Buyanov, Kinetics and Catalysis 46 (2005) 669.

[271] P. Burattin, M. Che, C. Louis, Journal of Physical Chemistry B 103 (1999) 6171.

[272] P. Burattin, M. Che, C. Louis, Journal of Physical Chemistry B 104 (2000) 10482.

[273] J.W. Geus, Studies in Surface Science and Catalysis 16 (1983) 1.

[274] B. Delmon, G.F. Froment, Catalyst deactivation, Elsevier, 1980.

3

Chapter Three

Equipment Description

This chapter is devoted to the description of the experimental apparatus that was used in this work. For the synthesis of multiwalled carbon nanotubes, a horizontal chemical vapor deposition (CVD) reactor was used; the catalyst synthesis did not require any equipment apart from glassware and finally the catalytic performance of the prepared catalysts were tested in a Fischer-Tropsch (FT) single micro reactor system.

3.1 The horizontal CVD reactor

The horizontal CVD reactor equipment shown in Figure 3.1 was made in the School of Chemistry, University of the Witwatersrand [1-3]. This equipment, similar to the CVD reactor used by other researchers [4-6], consists of the following:

- A tubular reactor, 510 mm long and 19 mm internal diameter, made of quartz glass in order to withstand high temperatures up to 1200^{o}C.
- A furnace (Lindberg Model LHTF 342C) that provided controllable heating with the maximum temperature located at the centre of the furnace (reaction zone).
- A quartz boat (120 mm long and 15 mm wide) used for introducing the catalyst into the reactor.
- A mass flow controller to control the flowrate of gases inside the reactor.
- A thermocouple placed inside the furnace and connected to a temperature controller in order to control the heating rate and the reaction temperature accurately.

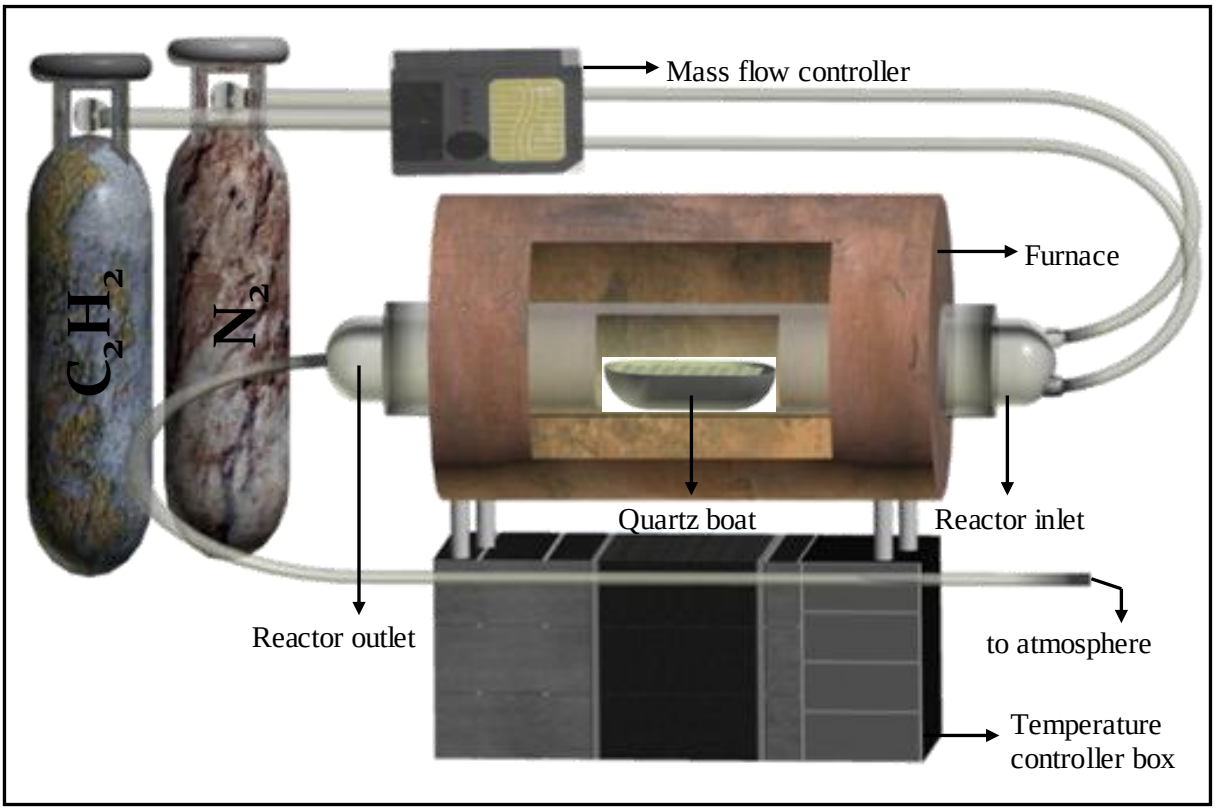


Figure 3.1: The horizontal CVD set up for the synthesis of carbon nanotubes

The quartz reactor inlet is connected to the gas sources (acetylene and nitrogen) via the mass flow controller and the outlet is connected to the exhaust pipe. The thermocouple is placed in such a way that the tip reaches the reaction zone i.e. zone of maximum temperature and where the quartz boat is placed. All reactions were carried out at atmospheric pressure.

3.2 The Fischer-Tropsch single micro reactor system

The Fischer-Tropsch synthesis can be defined as the catalytic conversion of syngas, a mixture of carbon monoxide and hydrogen, into hydrocarbons of various chain lengths. Various reactors have been used for the catalytic testing of the Fischer-Tropsch reaction such as: the constantly stirred basket reactor [7], the slurry reactor [7] and the fixed-bed reactor [8, 9]. Each reactor has its advantages and disadvantages. In this study a single fixed-bed micro reactor system was used for the catalytic conversion of syngas. The FT reactor system consists of three major parts: the fixed-bed micro reactor, the knock out pots and the gas chromatographs. Figure 3.2 shows the schematic representation of the FT single fixed-bed reactor system. The whole system (reactor, knock out pots and connecting lines), apart from the gas chromatographs, was made of stainless steel and mounted on a stainless steel frame. Stainless steel was the material of construction of choice because of:

- Its ability to withstand the high operating temperature (8 bar in this case)
- Its resistance to corrosion
- Its strength
- Its availability and low cost compared to other strong alloys.

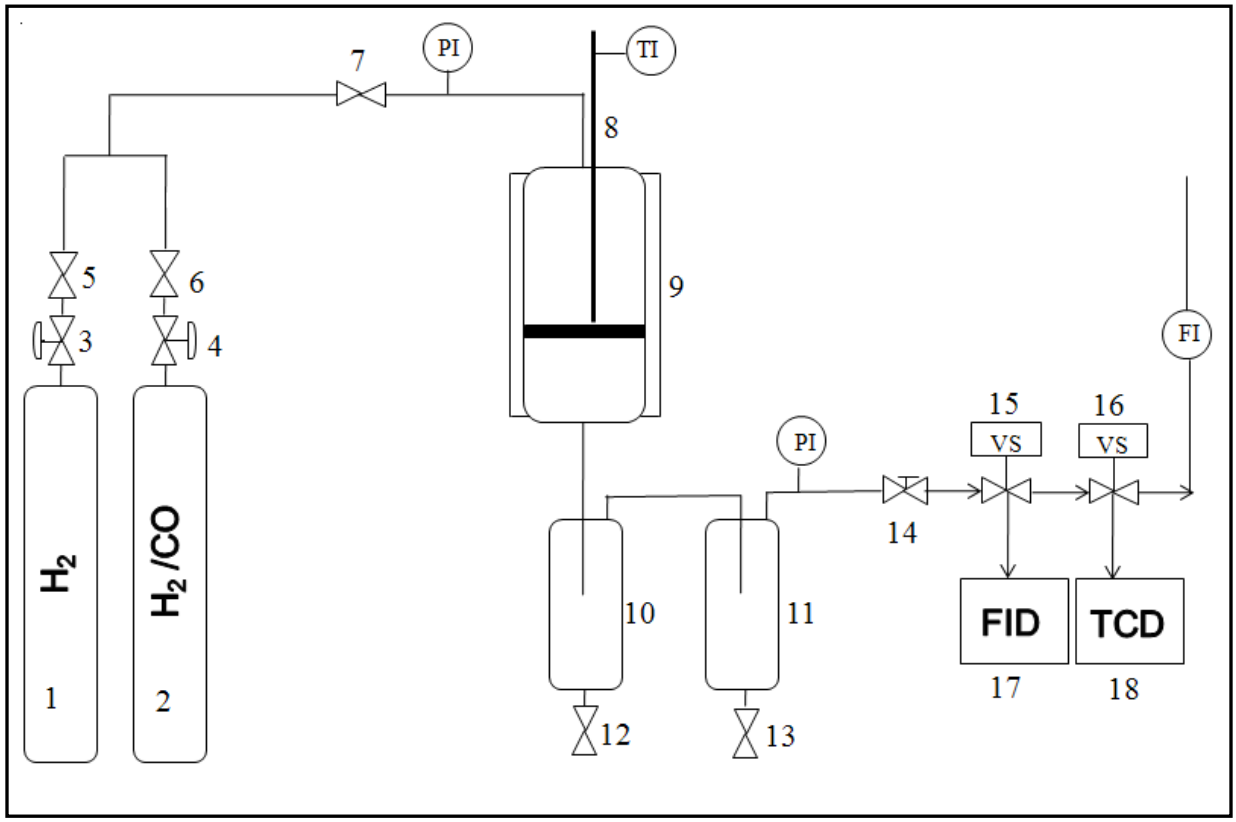


Figure 3.2: Schematic diagram of the Fischer-Tropsch single fixed-bed micro reactor system set up (not to scale)

PI = Pressure indicator; TI = Temperature indicator; FI = Flow indicator.
1: Hydrogen cylinder; 2: Syngas cylinder with H_2 : CO ratio of 2; 3 and 4: control valves; 5, 6, 7, 12 and 13: Shut off valves; 8: Temperature measuring device; 9: Fixed-bed micro reactor with heating jacket; 10: Wax trap (jacketed, maintained at 150^{o}C); 11: Liquid trap (maintained at room temperature); 14: Needle valve; 15 and 16: Solenoid valves; 17: GC with FID detector; 18: GC with TCD detector;

In the reactor set up presented above, the gas cylinders are connected to the fixed-bed reactor using 1/8'' stainless steel tubing. The ¼'' tubing was used to connect the reactor to the first knock out pot maintained at 150^{o}C for wax collection, then to the second knock out pot at room temperature for liquid (oil + water) collection. The

1/8'' tubing was used to convey the vapour sample exiting the reactor to the GCs for analysis. This line was maintained at 150^{o}C to avoid vapour condensation and line blockage. All the fittings, nuts and T-pieces used in connecting the different parts were Swagelock. The shut-off valves were SS Valco valves with viton seals and the needle valves were Whitey valves. The pressure gauges were purchased from Wika. The temperature inside the fixed-bed reactor was measured with a thermocouple (with the tip just above the catalyst bed). Figure 3.3 shows a photograph of the set up presented above.

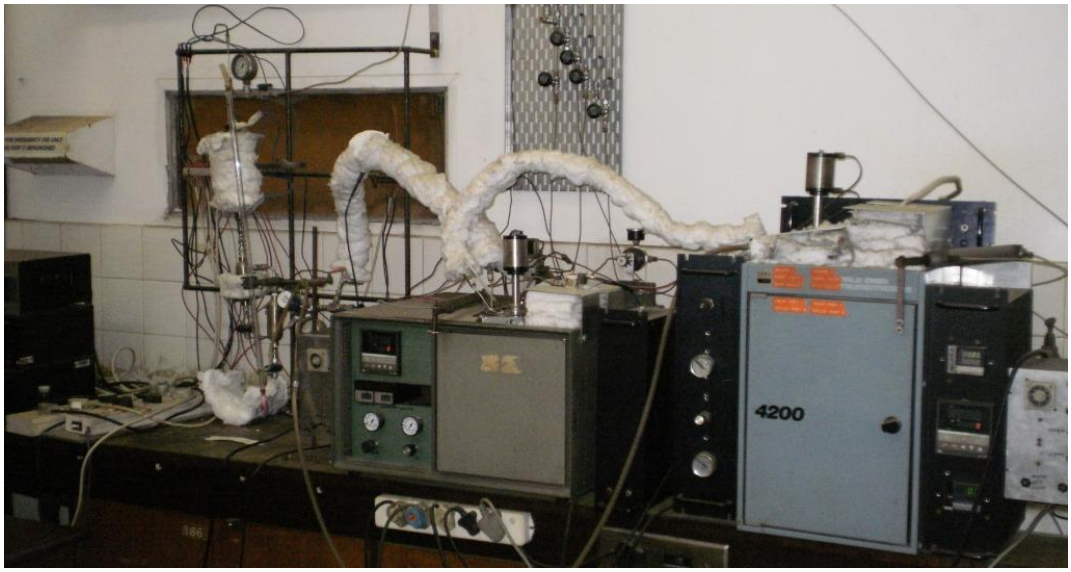


Figure 3.3: Photograph of the FT single micro reactor system set up

The operating pressure for all the runs done using the reactor described above was maintained at 8 bar, using the pressure regulator on the gas cylinder. The needle valve was used to control the gas flowrate in the reactor and to de-pressurize the outlet gas stream before it reached the GCs for analysis. A pressure indicator was used to check the total pressure in the reactor. Two solenoid valves, mounted after the needle valve automatically directed the reactor outlet gas to the GCs for analysis or vented it to the atmosphere. A new sample was analyzed every two hours.

3.2.1 The Fixed-bed micro reactor

The micro reactor is the heart of the Fischer-Tropsch reactor system. It is where the Fischer-Tropsch reactions take place. The micro reactor used in this study is a simple, stainless steel, tubular fixed-bed reactor with total height of 251 mm; internal diameter of 16 mm, and a thickness of 4.5 mm, with the catalyst bed situated at 88 mm from the bottom of the reactor tube. Steel balls (1mm) were used in the reactor in order to maintain constant temperature. The reactor tube is placed into a heating jacket surrounded with fiberglass insulation in order to achieve a uniform wall temperature along the length of the reactor. Electrical heating was provided to the jacket by a heating element with a 700 Watt rating. The syngas entered the system through the top of the reactor (8 bar) and products together with unreacted gases exited at the bottom. A schematic representation of the reactor body is shown in Figure 3.4.

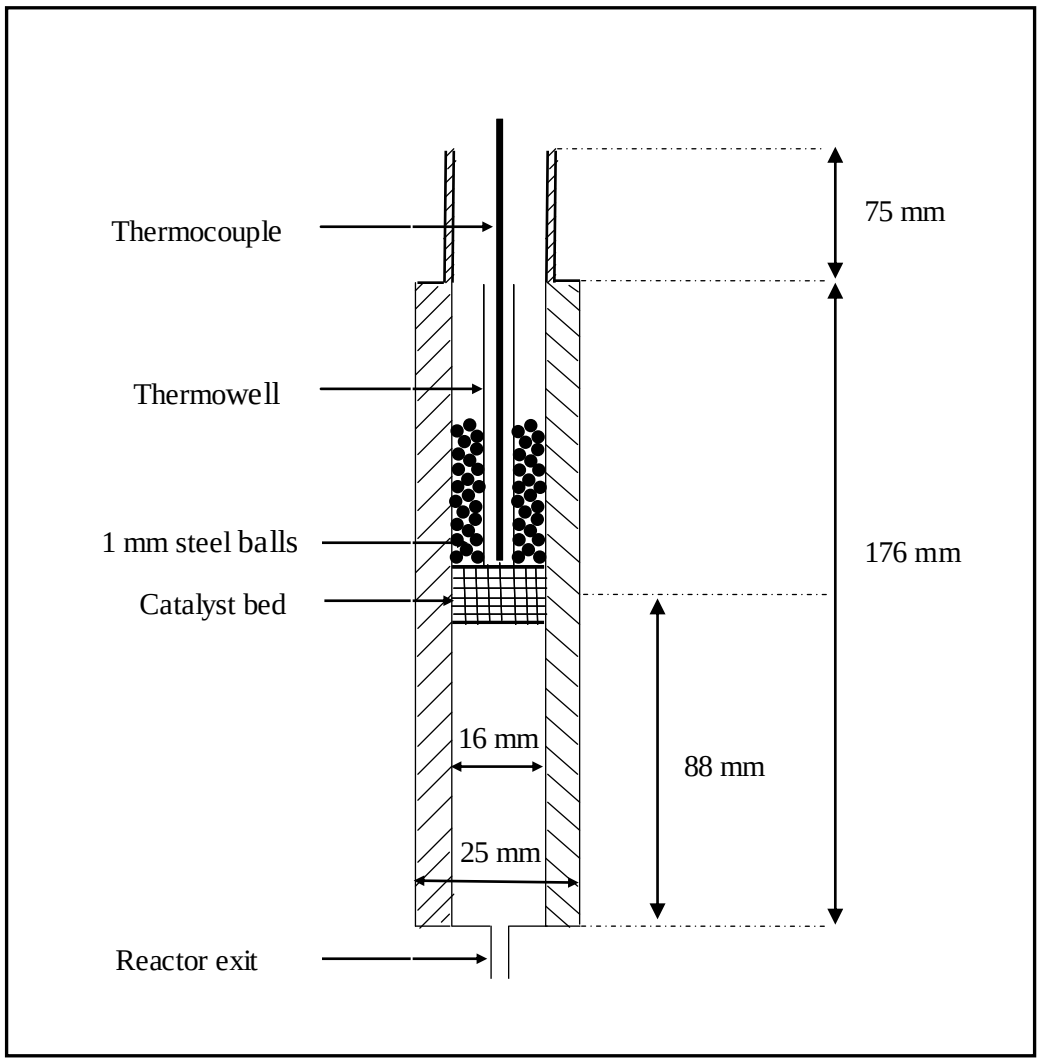


Figure 3.4: Schematic diagram of the fixed-bed micro reactor

A photograph of the assembled fixed-bed micro-reactor is shown in Figure 3.5 below. The reactor body, the thermocouple and the pressure gauge can clearly be seen.

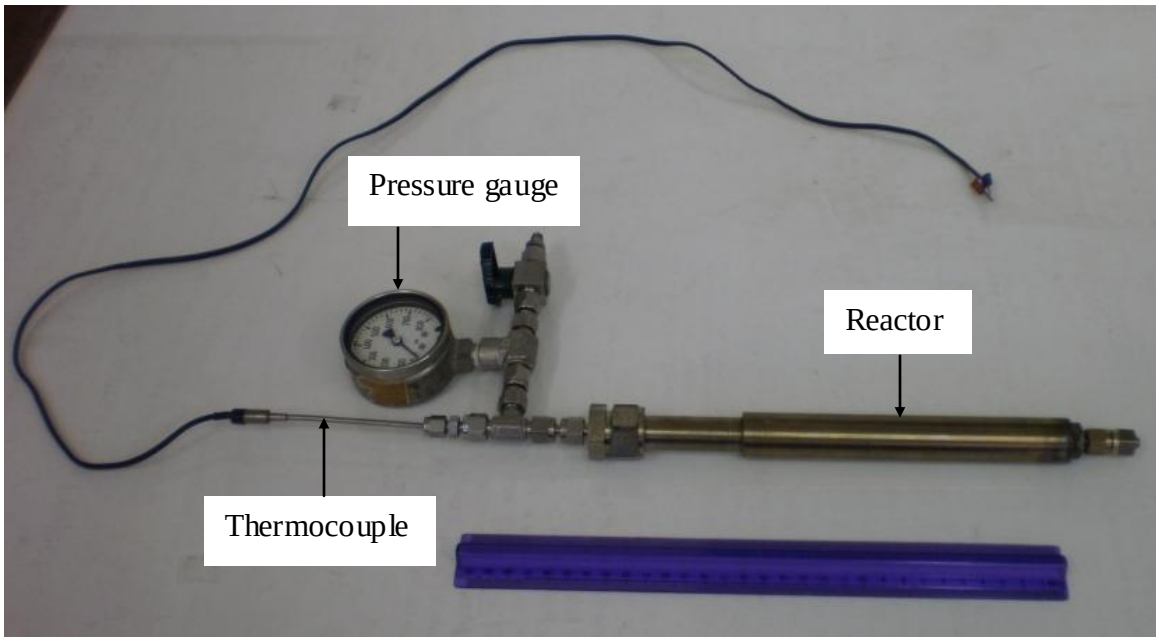


Figure 3.5: Photograph of the assembled fixed-bed micro reactor

3.2.2 Sampling and composition analysis

Liquid and wax samples, collected from the knock out pots, were analyzed using an offline GC equipped with an FID detector and a ZB-1 capillary column which was able to separate hydrocarbons from C_{9+}. Vapour samples were sent directly to the GCs via a heated (150^{o}C) gas line. Two 6-port external volume sample injector valves (VICI Valco Instruments Co. Inc.) were used in conjunction with solenoid valves for this purpose. Figure 3.6 below shows the connections of the valves and the stages in the sampling process.

Two online gas chromatographs (TCD an FID), controlled by their respective timers and connected to an amplifiers, were used to obtain the accurate composition of the vapour samples. The TCD gas chromatograph was fitted with a 2 m long, 1/8''O.D stainless steel carboxen S-II packed column for the analysis of H_2, N_2, CO and CO_2. Ultra high purity argon gas was used as the carrier gas in this gas chromatograph. A 2

m long poropak-Q (PPQ) column was used in the FID gas chromatograph to separate hydrocarbons from C_1 to C_8 and ultra high purity nitrogen gas was used as the carrier gas. The calibration procedure used for the GCs is presented in Chapter 4.

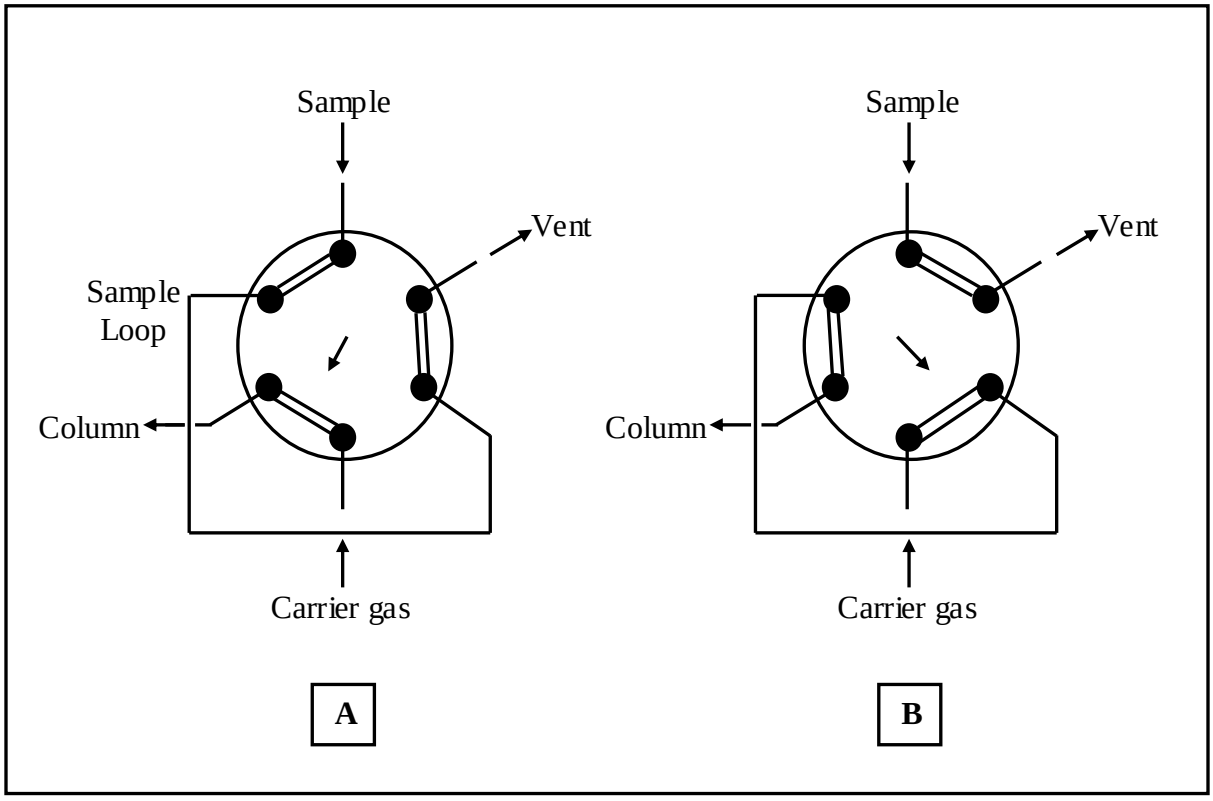


Figure 3.6: A schematic diagram of the valves viewed from the preload end (VICI Valco Instruments Co. Inc. Technical Note 203)

With the valve in position A, sample flows through the external loop while the carrier gas flows directly through to the GC column. When the valve is switched to position B, the sample contained in the sample loop and valve is displaced by the mobile phase and is carried into the column for separation and finally detection.

3.3 References

[1] X.Y. Liu, B.C. Huang, N.J. Coville, Carbon 40 (2002) 2791.

[2] X.Y. Liu, B.C. Huang, N.J. Coville, Fullerenes, Nanotubes and Carbon Nanostructures 10 (2002) 339.

[3] M.L. Mabudafhasi, R. Bodkin, C.P. Nicolaides, X.Y. Liu, M.J. Witcomb, N.J. Coville, Carbon 40 (2002) 2737.

[4] H.L. Ma, D.S. Su, A. Klein-Hoffmann, G.Q. Jin, X.Y. Guo, Carbon 44 (2006) 2254.

[5] D. Zhang, L. Shi, J. Fang, X. Li, K. Dai, Material Letters 59 (2005) 4044.

[6] W. Wasel, K. Kuwana, K. Saito, Chemical Physics Letters 422 (2006) 470.

[7] T. Chronis, "A Fischer-Tropsch study of Co/Ru catalysts", PhD thesis, University of the Witwatersrand, Johannesburg (1999).

[8] M.C. Bahome, "Synthesis and use of carbon nanotube as a support for the Fischer-Tropsch synthesis", PhD thesis, University of the Witwatersrand, Johannesburg (2008).

[9] W.M. Hexana, "A systematic study of the effect of chemical promoters on the precipitated Fe-based Fischer-Tropsch synthesis catalyst", PhD thesis, University of the Witwatersrand, Johannesburg (2009).

4

Chapter Four

Experimental Procedure

The Fischer-Tropsch synthesis is a very complex reaction because of the large number of products that are formed (from methane to heavy waxes). Although a large number of literature reports are available on the Fischer-Tropsch synthesis, there is still insufficient information available to predict the product spectrum under various operating conditions [1]. In an attempt to narrow the product spectrum and produce mainly the desired products, researchers are constantly designing new catalyst systems since the catalyst is the key element in the reaction. Fischer-Tropsch catalysts (Fe or Co) are generally supported on appropriate materials in order to reduce the catalyst cost, to provide a surface for better metal dispersion and to reduce metal sintering under the reaction conditions. In this study, carbon nanotubes were used as catalyst supports and the resulting catalyst system was tested for their performance in the Fischer-Tropsch synthesis (FTS).

This chapter describes in detail the method used for the synthesis of carbon nanotubes and their characterization, the procedure used for loading the active metals on the carbon nanotubes (catalyst preparation), the reactor set-up followed by catalyst testing in the Fischer-tropsch synthesis.

4.1 Materials and chemicals used

A variety of chemicals and gases were used for the synthesis and characterization of the catalysts as well as for the catalyst evaluation.

4.1.1 Chemicals

All the chemicals (solid or liquid) used were purchased from Sigma-Aldrich or Merck chemicals and were used without further purification. The water used was distilled or deionised water generated in the School of Chemistry.

4.1.2 Gases

All the gases used in this study were supplied by African Oxygen (AFROX). Each gas cylinder purchased was accompanied by a certificate indicating the purity of the gas mixture, the gas composition as well as the expiry date of the gas cylinder. The synthesis gas (syngas) used in the reactor experimental runs was a premixed gas with composition (10% N_2, 30% CO and 60% H_2, purity: 99.99%). This syngas composition was used for all the fixed-bed reactor experiments.

4.2 Carbon nanotubes, a support for the Fischer-Tropsch catalysts

Multiwalled carbon nanotubes were produced by a chemical vapour deposition method (CVD). The CVD method requires a carbon source and a catalyst. In this study, carbon nanotubes were made by the decomposition of acetylene (C_2H_2, Afrox South Africa) over a 10%Fe-Co/$CaCO_3$ catalyst prepared as described below.

4.2.1 Preparation of 10% Fe-Co/$CaCO_3$ catalyst

A 10%Fe-Co/$CaCO_3$ catalyst with 5 wt% Fe and 5 wt% Co metal loading was synthesized by the wet impregnation technique [2-4]. In this technique, $Fe(NO_3)_3 \cdot 9H_2O$, $Co(NO_3)_2 \cdot 6H_2O$ and $CaCO_3$ (Sigma Aldrich) were used to prepare the catalyst. A calculated amount of the Fe and Co nitrates were mixed and dissolved in distilled water to make a 0.3 M Fe-Co (50:50 w/w) precursor solution. This solution was added dropwise to the $CaCO_3$ support and the wetted slurry was left for 30 min while stirring. The metal-support mixture was then filtered and the product was first left to stand in air for 2 h at room temperature and then dried in an oven at 120^{o}C for 12 h. The product was removed from the oven and left to cool to room temperature. It was ground and screened through a 150 µm sieve. The catalyst powder obtained was then calcined at 400^{o}C for 16 h in a static air oven in order to decompose the nitrates.

4.2.2 Synthesis of multiwalled carbon nanotubes

The equipment used for the synthesis of carbon nanotubes is described in detail in Chapter 3. The optimization and effect of various production parameters in this equipment have been described [4]. In the synthesis of multiwalled carbon nanotubes (MWCNTs), the catalyst (1g) was spread uniformly in a quartz boat (120 mm × 15

mm), which was inserted in the centre of a tubular fixed-bed quartz tube reactor (Length: 510 mm, ID: 19 mm). The reactor, mounted horizontally in an electrical tube furnace, was then heated from room temperature to 700^{o}C at 10^{o}C/min while N_2 was flowing over the catalyst at 40 mL/min. When the temperature reached 700^{o}C, the N_2 flowrate was changed to 240 mL/min and acetylene, C_2H_2 was introduced at a flowrate of 90 mL/min. The reaction was allowed to take place for 60 min, thereafter, the C_2H_2 flow was stopped and the furnace was left to cool down to room temperature under the N_2 (40 mL/min). The boat was then removed from the reactor and approximately 3.5 g of black soot was collected. The morphologies and microstructures of the product were then evaluated using TEM and SEM.

4.2.3 Carbon nanotubes purification/functionalisation

The as-prepared CNTs were stirred in 30%HNO_3 or 55%HNO_3 at room temperature for 2 h or refluxed in 30%HNO_3 or 55%HNO_3 for 2 or 6 h (2 g of raw material was added to 200 ml of acid). At the end of the acid treatment, each mixture was diluted with distilled water followed by filtering and washing with distilled water until the pH of the filtrate was ~7. The obtained product was dried in an oven at 120^{o}C overnight.

4.2.4 Synthesis of nitrogen-doped multiwalled carbon nanotubes

Nitrogen-doped carbon nanotubes were obtained by post-treatment of CNTs in a nitrogen- containing atmosphere (known as post-doping). The set-up used for post-doping is similar to the one used for the synthesis of carbon nanotubes with a slight modification to allow for the introduction of the nitrogen source. In this experiment, CNTs were initially synthesized as described above, stirred in mild acid (30% HNO_3) for 2h at room temperature in order to remove residual metal catalyst as well as CaO.

The slurry was then filtered and washed with distilled water and dried at 120^{o}C overnight. The CNTs obtained were spread in a boat and placed in the reactor and then put in the horizontal furnace. A bubbler containing acetonitrile was placed before the reactor inlet. Argon was used as a carrier gas and was bubbled through acetonitrile at 78^{o}C and the vapour was carried through the reaction zone. The experiment was carried out at different temperatures (700^{o}C, 750^{o}C, 800^{o}C, 850^{o}C and 900^{o}C), constant reaction time (2 h) and constant flowrate (100 mL/min).

4.3 Synthesis of catalysts supported on carbon nanotubes

The catalysts were prepared according to the incipient wetness impregnation [5] and deposition precipitation methods [2]. All the catalysts used in this work had a 10% metal loading unless stated otherwise.

4.3.1 Deposition-Precipitation Method

A deposition-precipitation method (DPU) using urea [2, 3, 6] was employed to prepare catalysts supported on carbon nanotubes. For the preparation of the catalysts with 10% Fe loading, an appropriate amount of Fe precursor salts and urea (1.5 mol of urea per mol of iron) were dissolved in deionised water to make a 0.3 M Fe precursor solution and the solution was added dropwise to carbon nanotubes (2 g) initially suspended in deionised water (20 mL) and heated to 90^{o}C in an oil bath. The mixture was left to stir at this temperature for at least 2 h to allow for the decomposition of the urea. Thereafter, the temperature was decreased to 70^{o}C to allow a slow evaporation of the excess solvent. The catalysts were further dried in an oven at 100^{o}C overnight and heat treated for 150 min in nitrogen at an appropriate temperature (determined by TGA) in order to decompose the precursor salts.

4.3.2 Incipient wetness impregnation method [5]

The incipient wetness impregnation (IWI) method was used to make catalysts for comparison purposes. In this method, the pore volume of the support materials (the CNTs) had to be determined prior to catalyst preparation. The total pore volume of the CNTs was determined by titrating the CNT (1.00 g) with deionised water and the volume required to fill the pores to incipient wetness was determined by reading off the burette. The required amount of deionised water was then used to dissolve the desired amount of metal precursor salts and the solution was added dropwise to the CNTs. The metal and support were then well mixed and after aging the mixture for about 4 h in air at room temperature, it was placed in an oven at 100^{o}C overnight and heat treated for 150 min in nitrogen at 250^{o}C in order to decompose the precursor salts.

4.3.3 Synthesis of promoted catalysts supported on carbon nanotubes

The same procedure as described in section 2.3.1 was followed. The only difference being that a pre-determined amount of the promoter salts ($LiNO_3$, $NaNO_3$ KNO_3) was also added to the precursor salt and dissolved in deionised water.

4.4 Characterization techniques

4.4.1 Transmission Electron Microscopy (TEM)

The morphology and structure of the as-prepared and acid-treated CNTs as well as the catalysts were characterized by TEM. Sample specimens for TEM studies were prepared by ultrasonic dispersion of the sample in methanol. The suspensions were dropped onto a SPI-carbon coated copper grid. TEM investigations were carried out

using a FEI Tecnai Spirit G^2 transmission electron microscope operating at 120 kV. The inner and outer diameter distributions of the CNTs and the particle size of the active phase were obtained by using Image J software. About 120 CNT diameters and ~150 metal particles were measured.

4.4.2 Zeta potential measurements

Zeta potential measurements were used to quantify the electrical potential of the solid particles [7]. Zeta potentials of the as-grown and acid treated CNTs were measured using a Malvern Zetasizer nano series. CNTs were dispersed in deionised water at room temperature and the pH values of the suspension were adjusted from 2.0 to 12.0 by adding 0.1 M hydrochloric acid (HCl) or a 0.1 M sodium hydroxide (NaOH) solution to the glass beaker containing the CNTs. By measuring the zeta potential as a function of pH, the point of zero charge (the pH value at which the zeta potential is zero, i.e. the CNTs surface is electrically neutral) can be determined.

4.4.3 N_2 Physisorption (BET surface area)

The surface area and pore volume of the as-grown as well as the acid-treated CNTs were determined by N_2 physisorption using a Micromeritics TRISTAR 3000 analyzer. A sample of approximately 300 mg was degassed at 150^{o}C and 250^{o}C for 4 h under a flow of N_2, and then the surface areas and pore volumes were determined by the Brunauer-Emmett-Teller (BET) method as described by Idakiev et al. [8].

4.4.4 Thermogravimetric analysis (TGA)

The TGA analysis was done on a Perkin Elmer STA 4000 analyzer. About 5 to 10 mg of sample was placed in a ceramic pan and placed in the instrument's furnace. The

temperature of the sample was increased from room temperature to 900^{o}C at 10^{o}C/min under either an oxidative atmosphere (air, 20 mL/min) or an inert atmosphere (N_2, 20 mL/min). The TGA profile obtained gave information on the sample composition (including % metal loading in the case of a catalyst), thermal stability (under a specific atmosphere) and the purity. The derivative (DTG) curve was used to identify the decomposition temperature maxima. The extent to which oxygen was introduced during the purification step was also assessed from thermogravimetry analysis of the CNTs in an inert atmosphere [9].

The catalyst wt.% metal loading was also determined using TGA by simply burning off the carbon support in an oxidative environment. The % loading was calculated from the mass of the ash that remained assuming that the ash was only made up of the fully oxidized iron (Fe_2O_3). The value obtained was corrected for the ash that remained when the unsupported carbon support was oxidized.

4.4.5 Raman spectroscopy

A Raman spectrometer (Jobin-Yvon T64000 micro-Raman spectrometer) equipped with a liquid nitrogen cooled charge coupled device detector was employed to evaluate the quality of CNTs produced. All the samples were measured after excitation with a laser wavelength of 514.5 nm.

4.4.6 Fourier Transform Infra-red (FTIR) Spectroscopy

The presence of oxygen-containing surface groups on the CNTs was established by recording FTIR spectra on a Bruker TENSOR 27 FTIR spectrometer in the 400-4000 cm^{-1} wavenumber range, at a spectral resolution of 4 cm^{-1} using 64 scans per spectrum.

4.4.7 Temperature programmed reduction

Temperature programmed reduction (TPR) experiments were performed on a Micromeritics AutoChem11 Chemisorption analyser equipment to study the reduction behaviour of the catalysts. 100 mg sample of the catalyst was loaded into a U-shaped quartz tube reactor. The sample was first degassed in a flow of argon (20 mL/min) at 150^{o}C for 30 min to remove traces of water, and then cooled to 40^{o}C. The sample was then reduced in 5%H_2/Ar (50 mL/min) as the temperature was increased from 40^{o}C to 800^{o}C at a rate of 10^{o}C /min. A thermal conductivity detector (TCD) was used to measure H_2 consumption. The temperature and associated H_2 consumption was captured electronically to give the TPR profiles.

4.4.8 H_2 chemisorption and O_2 titration

H_2 chemisorption and O_2 titration were performed on a Micromeritics ASAP 2010 instrument. A sample of ~ 200 mg of iron catalyst was placed in a U shaped sample holder which was evacuated and the catalyst was degassed using pure helium (He) at 100^{o}C for 1.5 h. Degassing was continued at 350^{o}C with He and then catalyst reduction was performed using pure hydrogen (H_2) at 350^{o}C for 14 h. After reduction, the sample was evacuated with He at 325^{o}C for 1 h and then at 100^{o}C for 30 min. H_2 chemisorption was done at 220^{o}C. After H_2 chemisorption the sample was flushed and then evacuated using He at 100^{o}C for 30 min. Evacuation continued at 400^{o}C for 30 min after which oxygen titration was done using a stream of pure oxygen at 300^{o}C.

4.4.9 Elemental analysis

The nitrogen content in the N-CNTs was determined by elemental analysis using a Carlo Erba NA1500 Nitrogen Carbon Sulfur analyzer. Approximately 1.0-1.5 mg of powder sample was weighed into a tin foil container and ignited at high temperature (1020˚C) in oxygen (on a chrome oxide catalyst) to produce carbon dioxide, nitrogen gas and oxides of nitrogen (plus other oxides etc.). The gases produced pass through silvered cobalt oxide (to remove oxides of S and halogens etc.) and a column of copper (540˚C), which reduces the oxides of nitrogen to nitrogen gas (and removes excess free O_2). After removal of water vapour by a trap of anhydrous magnesium perchlorate, the N_2 gas and CO_2 are finally separated by gas chromatography using a helium carrier gas and detected by a thermal conductivity detector. These experiments were conducted at the Institute for Soil, Climate and Water based in Pretoria, South Africa.

An attempt to use the Inductively Coupled Plasma-Atomic Emission Spectroscopy (ICP-AES Analytical Instruments) for the determination of catalysis chemical composition was not successful.

4.5 Fischer-Tropsch studies

The catalytic testing for all the prepared catalysts was performed in a fixed-bed micro reactor. The experimental set-up was described in Chapter 3.

4.5.1 Gas Chromatograph (GC) calibration

Two online GCs (FID and TCD) were used to analyze the gaseous products exiting the reactor during the FTS. Prior to analysis, it was critical to calibrate the GCs using

a calibration gas mixture and syngas in order to determine the GC response. In a GC, the number of moles of a component i, n_i passing the detector is proportional to the peak area, A_i. The calibration gas mixture employed had the following composition: CH_4 (2.5%), C_2H_4 (0.2%), C_2H_6 (0.5%), CO (10%), CO_2 (5%) and Ar (81.1%). The syngas composition was: H_2 (60%), N_2 (10%) and CO (30%). Calibration of the GCs was done at the start of every catalyst test run. Typical traces produced from the calibration were recorded using Clarity (v. 2.5 a DataApex Chromatograph software package). These plots are illustrated in Figures 4.1, 4.2, &4.3 below.

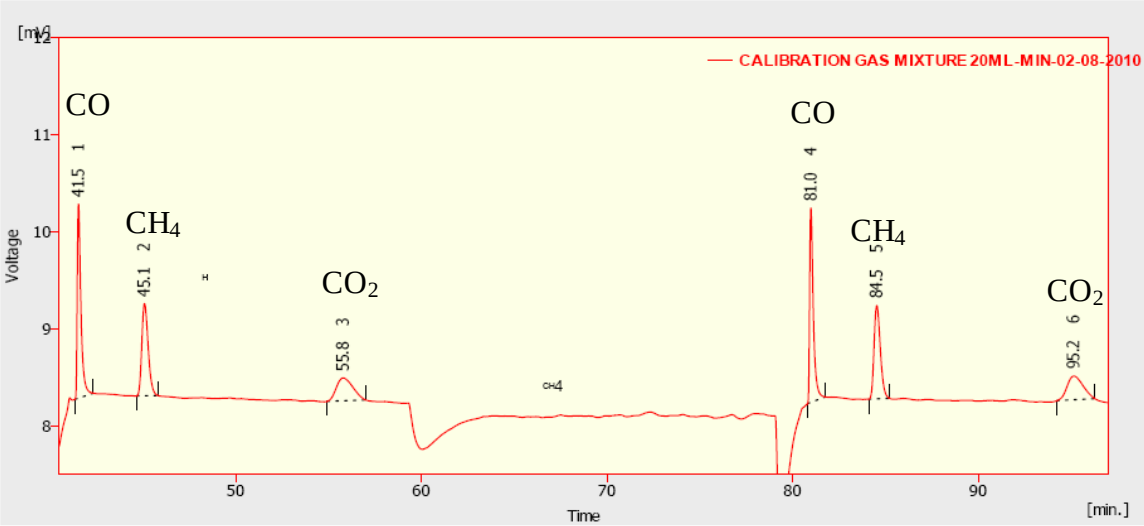


Figure 4.1: A trace for the calibration gas using the TCD GC and argon as a carrier gas

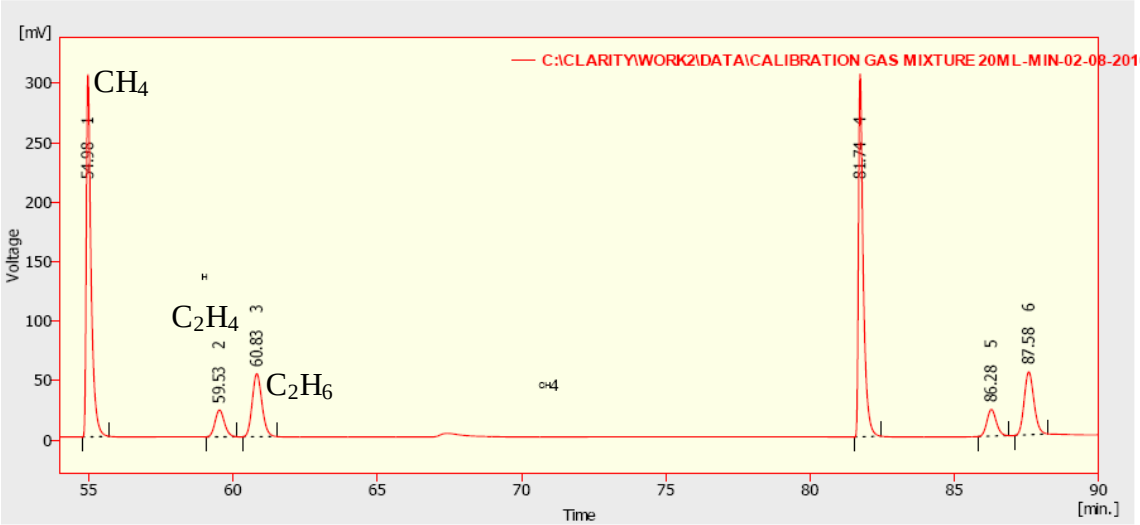


Figure 4.2: A trace for the calibration gas using the FID GC and nitrogen as a carrier gas

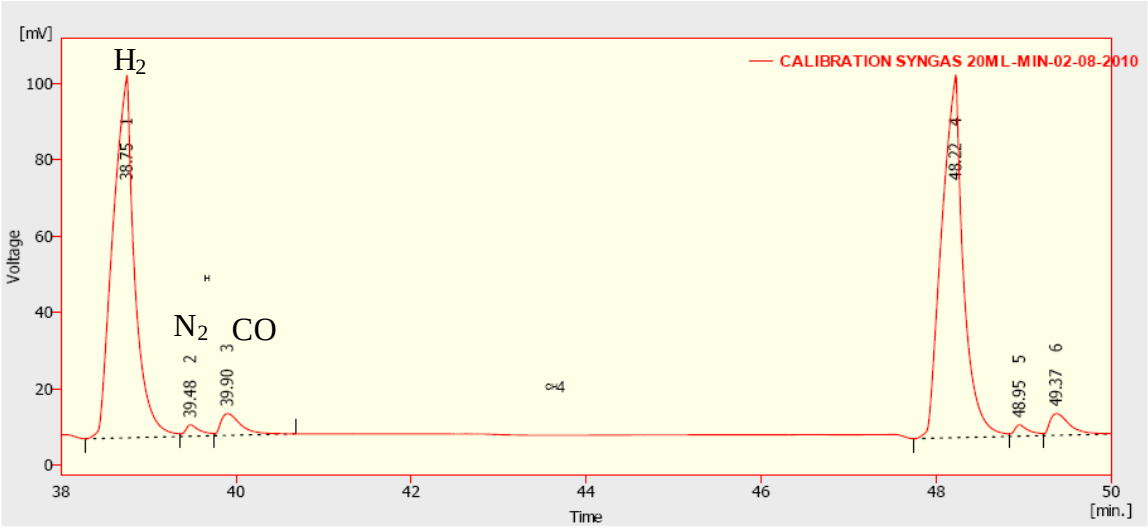


Figure 4.3: A trace for the syngas calibration using the TCD GC and argon as a carrier gas

Table 4.1: Operating conditions of the GCs used in this work

Operating Conditions	Gas Chromatographs	
	TCD	**FID**
Gas Flowrate (ml/min)	30	30
Oven Temperature Profile		
Initial Temperature (^{o}C)	Room temperature	Room temperature
Temperature Ramp (^{o}C/min)	10	10
Final Temperature (^{o}C)	200	200
Hold Time (min)	40	40
Detector Profile		
Detector Type	TCD-Gow-Mac detector	FID-Phillips detector
Temperature (oC)	220	220
Attenuation	1	1
Range	–	–
Injector Profile		
Temperature	100	100

4.5.2 Pressure testing/ leak detection and elimination

Precise measurement and control is only possible if the system is completely free of leaks. Thus the first stage in the operation of the FT system was the identification and successful elimination of all leaks. The determination of the presence of leaks in the system was achieved by pressurizing the system followed by complete isolation of the section to be checked using shut-off valves. The pressure reading on the display was then noted and the system was left at that condition for approximately 12 hours. Any leaks in the system were manifested in a decrease in pressure reading. As a way of detecting the individual leak if any, points on the system suspected of having leaks were sprayed with a small amount of soapy water and if there were any leak, bubbles would be seen. The identified leaks were then eliminated by tightening the nuts or changing them completely. All leaks were thereby eliminated by repeating the foregoing procedure.

4.5.3 Catalyst evaluation

The catalyst (0.5g) was loaded into the reactor and a thermocouple was placed in a removable stainless steel thermowell placed in the centre of the reactor with the tip of the thermocouple inside the catalyst bed. The reactor was then filled up with 1 mm diameter inert steel balls to ensure uniform heating inside the reactor. Prior to the start of the reaction, the system was pressure tested as described in section 2.5.2 above. When the system was judged to be leak tight, the in-situ reduction of the catalyst commenced under a stream of pure hydrogen (350 ^{o}C, 2 bar, 20 mL/min, ~20 h). After reduction, the reactor temperature was decreased to 275^{o}C, the pressure was increased gradually to 8 bar and a flow of syngas was passed over the catalyst bed with flowrate similar to hydrogen flowrate of 20 mL/min. The flow was controlled using a metering valve and measured with a bubble meter at atmospheric pressure. The gaseous product stream was analysed online and an offline GC was used to analyse the oil and wax. The standard FTS reaction ran for approximately 120 h, with steady state reached after about 10 h. Catalytic activity, product selectivity and the stability of the catalysts were evaluated during the reaction period of 120 h. In order to verify any poor heat exchange limitation during FTS runs, an experiment was conducted where the mass of catalyst used was doubled (1 g) and the flowrate on syngas doubled (40 mL/min).

4.5.4 Data analysis and calculations

The molar percentage of a component θ in the gas was calculated as:

$$\%\theta_{gas} = \left(\frac{A_{\theta,gas}}{A_{\theta,cal}} \right) \times \%\theta_{cal} \qquad [4.1]$$

Where:

$\%\theta_{gas}$ = molar percentage of compound θ in the analyzed gas;

$A_{\theta,gas}$ = integrated area of the GC peak corresponding to the compound θ in the analyzed gas;

$A_{\theta,cal}$ = integrated area of the GC peak corresponding to the compound θ in the calibration gas mixture;

$\%\theta_{cal}$ = molar percentage of compound θ in the calibration gas mixture.

For compounds whose calibration data could not be obtained directly from the calibration mixture, calibration data of a reference compound and relative molar response factors were used. Molar response factors for hydrocarbon products are presented in Table 4.2 [10, 11]. The following expression was used:

$$\%\theta_{gas} = \left(\frac{A_{\theta,gas}}{A_{\alpha,cal}} \right) \times \%\alpha_{cal} \times RF_{\theta,\alpha} \qquad [4.2]$$

Where:

$\%\alpha_{cal}$ = molar percentage of the reference compound α in the calibration gas mixture;

$A_{\alpha,cal}$ = integrated area of the GC peak corresponding to the reference compound α in the calibration gas mixture;

$RF_{\theta,\alpha}$ = relative response factor of the compound θ with respect to the reference compound α.

For olefins, the reference used was C_2H_4 whereas C_2H_6 was used as reference for paraffins.

The mass composition of oil and wax analyzed using an offline GC was obtained directly from GC peak area percentages as the mass response factors were assumed to be 1.00 [12, 13].

Table 4.2: Molar response factors for hydrocarbon products [10, 11].

Carbon number	Olefin	Paraffin
1	—	1.00
2	1.00	1.00
3	0.70	0.74
4	0.78	0.55
5	0.47	0.47
6	0.40	0.40
7	0.35	0.35
8	0.32	0.32
9	0.28	0.28
10	0.24	0.24
11	0.21	0.21
12	0.19	0.19
13	0.18	0.18
14	0.17	0.17
15	0.15	0.15

Mass balance calculations

The calculations used to determine the mass balance are similar to those used by numerous authors [12-14]. A mixture of hydrogen (60%), nitrogen (10%) and carbon monoxide (30%) was used as the feed into the micro reactor. Hydrogen and carbon monoxide were the reactants while nitrogen served as an internal standard. As an inert tracer during the FT reaction, nitrogen is present in the feed stream and in the reactor outlet gas stream in exactly the same amounts as it does not undergo any reactions in FTS. The nitrogen balance across the reactor was expressed as:

$$F_{in} \times X_{N_2,in} = F_{out} \times X_{N_2,out} \qquad [4.3]$$

and used to calculate $X_{N_2,out}$.

Where:

F_{in} = total molar flowrate (mol/min) of the reactor feed;

F_{out} = total molar flowrate (mol/min) of the system outlet gas stream (measured after the knockout pots); It was calculated from the total gas volumetric flowrate at the reactor exit using the ideal gas law (P = 1 bar, T = 298 K).

$X_{N_2,in}$ = molar fraction of nitrogen in the reactor feed;

$X_{N_2,out}$ = molar fraction of nitrogen in the reactor outlet gas.

The outlet flow stream was measured daily (many times during the day) for the duration of the reaction using a bubble meter and a stopwatch. Equation [4.3] was used to determine the feed flowrate into the reactor as no mass flow controllers were used.

The rate of CO conversion was calculated as follows:

$$r_{CO} = \frac{F_{CO,in} - F_{CO,out}}{m_{cat}} \qquad [4.4]$$

Where:

r_{CO} = rate of CO conversion (mol.min^{-1}.g$_{cat}^{-1}$) or (mol.min^{-1}.g$_{activemetal}^{-1}$);

$F_{CO,in}$ = molar flowrate (mol/min) of CO in the reactor feed;

$F_{CO,out}$ = molar flowrate (mol/min) of CO in the reactor outlet gas stream;

m_{cat} = mass (gram) of catalyst or mass (gram) of active metal.

$$F_{CO,in} = F_{in} \times X_{CO,in} \qquad [4.5]$$

$$F_{CO,out} = F_{out} \times X_{CO,out} \qquad [4.6]$$

$X_{CO,in}$ and $X_{CO,out}$ are the CO molar fractions in the reactor feed and in the outlet gas stream respectively. F_{in} and F_{out} were defined in equation [4.3].

The % CO conversion was calculated as follows:

$$\%CO_{conversion} = \frac{\left[X_{CO,in} - X_{CO,out} \times \left(\frac{X_{N_2,in}}{X_{N_2,out}} \right) \right]}{X_{CO,in}} \times 100 \qquad [4.7]$$

Where:

$\left(\frac{X_{N_2,in}}{X_{N_2,out}} \right)$ is the contraction factor.

The rate of Fischer-Tropsch synthesis r_{FTS} was calculated as follows:

$$r_{FTS} = r_{CO} - r_{WGS} \qquad [4.8]$$

$$r_{WGS} = r_{CO_2\,formation} \qquad [4.9]$$

Substituting for r_{WGS} into equation [4.8] gives

$$r_{FTS} = r_{CO} - r_{CO_2\,formation} \qquad [4.10]$$

Where:

r_{CO} = rate of CO consumption;

r_{WGS} = rate of water-gas-shift reaction, which is also the rate of CO_2 formation.

The percentage carbon balance was determined using equation [4.11] below:

$$\% \text{ carbon Balance } = \frac{TotalC_{out}}{TotalC_{in}} \times 100 \qquad [4.11]$$

The C being the atoms/moles of carbon. The number of moles of carbon that enter the reactor must equal the sum of the moles of carbon that exit from the reactor. The carbon balance was acceptable when the % error was $\leq 5\%$.

The product selectivity was calculated on moles of carbon basis.

$$Sel(\theta) = \frac{nC_{\theta}}{r_{CO} \times t} \qquad [4.12]$$

Where:

$Sel(\theta)$ = selectivity of product θ;

nC_{θ} = moles of carbon contained in the product θ;

t = mass balance time.

$Sel(CO_2)$ = (moles of CO_2 produced / moles of CO reacted) x 100

The olefin to paraffin ratio x_2 was given as:

$$\text{Olefin fraction } x_2 = \frac{m_{x_2^=}}{m_{x_2^=} + m_{x_2}} \qquad [4.13]$$

$m_{x_2^=}$ = mass of olefin containing two carbon atoms

$m_{x_2^=} + m_{x_2}$ = mass of total hydrocarbons containing 2 carbon atoms

4.6 References

[1] C.K. Rofer-DePoorter, Chemical Review 81 (1981) 447.

[2] E. van Steen, F.F. Prinsloo, Catalysis Today 71 (2002) 327.

[3] M.C. Bahome, L.L. Jewell, D. Hildebrandt, D. Glasser, N.J. Coville, Applied Catalysis A, General 287 (2005) 60.

[4] S.D. Mhlanga, K.C. Mondal, R. Carter, M.J. Witcomb, N.J. Coville, South African Journal of Chemistry 62 (2009) 67.

[5] J.T. Richardson, "Principles of Catalyst Development", (1989) 111.

[6] D. Barkhuizen, I. Mabaso, E. Viljoen, C. Welker, M. Claeys, E. van Steen, J.C.Q. Fletcher, Pure and Applied chemistry 78 (2006) 1759.

[7] Y.H. Li, S. Wang, Z. Luan, J. Ding, C. Xu, D. Wu, Carbon 41 (2003) 1057.

[8] V. Idakiev, Z.Y. Yuan, T. Tabakova, B.L. Su, Applied Catalysis A: General 281 (2005) 149.

[9] K.P. De Jong, J.W. Geus, Catalysis Reviews-Science and Engineering 42 (2000) 481.

[10] A.W. Dietz, Journal of Gas Chromatography 62 (1967).

[11] J.G. Price, "An investigation into novel bimetallic catalysts for use in the Fischer-Tropsch reaction", PhD Thesis, University of the Witwatersrand, Johannesburg, 1994.

[12] M.C. Bahome, "Synthesis and use of carbon nanotubes as a support for the Fischer-Tropsch Synthesis", PhD thesis, University of the Witwatersrand, Johannesburg (2008).

[13] W.M. Hexana, "A systematic study of the effect of chemical promoters on the precipitated Fe-based Fischer-Tropsch synthesis catalyst", PhD thesis, University of the Witwatersrand, Johannesburg (2009).

[14] K. Jalama, "Fischer Tropsch synthesis over supported cobalt catalysts: effect of ethanol addition, precursors and gold doping", PhD thesis, University of the Witwatersrand, Johannesburg (2008).

5

Chapter Five

Effect of acid treatment on the surface of multiwalled carbon nanotubes prepared from Fe-Co supported on $CaCO_3$: Correlation with Fischer-Tropsch catalyst activity[#]

5.1 Introduction

Carbon materials with various morphologies are widely used as adsorbents, as catalysts and /or catalyst supports and for structural reinforcement of polymers. The carbons often have relatively high surface areas, high thermal stability and show chemical inertness. Their surface chemistry, especially the presence of oxygen functionalities determines the application of the material [1, 2]. Historically, activated carbons and carbon blacks are the most commonly used forms of carbon in industry.

[#] Myriam A.M. Motchelaho et al. Journal of Molecular Catalysis A: Chemical 335, (2011) 189.

More recently, the use of carbon nanotubes, fullerenes and related materials in high-tech applications has attracted growing interest [3, 4].

Carbon nanotubes, popularised by studies by Iijima [5], represent one of the best examples of nanostructures derived by bottom-up chemical synthesis approaches [6]. Both single walled carbon nanotubes (SWCNTs) and multiwalled carbon nanotubes (MWCNTs) have a simple chemical composition and atomic bonding configuration but exhibit an extreme diversity and richness among nanomaterials in terms of structure and structure-property relations [7].

The synthesis, purification, properties, manipulation and more recently, the chemistry of nanotubes are all subjects of intensive investigations. There are three common methods used to make CNTs: laser ablation [8], electric arc discharge [9, 10] and chemical vapour deposition [11-14]. Catalytic chemical vapour deposition (CCVD) has proven to be an excellent method for large-scale production of high quality MWCNTs at relatively low cost [15-17]. By employing specific catalyst and carbon sources it is possible to control the structural characteristics of CNTs when CCVD is used [18].

The CCVD synthesis method consists of decomposing a carbon-containing gas over a supported catalyst. In order to improve the yield and quality of CNT production, various metal catalysts, supports and carbon sources have been investigated [19, 20]. The most widely used metals are Fe, Co and Ni as well as the alloys of these nanoparticles [21, 22]. Conventional supports such as SiO_2, Al_2O_3, and zeolite have been successfully used in the synthesis of CNTs but purification of the product has proven to be difficult. A detailed study by Magrez et al. [16] showed that $CaCO_3$ is an excellent support for CNT synthesis because of the good matching between the carbonate decomposition temperature and the nanotube growth. The removal of the residual CaO support can be easily done by a one step acid treatment [23, 24]. Earlier studies [19, 23] revealed that the order of catalyst activity in the CVD synthesis was

$Fe\text{-}Co/CaCO_3 >> Co/CaCO_3 > Fe/CaCO_3$. The Fe-Co bimetallic system supported on $CaCO_3$ was therefore used in this present study.

Regardless of the method used to make CNTs, there is always a significant amount of impurity present in the final product (graphitic debris, catalyst particles and fullerenes) [25]. These impurities often influence the desired properties of the CNTs. It is therefore important to both evaluate and reduce or completely eliminate impurities in the as-grown CNTs. Although there are many suggested methods for CNT purification, oxidation with concentrated HNO_3 or HNO_3-H_2SO_4 is the most widely used [1, 26-30]. However no purification method that fulfils all the requirements for technical processing is currently available [31]. The nature of the impurities depends on the synthesis method, reaction time, type of catalyst, catalyst support and carbon source employed.

One of the applications of CNTs that has received much attention in the literature recently is its use as a catalyst support. When CNTs are used as a catalyst support, the hydrophobic and inert nature of the as-grown CNTs can be unfavourable. It is therefore important to be able to modify their surface chemistry, for example, by the introduction of oxygen-containing surface groups. Upon oxidation, the hydrophobic CNTs become more hydrophilic so that wetting properties are enhanced and the CNT surface becomes more reactive [27, 32, 33]. Most importantly, the dispersion of an active metal phase during catalyst preparation increases with an increasing amount of surface oxygen [27, 34]. The presence of carboxyl groups on a CNT surface gives rise to cation-exchange sites [35] which can act as anchor positions for the metal particles. A critical survey of methods most frequently used for the determination of surface-oxygen groups and the use of nitric acid treatment to oxidize carbon surfaces has been given by Boehm [28]. Aqueous solutions of HNO_3 contain nitronium ions, NO_2^+, which are able to attack aromatic compounds and this is assumed to be the first step in the introduction of oxygen-containing surface groups [1]. Although the precise nature of carbon-oxygen structures is not well established, results from many studies

demonstrate that several types of surface oxygen-groups can be identified using FTIR spectroscopy, TGA in an inert environment and Boehm mass titration [27, 32, 33].

The chemical modification of carbon nanotubes represents an emerging area in research on nanotube-based materials [36]. In contrast to activated carbons and carbon blacks, the surface oxidation of the relatively new carbon nanotubes and nanofibres has been much less studied [27].

In a study focused on the use of a Fe/CNT catalyst in Fischer-Tropsch synthesis we observed that this catalyst proved to be an easy to use, stable catalyst with good activity [37]. Scanning transmission electron microscopy (STEM) studies revealed that the surface was heavily pitted and was populated with Fe and, unexpectedly, Ca^{2+} ions [38]. This led us to propose the concept of "docking stations" to explain the remarkable stability of the catalyst [38, 39]. These "docking stations" prevent or mitigate sintering which in turn suppresses deactivation. To further explore the origin of the surface roughness of the CNTs produced using $CaCO_3$ as a support, we herein report on a comprehensive investigation of the CNT surface after using a range of acid treatments, unlike previous studies which use relatively severe acid treatments. In particular, we have established that a correlation exists between surface roughness induced during acid treatment and the stability and activity of the Fe/CNT catalysts, and that this effect is related to CNT surface roughness.

5.2 Experimental section

5.2.1 Catalyst preparation

A 10%Fe-Co/$CaCO_3$ catalyst with 5 wt% Fe and 5 wt% Co metal loading was synthesized by the wet impregnation technique [37, 39]. In this technique, $Fe(NO_3)_3.9H_2O$, $Co(NO_3)_2.6H_2O$ and $CaCO_3$ (Sigma Aldrich) were used to prepare the catalyst. Calculated amounts of the Fe and Co nitrates were mixed and dissolved in distilled water to make a 0.3 M Fe-Co (50:50 w/w) precursor solution. This solution was added dropwise to the $CaCO_3$ support and the mixture was left for 30 min while stirring. The metal-support mixture was then filtered and the product was first left to stand in air for 2 h at room temperature and then dried in a static air oven at 120^oC for 12 h. The product was then removed from the oven and left to cool to room temperature. It was ground and screened through a 150 μm sieve. The catalyst powder obtained was then calcined at 400^oC for 16 h in a static air oven in order to decompose the nitrates.

5.2.2 Carbon nanotube synthesis

Multiwalled carbon nanotubes were produced by the catalytic decomposition of acetylene (Afrox South Africa) as the carbon source, on the 10%Fe-Co/$CaCO_3$ catalyst prepared as described above. Nitrogen (Afrox South Africa) was used as a carrier gas and as a diluent. Previous studies in our research group have focussed on the optimization procedure and effect of various parameters on the synthesis of carbon nanotubes [21]. The optimum conditions used in the CNTs synthesis were: Synthesis time: 1 h, reaction temperature: 700^oC, acetylene to nitrogen flowrate ratio of 1: 2.67.

In the synthesis of multiwalled carbon nanotubes (MWCNTs), approximately 1 g of the catalyst was spread uniformly in a quartz boat (120 mm × 15 mm), which was inserted in the centre of a tubular fixed-bed quartz tube reactor (length: 510 mm, ID: 19 mm). The reactor, mounted horizontally in an electrical tube furnace, was then heated from room temperature to 700^{o}C at 10^{o}C/min while N_2 flowed over the catalyst at 40 ml/min. When the temperature reached 700^{o}C, the N_2 flowrate was changed to 240 ml/min and acetylene was introduced at a flowrate of 90 ml/min. The reaction was allowed to take place for 60 min, thereafter, the C_2H_2 flow was stopped and the furnace was left to cool down to room temperature under N_2 (40 ml/min). The boat was then removed from the reactor and approximately 3.5 g of black soot was collected. The morphology and microstructure of the product was then evaluated using TEM.

5.2.3 Carbon nanotube purification/functionalisation

As-prepared CNTs were refluxed at 120^{o}C in 30%HNO_3 and 55%HNO_3 for 2 and 6 h respectively (about 2 g of raw material in 200 ml of acid). At the end of the acid treatment, each mixture was diluted with distilled water followed by filtering and washing with distilled water until the pH of the filtrate was ~7. The resulting product was dried in an oven at 120^{o}C overnight. The four purified materials were named: CNT-30R2 (i.e. CNT refluxed in 30% HNO_3 for 2 h), CNT-30R6, CNT-55R2 and CNT-55R6.

5.2.4 Characterisation techniques

The morphology and structures of the as-prepared and acid-treated CNTs were characterized by TEM and SEM. Sample specimens for TEM studies were prepared by ultrasonic dispersion of the sample in methanol. The suspensions were dropped

onto a SPI-carbon coated copper grid. TEM investigations were carried out using a FEI Tecnai Spirit G^2 transmission electron microscope operating at 120 kV. Energy dispersive X-ray spectroscopy (EDX) coupled with TEM was used to confirm the elemental composition of the sample. The inner and outer diameter distributions of the CNTs were obtained by using Image J software. About 120 CNT diameters were measured per sample. SEM analysis was carried out using a JSM-840 scanning microscope at an accelerating voltage of 10 kV and a working distance of 15 mm, which images the sample surface by scanning it with a high-energy beam of electrons in a raster scan pattern. Each SEM sample was sprinkled onto a disk and then coated with gold before analysis.

The zeta potential measurement was used to quantify the electrical potential of the solid particle [40]. Zeta potentials of the as-grown and acid treated CNTs were measured using a Malvern Zetasizer nano series instrument. CNTs were dispersed in deionised water at room temperature and the pH values of the suspension were adjusted from 2.0 to 12.0 by adding 0.1 M hydrochloric acid (HCl) or 0.1 M sodium hydroxide solution (NaOH) solution to the glass beaker containing the CNTs. By measuring the zeta potential as a function of pH, the point of zero charge (the pH value at which the zeta potential is zero i.e. the pH at which the CNTs surface is electrically neutral) was determined.

The surface area and pore volume of the as-grown as well as the acid-treated CNTs were determined by N_2 physisorption using a Micromeritics TRISTAR 3000 analyzer. A sample of approximately 300 mg was degassed at 150^{o}C and 250^{o}C for 4 h under a flow of N_2, and then the surface area and pore volume were determined by the Brunauer-Emmett-Teller (BET) method as described by Idakiev et al. [41].

The TGA analysis was done on a Perkin Elmer STA 4000 analyzer. About 5 to 10 mg of sample was placed in a ceramic pan and placed in the instrument's furnace. The temperature of the sample was increased from room temperature to 900^{o}C at

10^{o}C/min under either an oxidative atmosphere (air, 20 ml/min) or an inert atmosphere (N_2, 20 ml/min). The TGA profile obtained gave information on the sample composition, thermal stability under a specific atmosphere and purity. The derivative curve (DTG) was used to identify the decomposition temperature maxima. The extent to which oxygen was introduced during the purification step was also assessed from thermogravimetric analysis of the CNTs in an inert atmosphere [3].
Raman spectroscopy (Jobin-Yvon T64000 micro-Raman spectrometer) was employed to evaluate the quality of the CNTs.

The presence of oxygen-containing surface groups on the CNTs was established by recording FTIR spectra on a Bruker TENSOR 27 FTIR spectrometer in the 400 to 4000 cm^{-1} wavenumber range, at a spectral resolution of 4 cm^{-1} using 64 scans per spectrum.

5.2.5 Fischer-Tropsch

Catalyst preparation

All the catalysts used in the Fischer-Tropsch runs were prepared by the deposition precipitation (DPU) method using urea as the precipitating agent [37, 39]. A predetermined amount of $Fe(NO_3)_3.9H_2O$ (Sigma Aldrich), urea and deionised water were used in the preparation of a 10%Fe/CNT catalyst (the CNT used as a support had different degree of surface functional groups) . The resultant catalysts were dried (120^{o}C overnight) and calcined (heating in nitrogen at 250^{o}C for 150 min) to decompose the salts. The catalysts prepared were named: 10%Fe/CNT-as grown (CNT without any purification/functionalization), 10%Fe/CNT-30R2 (CNT refluxed in 30% HNO_3 for 2h) etc. The catalysts were characterized using BET surface area, H_2-chemisorption, TPR and TEM (refer to Chapter 4 for detailed description of the technique).

Fischer-Tropsch experiments

The Fischer-Tropsch synthesis was performed in a fixed-bed micro reactor [42, 43]. Gas cylinders containing $H_2/CO/N_2$ mixtures (60%H_2, 30%CO and 10% N_2; purity: 99.99%) were used to supply the reactant gas stream to the catalyst. Nitrogen was used as an internal standard in order to ensure an accurate mass balance.

Catalyst (0.5 g) was added to the reactor and reduced in situ at 350 °C for 20 h under a stream of pure hydrogen (2 bar pressure, 20 ml/minute). After reduction, the temperature was decreased to 275°C, the pressure was increased gradually to 8 bar and a flow of syngas was passed over the catalyst bed with a flowrate similar to the hydrogen flowrate of 20 mL/min (GHSV = 2400 h^{-1}). All gas lines after the reactor were kept at 150°C and the hot trap placed immediately after the reactor was held at 150°C in order to collect wax. A second trap kept at ambient temperature was used to collect the oil and water mixture. The flow of gases was controlled using a metering valve and measured with a bubble meter. The gaseous product stream was analyzed online using two gas chromatographs. An offline GC was used to analyze the oil and wax. Data analysis used in our study was performed according to standard procedures as described elsewhere [37, 43].

5.3 Results and Discussion

5.3.1 Electron microscopy

Among the numerous known techniques employed to synthesize CNTs, the catalytic chemical vapour deposition is the most reproducible, cheapest and easily scalable method [16, 17]. This method was therefore used in this study to synthesize CNTs. The majority of the tubes had outer diameters ranging from 20 to 35 nm and inner diameters ranging from 8 to 18 nm (Figures 5.1 and 5.2). After acid treatment using the harshest oxidizing condition (sample CNT-55R6), the CNT inner diameter remained unchanged but the outer diameter decreased relative to the non acid treated sample. This reduction in diameter is due to the interaction of acid with the outermost graphene layers (Figure 5.2). The decreased outer diameter is also attributed to wall damage during acid treatment and this is confirmed by TEM micrographs (Figure 5.3).

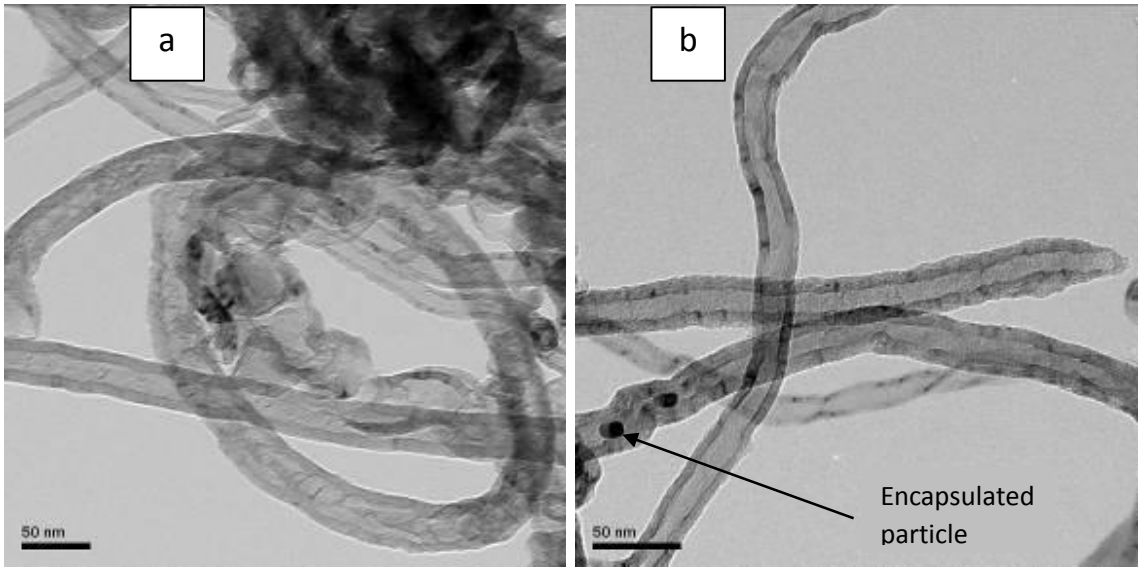


Figure 5.1: a) TEM image of as-grown CNTs and b) TEM image of as-grown CNTs showing some encapsulated metal particles indicated by arrow.

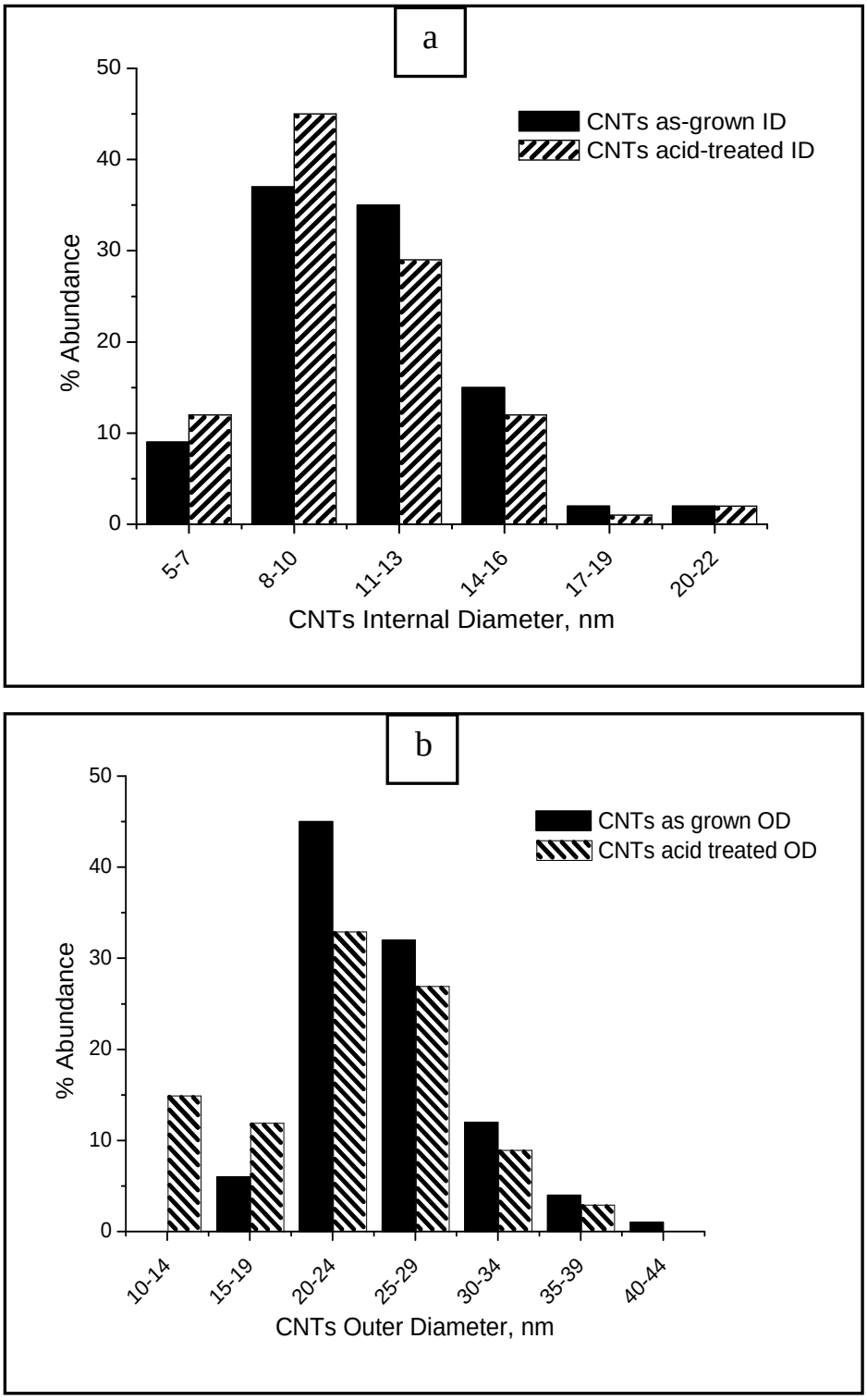


Figure 5.2: Diameter size distribution before and after acid treatment. a) Comparison of inner diameters; b) comparison of outer diameters.

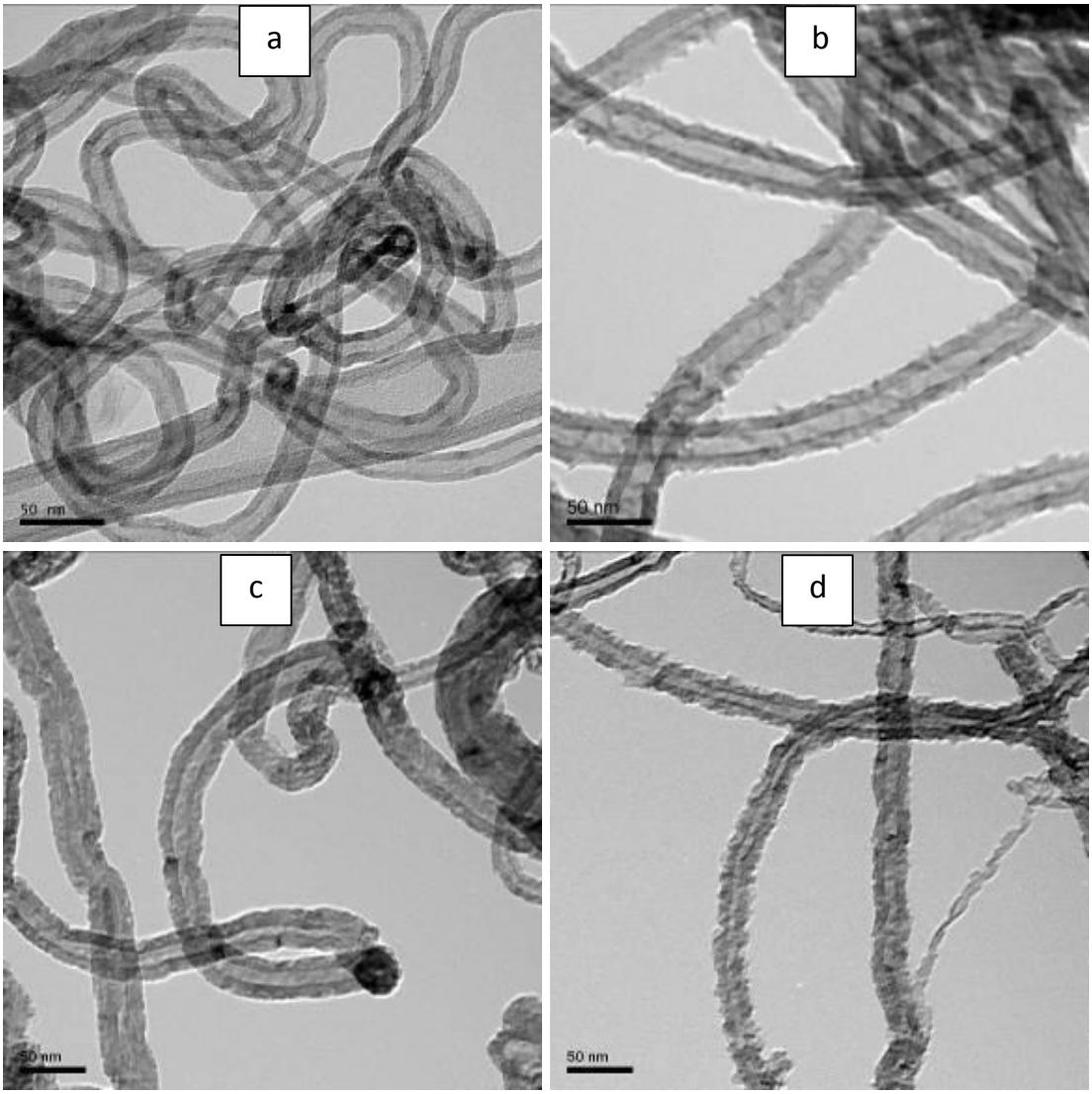


Figure 5.3: Effect of acid treatment on the texture and morphologies of CCVD synthesized CNTs: a) CNTs-30R2; b) CNT-30R6; c) CNT-55R2; d) CNT-55R6.

TEM images of the as-grown CNTs (Figure 5.1b) reveal encapsulated metal particles which were shown by EDX analysis to be Fe and Co (Figure 5.4a). After acid treatment, the residual catalyst was removed (Figure 5.4b) due to the dissolution of the metal catalysts by nitric acid. However removal of all the Fe and Co catalyst that was observed within the tubes was not possible. The TEM images also revealed that

the roughness increased with nitric acid concentration and time of reaction. The tubes became thinner and the surface rougher (Figure 5.3a-d).

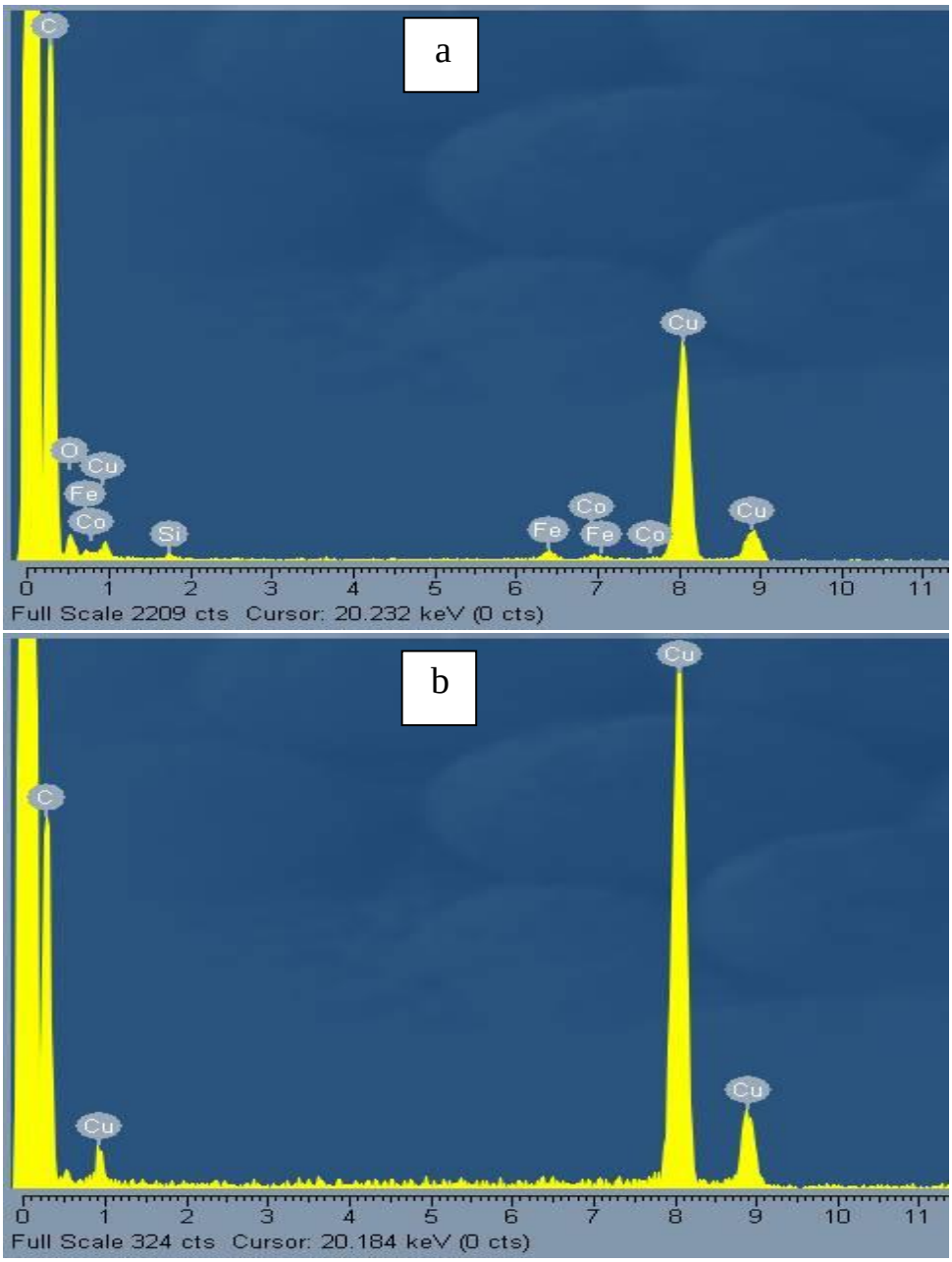


Figure 5.4: EDX spectrum of: (a) as grown CNT showing the presence of residual metal and (b) acid treated, CNT-55R6 showing that most of the residual metal particles are removed.

5.3.2 Zeta potential measurements

The determination of the zeta potential of the CNTs can be used to study the presence of oxygen surface groups. The presence of acidic groups causes the carbon surface to be more hydrophilic, increasing the negative surface charge density and decreasing the pH of the point of zero charge (PZC) [35, 45]. Figure 5.5 shows the plots of zeta potential of the as-grown and oxidised CNTs as a function of pH. The PZC for the as-grown CNT occurs at pH = 4.9. That is at pH < 4.9, the surface of the CNTs is positively charged and at pH > 4.9, the surface is negatively charged. This result is in good agreement with results obtained by Li [40] (see footnote to Table 5.1). After acid treatment, the PZC shifts to lower pH values due to the introduction of surface oxygen groups (Table 5.1). CNT-30R2, CNT-30R6 and CNT-55R2 all have values very close to a pH_{pzc} around 2.6 with CNT-55R6 having the lowest PZC. These results suggest that acidic functional groups are formed on the carbon nanotubes surface and their concentration increases with treatment time and acid strength.

Table 5.1: Point of zero charge (PZC) obtained from zeta potential measurements

Sample	PZC
As grown CNTs [a]	4.9
CNT-30R2	2.9
CNT-30R6	2.7
CNT-55R2	2.5
CNT-55R6	< 0

[a]PZC = 5.0 [40]

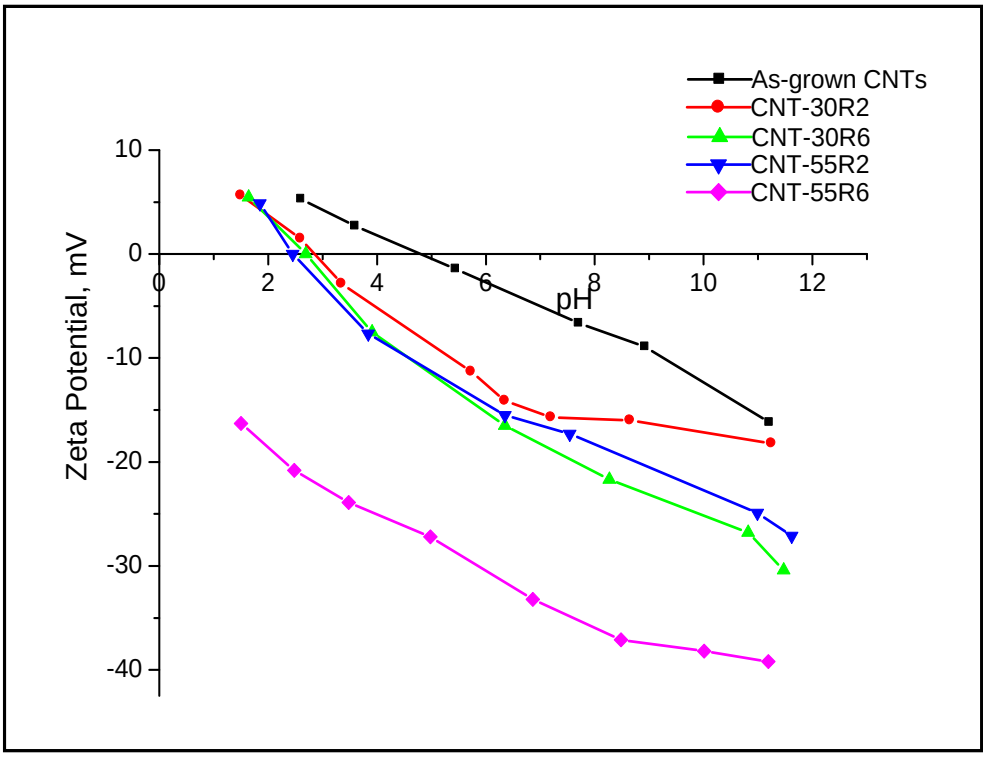


Figure 5.5: Zeta potential measurements of as-grown and acid treated CNTs as a function of pH.

5.3.3 Surface Area and Pore volume measurements

Nitrogen adsorption represents the most widely used technique to determine a materials surface area and to characterize its porous structure [46]. The surface area and pore volume of the as-grown and acid-treated CNTs are given in Table 5.2. Prior to the surface area and pore volume analysis, the effect of degassing temperature was investigated and it was demonstrated that whether the sample is degassed at 150^{o}C or at 250^{o}C for 4 h the surface area and pore volume values are the same within experimental error (Table 5.2). The surface area and pore volume increased with the initial acid treatment due to the removal of the low surface area residual CaO and

possibly opening of the ends of the tubes, but did not however change significantly on further treatment.

Table 5.2: Surface area and pore volume of as-grown and acid-treated CNTs.

Sample ID	BET Surface area (m^2/g) [a]	Pore Volume (cm^3/g)	BET Surface area (m^2/g) [a]	Pore Volume (cm^3/g)
	degassed under N_2 at 150°C[b]		degassed under N_2 at 250°C[b]	
CNT-as grown	80	0.27	77	0.27
CNT-30R2	105	0.34	103	0.35
CNT-30R6	112	0.35	114	0.34
CNT-55R2	108	0.35	–	–
CNT-55R6	100	0.33	–	–

[a] ±5% experimental error

[b] 4 hours

5.3.4 Thermogravimetric analysis (TGA)

Thermogravimetric analysis (TGA), coupled with a derivative curve of the weight loss (DTG), is often used to investigate the thermal stability as well as the composition and purity of carbons. It is an effective way to quantitatively evaluate CNTs, in particular, the content of residual metal. It is easy to obtain the residual metal content using this technique by simply oxidising the CNT samples in air. The carbon material is converted to CO/CO_2 and the metal catalyst is converted to an oxide [47].

Figure 5.6 shows the TGA and DTG profiles of the as-grown CNTs. The residual catalyst and CaO makes up ~17% of the mass so that 83% of the sample is due to carbonaceous materials. There is no significant weight loss before 500°C in the as-grown CNTs, thus ruling out the presence of a significant amount of amorphous carbon. In the product, most of the carbon decomposes at 642°C with a small amount

decomposing at 729°C as seen from Figure 5.6. This is a typical decomposition profile for multiwalled carbon nanotubes (MWCNTs) [47], and confirms that the carbon nanotubes were multiwalled. The small proportion of CNTs oxidising at the higher temperature could be those CNTs not in proximity to residual catalyst or due to the presence of some highly graphitized carbon.

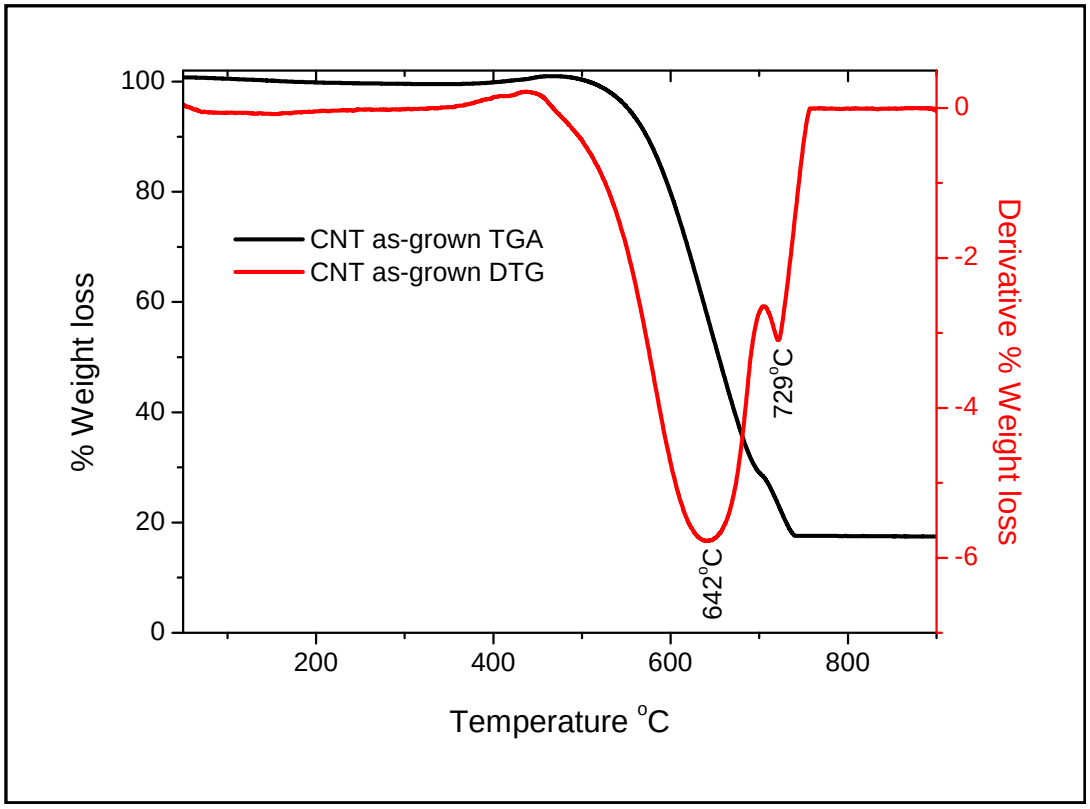
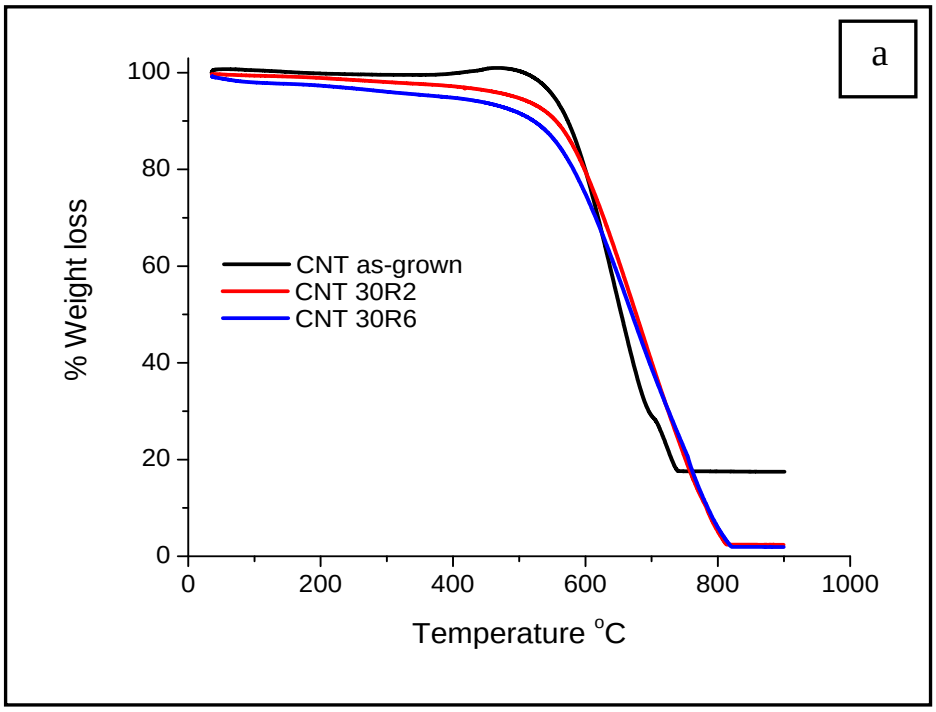


Figure 5.6: TGA and DTG profiles of as-grown CNTs under air atmosphere.

After refluxing in nitric acid, the impurity content decreased to less that 1%, with values dependent on the treatment time and acid strength. Figures 5.7 and 5.8 show an increase in sample mass at 500°C due to the oxidation of residual Fe-Co metal; the derivative peak breadth showed an increase upon oxidation due to an increase in the number of defects. When the as-grown CNTs were refluxed in 30% HNO_3 for 2 h and 6 h, the thermal stability of the CNTs improved slightly (Figure 5.7) and the CNT

decomposition temperature increased from 642°C to 685°C and 690°C respectively. This improvement is attributed to the removal of catalyst which is known to aid the oxidation of carbon. On the other hand, when the as-grown CNTs were refluxed in 55% HNO_3 for 2 and 6 h, the thermal stability maxima of the CNTs decreased slightly with the decomposition temperature dropping to 633 and 639°C for the 2 h and 6 h treatments respectively (Figure 5.8), although the purity of the CNTs was improved. The drop in temperature can be attributed to the damage of the outer structure as confirmed by TEM and Raman spectroscopy. These observations suggest that acid concentration and not temperature has the more significant effect on achieving wall defects on CNTs. In summary, the position of the decomposition peak maximum is affected by the amount of residual catalyst in the sample, the defect content on the surface of the CNTs and the amount of amorphous carbon present.



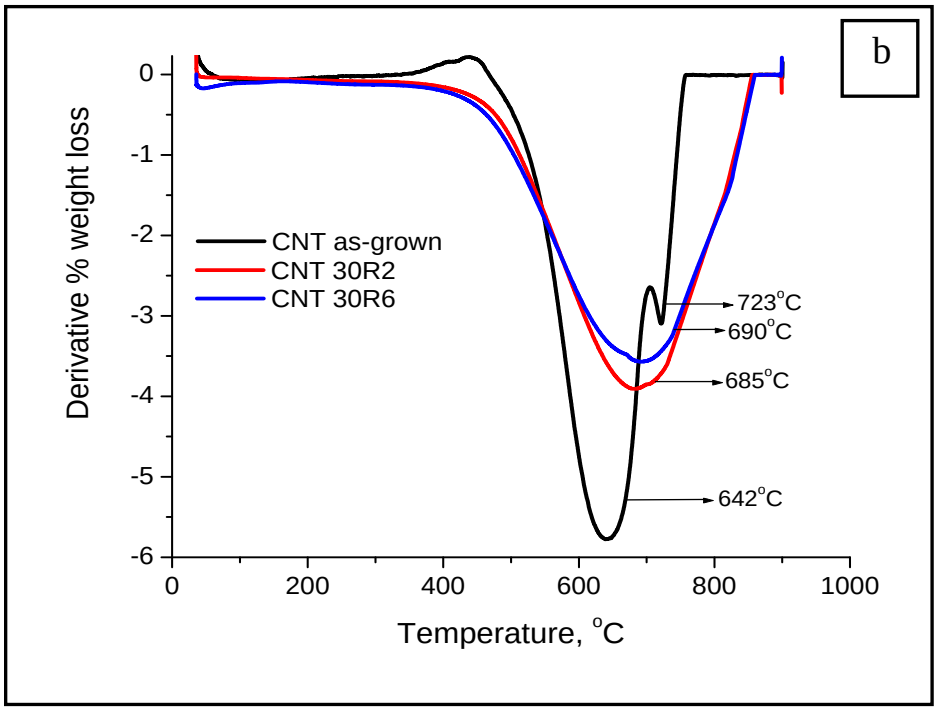


Figure 5.7: a) TGA and b) DTG profiles of as-grown CNTs as well as purified CNTs in 30%HNO_3 under air atmosphere.

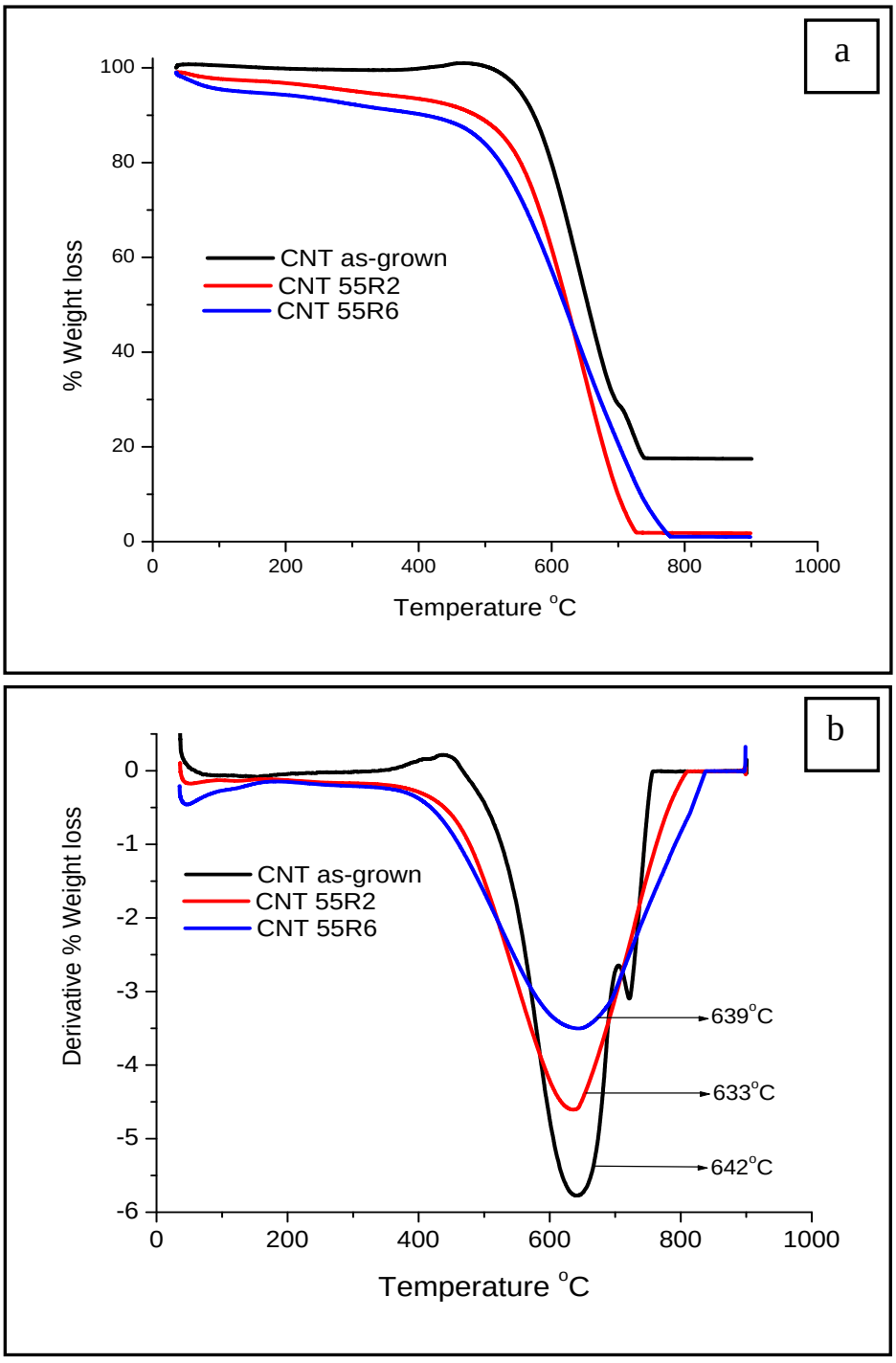
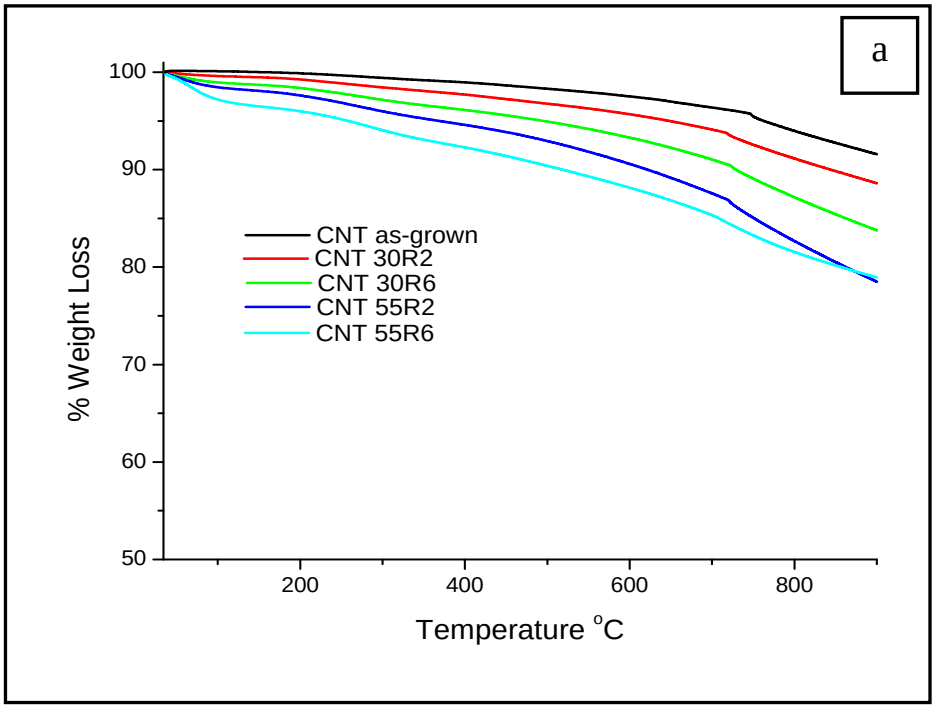


Figure 5.8: a) TGA and b) DTG profiles of as-grown CNTs as well as purified CNTs in 55%HNO_3 under air atmosphere.

TGA profiles of the as-grown as well as the acid-treated CNTs were also recorded under a N_2 atmosphere in order to determine the oxygen surface group content on the CNTs. The weight loss occurring from 150^{o}C to 400^{o}C corresponds to the evolution of gaseous CO_2 [48] while the total weight loss from 100^{o}C to 900^{o}C was correlated with the weight loss due to the formation of both CO and CO_2 [3] (Figure 5.9). The derivative curve for the acid treated samples is shown in Figure 8b. The onset before 100^{o}C is due to H_2O loss, between 150 and 400^{o}C CO_2 is evolved from acid (COOH) groups and the weight loss at temperature > 400^{o}C could be due to the loss of oxygen atoms tightly bonded to the surface of the CNTs or other non-graphitic carbonaceous species.



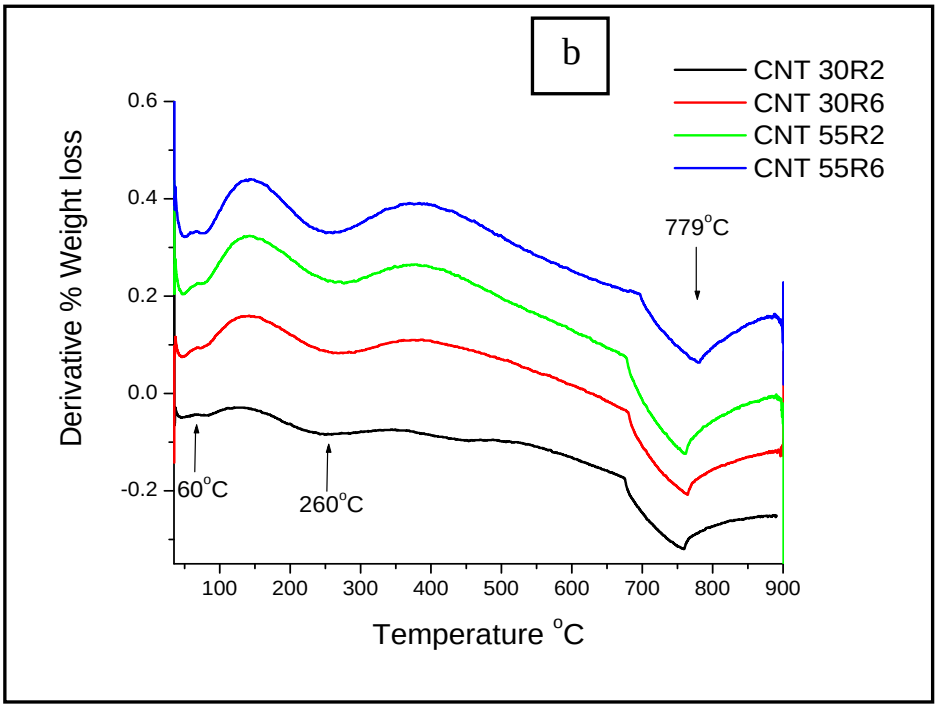


Figure 5.9: a) TGA and b) DTG profiles of as-grown and acid treated CNTs under N_2 atmosphere.

Table 5.3 shows the % CO_2 and CO formed during the experiment which corresponds to the weight loss of CNTs in a N_2 atmosphere. The weight loss is plotted against the reflux time in Figure 5.10, showing an increase in the amount of CO_2 evolved with increasing reflux time and acid concentration. A similar trend was observed by de Jong when working with carbon nanofibers [3].

Table 5.3: Weight loss of CNTs due to the formation of CO/CO_2 on heating in N_2

Sample ID	150°C-400°C	100°C-900°C
	$\%CO_2$	$\%(CO_2 + CO)$
CNT as-grown	0.95	8.36
CNT-30R2	1.81	11.04
CNT-30R6	2.75	15.14
CNT-55R2	3.52	19.95
CNT-55R6	4.27	18.78

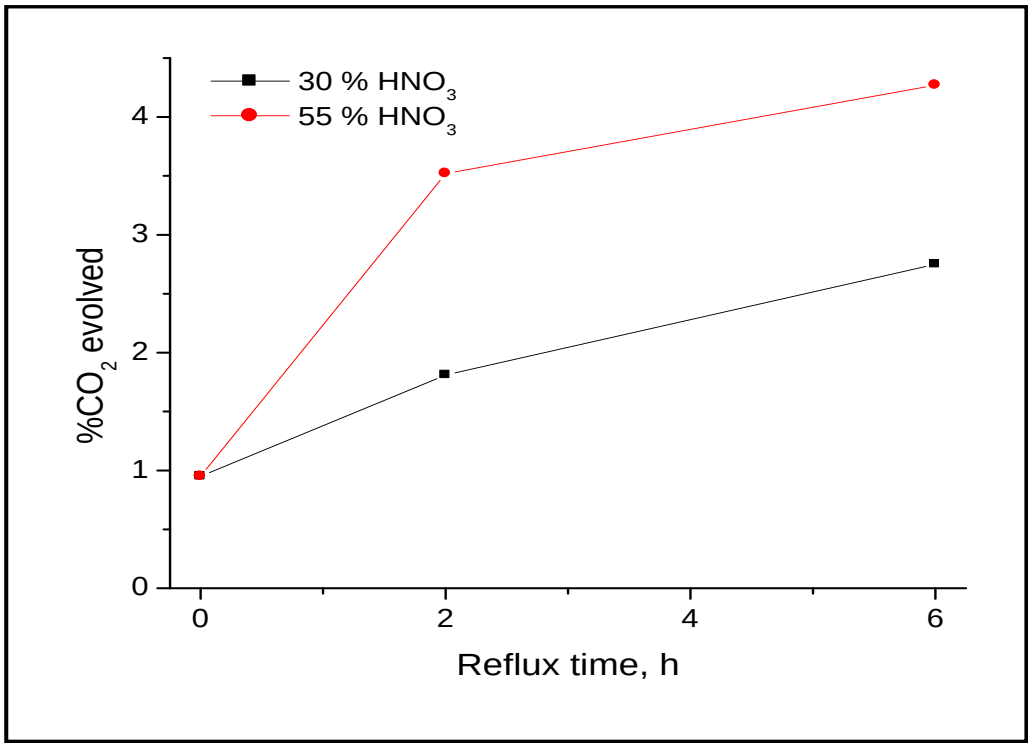


Figure 5.10: Evolution of oxygen as CO_2 versus reflux time.

5.3.5 Raman analysis

Raman spectral analysis was used to determine the long range structure of the CNTs [49, 50]. A major drawback of Raman spectroscopy is that it cannot provide direct information on the nature of metal impurities, and it is not very effective in studying CNT samples with a low content of amorphous carbon [51, 52]. However, Raman spectra for as-grown as well as acid-treated CNTs show two characteristic peaks in all samples, one at ~1350 cm^{-1} corresponding to the disorder-induced band (D band) and the other at ~1590 cm^{-1} corresponding to the tangential mode (G band) (Figure 5.11). The D mode indicates the disorder features of the CNTs whereas the G mode is associated with the ordered graphite in the CNTs [53]. The area ratio of the D band to the G band (I_D/I_G) was used to estimate the amount of disorder or defects present in the walls of the CNTs. The (I_D/I_G) ratio was found to increase with increasing reflux time/acid strength indicating that the longer the reflux time, the more defects are added to the CNTs. These results are in good agreement with the TEM observations.

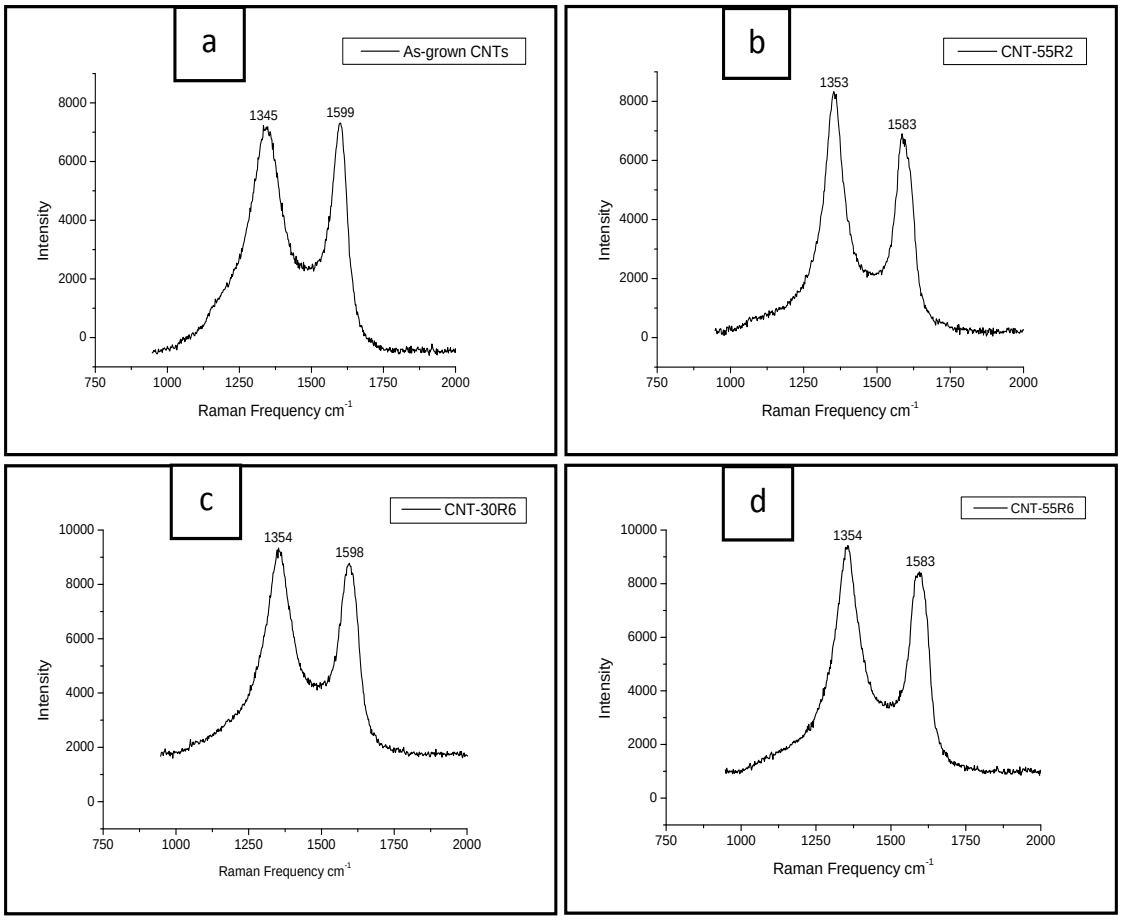


Figure 5.11: Raman spectra of CNTs: a) as-grown CNTs, b) CNT-55R2, C) CNT-30R6, d) CNT-55R6.

Table 5.4 below shows the position of the D and G band as well as the ratio of areas for the as-grown and acid treated CNTs. From the results, it is observed that there is an upshift of the D-band for the acid-treated CNTs with respect to the as-grown CNTs. Similar observations were obtained by Okpalugo et al. and correlated with the inter-tubular coupling resulting from Van der Waals repulsions [54].

Table 5.4: Raman data for as-grown and acid-treated CNTs

Sample ID	Peak position (cm^{-1})		I_D/I_G
	D-band	G-Band	
CNT As-grown	1345	1599	2.88
CNT 30R6	1354	1598	2.83
CNT 55R2	1353	1583	2.41
CNT 55R6	1354	1583	3.79

Error bar ± 2 cm^{-1}

5.3.6 FTIR analysis

FTIR spectroscopy is a very useful and direct technique for the study of the nature of oxygen surface groups. However there are well-known experimental difficulties involved in obtaining IR spectra of carbon materials [34]. FTIR can only be used for highly oxidized carbon surfaces; otherwise the intensity of the absorption bands is very poor [55]. The FTIR data are presented in Figure 5.12. When comparing the FTIR spectra, peaks appear at 1737 cm^{-1}, 1364 cm^{-1} and 1217 cm^{-1} for the acid-treated CNTs relative to the as-grown CNTs. This clearly shows that acid treatment has introduced some functional groups onto the surface of the CNTs. The amount of these functional groups present on the surface depends on the reflux time and/or the acid strength. The peak appearing at ~1737 cm^{-1} can be ascribed to the C=O stretching vibration of carboxyl or carbonyl groups [56-58] while that at 1364 cm^{-1} is associated with NO_2 stretching vibrations [59, 60] and the peak at 1217 cm^{-1} corresponds to C-O stretching and O-H bending vibrations [56-58]. It can be concluded that FTIR analysis also provides evidence for the existence of defects in the all of CNTs. This result is in good agreement with the Raman analysis.

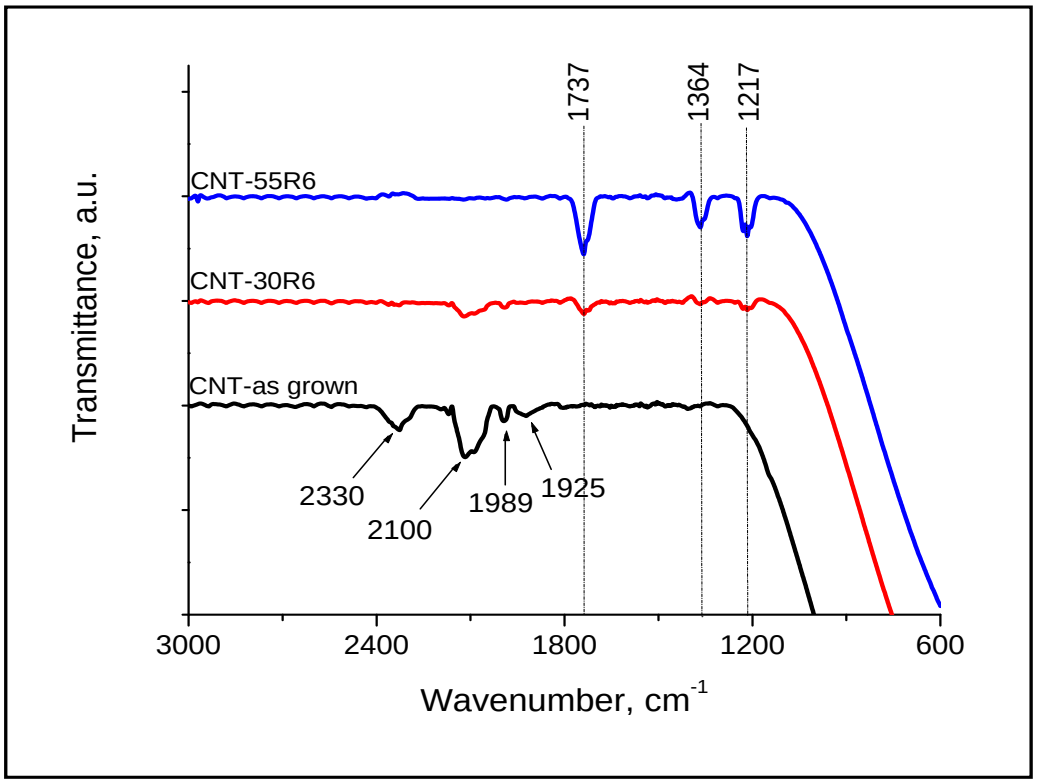


Figure 5.12: FTIR spectra of untreated (CNT-as grown) and oxidized carbon nanotubes.

5.3.7 Fischer-Tropsch catalyst data

Catalysts characterisation

The TEM images of the 10%Fe/CNT-as grown and 10%Fe/CNT-55R6 (the two extreme cases) are presented in Figure 5.13. It can be seen that the as- grown carbon nanotube is poor at dispersing the metal particle because the only metal anchoring sites are the surface defects that originated from the CNT synthesis. Whereas in the

case of the 10%Fe/CNT-55R6 catalysts, a much better dispersion is achieved and this is attributed to the extra metal anchoring site created by the surface functional groups.

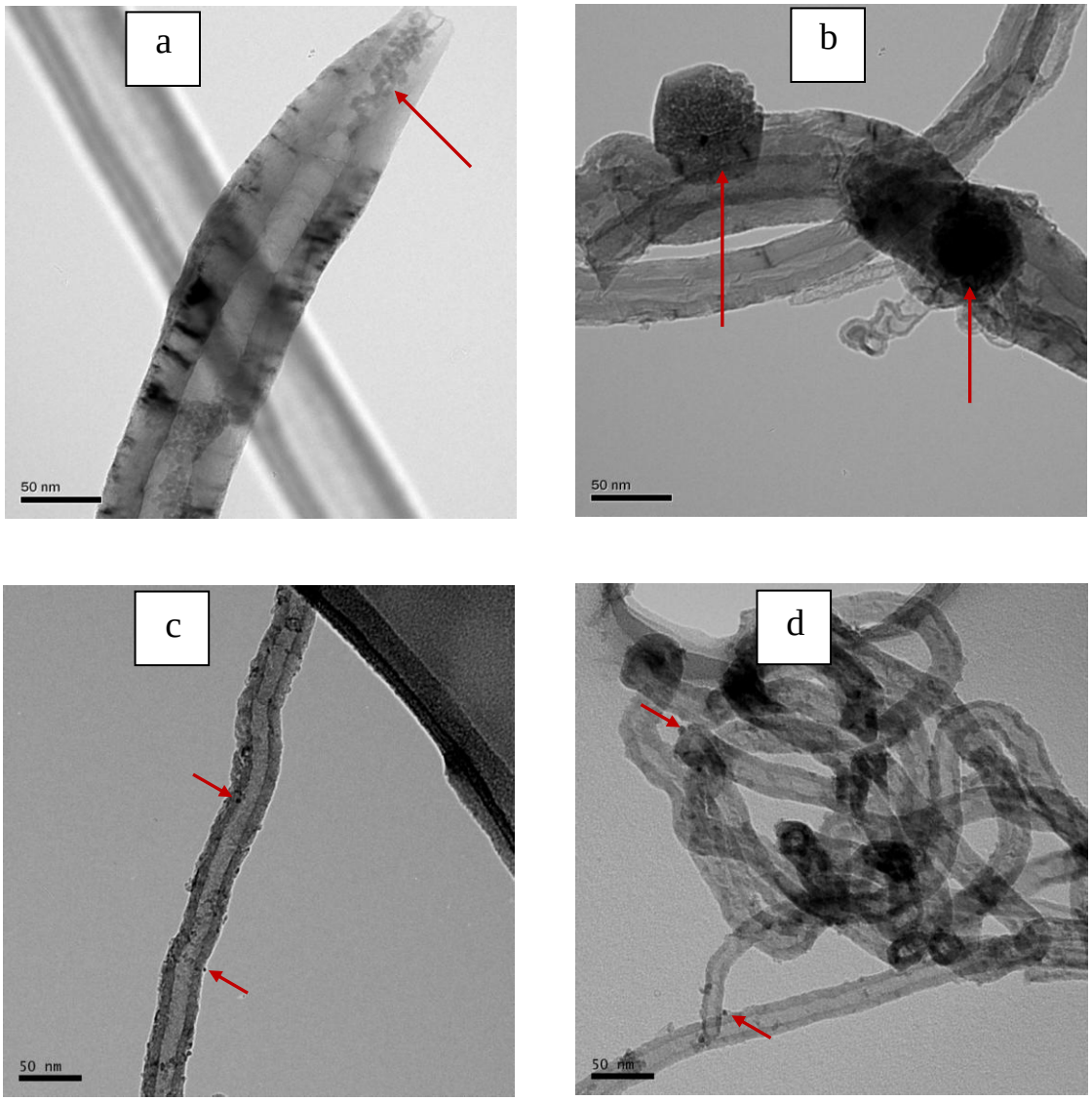


Figure 5.13: a) and b) TEM images of 10%Fe/CNT-as grown with arrow indicating large Fe clusters (iron cluster size ~ 35±5 nm based on 10 particles) ; c) and d) TEM images of 10%Fe/CNT-55R6 with arrow indicating small Fe particle (iron particle size ~ 6±1 nm based on 50 particles);

Surface area and pore volume measurements

The surface area and pore volume of the 10%Fe/CNT catalysts are presented in Table 5.5. The surface area and pore volume increased upon acid purification. The 10%Fe/CNT-as grown catalyst presents a very low surface area because the CNT used as the support was not purified therefore, still contain the residual growth reagents.

All the catalysts except the 10%Fe/CNT-as grown have similar surface area. This is due to the fact that the same amount of Fe was loaded onto the CNT with very similar surface area

Table 5.5: Surface area and pore volume of Fe catalysts supported on differently functionalised CNTs

Sample ID	Metal loading (%wt.)[a]	BET Surface area m^2/g[b]	Pore Volume cm^3/g
10%Fe/CNT-as grown	11.8	30	0.14
10%Fe/CNT-30R2	9.6	125	0.32
10%Fe/CNT-30R6	10.1	126	0.33
10%Fe/CNT-55R2	10.1	117	0.31
10%Fe/CNT-55R6	10.6	123	0.32

[a]Determined by TGA

[b]Error ± 5%

H_2 Chemisorption data

The H_2 chemisorption data obtained for the different iron catalysts are presented in Table 5.6. In general, The H_2 chemisorption studies reveal that acid treatment can result in higher metal dispersion with Fe/CNT-as grown having the lowest dispersion

and Fe/CNT-55R6 the highest dispersion. The higher the dispersion the smaller the metal particle sizes as confirmed by TEM. The Fe particle size increases in the order Fe/CNT-55R6 < Fe/CNT-55R2 < Fe/CNT-30R6 < Fe/CNT-30R2 < Fe/CNT-as grown. There is a clear correlation between iron dispersion and the degree of functionalization of the CNT support.

Table 5.6: Fe dispersion and degree of reduction for Fe catalysts

Sample ID	**amount of H_2 chemisorbed (µmol/g catal)**	**O_2 consumption (mmol/g catal)[a]**	**Fe dispersion (%)[b]**
Fe/CNT-as grown	3.52	1.02	0.52
Fe/CNT-30R2	9.15	1.18	1.17
Fe/CNT-30R6	10.23	1.20	1.28
Fe/CNT-55R2	12.70	1.05	1.81
Fe/CNT-55R6	17.32	1.11	2.34

[a] Based on the O_2 consumption at 300°C after the catalyst was reduced at 350°C for 16h.

[b] Assuming H_2:Fe stoichiometry of 1:2.

Temperature programmed reduction (TPR)

The TPR profile of the CNT support and that of 10%Fe/CNT-55R2 and 10%Fe/CNT-55R6 catalysts are shown is Figure 5.14. It can be seen that there is only one peak (T > 600°C) present in the reduction profile of the CNT-support. The same peak is present in the profile of the supported catalysts. This peak is attributed to the gasification of CNT at high temperature to produce methane [39]. For 10%Fe/CNT-55R2 and 10%Fe/CNT-55R6 catalysts, the TPR profiles show three reduction peaks. For the 10%Fe/CNT-55R2 catalyst, the first peak which corresponds to the reduction of Fe_2O_3 to Fe_3O_4 [44] appears at T =335°C. The second peak which corresponds to the reduction of Fe_3O_4 to Fe [44] occurs at 439°C. The third peak which occurs at

530°C could be attributed to those smaller metal particles that are difficult to reduce due to the stronger interaction between the metal and the support. There is a clear shift toward higher temperatures for the 10%Fe/CNT-55R6 catalyst, indicating that the catalyst is more difficult to reduce compared to the 10%Fe/CNT-55R2. This difference in reduction behavior is attributed to the difference in particle sizes (smaller metal particles interact more strongly with the support). Also, the carbon support reduction peaks are so small for the catalyst containing cases relative to that of the carbon support only because the presence of metal on the carbon catalyses the methanation reaction, and as a result, some of the carbon reduction peak probably overlaps with the last reduction peak of the metal.

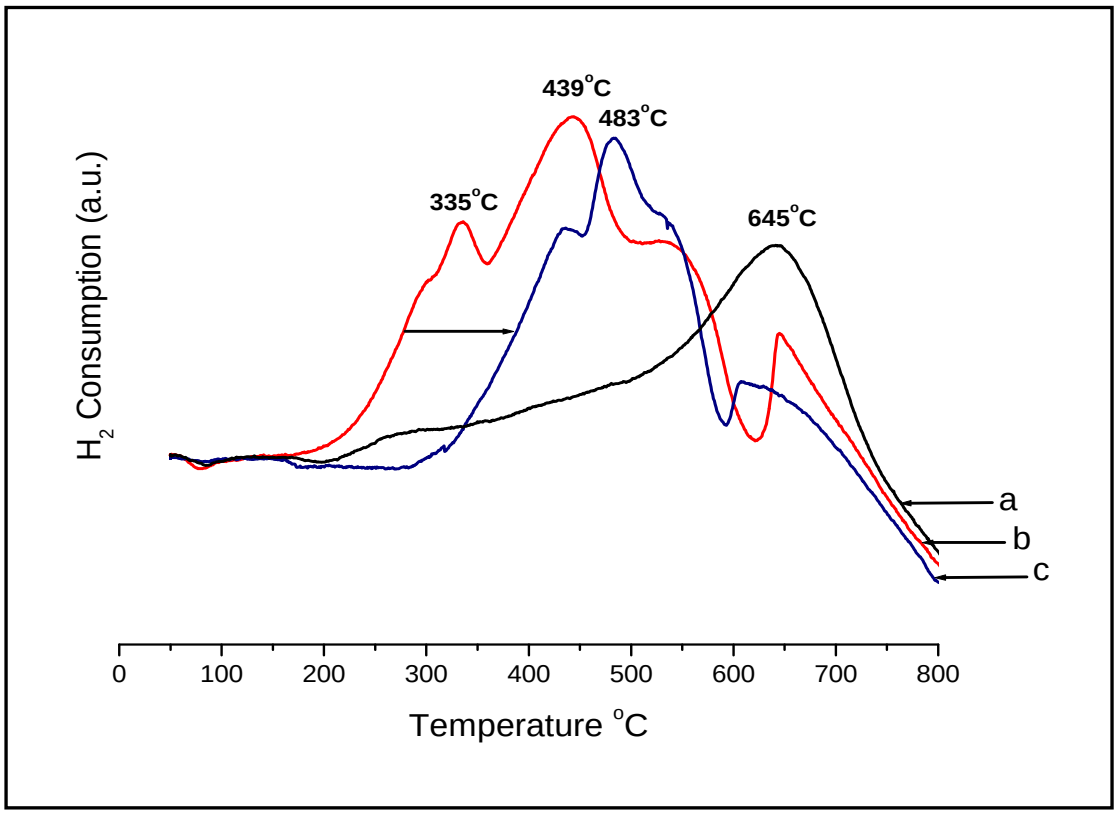


Figure 5.14: TPR profiles of a) CNT-55R2 support, b) 10%Fe/CNT-55R2 catalyst and c) 10%Fe/CNT-55R6 catalyst.

Catalytic activity

In order to check for reproducibility, a duplicate run was performed on the 10% Fe/CNT-55R2 catalyst (same conditions as for the actual runs) and the CO conversion with time on stream is shown in Figure 5.15. The data show that the experiment is reproducible.

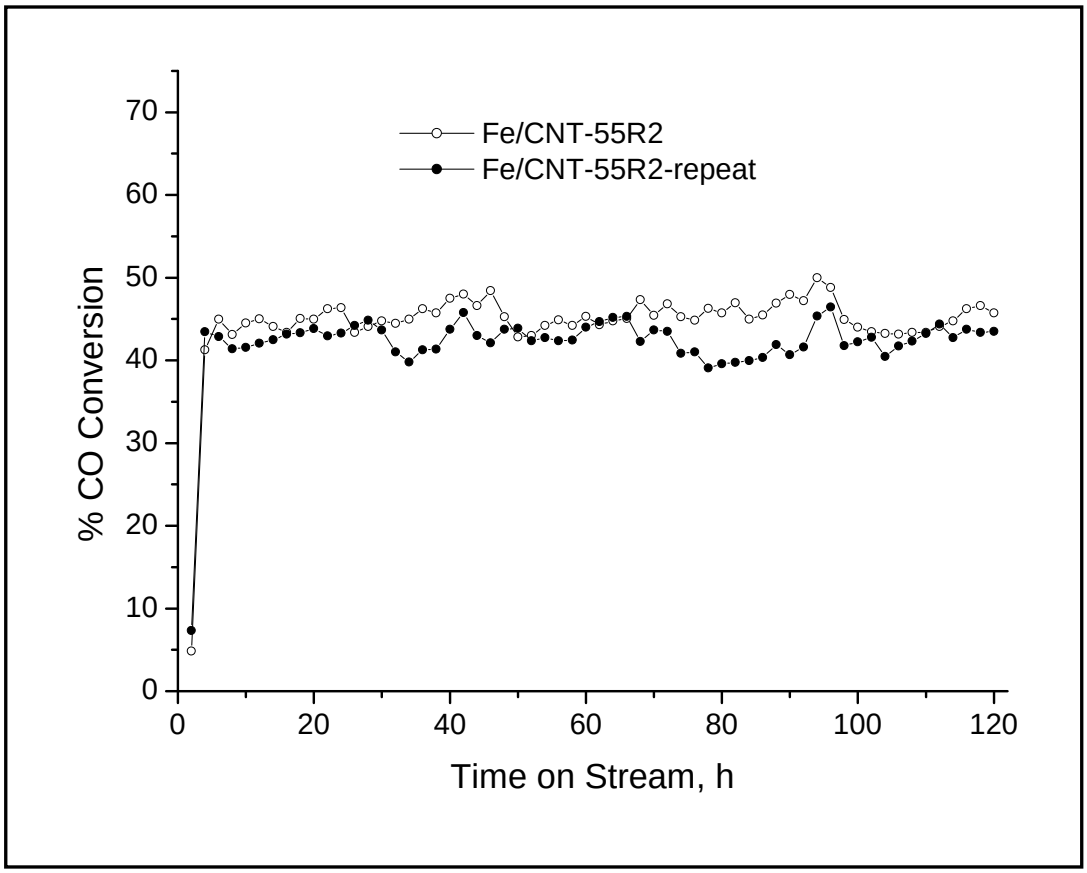


Figure 5.15: CO conversion with time on stream showing reproducibility of results

All FT reactions were performed under fixed conditions (275^{o}C, 8 bar, H_2:CO = 2, GHSV = 2400 h^{-1}). Figure 5.16 shows a plot of the catalytic activity in terms of the percentage conversion of CO, as a function of time on stream. The conversion for all the catalysts was initially low and increased significantly before leveling off within

10 h on stream; afterward the catalyst remained stable for the entire experiment (15-120 h). A comparison of the FTS data obtained from the 10% catalysts prepared on differently functionalised CNTs (Table 5.7) reveals that the %CO conversions, FT activity and hydrocarbons selectivity are all dependent on the support acid pre-treatment. Thus, the 10%Fe/CNT-as grown catalyst not only has the poorest FT performance but the highest methane selectivity and lowest C_{5+} product content of the tested catalysts. The FT activity data presented in Table 5.7 is given per g of catalyst, rather than as a turnover frequency. Attempts to use H_2 chemisorption to determine the surface area of the active metal were unsuccessful, presumably because the particles are too small [38], as reflected by TEM (and carbons as the catalyst support seem to be problematic since they gasified under chemisorption conditions). Consequently the turnover frequency could not be calculated.

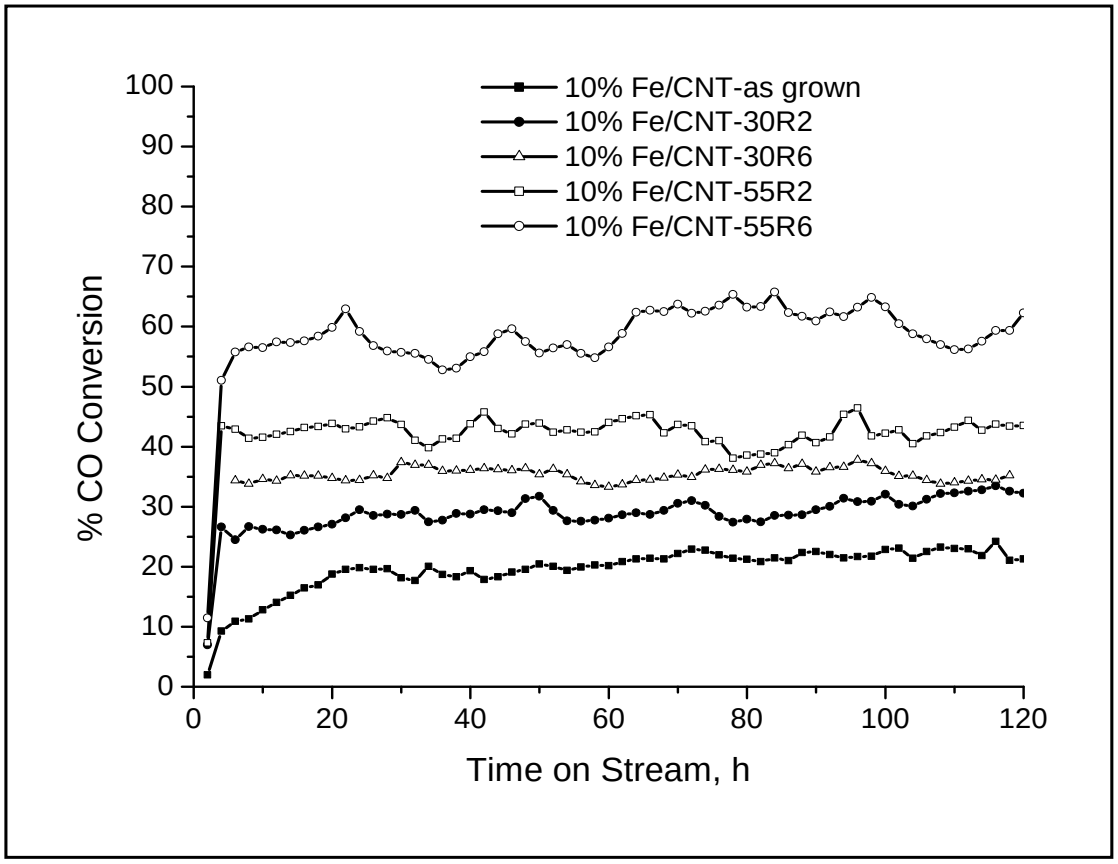


Figure 5.16: CO conversion with time on stream.

Table 5.7: Activity and selectivity of iron catalyst supported on differently functionalized CNTs in Fischer-Tropsch synthesis

Catalyst	%CO Conversion	FT Activity µmol/min.gCat	Hydrocarbons Selectivity (mol %)				
			C_1	C_2	C_3	C_4	C_{5+}
10%Fe/CNT-as grown	20	71	48	15	13	7.7	17
10%Fe/CNT-30R2	29	153	30	15	19	13	24
10%Fe/CNT-30R6	35	179	31	8.0	7.3	3.6	50
10%Fe/CNT-55R2	44	214	29	8.4	6.0	2.6	54
10%Fe/CNT-55R6	59	322	19	8.3	9.2	5.4	58

Conditions: 8 bar, 275^{o}C, CO:H_2 = 1:2, GHSV = 2400 h^{-1}.

It was observed that the FT activity increased with increasing amount of oxygen functional groups on the support i.e. the FT activity followed the order Fe/CNT-55R6 > Fe/CNT-55R2 > Fe/CNT-30R6 > Fe/CNT-30R2 > Fe/CNT-as grown. From the zeta potential measurements, it can be seen that CNT-55R6 has the highest concentration of negative charge and should lead to a better Fe dispersion; this is also the catalyst with the highest activity. The better dispersion of the metal particles on the surface of CNT-55R6 is due to the availability of the extra anchoring sites for the Fe particles, leading to the smaller Fe particles [38] and the better performance during FTS.

This study thus reveals that CNTs that are functionalized using vigorous acid treatments generate *stable* carbon materials that can be used as supports in catalytic reactions. The role of the acid treatment is to create roughened carbon surfaces that facilitate metal binding to the surface though COOH (and possibly OH) groups. The study thus confirms the earlier proposals relating to the role of 'docking stations' generated by acid treatment of CNTs. [38].

5.4 Conclusion

Carbon nanotubes were successfully synthesized using the CCVD method. The as-grown CNTs were purified by refluxing the obtained product in nitric acid. Purification not only removes the impurities, but also introduces oxygenated surface groups onto the CNTs. The presence of those groups altered the surface chemistry of CNTs. The different oxygen functional groups on the CNT surfaces were qualitatively identified by FTIR spectroscopy. Their presence was also detected by Raman spectroscopy where the amount of disorder was related to the presence of surface defects introduced by nitric acid treatment. Zeta potential measurements show that the PZC decreased with increasing treatment duration/acid concentration indicating an increase in the concentration of surface acid groups with time.

Thermogravimetric analysis revealed that the CNTs produced were multiwalled as indicated by the oxidation temperature profiles typical of MWCNTs. The amount of CO_2/CO desorbed from the surface of CNTs was a function of CNTs treatment time/acid strength. Refluxing CNTs in HNO_3 is suitable for the creation of surface functional groups. In summary, acid treatment of CNTs produced from Fe-Co on $CaCO_3$ can readily generate roughened CNT surfaces and these carbons can be used as stable supports for Fischer-Tropsch catalysts as shown here and in other studies [38]. The activity of the FT catalysts correlates with the degree of acid functionalisation of the support, indicating that the surface groups introduced during the acid treatment are linked to the active sites.

5.5 References

[1] M.L. Toebes, J.M.P. van Heeswijk, J.H. Bitter, A. Jos van Dillen, K.P. de Jong, Carbon 42 (2004) 307.

[2] J.H. Zhou, Z.J. Sui, J. Zhu, P. Li, D. Chen, Y.C. Dai, W.K. Yuan, Carbon 45 (2007) 785.

[3] K.P. De Jong, J.W. Geus, Catalysis Reviews Science and Engineering 42 (2000) 481.

[4] M.L. Toebes, J.H. Bitter, A.J. van Dillen, K.P. de Jong, Catalysis Today 76 (2002) 33.

[5] S. Iijima, Nature 354 (1991) 56.

[6] H. Dai, Accounts of Chemical Research 35 (2002) 1035.

[7] M.S. Dresselhaus, G. Dresselhaus, P.C. Eklund, D.E.H. Jones, Science of fullerenes and carbon nanotubes, Academic Press San Diego, 1996, p. 1-985.

[8] A. Thess, R. Lee, P. Nikolaev, H. Dai, P. Petit, J. Robert, C.H. Xu, Y.H. Lee, S.G. Kim, A.G. Rinzler, D.T. Colbert, G.E. Scuseria, D. Tomanek, J.E. Fischer, R.E. Smalley, Science 273 (1996) 483.

[9] T.W. Ebbesen, P.M. Ajayan, Nature 358 (1992) 220.

[10] C. Journet, W.K. Maser, P. Bernier, A. Loiseau, M.L. delaChapelle, S. Lefrant, P. Deniard, R. Lee, J.E. Fischer, Nature 388 (1997) 756.

[11] C. Bower, O. Zhou, W. Zhu, D.J. Werder, S. Jin, Applied Physics Letters 77 (2000) 2767.

[12] S.S. Fan, M.G. Chapline, N.R. Franklin, T.W. Tombler, A.M. Cassell, H.J. Dai, Science 283 (1999) 512.

[13] M. Su, B. Zheng, J. Liu, Chemical Physics Letters 322 (2000) 321.

[14] Z.F. Ren, Z.P. Huang, J.W. Xu, J.H. Wang, P. Bush, M.P. Siegal, P.N. Provencio, Science 282 (1998) 1105.

[15] Z. Li, E. Dervishi, Y. Xu, X. Ma, V. Saini, A.S. Biris, R. Little, A.R. Biris, D. Lupu, Journal of Chemistry and Physics 129 (2008) 074712.

[16] A. Magrez, J.W. Seo, C. Miko, K. Hernadi, L. Forro, Journal of Physical Chemistry B 109 (2005) 10087.

[17] E. Couteau, K. Hernadi, J.W. Seo, L. Thiên-Nga, C. Mikó, R. Gaál, L. Forró, Chemical Physics Letters 378 (2003) 9.

[18] S. Porro, S. Musso, M. Giorcelli, A. Chiodoni, A. Tagliaferro, Physica E: Low-dimensional Systems and Nanostructure 37 (2007) 16.

[19] H. Kathyayini, N. Nagaraju, A. Fonseca, J.B. Nagy, Journal of molecular Catalysis A: Chemical 223 (2004) 129.

[20] J.A. Seo, E. Couteau, P. Umek, K. Hernadi, p. Marcoux, B. Lukic, L. Forro, New Journal of Physics 5 (2003) 120.

[21] S.D. Mhlanga, K.C. Mondal, R. Carter, M.J. Witcomb, N.J. Coville, South African Journal of Chemistry , 62 (2009) 67.

[22] M. Kumar, Y. Ando, Journal of Nanoscience and Nanotechnology 10 (2010) 3739.

[23] S.D. Mhlanga, N.J. Coville, Diamond & Related Materials 17 (2008) 1489.

[24] Z. Li, E. Dervishi, Y. Xu, X. Ma, V. Saini, A.S. Biris, R. Little, A.R. Biris, D. Lupu, Journal of Chemical Physics 129 (2008) 074712.

[25] D. Vairavapandian, P. Vichchulada, M.D. Lay, Analytica Chemica Acta 626 (2008) 119.

[26] I.D. Rosca, F. Watari, M. Uo, T. Akasaka, Carbon 43 (2005) 3124.

[27] T.G. Ros, A.J. Van Dillen, J.W. Geus, D.C. Koningsberger, Chemistry European Journal 8 (2002) 1151.

[28] H.P. Boehm, Carbon 40 (2002) 145.

[29] K. Esumi, M. Ishigami, A. Nakajima, K. Sawada, H. Honda, Carbon 34 (1996) 279.

[30] P. Serp, M. Corrias, P. Kalck, Applied Catalysis A: General 253 (2003) 337.

[31] W. Chen, J. Li, L. Liu, Z. Jia, Y. Yu, Z. Zhang, Journal of Applied Electrochemistry 33 (2003) 755.

[32] H.P. Boehm, Adv. Catal. Relat. Subj 16 (1966) 179.

[33] F. Rodríguez-Reinoso, Carbon 36 (1998) 159.

[34] C. Prado-Burguete, A. Linares-Solano, F. Rodriguez-Reinoso, C. de Lecea, Journal of Catalysis 115 (1989) 98.

[35] H.P. Boehm, Carbon 32 (1994) 759.

[36] Y.P. Sun, K. Fu, Y. Lin, W. Huang, Accounts of Chemical Research 35 (2002) 1096.

[37] M.C. Bahome, L.L. Jewell, D. Hildebrandt, D. Glasser, N.J. Coville, Applied Catalysis A: General 287 (2005) 60.

[38] U.M. Graham, A. Dozier, R.A. Khatri, M.C. Bahome, L.L. Jewell, S.D. Mhlanga, N.J. Coville, B.H. Davis, Catalysis Letters 129 (2009) 39.

[39] E. van Steen, F.F. Prinsloo, Catalysis Today 71 (2002) 327.

[40] Y.H. Li, S. Wang, Z. Luan, J. Ding, C. Xu, D. Wu, Carbon 41 (2003) 1057.

[41] V. Idakiev, Z.Y. Yuan, T. Tabakova, B.L. Su, Applied Catalysis A: General 281 (2005) 149.

[42] M.E. Dry, Applied Catalysis A: General138 (1996) 319.

[43] D.J. Duvenhage, N.J. Coville, Applied Catalysis. A: General 153 (1997) 43.

[44] R.M.M. Abbaslou, A. Tavasoli, A.K. Dalai, Applied Catalysis. A: General 355 (2009) 33.

[45] C. Moreno-Castilla, M.A. Ferro-Garcia, J.P. Joly, I. Bautista-Toledo, F. Carrasco-Marin, J. Rivera-Utrilla, Langmuir 11 (1995) 4386.

[46] G. Leofanti, M. Padovan, G. Tozzola, B. Venturelli, Catalysis Today 41 (1998) 207.

[47] A.R. Harutyunyan, B.K. Pradhan, J. Chang, G. Chen, P.C. Eklund, Journal of Physical Chemistry B 106 (2002) 8671.

[48] M.N. Kirikova, A.S. Ivanov, S.V. Savilov, V.V. Lunin, Russian Chemical Bulletin 57 (2008) 298.

[49] J. Kastner, T. Pichler, H. Kuzmany, S. Curran, W. Blau, D.N. Weldon, M. Delamesiere, S. Draper, H. Zandbergen, Chemical Physics Letters 221 (1994) 53.

[50] F.X. Wang, X.P. Gao, Z.W. Lu, S.H. Ye, J.Q. Qu, F. Wu, H.T. Yuan, D.Y. Song, Journal of Alloys Compounds 370 (2004) 326.

[51] P.X. Hou, C. Liu, H.M. Cheng, Carbon 46 (2008) 2003.

[52] T.J. Park, S. Banerjee, T. Hemraj-Benny, S.S. Wong, Journal of Material Chemistry 16 (2006) 141.

[53] A. Jorio, M.A. Pimenta, A.G. Souza Filho, R. Saito, G. Dresselhaus, M.S. Dresselhaus, New Journal of Physics 5 (2003) 139.

[54] T.I.T. Okpalugo, P. Papakonstantinou, H. Murphy, J. Mclaughlin, N.M.D. Brown, Carbon 43 (2005) 2951.

[55] S. Kundu, Y. Wang, W. Xia, M. Muhler, Journal of Physical Chemistry C 112 (2008) 16869.

[56] W.M. Prest, R.A. Mosher, in: Anonymous, Colloids and Surfaces in Reprographic Technology, ACS Symposium Series 1982.

[57] P. Painter, M. Starsinic, M. Coleman, IV edited by J.R. Ferraro and L.L. Basile (Academic Press, Orlando, 1985) (1985) 169.

[58] M.S.P. Shaffer, X. Fan, A.H. Windle, Carbon 36 (1998) 1603.

[59] U. Zielke, K.J. Hüttinger, W.P. Hoffman, Carbon 34 (1996) 983.

[60] M.M. Keyser, F.F. Prinsloo, in: B.H. Davis and M.L. Occelli (Eds.) Studies of Surface Science and Catalysis, Elsevier, 2007, p. 45.

6

Chapter Six

Fe/CNT catalyzed Fischer-Tropsch synthesis: The effect of iron precursor and solvent

6.1 Introduction

Fischer-Tropsch synthesis (FTS) is a surface catalyzed polymerization reaction in which syngas, a mixture of H_2 and CO, reacts to produce hydrocarbons of various chain lengths [1, 2]. It is one of the leading gas-to-liquid (GTL) options to transport remote natural gas [3]. The FTS process is catalyzed by various transition metals, with Co, Fe, and Ru presenting the highest activity [4]. Fe and Co-based catalysts are the most frequently used but the Fe-based catalyst system remains the preferred choice in commercial F-T synthesis plants when a high olefin content in the hydrocarbon distribution is required [2, 5, 6]. However, low space-time-yield, low product selectivity for the higher molecular weight hydrocarbon and sintering are

major drawbacks of the Fe-based catalyst system when operating at temperatures between 260 and 300^{o}C [2, 6, 7].
Although the iron-based FTS catalyst system is one of the oldest and perhaps most studied systems known in the field of heterogeneous catalysis [8], ongoing research to improve the catalyst activity and selectivity continues. The catalyst performance can be altered by varying the promoters [9], support materials [10], the active metal precursor salts [11] and solvents [12].

Little work has been reported on the use of different iron sources on carbon supports. In one example, Xiong et al. [13] investigated the effect of iron precursors on the performance of a carbon sphere supported iron catalyst (Fe/CS) for FTS and found that an iron acetate precursor showed higher CO conversion than an iron nitrate precursor. However, the study was limited to Fe (nitrate) and Fe (acetate) precursors supported on carbon nanospheres.

The performance of the catalysts is known to be dependent on the metal crystallite size [14], and it is one the main factors that influences the catalytic activity and selectivity during FTS. Several researchers have investigated the effect of cobalt crystallite size on FTS and found that the turnover frequency depends on the Co crystallite size when the size is less than 8 nm but it is independent of the crystallite size when the size is greater than 8-10 nm [14, 15]. Some work has been reported on the use of iron based FT catalysts as far as the particle size effect is concerned. Mabaso et al. [16] investigated the effect of crystal size on carbon supported iron catalysts prepared by the reverse micelle technique. They reported that a lower turnover frequency and a higher selectivity toward methane are observed when the particle size is smaller than 7-9 nm.

Traditionally, researchers have tried to control the catalyst particle size by synthetic procedures that include impregnation, deposition-precipitation, ion-exchange and reverse micelle procedures. Additionally various supports have been used as a means

to control particle size [11, 17]. The particle size can also be modified by varying the reaction temperature [18]. In this study we have investigated the effect of the precursor salt and solvent on the particle size and its distribution. The catalysts were prepared using $Fe(C_5H_8O_2)_3$, $Fe(OOCCH_3)_2$, $Fe(NO_3)_3{\cdot}9H_2O$ and $Fe(C_2O_4){\cdot}2H_2O$ as the precursor and dissolved in either water or acetone as the solvent.

6.2 Experimental Section

6.2.1 Carbon nanotube synthesis

Multiwalled carbon nanotubes were produced by the catalytic decomposition of acetylene (Afrox South Africa) as the carbon source, over a 10%Fe-Co/$CaCO_3$ catalyst prepared as described elsewhere [19, 20]. The optimal condition used in this study to produce high quality and relatively high purity CNTs has previously been established in our research group [19]. The detailed procedure for the synthesis of carbon nanotubes is provided in Chapters 4 and 5.

6.2.2 Carbon nanotube purification/functionalisation

As-prepared CNTs were refluxed at 120^{o}C in 55% HNO_3 for 2 h (about 5 g of raw material was added to 500 ml of acid) in order to remove residual metal catalyst as well as to introduce surface oxygen groups which render the CNT surfaces less hydrophobic and as a result enhance the wettability for polar solvents such as water [21]. At the end of the acid treatment, the mixture was diluted with distilled water followed by filtering and washing with distilled water until the pH of the filtrate was ~7. The resulting product was dried in an oven at 120^{o}C overnight.

6.2.3 Catalyst preparation

All the catalysts were prepared by the deposition precipitation (DPU) method using urea as the precipitating agent as described elsewhere [20, 22, 23]. The solvent used in the preparation of the catalysts was either de-ionised water or acetone. Briefly, for the preparation of catalysts with a 10% Fe loading, an appropriate amount of Fe salt containing different counter-ions (acetylacetonate, acetate, nitrate or oxalate) and urea (1.5 mol of urea per mol of iron) were dissolved in either de-ionised water or acetone and added dropwise to the functionalized carbon nanotubes (2 g) slurried in de-ionised water (20 ml) and heated to 90^{o}C in an oil bath. The mixture was left to stir at this temperature for at least 2 h to allow for the decomposition of urea. Thereafter, the excess solvent was left to evaporate at 90^{o}C. The catalysts were further dried in an oven at 100^{o}C overnight and heat treated for 150 min in nitrogen at an appropriate temperature as inferred from TGA data in order to decompose the precursor salts. An overview of the reaction conditions used for the catalysts is given in Table 6.1.

Table 6.1: Overview of the prepared catalysts[a]

Name of catalyst	Fe-counter-ion	Solvent	Pre-treatment Temperature ^{o}C[b]
Fe-acac[c]	acetylacetonate(acac)	acetone	250
Fe-acac-350[d]	acetylacetonate (acac)	acetone	350
Fe-acet	acetate (acet)	de-ionised water	250
Fe-nitr	nitrate (nitr)	de-ionised water	250
Fe-oxal	oxalate (oxal)	de-ionised water	350
Fe-acet-1[c]	acetate (acet)	acetone	250
Fe-nitr-1[c]	nitrate (nitr)	acetone	250

[a]All the catalysts were supported on CNTs and were prepared using the deposition precipitation method with urea (DPU).
[b]Thermal treatment of catalyst under nitrogen to decompose the precursor salt.
[c]Reaction in acetone
[d]pre-treatment temperature = 350^{o}C

6.2.4 Carbon nanotubes and iron catalyst characterization

The morphology and structures of the as-prepared and acid-treated CNTs as well as the Fe/CNT catalysts were characterized by TEM. Sample specimens for TEM studies were prepared by ultrasonic dispersion of the sample in methanol. The suspensions were dropped onto a SPI-carbon coated copper grid. TEM investigations were carried out using an FEI Tecnai Spirit G^2 transmission electron microscope operating at 120 kV. The inner and outer diameter distributions of the CNTs and the particle size of the active phase were obtained by using Image J software. About 120 CNT diameters and ~150 particles were measured per sample.

The surface area and pore volume of the as-grown CNTs, the acid-treated CNTs and the Fe/CNT catalysts were determined by N_2 physisorption using a Micromeritics TRISTAR 3000 analyzer. A sample of approximately 300 mg was degassed at 150^{o}C for 4 h under a flow of N_2. Thereafter the surface areas and pore volumes were determined by the Brunauer-Emmett-Teller (BET) method.

The TGA analysis was done on a Perkin Elmer STA 4000 analyzer. About 5-10 mg of sample was placed in a ceramic pan and placed in the instrument's furnace. The temperature of the sample was increased from room temperature to 900^{o}C at 10^{o}C/min under either an oxidative atmosphere (air, 20 ml/min) or inert atmosphere (N_2, 20 ml/min). The percentage Fe loading in all the catalysts was determined using the % residual ash that remained after burning the carbon from the catalyst and assuming that the ash consists only of Fe_2O_3. The value obtained was corrected for the ash that remains when the support alone is oxidized.

Temperature programmed reduction (TPR) experiments were performed on a Micromeritics AutoChem11 Chemisorption analyzer to study the reduction behaviour of the catalysts. A sample of the catalyst (100 mg) was loaded into a U-shaped quartz tube reactor, fitted with a thermocouple for continuous temperature measurement.

Prior to the H_2-TPR analysis, the sample was first degassed in a flow of high purity argon (20 ml/min) at 150^oC for 30 min to remove traces of water, and then cooled to 40^oC. The sample was then reduced in 5%H_2/Ar (50 ml/min) as the temperature was increased from 40^oC to 800^oC at a rate of 10^oC /min. The gas flow through the reactor was controlled by three Brooks mass flow controllers. A thermal conductivity detector (TCD) was used to measure the H_2 consumption. The temperature and associated H_2 consumption was captured automatically by a PC to give the TPR profiles.

X-ray powder diffraction (XRD) patterns for the support and the Fe/CNT catalysts were recorded with a Brucker D2 phaser diffractometer using a Cu source (1.5418 Å) and a LynxEye detector. The scan was within a 2θ range of 5-90^o with 0.03^o steps at 25^oC.

6.2.5 Catalyst evaluation and data analysis

The catalysts'performance during FTS was tested using a fixed-bed micro reactor. A detailed description of the experimental set-up and procedures has been given in Chapters 3 and 4. Catalytic activity, product selectivity and the stability of the catalysts were evaluated during a reaction period of 120 h.

The calculations used to determine the mass balance are similar to those used previously in our group [24]. Selectivity is reported as the percentage of CO converted into a certain product expressed in C atoms. C_2-C_4 refers to hydrocarbons containing 2-4 carbon atoms and C_{5+} to hydrocarbons containing 5 or more carbon atoms [25]. Refer to Chapter 4 for the different formulae used.

6.3 Results and discussion

6.3.1 X-ray diffraction analysis (XRD)

Table 6.2, Figures 6.1a and 6.1b below show the XRD patterns of the CNT support and the Fe/CNT catalysts prepared using different precursors and solvents as well as the d-space values and corresponding reflection planes for all the phases identified in XRD figures. The peaks at 2θ values of 26^o and 45^o correspond to graphite layers of multiwalled carbon nanotubes [26]. The peaks at 30^o and 33^o correspond to the presence of the magnetite (Fe_3O_4) phase and hematite (Fe_2O_3) phase respectively and the peak at 35.5^o corresponds to the presence of either hematite or magnetite or both phases. The broad peak at 2θ = 43^o is attributed to the presence of small amounts of carbides as well as residual catalyst from the CNTs synthesis [27].

Table 6.2: d-space values and corresponding reflection planes for all the phases identified in XRD figures

Phases Identified	2θ(^{o})	d-spacing (Å)	h k l plane
graphite	26	3.37	002
	45	2.04	101
Hematite (Fe_2O_3)	33	2.70	104
	35.5	2.52	110
Magnetite (Fe_3O_4)	30	2.97	220
	35.5	2.53	311
Fe_3C	43	2.10	211
Co_2C	43	2.12	111
Fe-Co	45	2.02	110

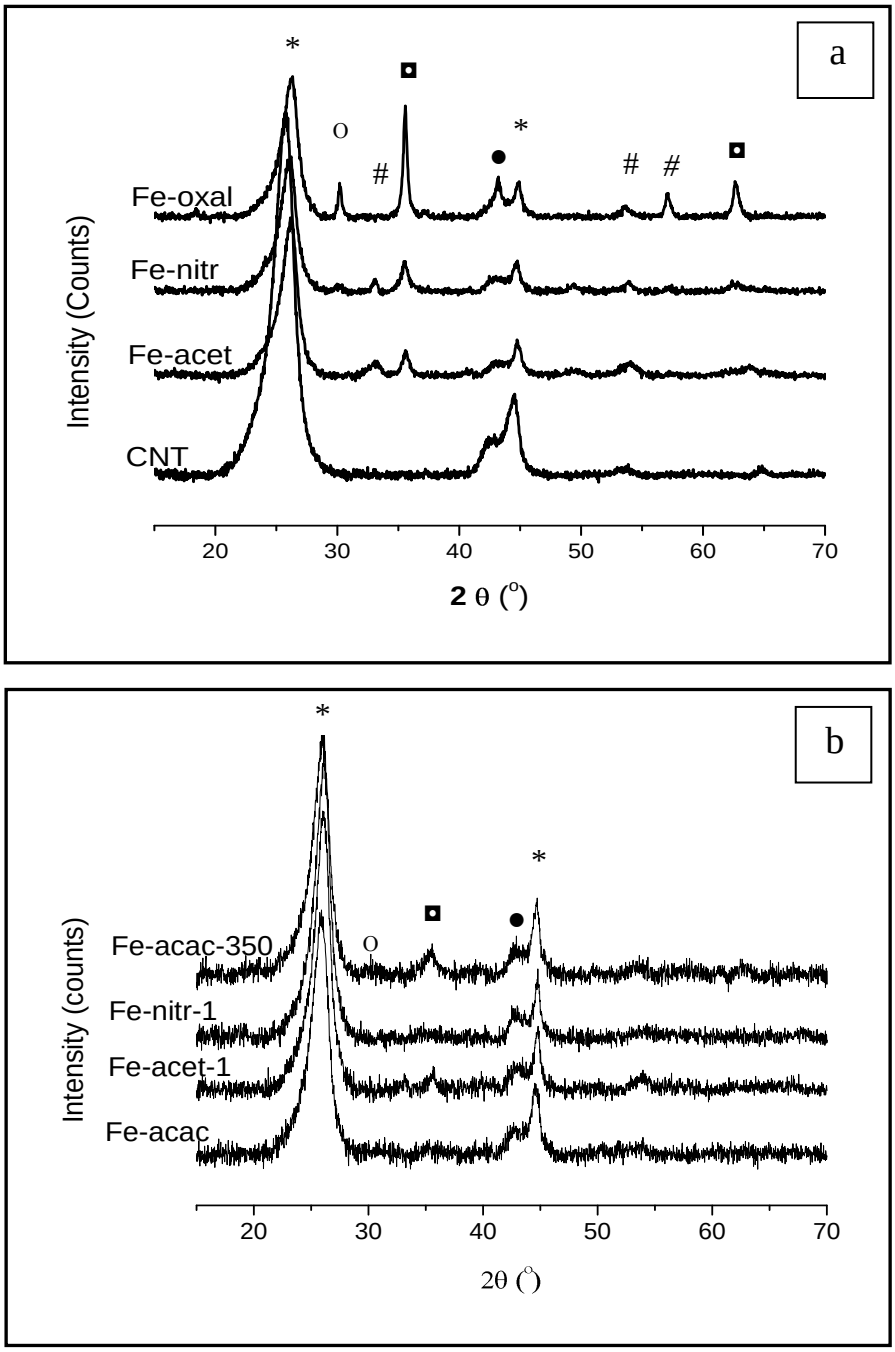


Figure 6.1: XRD data of Fe/CNT catalysts prepared using different iron precursors and either a) water or b) acetone as solvents: * = graphite; o = Fe_3O_4; # = Fe_2O_3; ◘ = Fe_2O_3 and Fe_3O_4; ● = Co-Fe, Fe_3C, Co_3C or Co_2C [13, 27]

When comparing the XRD patterns of the catalysts studied, it is clear that the precursor salts and the solvent used in the catalysts preparation had an effect on the catalysts' phase composition (different diffraction patterns). The Fe crystallite sizes were determined using the Scherrer equation and the line broadening of the peak at $2\theta = 33^{o}$ since it corresponds to the Fe_2O_3 most intense peak. The peak at $2\theta = 35.5$ could not be used because it is a mixture of the hematite and magnetite phases. Using the Scherrer equation, the crystallite size of only Fe-acet and Fe-nitr could be estimated and were found to be 5.5 and 7 nm respectively. The other catalysts crystallite sizes could not be determined probably because they were very small and below the detection limit of the XRD. In general, the catalysts prepared using acetone as the solvent had smaller iron particle sizes than the ones prepared using water. Similar observations were made by Chronis [12] and correlates with the difference in the solvent volatility (The catalyst particle sizes tended to decrease with decrease in the solvent boiling point).

6.3.2 TEM analysis

The morphology and structure of the carbon nanotubes were confirmed by TEM and HRTEM analysis. It was shown that the CNTs produced are multiwalled carbon nanotubes with a distance of 0.34 nm between the graphene layers (Figures 6.2a and 6.2b). The inner diameters of the CNTs are not uniform throughout the length of the tubes (Figure 6.2b) due to the restructuring of enclosed metal particle morphology and orientation during CNT growth [28]. The outermost layers are typically covered by carbon flakes (amorphous carbon) as indicated in Figure 6.2b (ovals). The build-up of amorphous carbonaceous materials is due to the prolonged synthesis time used [19]. Acid treatment was used to remove impurities (residual metal catalyst except for the encapsulated metal particles, support, and some amorphous carbon) as well as to introduce oxygen functional groups (carboxyl, carbonyl, phenol etc.). A degree of surface roughness is brought about by the acid treatment (Figure 6.3). This roughness

is required for the preparation of stable metal catalysts since they act as additional anchoring sites for the catalyst particles [29, 30].

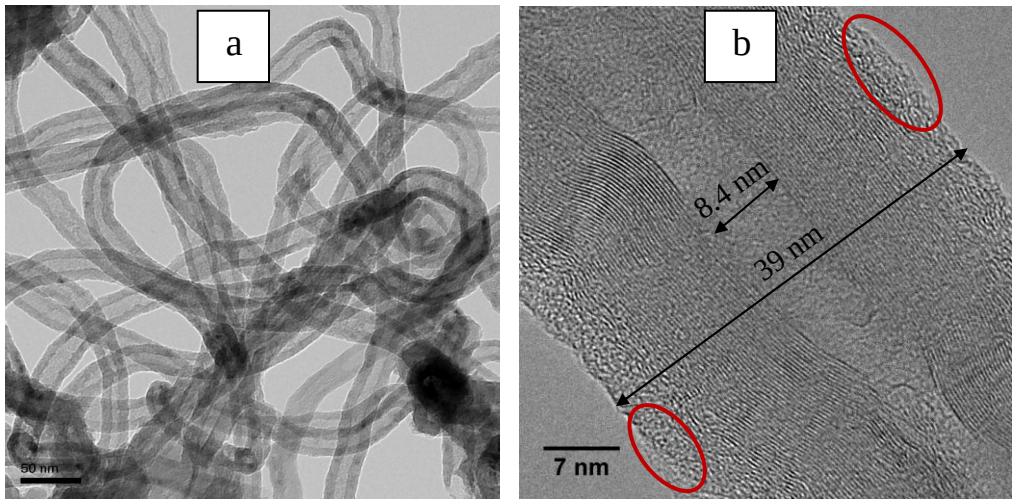


Figure 6.2: CNT-as grown: a) TEM, b) HRTEM with ovals representing amorphous carbon

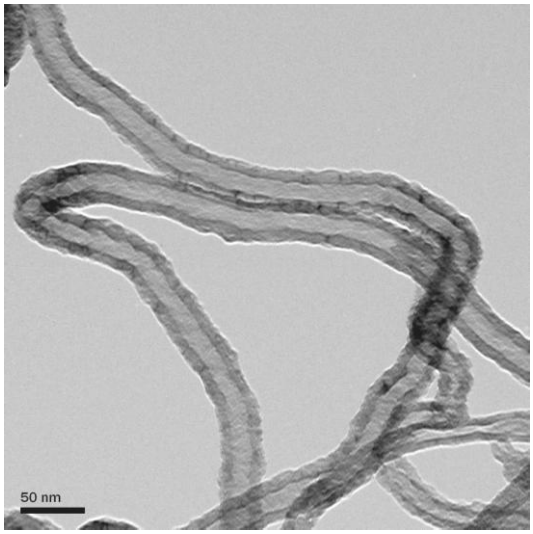


Figure 6.3: TEM image of CNTs after reflux in 55% HNO_3 for 2 h

Fe-based catalysts were prepared by a deposition precipitation method using different iron precursors and water or acetone as the solvent (see Table 6.1 for details). The purpose of using two different solvents was to try and control the particle size during catalyst preparation. TEM analysis of the fresh catalyst (before FTS) revealed that the metal particle size depended on the solvent used in the preparation of the catalyst (water, acetone), the pre-treatment temperature used (250^{o}C, 350^{o}C) and less significantly on the iron precursor (Table 6.3).

TEM images and particle size distributions for the catalysts prepared from Fe-acet, Fe-nitr, Fe-oxal, Fe-acet-1, Fe-nitr-1, Fe-acac and Fe-acac-350 are shown in Figures 6.4 – 6.10. For the catalyst prepared using water as the solvent, the particle size increased in the order Fe-acet < Fe-nitr < Fe-oxal. When acetone is used as the solvent in the catalyst preparation, the average Fe particle size is very similar (2-5 nm) and independent of the precursor used. The variation of particle size with the precursor and/or the solvent is due to the precursor-solvent-support interaction. The mechanism of this interaction is not well understood [11]. Fe-acac-350 which was prepared using acetone and pre-treated at 350^{o}C to decompose the salt, showed a slight increase in particle size (4-8 nm, Table 6.3, Figure 6.10) confirming that the pre-treatment temperature influenced the Fe particle size. It was also noticed that Fe-oxal showed an increase in particle size when compared to Fe-acet and Fe-nitr and this was due to metal sintering as Fe-oxal had to be pretreated at a higher temperature (350^{o}C) due to the higher decomposition temperature for the oxalate salt. The TEM data agrees well with the XRD findings.

Table 6.3: Particle size comparison

Catalyst	Fe Particle size, nm	
	TEM (Before FTS)	XRD (Fe_2O_3)
Fe-acet	3-5	5.5
Fe-nitr	4-7	7
Fe-oxal	5-12	—[a]
Fe-acet-1	2-5	—[a]
Fe-nitr-1	2-5	—[a]
Fe-acac	2-5	—[a]
Fe-acac-350	4-8	—[a]

[a] Could not be determined using XRD.

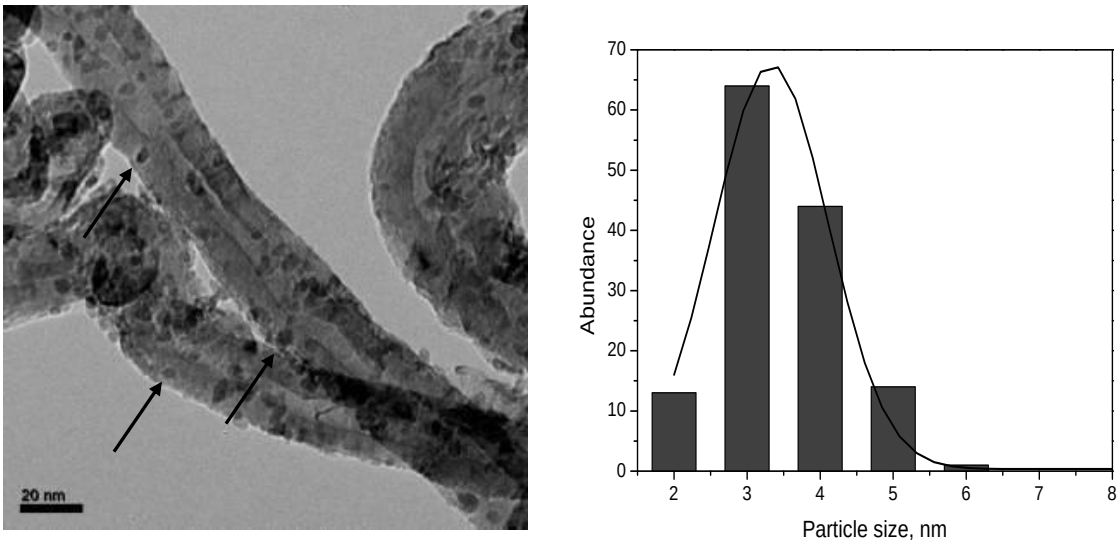


Figure 6.4: TEM image with arrows indicating the Fe particles, and Fe particle size histogram for the Fe-acet catalyst.

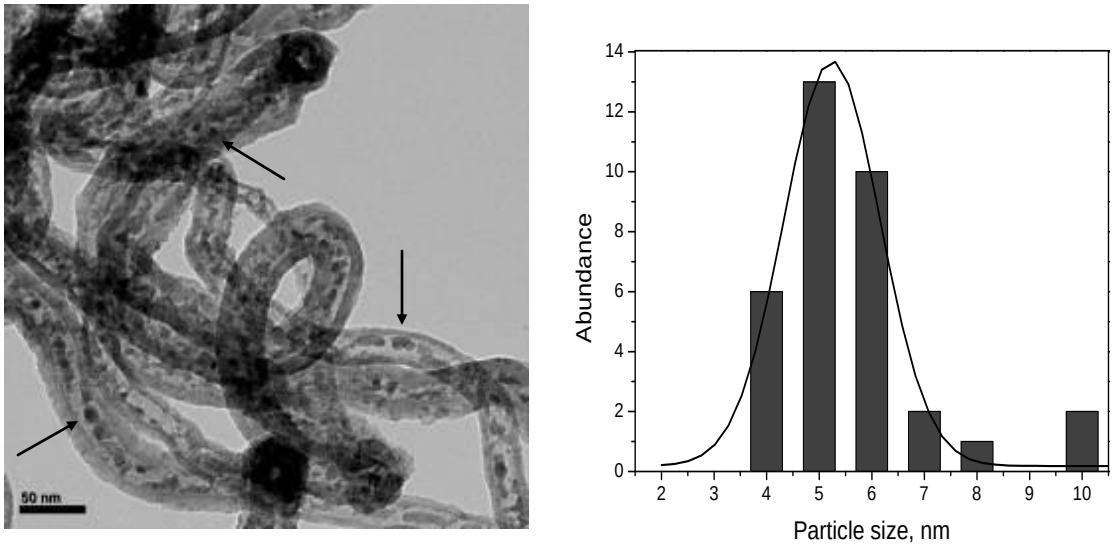


Figure 6.5: TEM image with arrows indicating the Fe particles, and Fe particle size histogram for the Fe-nitr catalyst.

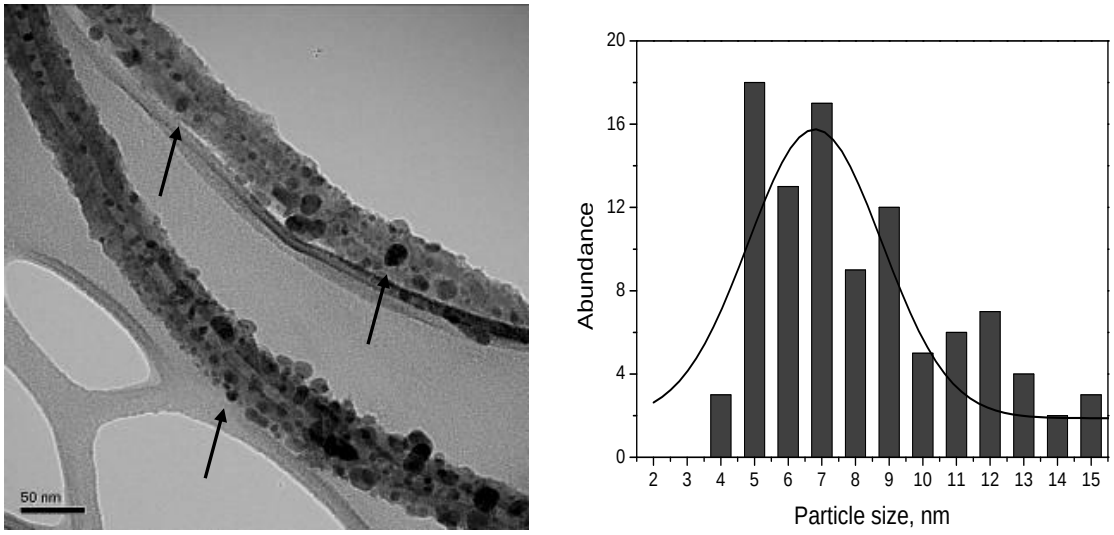


Figure 6.6: TEM image with arrows indicating the Fe particles, and Fe particle size histogram for the Fe-oxal catalyst.

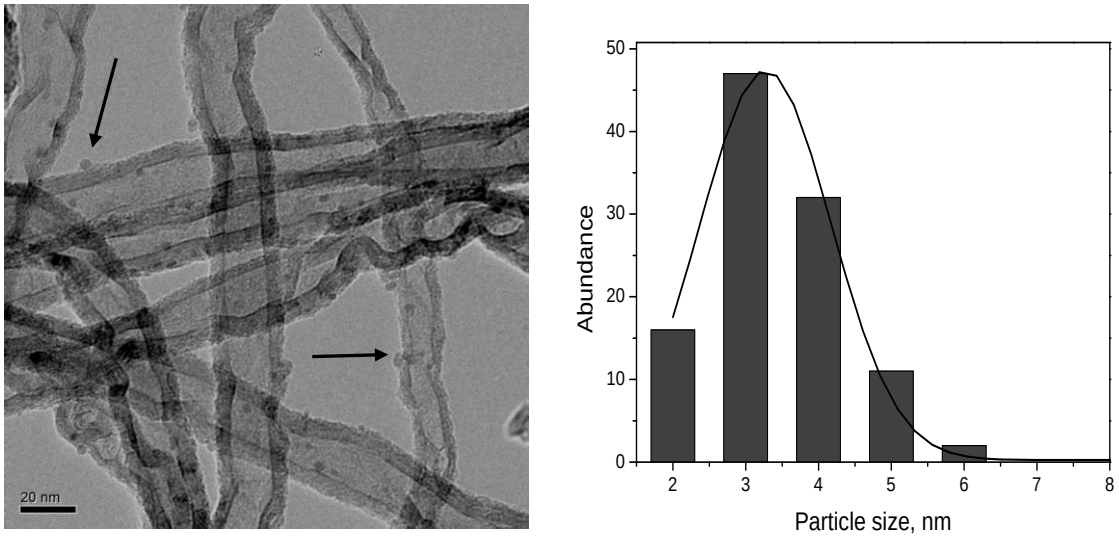


Figure 6.7: TEM image with arrows indicating the Fe particles, and Fe particle size histogram for the Fe-acet-1 catalyst.

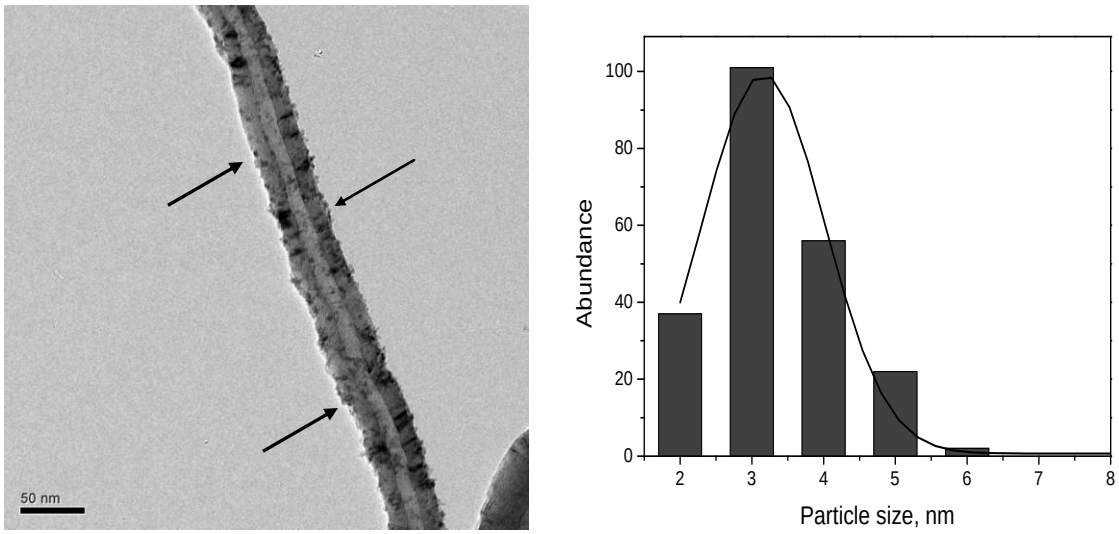


Figure 6.8: TEM image with arrows indicating the Fe particles, and Fe particle size histogram for the Fe-nitr-1 catalyst.

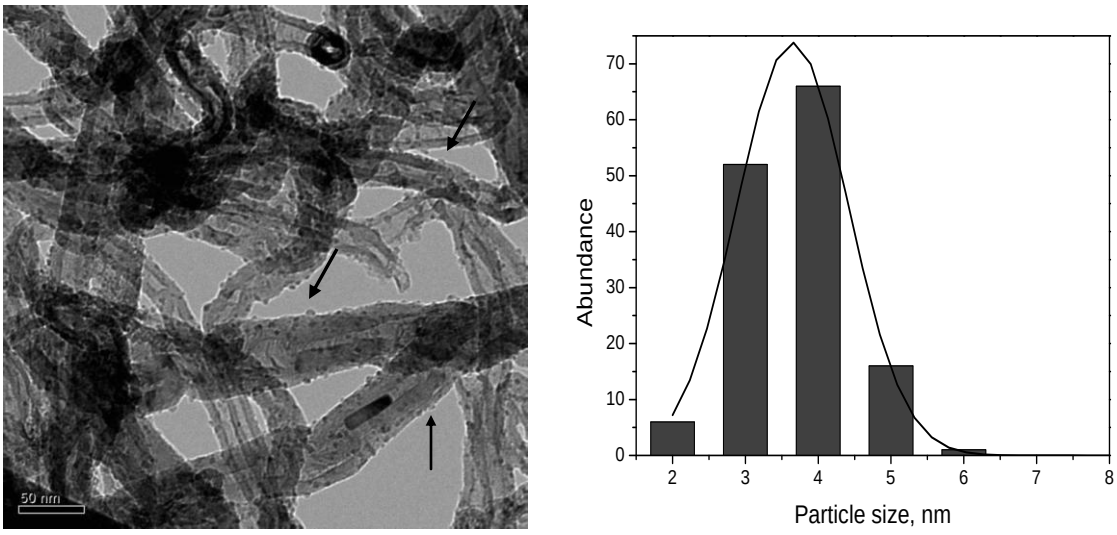


Figure 6.9: TEM image with arrows indicating the Fe particles, and Fe particle size histogram for the Fe-acac catalyst.

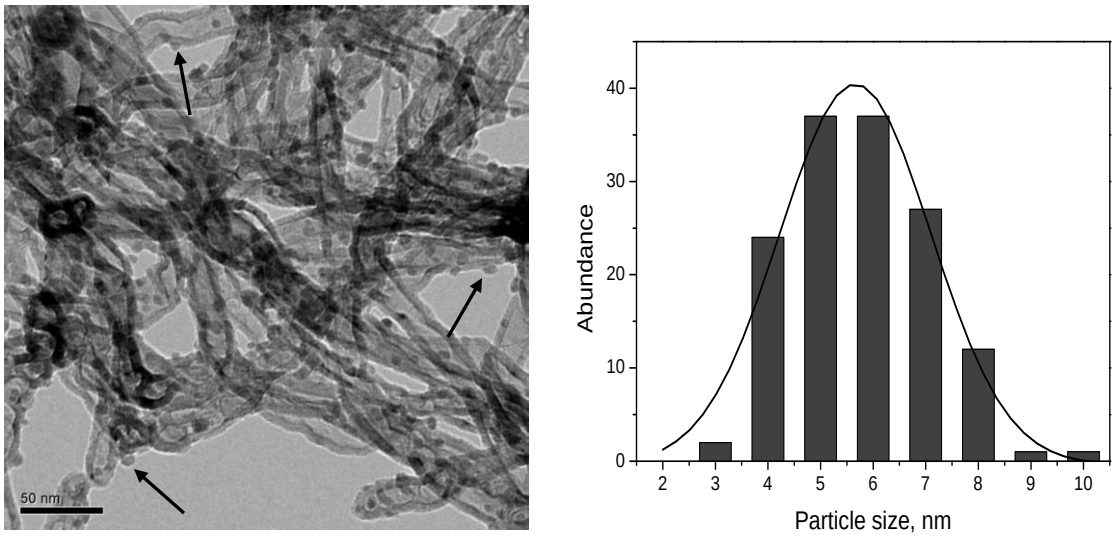


Figure 6.10: TEM image with arrows indicating the Fe particles, and Fe particle size histogram for the Fe-acac-350 catalyst.

6.3.3 Thermogravimetric analysis (TGA)

TGA was used to determine the decomposition temperature of the precursor, the thermal stability and the composition of the CNT support and the Fe/CNT catalysts. TGA of all the catalysts before heat treatment in nitrogen was performed in an air atmosphere (flowrate: 20 ml/min, heating rate: 10 ^{o}C/min) in order to determine the temperature at which the precursor salt decomposed to form the metal oxide (Figures 6.11a and 6.12a). After heat treatment in a nitrogen atmosphere at the desired temperature (250^{o}C or 350^{o}C) for 150 min, the TGA analysis was performed in an air atmosphere to confirm the removal of the precursor salt (Figure 6.11b and Figure 6.12b). In Figure 6.11a, the weight loss at 180^{o}C is attributed to the decomposition of acetylacetonate whereas the peak at 500^{o}C is due to the oxidation of the CNT. Heat-treatment of the catalyst at 250^{o}C for 150 min under nitrogen was sufficient to convert Fe-acac into Fe_2O_3 (Figure 6.10b). In Figure 6.12a, the weight loss for Fe-oxal before 100^{o}C is attributed to the loss of moisture. Between 140 and 300^{o}C, the decomposition of oxalate salt takes place and the peak at 500^{o}C corresponds to the oxidation of CNTs. This suggests that in order to decompose the oxalate, the catalyst must be heated at 350^{o}C in nitrogen for 150 min (Figure 6.12b).

TGA and DTA profiles (in air) of some of the prepared catalysts are shown in Figures 6.13a and b. Upon adding the active metal (iron) to the CNT, the thermal stability of the CNT decreased from 675^{o}C to ~ 495^{o}C since the presence of iron aids/catalyses the oxidation of the CNTs [31]. The breadth of the DTA peak increased upon adding the Fe metal (Figure 6.13b) due to the added defects on the surface of the CNT (The defects came from the acid treatment of the CNTs). There was also an increase in the residual mass due to the presence of the added iron.

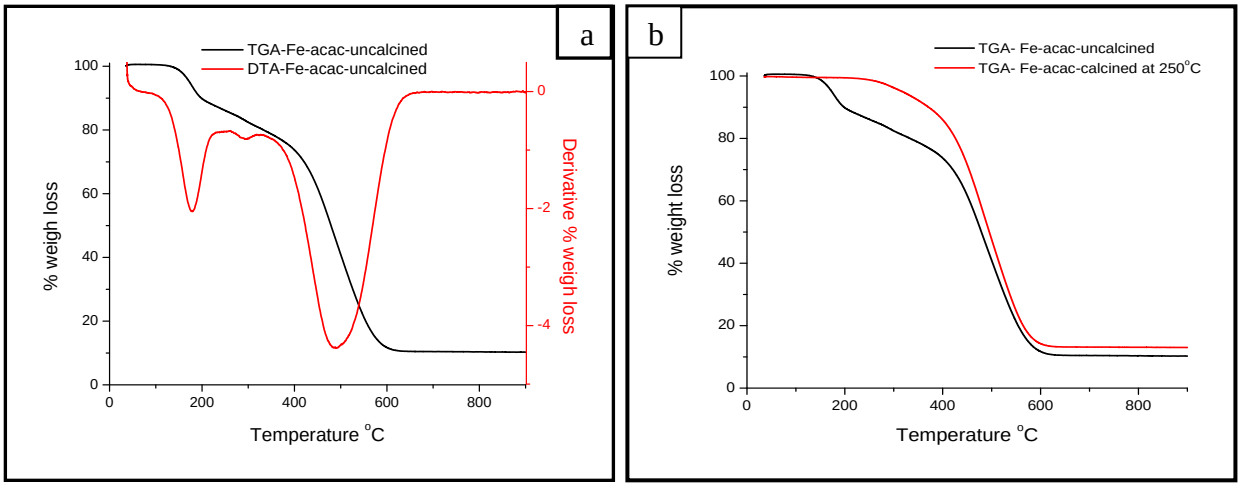


Figure 6.11: TGA profile in air atmosphere for the Fe-acac catalyst: a) before heat treatment together with the derivative plot and b) before heat treatment and after heat treatment (250°C, 150 min).

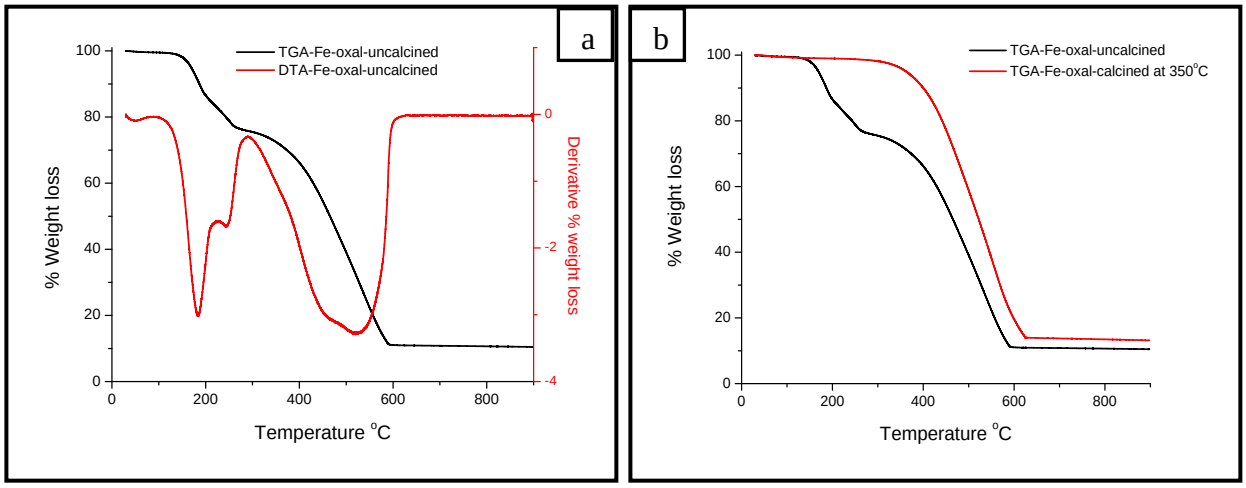


Figure 6.12: TGA profile for the Fe-oxal catalyst in air atmosphere; a) before heat treatment together with the derivative plot and b) before heat treatment and after heat treatment (350°C, 150 min).

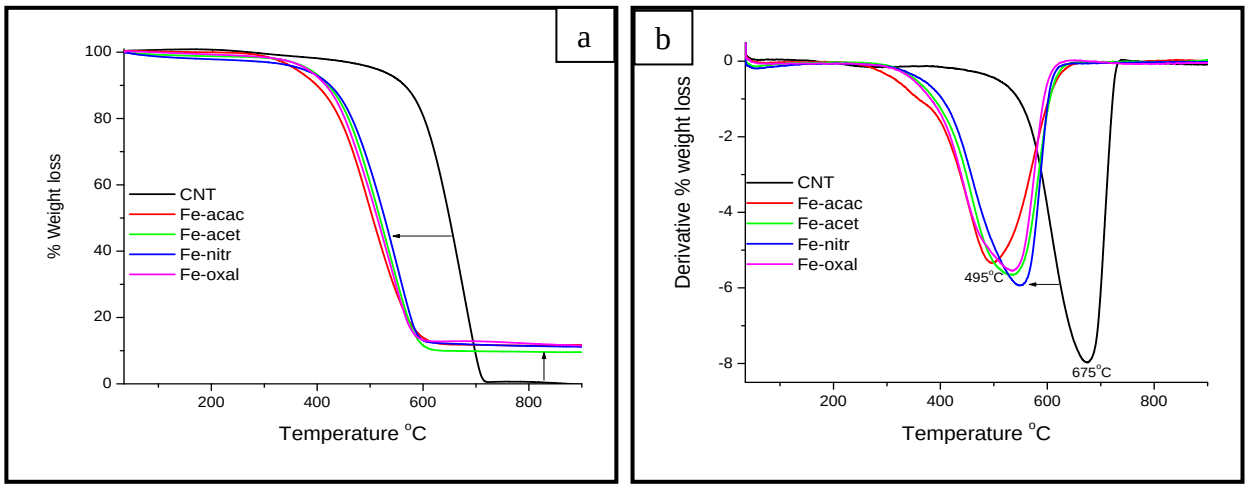


Figure 6.13: a)-TGA and b)-DTA of Fe-acac, Fe-acet, Fe-nitr and Fe-oxal.

6.3.4 Surface area and pore volume analysis

The surface area and pore volume of the support and prepared catalysts are presented in Table 6.4. Apart from the Fe-acac and Fe-acac-350 catalysts that showed a lower surface area and pore volume, the other catalysts have in general a slightly higher surface area relative to the CNT support. The decrease in surface area and pore volume for the catalyst prepared from acetylacetonate precursor is attributed to pore blockage. The precursor and the solvent used in the catalyst preparation did not seem to have any major effect on the surface area of the Fe/CNT catalysts. It was expected that the catalyst with the smaller metal particle would have a higher surface area but this was not the case.

Table 6.4: BET surface area and pore volume and of the support (CNT) and Fe/CNT catalysts.

Sample ID	Metal loading (wt. %)[a]	Surface Area ($m^2.g^{-1}$) [b]	Pore Volume ($cm^3.g^{-1}$)
CNT	-	108	0.35
Fe-acet	9.2	119	0.32
Fe-nitr	10.4	123	0.28
Fe-oxal	10.6	101	0.30
Fe-acet-1	9.5	103	0.29
Fe-nitr-1	9.9	112	0.28
Fe-acac	10.3	67.0	0.25
Fe-acac-350	10.1	72.1	0.26

[a]determined using TGA analysis
[b]error bar ±5%.

6.3.5 Temperature programmed reduction (TPR)

TPR analysis was performed to assess the reducibility of the catalysts. The reduction of Fe_2O_3 to Fe normally takes place in three steps:

$$Fe_2O_3 \xrightarrow{1} Fe_3O_4 \xrightarrow{2} FeO \xrightarrow{3} Fe$$

Since FeO is thermodynamically unstable compared to Fe and Fe_3O_4 [26], the transition to and from FeO is generally not expected to appear in the TPR profile and as a result the reduction of Fe_2O_3 to Fe normally takes place in two steps:

$$Fe_2O_3 \xrightarrow{1} Fe_3O_4 \xrightarrow{2} Fe$$

It is generally accepted that the first peak in the TPR profile corresponds to the reduction of Fe_2O_3 to Fe_3O_4, and the second peak corresponds to the reduction of Fe_3O_4 to Fe [20, 32]. It is also known that a transition metal acts as a methanation catalyst in the presence of H_2 at temperatures greater than 550^oC [22].

The H_2-TPR profiles of the functionalized CNTs as well as the Fe/CNTs catalysts are shown in Figure 6.14. It can be seen that only one peak occurs in the TPR profile of the CNTs; at ~645 ^oC. This is due to the gasification of carbon in the presence of H_2 at high temperature to produce methane. After loading the iron, the gasification temperature is shifted slightly to lower temperature (ca. 630^oC). This shift to lower temperature can be attributed to the iron acting as a catalyst for the gasification reaction [20]. The H_2-TPR profiles of the Fe/CNT catalysts prepared using different precursors show different reducibility behaviour which is attributed to the difference in metal particle size which leads to different metal-support interactions. Table 6.5 summarises the temperature data for each reduction step. The most important features to note are: for the Fe-nitr catalyst, the first reduction step which corresponds to $Fe_2O_3 \rightarrow Fe_3O_4$ occurs as two peaks (306^oC and 340^oC). The presence of these two peaks could be related to the reduction of iron oxide located in the inner and outer walls on the CNTs respectively [26]. The TEM image of Fe-nitr actually confirms that some Fe particles are located inside the tube (Figure 6.5). The second reduction step which corresponds to $Fe_3O_4 \rightarrow Fe^o$ occurs at 441^oC and the third peak which occurs at 530^oC could be attributed to those smaller metal particles that are difficult to reduce due to the stronger interaction between the metal and the support. The second reduction step for the Fe-oxal occurs at slightly higher temperature (491^oC) and this step consumed much more H_2 compared to the second peak of all the catalysts studied. This suggests that Fe-oxal is easier to reduce from Fe_3O_4 to Fe.

Table 6.5: Temperature of the peak maxima at which each reduction steps occured during the H_2-TPR

	Temperature (^oC)		
Sample ID	$Fe_2O_3 \rightarrow Fe_3O_4$	$Fe_3O_4 \rightarrow Fe^o$	$CNT \rightarrow CH_4$
CNT	–	–	645
Fe-acet	352	445	636
Fe-nitr	306, 340	441	635
Fe-oxal	346	491	628

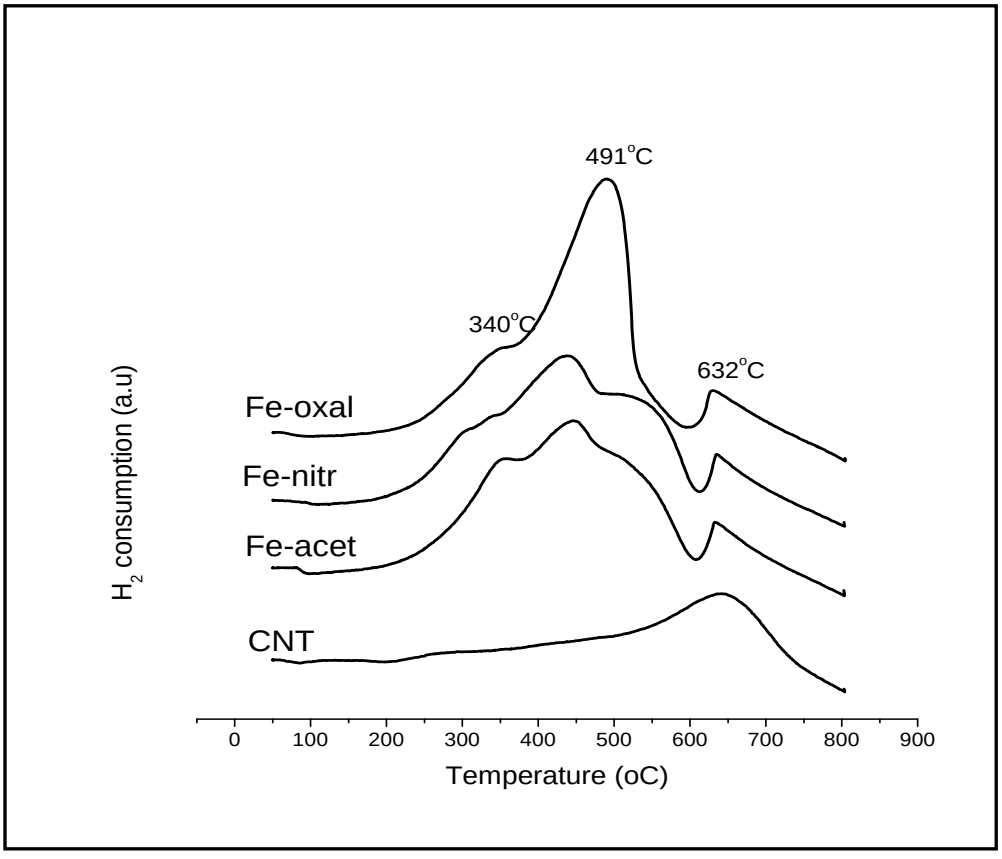


Figure 6.14: TPR profiles of the support and the Fe/CNT catalysts prepared using water as the solvent.

The TPR profiles of the Fe/CNT catalysts prepared using acetone as the solvent are presented in Figure 6.15. The first reduction peak (Fe_2O_3 to Fe_3O_4) occurs at 350°C, 401°C and 422°C for Fe-nitr-1, Fe-acet-1 and Fe-acac respectively. The shift to higher temperature is attributed to the strength in the metal-support interaction. The stronger the interaction, the more difficult it is to reduce the catalyst. The second reduction process (Fe_3O_4 to Fe) follows the same trend as the first step with Fe-acac being slightly more difficult to reduce. The third peak probably corresponds to the small particles that are difficult to reduce and the last peak corresponds to the gasification of CNTs. From the TPR reduction data, it is observed that catalysts prepared using acetone are more difficult to reduce compared to the ones prepared using de-ionised water. This indicated that the Fe catalysts prepared using acetone have smaller particle size and this is in agreement with the TEM and XRD data (Table 6.2).

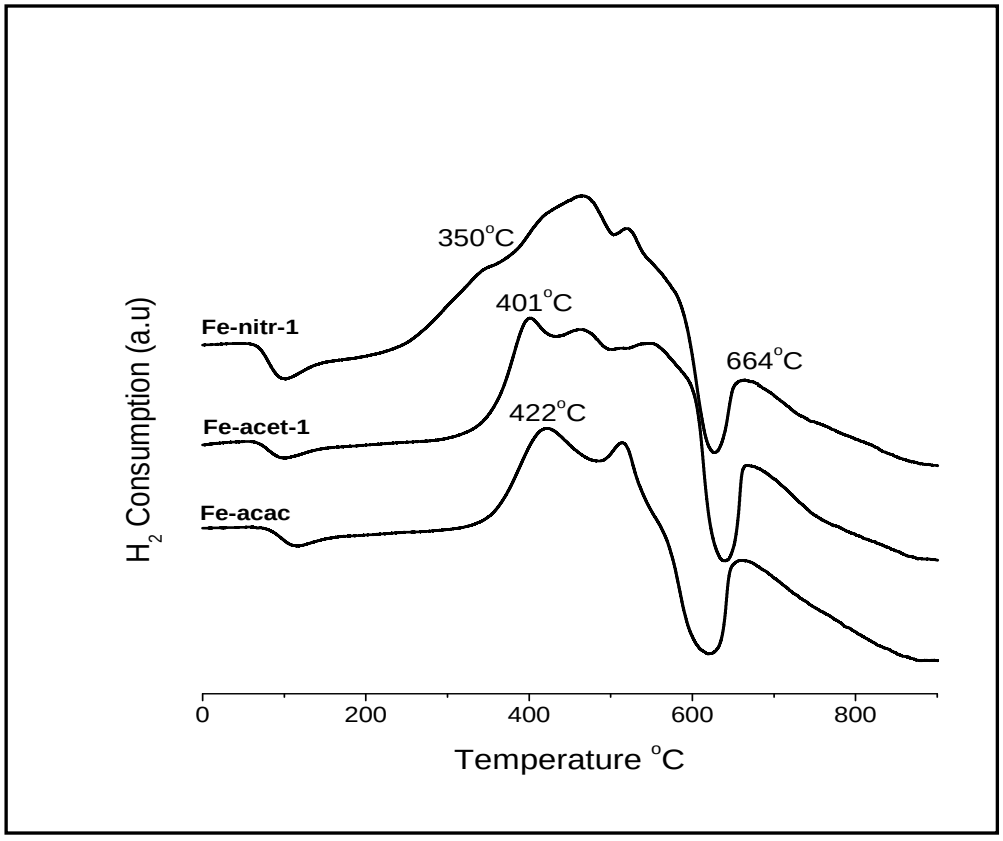


Figure 6.15: TPR profiles of Fe/CNT catalysts prepared using acetone as the solvent.

6.4 Fischer-Tropsch synthesis

The performance of the iron catalysts (prepared using different precursors and solvent) in the Fischer-Tropsch synthesis was tested in a fixed-bed micro reactor. All the reactions were performed under a set of standard conditions (275^{o}C, 8 bar, 2400 h^{-1}, H_2 : CO = 2) as established from preliminary experiments [24, 33]. Based on the temperature at which FTS was conducted in this study, no gasification of CNTs should occur. A blank FTS run was performed on the purified CNTs-support (no iron loaded) under the same operating conditions as used for the iron loaded catalysts. In the blank reaction, the product that formed at very low conversion (<3% CO conversion) was methane with almost no other hydrocarbons formed. This result implies that the residual iron particles from the CNT synthesis after acid treatment of the CNTs have little impact on the FTS reaction.

The percentage CO conversion as a function of time on stream for Fe-acet, Fe-nitr and Fe-oxal catalysts is shown in Figure 6.16. The activity for all the iron catalysts studied was initially low but increased significantly and the catalysts reached their highest activity within 10 h on stream. Thereafter, they remained stable for the entire run (120 h). There is no obvious evidence of deactivation for all these catalysts within 120 h. The stability of the catalyst may be attributed to the initial presence of functional groups on the CNTs which act as anchoring sites for the iron particles. The catalyst activity, under similar reaction conditions, increased in the order: Fe-acet ≤ Fe-oxal < Fe-nitr. The difference in activity is generally related to the difference in catalyst reducibility, dispersion and active sites available for FTS. The Fe/CNT prepared from the nitrate precursor gave enhanced selectivity towards higher molecular weight products which is often desirable in FTS. The olefin to paraffin ratio was very poor for all the catalysts studied. The CO_2 production rates, under fixed FTS conditions, increased in the order: Fe-oxal < Fe-acet < Fe-nitr.

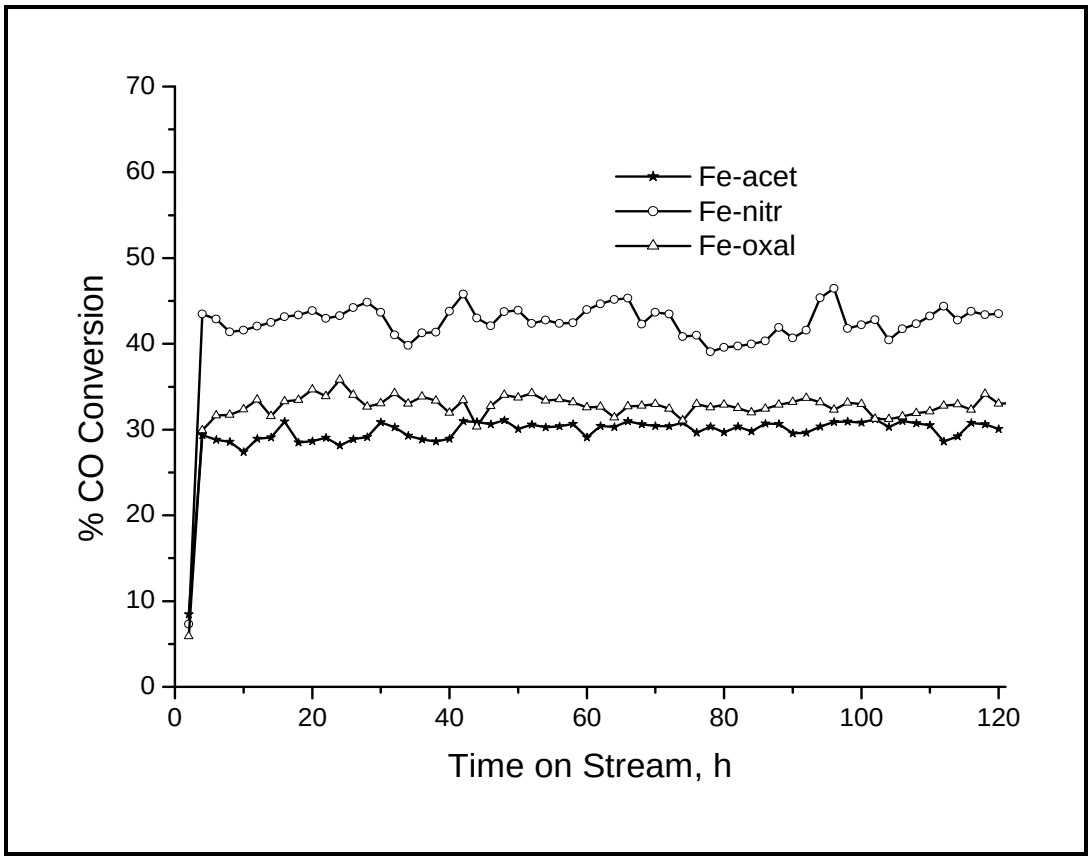


Figure 6.16: CO conversion as a function of time on stream.

Table 6.6 summarizes the results obtained from the FT reaction for the Fe/CNT catalysts. It can be seen that the performance of the various catalysts during the FT reaction is quite different. The difference in catalyst performance is attributed to the different types of interactions that exist between the Fe precursor and the support and the possible difference in particle size. It can be concluded that the metal precursor has an effect on the catalyst activity and selectivity during FTS. In a similar study but with a different active metal (Co) and support (TiO_2), Kraum et al. [11] have shown that the type of cobalt precursor used for the preparation of TiO_2 supported catalysts affects activity and chain growth probability under fixed FTS conditions.

Table 6.6: Activity and selectivity of iron catalysts supported on CNTs (prepared using water as solvent) in FTS[a]

Catalyts	Fe-acet	Fe-nitr	Fe-oxal
TOS (h)	120	120	120
% CO Conversion	29.5	46.4	32.3
$10^6 \times$ CO rate[b]	1.10	1.79	1.16
$10^6 \times CO_2$ rate (WGS)	0.49	0.99	0.36
$10^6 \times$ FTS rate	0.61	0.80	0.80
Activity (μmol/s.gFe)	22.0	35.8	23.2
Selectivity (mol % C)			
C_1	44.1	29.1	34.2
C_2-C_4	18.7	13.5	40.6
C_{5+}	37.2	57.4	25.2
O/O+P ratio[c]	0.036	0.023	0.050
CO_2 (% produced)	4.08	9.36	3.13

[a]Conditions: 8 bar, 275 ^oC, CO:H_2 = 1:2, GHSV = 2400 h^{-1}

[b] Rate are expressed in mol/s.

[c] $C_3^=/(C_3^=+C_3)$.

Figure 6.16 below shows the percentage CO conversion as a function of time on stream for the catalysts prepared using acetone as the solvent and the summary of the calculated parameters are presented in Table 6.7. It can be seen that apart from Fe-acet-1, all the other catalysts have the same CO conversion. The CO conversion and activity of Fe-acet-1 and Fe-nitr-1 improved over that of their counterparts prepared using de-ionised water. These findings suggest that the solvent used influences the catalysts' preparation and in turn increases the performance during FTS, probably as a result of more active sites being created. The dispersion of metal particles on the support is probably enhanced when acetone is used as solvent.

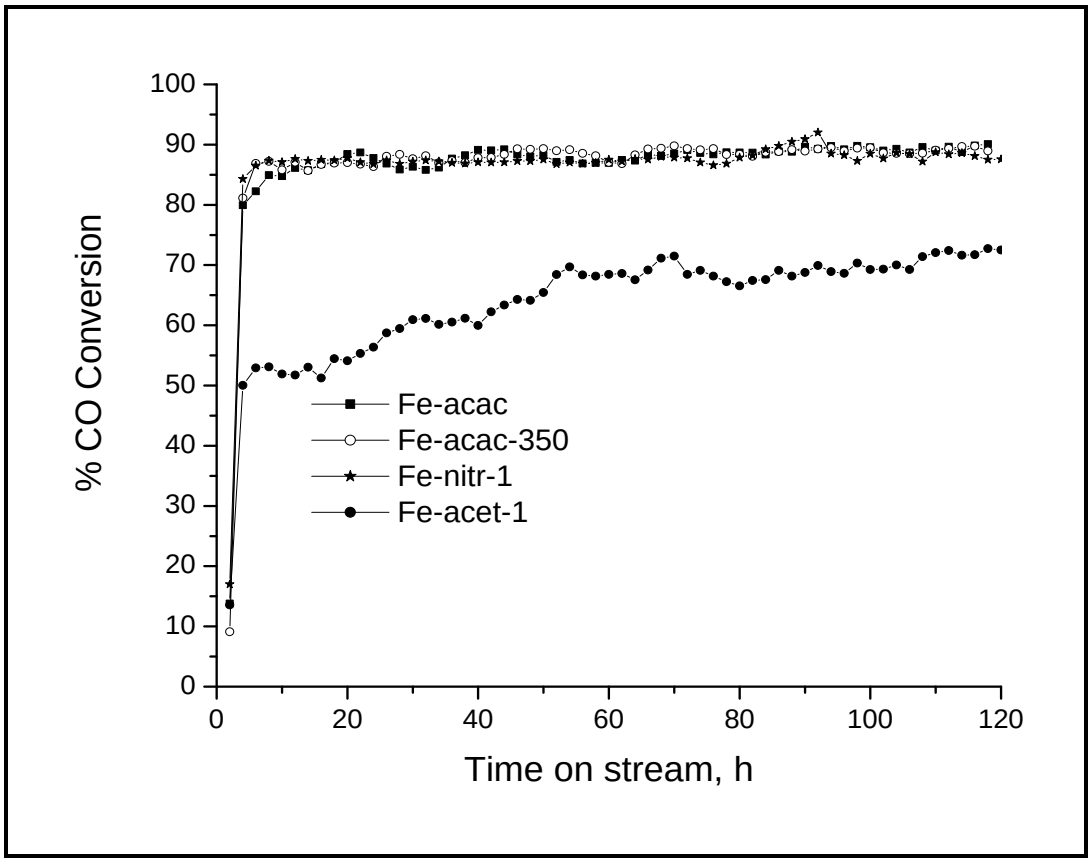


Figure 6.16: CO conversion with time on stream for catalysts prepared using acetone as solvent.

Table 6.7: FTS[a] activity and selectivity of iron catalysts supported on CNTs prepared using acetone as a solvent.

Catalyts	Fe-acac	Fe-acac-350	Fe-acet-1	Fe-nitr-1
Calcination Temp ^{o}C	250	350	250	250
TOS (h)	120	120	120	120
% CO Conversion	88.0	88.3	69.0	87.7
$10^6 \times$ CO rate[b]	3.73	3.23	2.54	4.03
$10^6 \times CO_2$ rate (WGS)	2.09	1.82	1.37	2.23
$10^6 \times$ FTS rate	1.64	1.41	1.17	1.80
Activity (µmol/s.gFe)	74.6	64.6	50.8	80.6
Alpha (α)	0.64	0.54	0.67	0.69
Selectivity (mol C %)				
C_1	29.9	38	25.0	18.8
C_2-C_4	27.9	29.7	25.3	30.1
C_{5+}	42.2	31.9	49.8	51.1
O/O+P ratio[c]	0.11	—[d]	0.19	0.17
CO_2 (% produced)	20.3	17.4	13.3	19.8

[a]Conditions: 8 bar, 275 ^{o}C, CO:H_2 = 1:2, GHSV = 2400 h^{-1}.
[b] Rate are expressed in mol/s.
[c] $C_2^{=}/(C_2^{=}+C_2)$.
[d]Not detected.

When comparing data for Fe-acac, Fe-acac-350 and Fe-nitr-1 which were recorded at the same conversion level, it is clear that Fe-nitr-1 is a better catalyst: It has the highest FTS rate and is less selective toward methane. The chain growth probability and the olefin to paraffin ratio are also high for Fe-nitr-1. The CO_2 production rate is similar for Fe-acac and Fe-nitr-1 which means that these catalysts are active for the water gas shift reaction. The higher selectivity of Fe-nitr-1 catalyst toward C_{5+} results from the lower rate of H_2 adsorption. It is known that H_2 adsorption is responsible for chain termination. The less H_2 adsorbed on the surface of the catalyst, the longer the hydrocarbons chain formed and the higher the α-olefin content. Fe-acac-350 had

similar CO conversion as Fe-acac but was more selective towards lower molecular weight product. The difference in the activity and selectivity of the two catalysts is attributed to the difference in the particle size.

6.5 Catalyst characterization after FTS

TEM images of the Fe-nitr-1 catalyst after 12 h (steady state condition) and after 120 h on stream were compared (Figures 6.17 and 6.18). It was interesting to note that the catalyst particle size increased significantly during the first 12 h of the reaction and this is attributed to the catalyst structural changes under FTS conditions. Further increase in the average particle size distribution after prolonged synthesis time (120 h) was noted. The further increase in the size of the particle is due to sintering of the catalyst particle during FTS. TEM image of the Fe-acet catalyst after 120 h time on stream is also presented (Figure 6.19). It was observed that all the catalysts prepared have the similar average particle size after 120 h time on stream (Table 6.8).

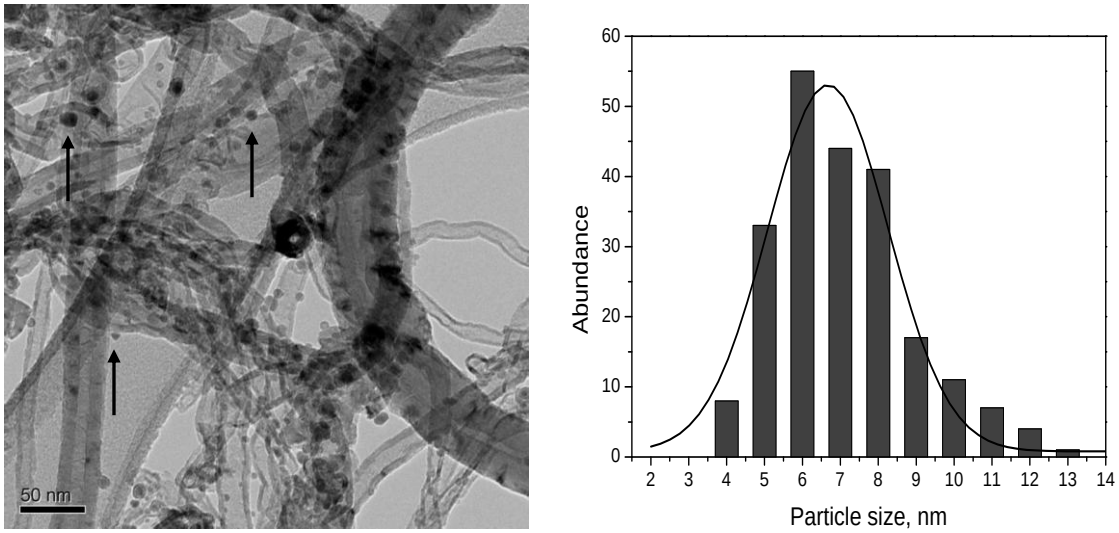


Figure 6.17: TEM image with arrows indicating the Fe particles, and Fe particle size histogram for the Fe-nitr-1 after 12 h time on stream (particle size: 5-10 nm).

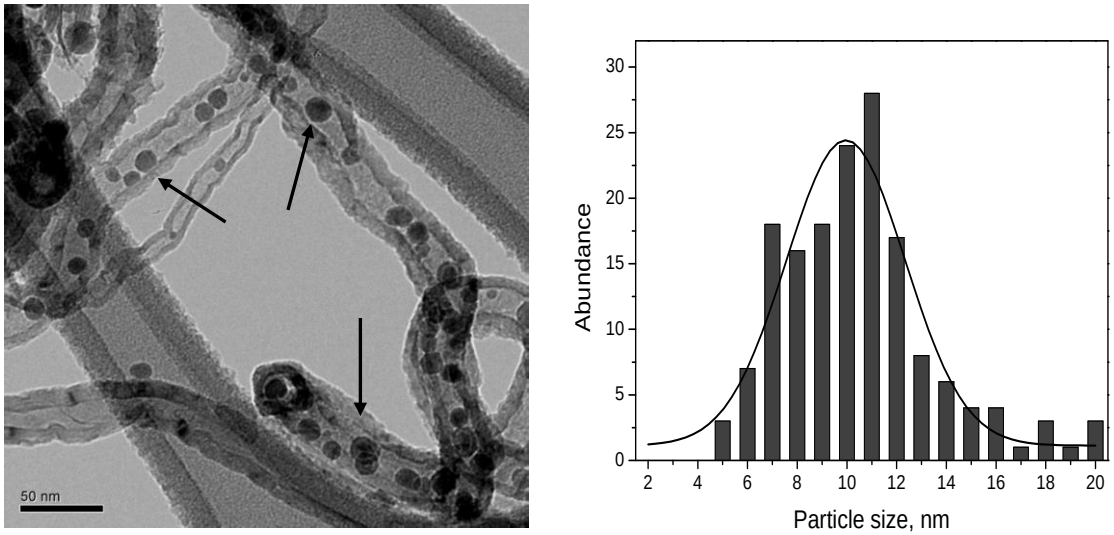


Figure 6.18: TEM image with arrows indicating the Fe particles, and Fe particle size histogram for the Fe-nitr-1 after 120 h time on stream (particle size: 7-14 nm).

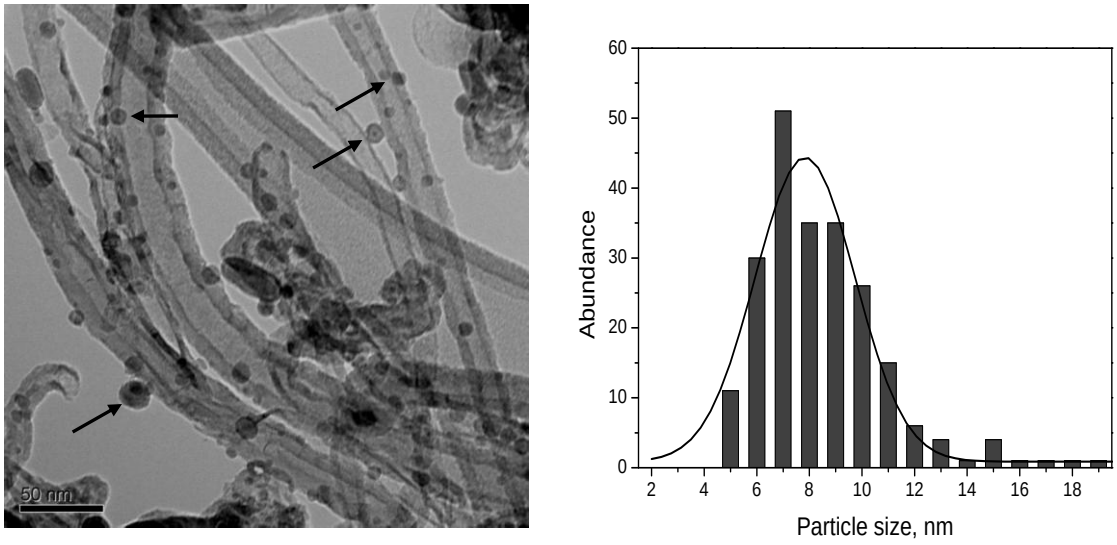


Figure 6.19: TEM image with arrows indicating the Fe particles, and Fe particle size histogram for the Fe-acet after 120 h time on stream (particle size: 5-12 nm).

Table 6.8: Particle size comparison

Catalyst	Fe Particle size, nm		
	TEM (Before FTS)	TEM after 12 h TOS[a]	TEM after 120 h TOS
Fe-acet	3-5	—[b]	5-12
Fe-nitr	4-7	—	6-13
Fe-oxal	5-12	—	6-15
Fe-acet-1	2-5	—	6-11
Fe-nitr-1	2-5	5-10	6-12
Fe-acac	2-5	—	5-11
Fe-acac-350	4-8	—	7-12

[a]Time on stream

[b]data not measured

6.6 Conclusion

The effect of precursor and solvent used in the preparation of iron supported on CNTs catalysts has been investigated by TEM, TGA, TPR, BET and XRD. The Fe/CNT catalysts have been tested for CO hydrogenation activity in a fixed-bed micro reactor. It was found that all the catalysts were stable after 12 h for the entire duration of the test (120 h) and the average particle size of the catalysts after 120 h time on stream were found to be very similar. It was also interesting to note that the average Fe particle size responsible for the catalyst performance during FTS ranged from 5 to 10 nm (size obtained after ~12 h time on stream). For the catalysts prepared by dissolving the precursors in de-ionised water, the activity increased in the order Fe-acet ≤ Fe-oxal < Fe-nitr. The precursor salts used in the preparation of the catalyst has an influence on the catalyst performance. The counter-ions probably play a role in the way the active metal interacts with the support thereby affecting the metal particle

size, the reducibility and the dispersion, which in turn affect the catalyst performance in the FTS. The mechanism by which the counter-ions affect the active metals deposition onto the support is not well understood. The solvent used in the preparation of the catalyst also has an effect on the properties of the final catalysts. The choice of the solvent did influence the metal dispersion, catalyst particle size, catalyst reducibility and active site availability. Improvements in metal dispersion created more active metal site available for FTS reaction and as a result enhanced the catalyst activity. Catalysts prepared using acetone exhibited better performance during FTS.

6.7 References

[1] M.E. Dry, Catalysis Letters 7 (1990) 241.

[2] H. Schulz, Applied Catalysis A, General 186 (1999) 3.

[3] S.T. Sie, Reviews in Chemical Engineering 14 (1998) 109.

[4] M.A. Vannice, Journal of Catalysis 50 (1997) 228.

[5] R.L. Espinoza, A.P. Steynberg, B. Jager, A.C. Vosloo, Applied Catalysis A: General 186 (1999) 13.

[6] M.E. Dry, In: Anderson J. R. Boudart M (Eds) Catalysis Science and Technology, Vol 1 Berlin: Springer-Verlap (1981) 159.

[7] E. Iglesia, S.C. Reyes, R.J. Madon, S.L. Soled, Advances in Catalysis 39 (1993) 221.

[8] E. de Smit, B.M. Weckhuysen, Chemical Society Reviews 37 (2008) 2758.

[9] W. Ngantsoue-Hoc, Y. Zhang, R.J. O'Brien, M. Luo, B.H. Davis, Applied Catalysis A: General 236 (2002) 77.

[10] J.A.L. Lodya, T. Seda, A.M. Strydom, S.S. Manzini, in: Anonymous , Characterization of Fe/C catalysts supported on Al_2O_3, SiO_2 and TiO_2, Journal of Physics: Conference Series, IOP Publishing, 2010, p. 082016.

[11] M. Kraum, M. Baerns, Applied Catalysis A: General 186 (1999) 189.

[12] T. Chronis, "A Fischer-Tropsch study of Co/Ru Catalysts" PhD thesis, University of the Witwatersrand, Johannesburg (1999).

[13] H. Xiong, M. Moyo, M.A.M. Motchelaho, L.L. Jewell, N.J. Coville, Applied Catalysis A: General (2010).

[14] G.L. Bezemer, J.H. Bitter, H.P. Kuipers, H. Oosterbeek, J.E. Holewijn, X. Xu, F. Kapteijn, A.J. van Dillen, K.P. de Jong, Journal of the American Chemical Society 128 (2006) 3956.

[15] H. Xiong, M.A.M. Motchelaho, M. Moyo, L.L. Jewell, N.J. Coville, Journal of Catalysis (2010).

[16] E.I. Mabaso, E. van Steen, M. Claeys, DGMK Tagungsbericht 4 (2006) 93.

[17] V.K. Jones, L.R. Neubauer, C.H. Bartholomew, Journal of Physical Chemistry 90 (1986) 4832.

[18] J.Y. Park, Y.J. Lee, P.K. Khanna, K.W. Jun, J.W. Bae, Y.H. Kim, Journal of Molecular Catalysis A: Chemical 323 (2010) 84.

[19] S.D. Mhlanga, K.C. Mondal, R. Carter, M.J. Witcomb, N.J. Coville, South African Journal of Chemistry 62 (2009) 67.

[20] M.C. Bahome, L.L. Jewell, D. Hildebrandt, D. Glasser, N.J. Coville, Applied Catalysis A, General 287 (2005) 60.

[21] M.L. Toebes, J.M.P. van Heeswijk, J.H. Bitter, A. Jos van Dillen, K.P. de Jong, Carbon 42 (2004) 307.

[22] E. van Steen, F.F. Prinsloo, Catalysis Today 71 (2002) 327.

[23] D. Barkhuizen, I. Mabaso, E. Viljoen, C. Welker, M. Claeys, E. van Steen, J.C.Q. Fletcher, Pure and Applied Chemistry 78 (2006) 1759.

[24] K. Jalama, "Fischer-Tropsch over supported cobalt catalysts: effect of ethanol addition, precursors and gold doping", PhD thesis, University of the Witwatersrand, Johannesburg (2008).

[25] W. Chen, Z. Fan, X. Pan, X. Bao, Journal of the American Chemical Society 130 (2008) 9414.

[26] R.M.M. Abbaslou, A. Tavasoli, A.K. Dalai, Applied Catalysis A: General 355 (2009) 33.

[27] S.D. Mhlanga, "Synthesis and study of carbon nanotubes and carbon spheres" PhD thesis, University of the Witwatersrand, Johannesburg (2009).

[28] M. Moseler, F. - , A.C. Ferrari, ACS Nano (2010) 88.

[29] S. Kundu, Y. Wang, W. Xia, M. Muhler, Journal of Physical Chemistry C 112 (2008) 16869.

[30] P. Serp, M. Corrias, P. Kalck, Applied Catalysis A, General 253 (2003) 337.

[31] M.A.M. Motchelaho, H. Xiong, M. Moyo, L.L. Jewell, N.J. Coville, Journal of Molecular Catalysis A: Chemical 335 (2011) 189.

[32] H. Hayakawa, H. Tanaka, K. Fujimoto, Applied Catalysis A: General 310 (2006) 24.

[33] M.C. Bahome, "Synthesis and use of carbon nanotubes as a support for the Fischer-Tropsch Synthesis" PhD thesis, University of the Witwatersrand, Johannesburg (2008).

7

Chapter Seven

Fe/CNT catalyzed Fischer-Tropsch synthesis: effect of group 1 alkali promoters

7.1 Introduction

The Fischer-Tropsch synthesis is a carbon chain building reaction that is known to give a wide product distribution described by the Anderson-Schultz-Flory model [1]. It is possible to alter this distribution to favour certain parts of the product spectrum through the use of promoters [2]. Promoters are a subject of great interest in catalyst research due to their remarkable influence on the activity, selectivity and stability of industrial catalysts [3]. Typical iron-based catalysts contain varying amounts of structural and chemical promoters known to increase the overall FTS activity or to facilitate the reduction of iron oxide to metallic iron during hydrogen activation [4, 5]. A promoter is regarded as a component of the catalyst that does not take part in the reaction, but changes the catalytic properties of the catalyst [2, 3]. It has been

shown that promoting Fe catalysts with group 1 alkali metals has a strong influence on the product selectivity, and that other promoters have a lesser influence [6]. The basicity of the alkali metals is one of the reasons for the significant influence of these metals on the catalyst performance during FTS; it has been shown that, for equivalent amounts of alkali present the basicity of the reduced catalysts increased in the order Li < Na < K< Rb [7]. The more basic the alkali metal, the more readily it can donate its electrons to the metal (Fe) and facilitate CO chemisorption, since CO tends to accept electrons from iron [8]. Alkali metals strengthen the Fe-C bond and weaken the Fe-H bond [9-11]. Alkali promoted Fe catalysts suppress the formation of methane and the amount of methane produced during FTS decreases as the surface basicity increases [7, 12].

Promoters, especially K-promoted catalysts, have been shown to either increase or decrease the activity of Fe-based FTS catalysts [13], and to promote the selective formation of C_2-C_5 olefins on alumina-supported Fe catalysts [14]. Ngantsoue-Hoc et al. [5] studied the impact of the group 1 alkali metals upon the activity and selectivity of a precipitated iron-silica catalyst and they reported that the relative impact of the alkali metal depends upon the conversion level with potassium being the promoter that has the highest impact on the activity at all conversion levels. Their results also showed that Na and K exhibit much higher WGS rates than the other alkali promoted catalysts. A similar study by An et al. [15] compared the effect of a K or Na promoted $FeCu/SiO_2$ catalysts and they found that the addition of K or Na can improve the catalytic activity during FTS and shift the product distribution to heavy hydrocarbons to different extents. Alkali promoters have been shown to be very important but data to document their relative influence during FTS synthesis are not abundant [5]. Moreover, most of the alkali-promoted Fe-based catalysts available in the literature were obtained with precipitated or co-precipitated Fe/silica catalysts. A literature survey revealed that, in terms of carbon nanomaterials (CNTs, CNFs or CSs) as support, the most widely studied group 1 alkali promoter is potassium [16-19]. Bahome et al. [17] investigated the promotion of carbon nanotube-supported iron

catalysts by potassium. Fischer-Tropsch synthesis (conditions: 8 bar, 275^{o}C, CO/H_2 ratio of 1:2) results revealed that the potassium promoted catalyst was very active for the water gas shift reaction (higher yields of CO_2), less selective to methane and produced more olefins compared to the unpromoted catalysts. Similar observations were reported by Xiong et al. [19].

The focus of this study is to investigate the influence of alkali promoted Fe/CNT catalysts on the Fischer-Tropsch synthesis. We herein present preliminary results obtained when group 1 alkali metals (Li, Na, K) were used as promoters for CNT supported Fe-based FT catalysts. The amount of promoter was not optimized. The focus here is on a comparative study of the effect of equimolar amounts of alkali metals on an Fe Fischer-Tropsch catalyst.

7.2 Experimental section

Carbon nanotubes were synthesized by the catalytic decomposition of acetylene at 700^{o}C over a bimetallic Fe-Co catalyst supported on $CaCO_3$. A more detailed description of the experimental procedure for the synthesis of this bimetallic catalyst as well as the CNT synthesis was given in Chapter 5 and will not be repeated here. The as-grown CNTs were refluxed in 55% HNO_3 at 120^{o}C for 2 h in order to remove residual catalyst and to functionalize the CNT surface. These purified and functionalized CNTs were used as the catalyst support in this study.

The alkali promoted FT catalysts supported on CNTs were prepared by the deposition-precipitation method using urea as described elsewhere [16, 17]. The Fe-Li/CNT, Fe-Na/CNT and Fe-K/CNT catalysts were prepared in such a way that the molar ratio was kept constant at a ratio of 100 : 3.4 moles of Fe/promoter. The catalyst will be described as 100 Fe-3.4A/CNT (where A = Li, Na or K) in this study. A 100Fe/CNT unpromoted catalyst was also prepared and used as the reference

catalyst. The nitrate salts of Fe and the alkali promoters were used during the preparation because they mixed easily in aqueous solution and the nitrates are readily removed without undesired residues being left on the catalyst after calcination [20]. Typically, $Fe(NO_3)_3.9H_2O$ (1.44 g) and urea (0.32 g; 1.5 moles urea per mole of iron) were dissolved in de-ionised water (20 ml). To this Fe solution was added $LiNO_3$ (0.0083 g, 0.04 wt.% Li), or $NaNO_3$ (0.0101 g, 0.14 wt.% Na) or KNO_3 (0.012 g, 0.23 wt.% K) and the resulting mixture was added dropwise to the carbon nanotube support (2 g) slurried in de-ionised water (20 mL). After allowing about 2 h for the hydrolysis of the urea at 90^{o}C, the sample was dried by evaporating the excess solvent at 90^{o}C. The different catalysts prepared were further dried in an oven (120^{o}C, in static air overnight) and then heat-treated in nitrogen at 250 ^{o}C for 150 min in order to decompose the nitrates. Additionally, 100Fe-12Na/CNT and 100Fe-24Na/CNT were also prepared by following the procedure described above. Table 7.1 below gives a summary of the catalysts prepared.

TEM, XRD, TGA, BET and TPR techniques were used to characterize the CNTs, as well as the promoted and unpromoted Fe/CNT catalysts. All characterization analyses were performed according to standard procedures as described in Chapter 4. The catalysts' performance during FTS was tested using a fixed-bed micro reactor. A detailed description of the experimental set-up and procedures has been given in Chapters 3 and 4 and will not be repeated here.

Table 7.1: Summary data of the catalysts prepared

Catalysts	Mass of Fe salt (g)[a]	Mass of alkali salt (g)[b]	Mass of CNT support (g)	Calculated molar ratio (Fe:alkali)	Promoter wt. %
100Fe/CNT	1.44	—	2	—	—
100Fe-3.4Li/CNT	1.44	0.0083	2	100 : 3.38	0.042
100Fe-3.4Na/CNT	1.44	0.010	2	100 : 3.35	0.14
100Fe-3.4K/CNT	1.44	0.012	2	100 : 3.31	0.23
100Fe-12Na/CNT	1.44	0.037	2	100 : 12.4	0.51
100Fe-24Na/CNT	1.44	0.074	2	100 : 24.3	1.00

[a] $Fe(NO3)_3 \cdot 9H_2O$
[b] $LiNO_3$ or $NaNO_3$ or KNO_3

7.3 Results and discussion

7.3.1 Effect of alkali promotion (Li, Na, K)

TEM analysis

Figures 7.1a and 7.1b show the TEM and HRTEM images of the as-grown CNTs; where the morphology and the structure can clearly be seen. The CNTs produced are multiwalled carbon nanotubes with outer diameters ranging from 20 to 40 nm, and length ranging from hundreds of nanometers to micrometers. Since the as-grown CNTs contained some non-carbonaceous materials (residual growth reagents), purification is an essential step to remove the non-carbon materials. In the process, the CNTs are functionalized and as a result become less hydrophobic. Figures 7.2a and 7.2b show the TEM and SEM images of the purified CNTs. It is clearly seen from TEM images (Figure 7.2a) that the CNT surface is roughened upon purification.

This roughness is required for the preparation of stable metal catalysts since they act as additional anchoring sites for the catalyst particles [21, 22]. Residual metal in the form of encapsulated particles (Figure 7.1a) are generally not removed in the acid washing.

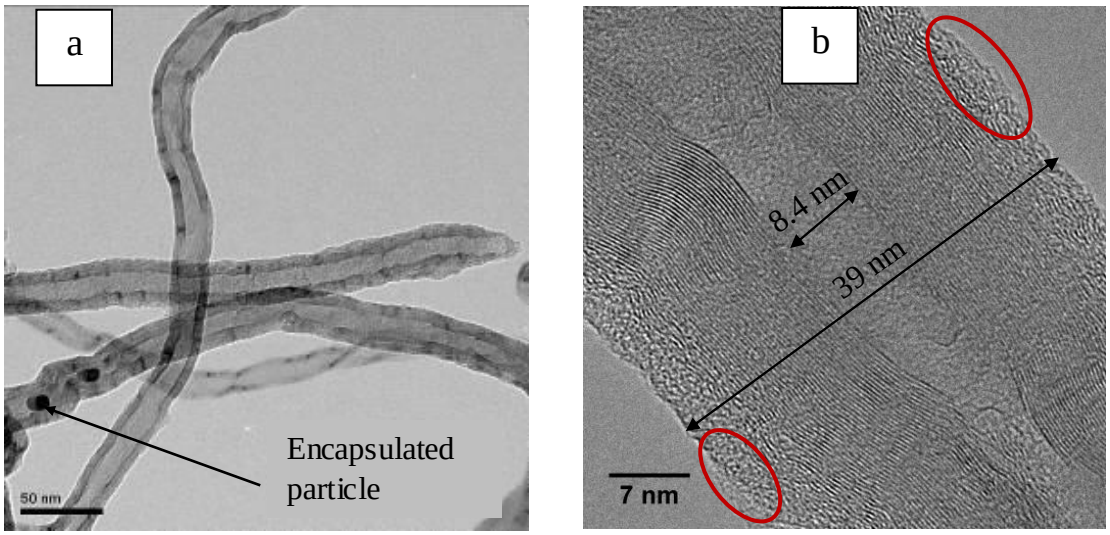


Figure 7.1: CNTs as-grown - a) TEM, b) HRTEM with red oval representing amorphous carbon.

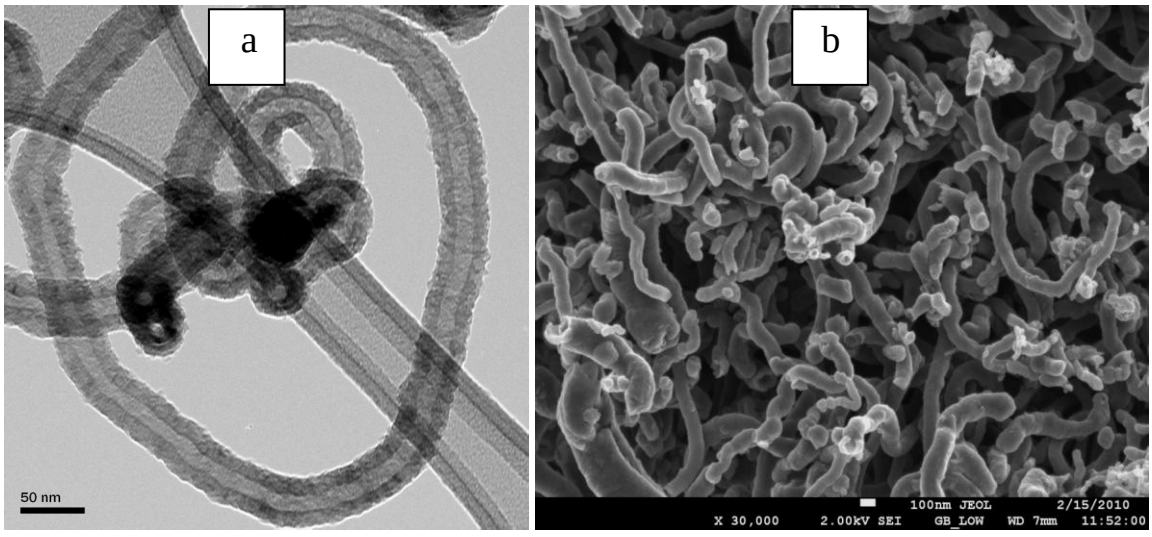


Figure 7.2: Purified CNTs a) TEM, b) SEM

Fe-based catalysts (promoted and unpromoted) were prepared by a deposition precipitation method using urea as a precipitating agent. A TEM image and an EDX spectrum of the fresh, unpromoted catalyst is presented in Figure 7.3. Small Fe particles can be seen dispersed on the surface of CNTs and some are indicated using an arrow (Figure 7.3a and b). The presence of Fe on the surface of the CNT is also confirmed by an EDX spectrum (Figure 7.3c). TEM images of Li and Na promoted Fe/CNT catalyst are presented in Figures 7.4 and 7.5 respectively. Figure 7.6 presents the TEM and EDX spectrum of the potassium promoted Fe catalyst. The presence of potassium could not be detected using EDX, probably due to the low levels of K used relative to the Fe. TEM images suggest no difference in the morphology of CNTs in the presence or absence of K (or Na or Li). From the TEM images, it can be determined that the addition of alkali promoter to the Fe/CNT catalyst caused a slight increase in the Fe particle size when compared to the unpromoted catalysts.

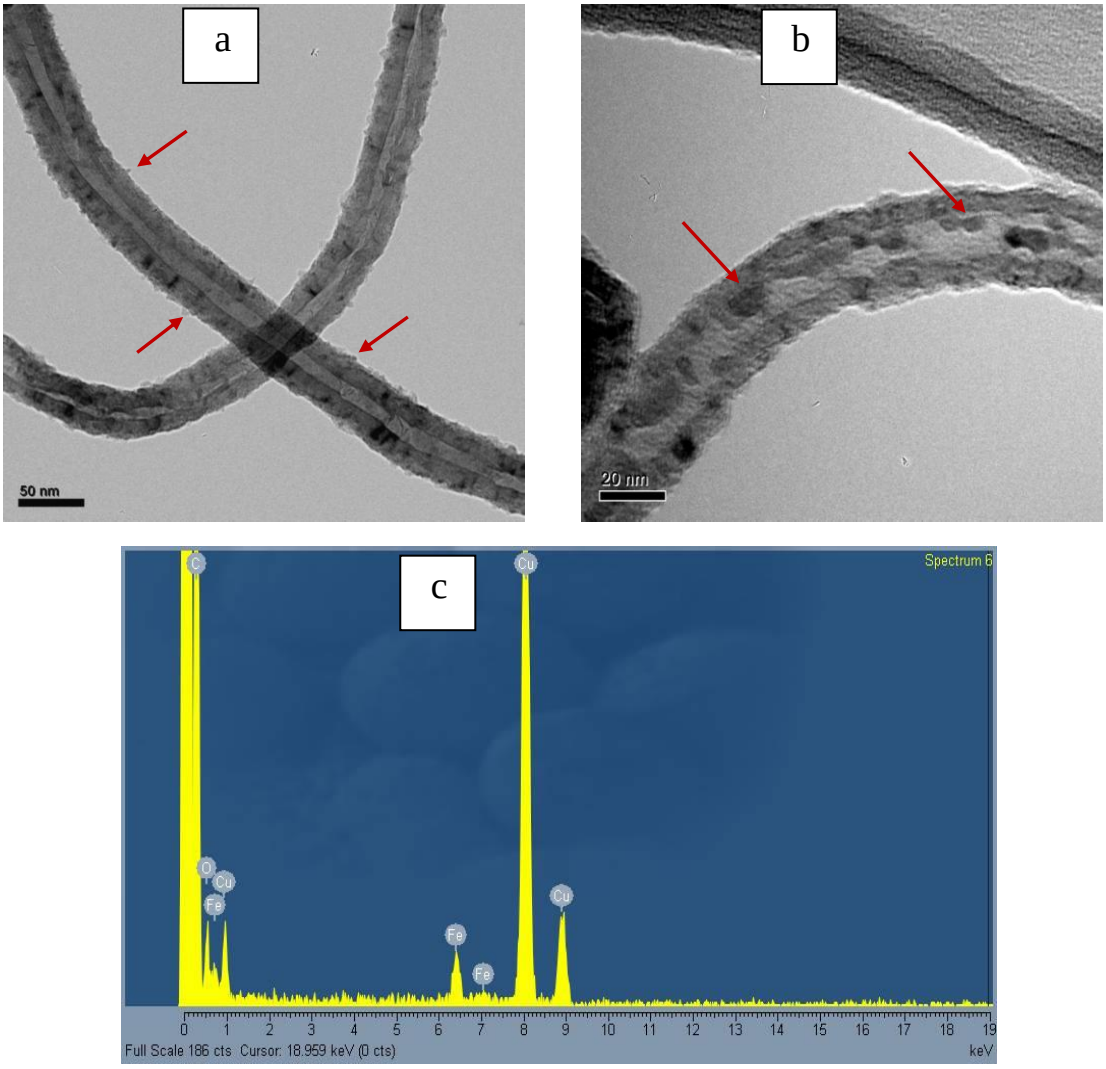


Figure 7.3: a) TEM image and b) EDX spectrum of unpromoted Fe/CNT catalyst with arrows indicating the Fe particles

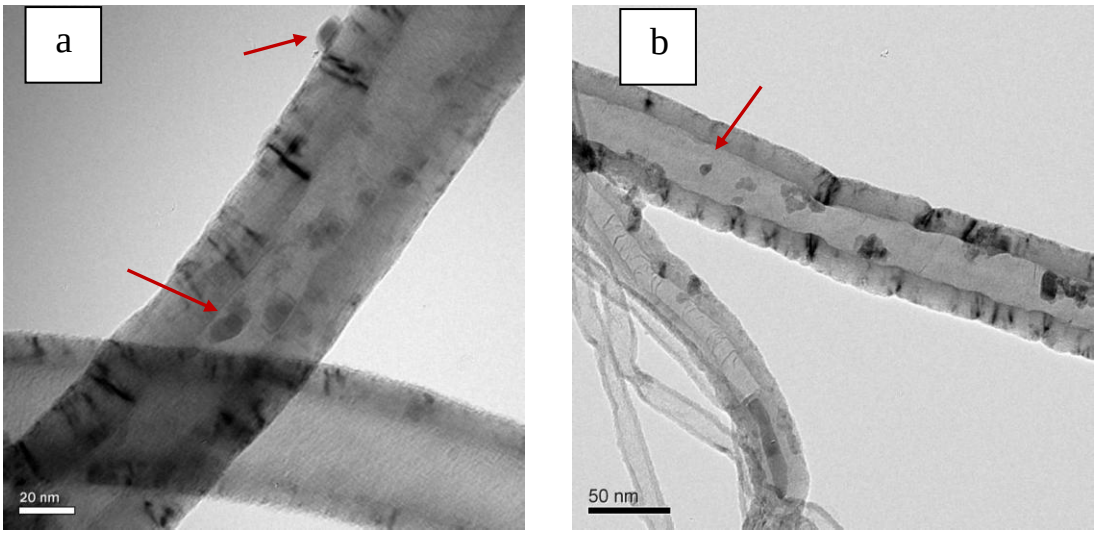


Figure 7.4: a) and b) TEM images of Li promoted Fe/CNT catalysts (100Fe-3.38K/CNT) with arrows indicating the Fe particles

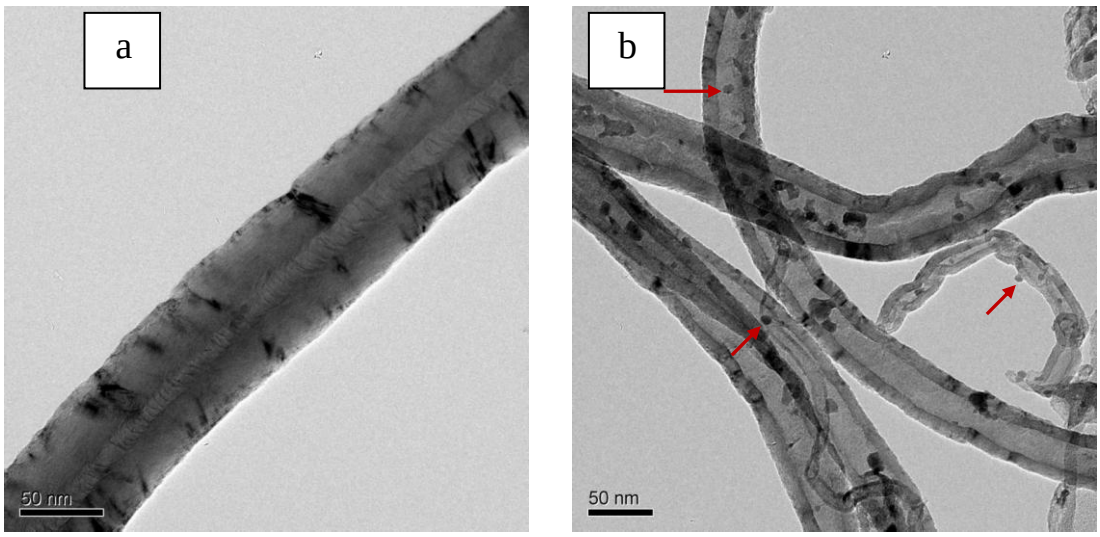


Figure 7.5: a) and b) TEM images of Na promoted Fe/CNT catalysts (100Fe-3.35K/CNT) with arrows indicating the Fe particles

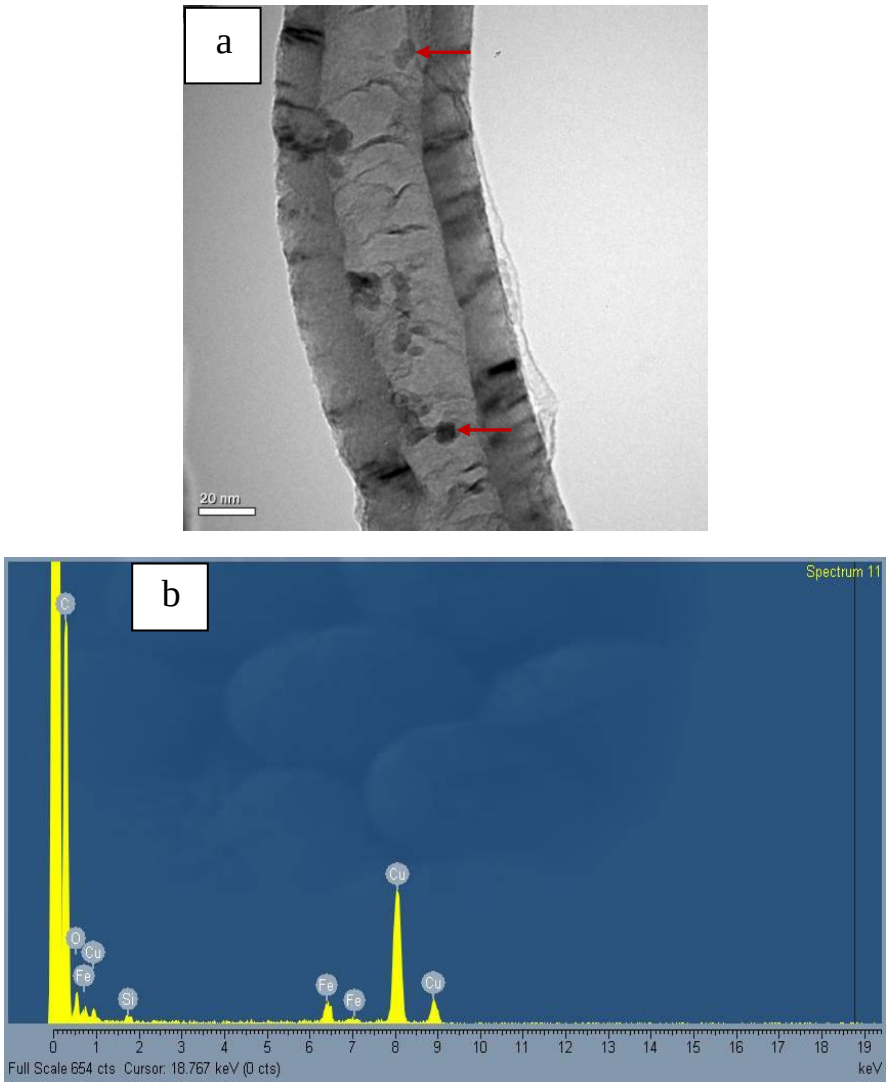


Figure 7.6: Potassium promoted Fe/CNT catalyst (100Fe-3.31K/CNT): a) TEM image with arrow indicating an Fe particle and b) EDX spectrum

Thermogravimetric analysis (TGA)

TGA was used to determine the thermal stability and the composition of the CNTs as well as the unpromoted and promoted Fe catalysts. TGA and DTA profiles (in an air atmosphere) of all the catalysts are shown in Figures 7.7a and b. The analysis shows that the unloaded CNTs are stable up to 500^{o}C with the majority of the materials oxidizing by 674^{o}C (half width information). The CNTs consist of about 99% carbonaceous materials and the remaining 1% is the residual encapsulated growth catalyst (Fe-Co) that could not be removed by acid treatment. Upon adding the active metal (iron) to the CNTs, the thermal stability of the catalyst decreased from 674^{o}C to 520^{o}C (Figure 7.7b) because the presence of iron aids/catalyses the oxidation of the CNTs [23]. There was no further decrease in the thermal stability upon adding the promoters. This result was expected because a very small amount of promoter was added to the catalyst. The ~ 10 wt. % difference after complete weight loss of the CNTs indicates the amount of iron on the support (Figure 7.7a (b)). The slight difference observed in the wt. % residual mass could be due to the mass of K, Na and Li.

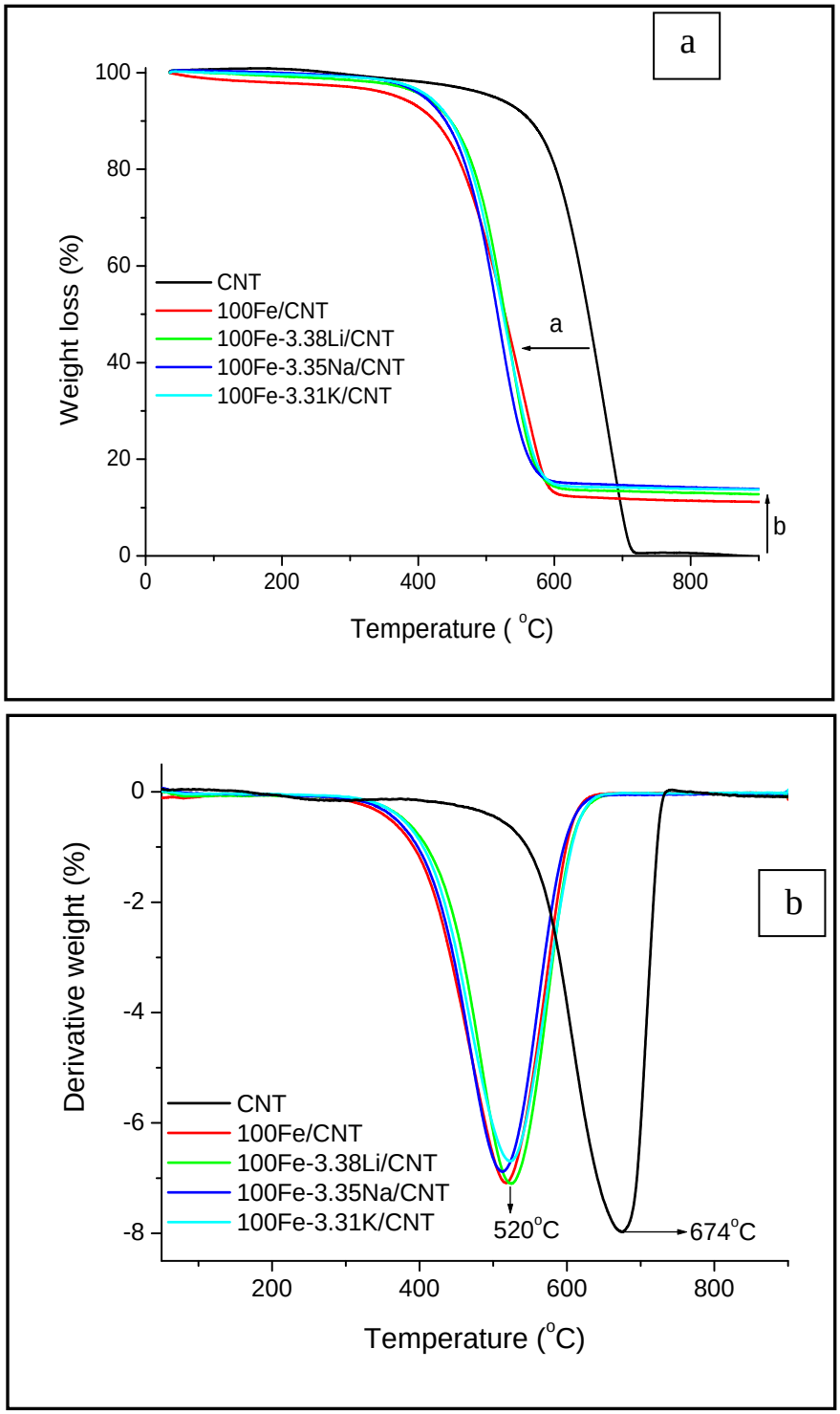


Figure 7.7: a) TGA and b) DTA of CNTs, and promoted and unpromoted Fe catalysts

Temperature programmed reduction (TPR)

H_2-TPR was used to investigate the effect of various group 1 alkali promoters (Li, Na, K) on the catalyst reducibility and the profiles are shown is Figure 7.8. It is worth mentioning again that the catalysts have the same number of moles of alkali. Four major peaks are present in each profile except that of the CNT where only one peak is present (peak 4). Peak 1 corresponds to the reduction of Fe_2O_3 to Fe_3O_4; peak 2 corresponds to the reduction of Fe_3O_4 to Fe; peak 3 is associated with the presence of small iron oxide particles that are difficult to reduce and peak 4 corresponds to the gasification of the CNTs in the presence of H_2 at elevated temperature (~ 600^{o}C) to produce methane [16]. The presence of the peak 1' is ascribed to the reduction of Fe_2O_3 found inside the tubes. It has been reported that Fe_2O_3 inside the tubes reduces at a lower temperature (301^{o}C) when compared to the Fe_2O_3 found on the outside of the tubes (339^{o}C) [24, 25].

The addition of the alkali promoters influenced the reduction behavior of the catalyst differently in each case. Li shifted the reduction peaks to slightly lower temperatures whereas Na and K shifted the peaks to higher temperature relative to the unpromoted Fe/CNT catalyst (Figure 7.8, Table 7.2). It can therefore be concluded that Li enhances the reducibility of the catalyst whereas Na and K inhibit its reduction. The retarded reduction of Na and K-promoted catalysts can be explained in terms of the strong interaction between sodium oxide and iron oxide as well as potassium oxide and iron oxide. This interaction could result in the suppression of H_2 adsorption on the catalyst surface [26].

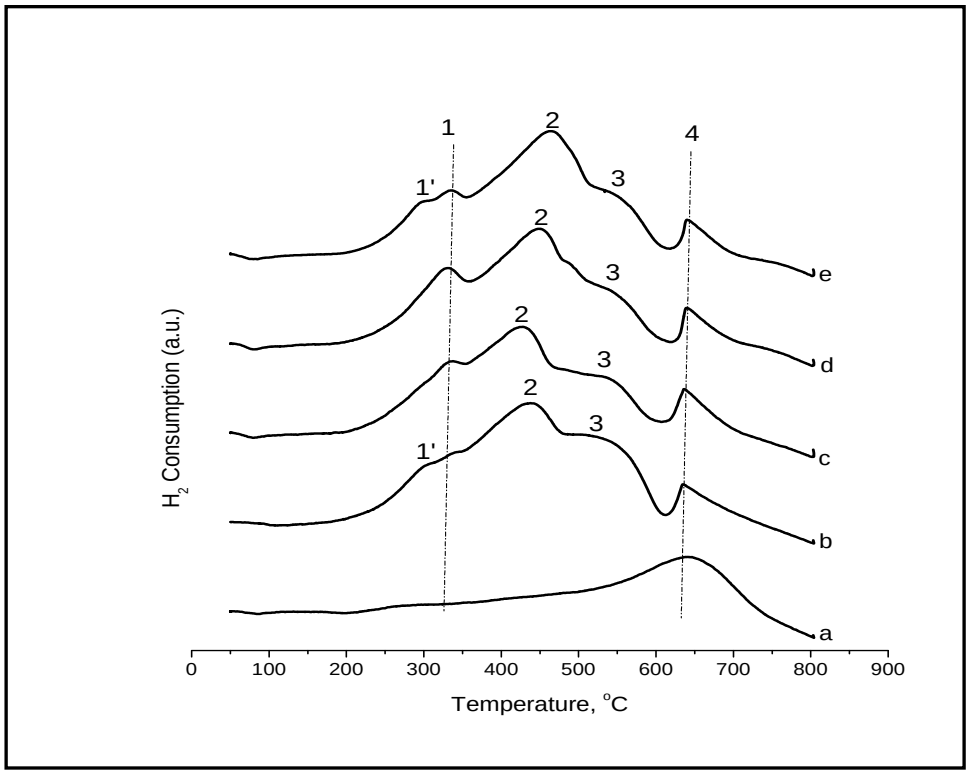


Figure 7.8: TPR profiles of the CNT, unpromoted and alkali-promoted Fe-catalysts: a) CNT support, b) 100Fe/CNT, c) 100Fe-3.38Li/CNT, d) 100Fe-3.35Na/CNT, e) 100Fe-3.31K/CNT.

Table 7.2: Temperature of the peak maxima at which each reduction steps occured during the H_2-TPR

	Temperature (^oC)		
Sample ID	$Fe_2O_3 \rightarrow Fe_3O_4$	$Fe_3O_4 \rightarrow Fe^o$	$CNT \rightarrow CH_4$
CNT	–	–	> 600
100Fe/CNT	301, 339	435	635
100Fe-3.38Li/CNT	334	426	637
100Fe-3.35Na/CNT	330	451	640
100Fe-3.31K/CNT	300, 338	466	640

X-ray diffraction (XRD) data

The powder X-ray diffraction patterns for the CNTs, unpromoted and alkali promoted Fe/CNT catalysts are shown in Figure 7.9 with the most pronounced lines indicated. The peaks appearing at 2θ values of 26°, 44.8° are present in all five XRD patterns and are characteristic of the graphitic walls of the CNTs [27]. The broad peak at a 2θ value of 43° is attributed to the presence of small amounts of carbides as well as residual catalyst from the CNT synthesis in the samples (Fe-Co, Fe_3C, Co_3C or Co_2C) [27]. The peaks at a 2θ of 30° and 33° correspond to the presence of the magnetite (Fe_3O_4) and hematite (Fe_2O_3) phases respectively and the peak at 35.5° is related to the presence of both hematite and magnetite phases.

The peak at 2θ value of 33° is the most intense peak of Fe_2O_3 in the XRD spectrum of the catalysts. Due to the low content of alkali promoters in the Fe/CNT catalyst, no peak was observed indicating the diffraction lines of lithium oxide, sodium oxide and potassium oxide. The iron oxide average crystallite size for the catalysts was measured using the line broadening of the peak at the 2θ value of 33° and the Scherrer equation. The data are presented in Table 7.3. The XRD data are in good agreement with TEM data.

The peak intensity of Fe_2O_3 in the alkali promoted samples is higher than that of the unpromoted catalyst and increases in the order Li ≤ Na ≤ K. It implies that the addition of alkali promoter to the Fe/CNT catalyst promotes the aggregation of Fe_2O_3 crystallites. This is consistent with the observed decrease in the promoted catalyst surface area.

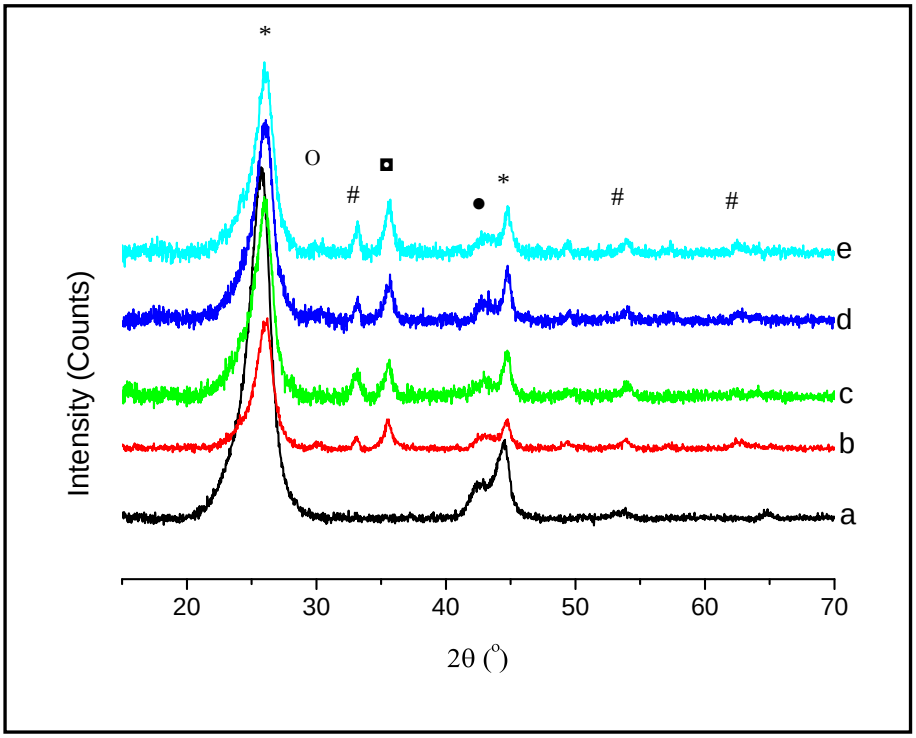


Figure 7.9: XRD patterns of CNTs, unpromoted and alkali promoted Fe/CNT catalysts: a) CNT support, b) 100Fe/CNT, c) 100Fe-3.38Li/CNT, d) 100Fe-3.35Na/CNT, e) 100Fe-3.31K/CNT; * = graphite; o = Fe_3O_4 ; # = Fe_2O_3; ◘ = Fe_2O_3 and Fe_3O_4; ● = Co-Fe, Fe_3C, Co_3C or Co_2C [19, 27].

Table 7.3: Iron particle size measured using XRD and for comparison TEM data are added.

	Fe_2O_3 average particle size, nm	
Catalyst	**TEM**	**XRD[a]**
100Fe/CNT	5-11	8.5
100Fe-3.38Li/CNT	7-13	12.7
100Fe-3.35Na/CNT	8-12	14.7
100Fe-3.31K/CNT	8-12	14.5

[a]Error ± 1 nm

Surface area and pore volume measurements

The surface area and pore volume of the CNTs, unpromoted (Fe/CNT) and alkali promoted Fe/CNT catalysts are presented in Table 7.4.

Table 7.4: BET surface area and pore volume of the CNT, unpromoted and promoted catalysts.

Sample ID	Surface area (m^2/g)[a]	Pore volume (cm^3/g)
CNT	105	0.35
Fe/CNT	123	0.28
100Fe-3.38 Li/CNT	106	0.31
100Fe-3.35 Na/CNT	92	0.27
100Fe-3.31K/CNT	89	0.30

[a]error bar ±5%

The presence of Li, Na and K clearly has an effect on the surface area relative to that of the unpromoted catalyst. The analysis of the BET results shows that the surface area decreased in the order 100Fe/CNT > 100Fe-3.38 Li/CNT > 100Fe-3.35Na/CNT ≥ 100Fe-3.31K/CNT and it is observed that the more basic the alkali added, the greater the loss in surface area (the basicity of the alkali increases in the order Li < Na < K [5, 20]). The pore volume however, is not affected by the addition of alkali promoters. TEM and XRD studies of the freshly prepared unpromoted and alkali-promoted Fe/CNT revealed that the promoted catalysts have larger Fe crystallites than the unpromoted catalyst hence the decrease in surface area could be due to crystallite growth and not pore blocking since the presence of alkali could improve the agglomeration of the iron precursor and as a result enlarge the crystallite size of iron oxide [28, 29].

Catalytic testing

The performance of the iron catalysts (promoted and unpromoted) in the Fischer-Tropsch synthesis was tested in a fixed-bed micro reactor. All the reactions were performed under a set of standard conditions (275^{o}C, 8 bar, 2400 h^{-1}, H_2 : CO = 2) as established from preliminary experiments [17]. The activities, stabilities and product selectivities were tested over a period of 72 h. A blank FTS run was first performed on the purified CNTs-support (no iron loaded) and the product formed at very low conversion (< 3% CO conversion) was methane with almost no other hydrocarbons formed. This result implies that the residual iron particles after acid treatment of the CNTs have little impact on the FTS product range.

The CO conversion was used as an indication of the overall Fischer-Tropsch activity. The % CO conversion as a function of time on stream is shown in Figure 7.10. The initial CO conversion for all the catalysts under investigation was initially low. However, it increased rapidly and stabilized within 12 h time on stream. The results obtained show that the CO conversion increased in the order 100Fe-3.31K/CNT < 100Fe/CNT < 100Fe-3.38Li/CNT < 100Fe-3.35Na/CNT. Under fixed operating conditions, the potassium promoted catalyst, 100Fe-3.31K/CNT shows the lowest fraction of CO transformed into hydrocarbon products; the lowest CO conversion observed may be due to K ions covering some of the Fe active sites or could also result from carbon deposition on the Fe-K surface, which leads to the formation of inactive carbon covering the active surface sites [8, 30].

The Na-promoted catalyst, 100Fe-3.35Na/CNT, exhibits the highest CO conversion. The 100Fe-3.35Na/CNT catalyst is more efficient in converting syngas to product than the other promoted or unpromoted catalysts when studied under similar FT conditions. The water-gas-shift reaction is an important side reaction during FTS because it generates hydrogen. Carbon monoxide can be converted either into hydrocarbon products and water (FTS) or into carbon dioxide and hydrogen (WGS).

The Na-promoted catalyst exhibits the highest water-gas shift rate. This means that Na can effectively be used as a promoter for an Fe/CNT catalyst that is used for the conversion of low hydrogen-containing feedstock.

The hydrocarbon product distribution of the catalysts studied is shown in Table 7.5. It can be seen that both potassium and sodium enhance the selectivity to olefins. The result also shows that the selectivity to methane decreases in the order unpromoted ≥ Li-promoted > K-promoted > Na-promoted catalyst, whereas the probability of chain growth (α) increased in the order Li-promoted ≤ unpromoted < K-promoted < Na-promoted catalyst. Several studies [5, 15, 31, 32] have indicated that the presence of alkali enhances the surface basicity of catalysts and as a result suppresses the selectivity to methane. It has been shown that the effectiveness of the alkali promoter decreases in the order Rb > K > Na > Li [33]. It is generally accepted that the effect of alkali promoters is to inhibit the hydrogenation steps [34]; alkali may act to reduce the availability of hydrogen, and modify the rate at which hydrogen adds to carbon [34]. It could also inhibit the mobility of H_2 by blocking the low-coordination edge and corner sites for dissociative adsorption of hydrogen [35]. Inhibition of the hydrogenation steps leads to a decrease in H_2 conversion, increase in selectivity towards longer chain hydrocarbons (implying increased chain growth probability) and increase in the olefin content as found in this investigation (Table 7.5). Previous studies in this area have revealed that K is a better promoter than Na [5, 15, 31, 32]. However, in the present study, Na seems to be a better promoter when compared to K. The change could result from the use of CNT as a support, the amount of the promoter used and/or the catalyst preparation method. A comparison of these two promoters at the same conversion level should be done in order to properly effectively assess their influence on the product distribution. Unfortunately, a comparison could not be made with the data available in the literature because the data are collected at different FT conditions or different Fe/promoter ratio or prepared on different supports using different catalyst preparation methods. It was noticed from this study that the potassium promoted catalyst appeared to be out of line

regarding the basicity aspect. The FT runs were repeated and results within experimental error were obtained.

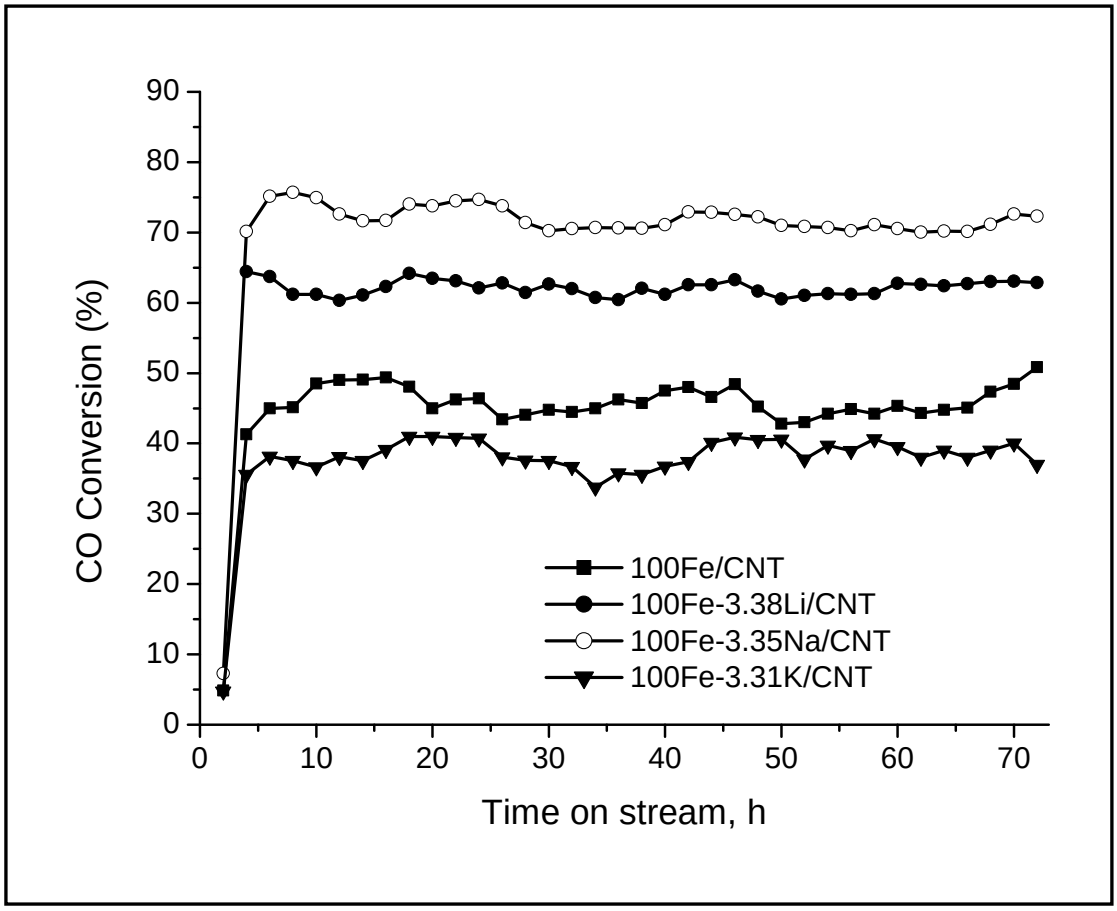


Figure 7.10: % CO conversion versus time on stream for unpromoted and alkali promoted Fe/CNT catalysts.

Table 7.5: Activity and selectivity of unpromoted and alkali promoted iron catalysts supported on CNTs during FTS[a].

Catalyts	100Fe/CNT	100Fe-3.38Li/CNT	100Fe-3.35Na/CNT	100Fe-3.31K/CNT
% CO Conversion	46.4	62.2	73.0	38.4
10^6 × CO rate[b]	1.79	2.74	2.94	1.44
10^6 × CO_2 rate (WGS)	0.99	1.18	1.49	0.93
10^6 × FTS rate	0.80	1.56	1.45	0.51
Activity (µmol/s.gFe)	35.8	54.8	58.8	28.8
Alpha (α)	0.53	0.52	0.63	0.68
Selectivity (mol % C)				
C_1	29.1	30.2	12.0	13.6
C_2-C_4	13.5	17.6	25.1	29.9
C_{5+}	57.4	52.2	63.0	56.5
O/O+P (weight ratio)[c]	0.023	-[d]	0.58	0.39
CO_2 (% produced)	9.36	10.31	14.01	8.52

[a]Conditions: 8 bar, 275 ^oC, CO:H_2 = 1:2, GHSV = 2400 h^{-1}
[b]Rates are expressed in mol/s.
[c]$C_3^=/(C_3^=+C_3)$.
[d]not detected.

7.3.2 Effect of varying the sodium loading

Preparation

Since this study revealed that Na was an effective promoter for the Fe/CNT catalyst, a more detailed study on the Na promoted Fe/CNT catalyst was undertaken. A series of catalysts were prepared in which the sodium content was varied. In addition to the 100Fe-3.35Na/CNT, two other sodium promoted catalysts were prepared: 100Fe-12Na/CNT and 100Fe-24Na/CNT (refer to experimental section 7.2).

X-ray diffraction (XRD) data

The X-ray diffraction patterns for the unpromoted and Na promoted Fe/CNT catalysts are shown in Figure 7.11 with the most pronounced lines indicated. The peaks that appeared at 2θ values of 26° and 44.8° are characteristic of carbon nanotubes [27]. The broad peak at 2θ value of 43° is attributed to the presence of small amounts of carbides as well as residual catalyst from the CNT synthesis in the samples (Fe-Co, Fe_3C, Co_3C or Co_2C) [27]. The peak at 2θ of 30° and 33° correspond to the presence of the magnetite (Fe_3O_4) and hematite (Fe_2O_3) phases respectively and the peak at 35.5° is related to the presence of both hematite and magnetite phases. It is observed from the XRD patterns that varying the amount of Na in the catalyst gave rise to different XRD patterns. This indicates that the iron phases present in the catalyst are different or the relative amount of each phase present is different. For instance the XRD pattern of the 100Fe-3.35Na/CNT catalyst shows the presence of the hematite peak at 2θ of 33° and when the sodium loading is increased 7.2 fold (100Fe-24Na/CNT catalyst), the hematite peak at 2θ of 33° is no longer detected and instead, the peak at 2θ of 35.5° is broadened.

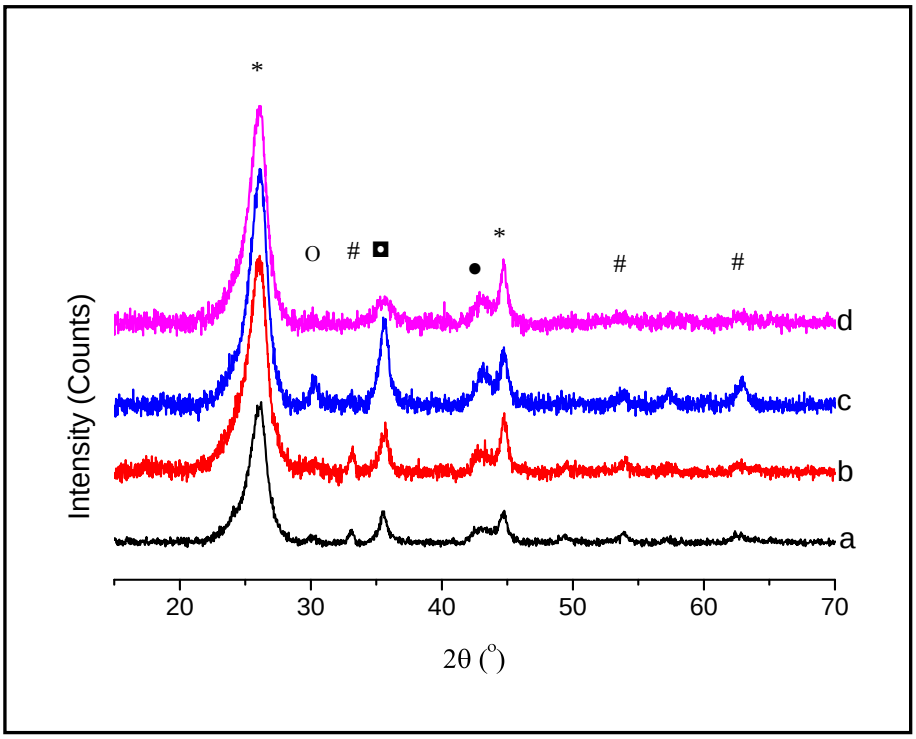


Figure 7.11: XRD patterns of unpromoted and Na promoted Fe/CNT catalysts: a) 100Fe/CNT, b) 100Fe-3.35Na/CNT, c) 100Fe-12Na/CNT, d) 100Fe-24Na/CNT; * = graphite; o = Fe_3O_4 ; # = Fe_2O_3; ◘ = Fe_2O_3 and Fe_3O_4; ● = Co-Fe, Fe3C, Co3C or Co2C ;

Temperature programmed reduction (TPR)

H_2-TPR was used to investigate the effect of varying the Na loading on the reducibility of the Na-promoted catalysts and the profiles are shown in Figure 7.12. As discussed earlier, the reduction of Fe_2O_3 to Fe takes place in 2 steps with peak 4 corresponding to the gasification of the CNTs [16]. In general, the addition of Na to the Fe/CNT catalyst inhibits its reduction due to the interaction of iron oxide with sodium oxide. However, increasing the Na content 3.7 and 7.2 fold did not have a significant influence on the reducibility of the catalyst (Figure 7.12, Table 7.6).

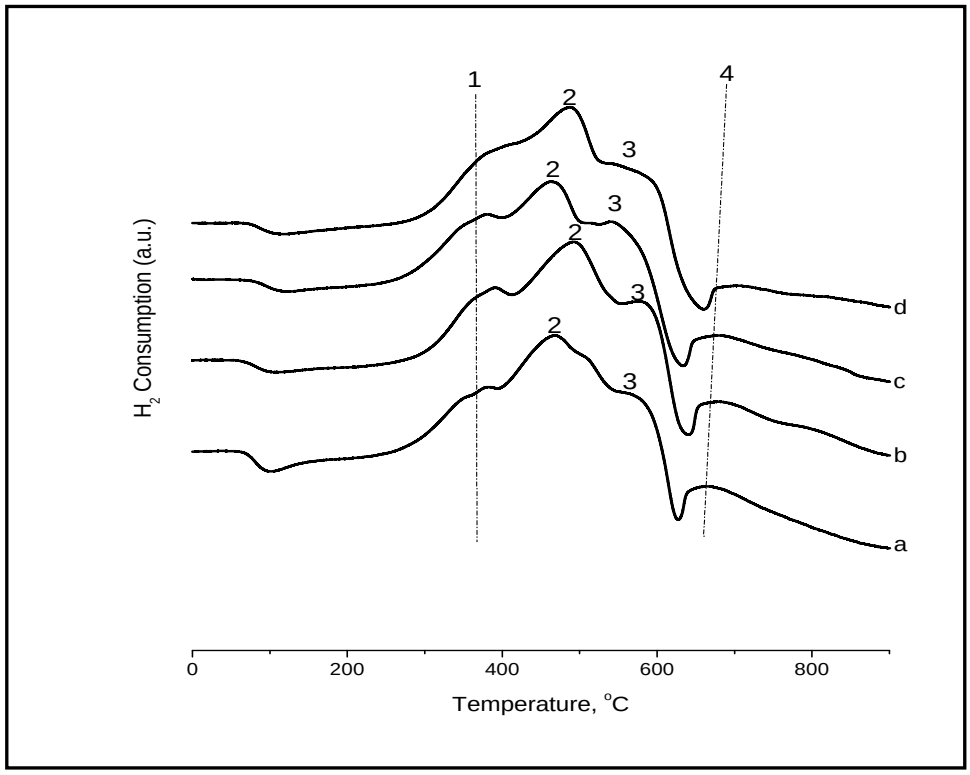


Figure 7.12: H_2-TPR profiles of the unpromoted and Na-promoted Fe-catalysts supported on CNTs: a) 100Fe/CNT, b) 100Fe-3.35Na/CNT, C) 100Fe-12Na/CNT; d) 100Fe-24Na/CNT.

Table 7.6: Temperature of the peak maxima at which each reduction steps occured during the H_2-TPR

	Temperature (^{o}C)		
Sample ID	$Fe_2O_3 \rightarrow Fe_3O_4$	$Fe_3O_4 \rightarrow Fe^o$	$CNT \rightarrow CH_4$
CNT	—	—	> 600
Fe/CNT	361	467	650
100Fe-3.35Na/CNT	392	492	662
100Fe-12Na/CNT	381	464	657
100Fe-24Na/CNT	395	497	678

Surface area and pore volume measurements

The surface areas and pore volumes of the Na-promoted catalysts are presented in Table 7.7. The surface area decreased upon adding the promoter. However, there is no significant decrease in surface area and pore volume with increasing Na loading. The surface area data are within ± 5% experimental error.

Table 7.7: BET surface area and pore volume of the unpromoted and Na promoted catalysts.

Sample ID	Surface area (m^2/g)[a]	Pore volume (cm^3/g)
100Fe/CNT	123	0.28
100Fe-3.35Na/CNT	92	0.27
100Fe-12Na/CNT	86	0.28
100Fe-24NaCNT	85	0.28

[a]error bar ±5%.

Catalytic testing

The performance of the Na-promoted iron catalysts with different amounts of Na was tested for Fischer-Tropsch synthesis using a fixed-bed micro reactor as described before. The unpromoted Fe catalyst was used as a reference.

From Figure 7.13 and Table 7.8, it is observed that the % CO conversion/activity of the Na-promoted catalysts significantly increases relative to the unpromoted one, this increase in activity could be due to the increase in concentration of surface active sites in the Na promoted catalysts. However, the % CO conversion/activity did not change significantly with increasing sodium loading. The selectivity to olefins, the

selectivity towards C_{5+} and the chain growth probability were found to increase with increasing Na loading (Table 7.8). The selectivity to methane was found to decrease upon promotion with sodium relative to the unpromoted catalyst. A further decrease in the methane selectivity was noticed with increasing sodium content in the catalyst. Such effects are attributed minimally to the geometric effects of surface alkalis, which can block active catalyst sites, and mostly to the electronic effects which have been shown previously to affect H_2 and CO adsorption and dissociation (Table 7.8). Increasing the sodium content beyond that of the 100Fe-3.5Na/CNT sample did not have a significant effect on the water gas shift reaction as seen by the fraction of CO_2 produced (Table 7.8).

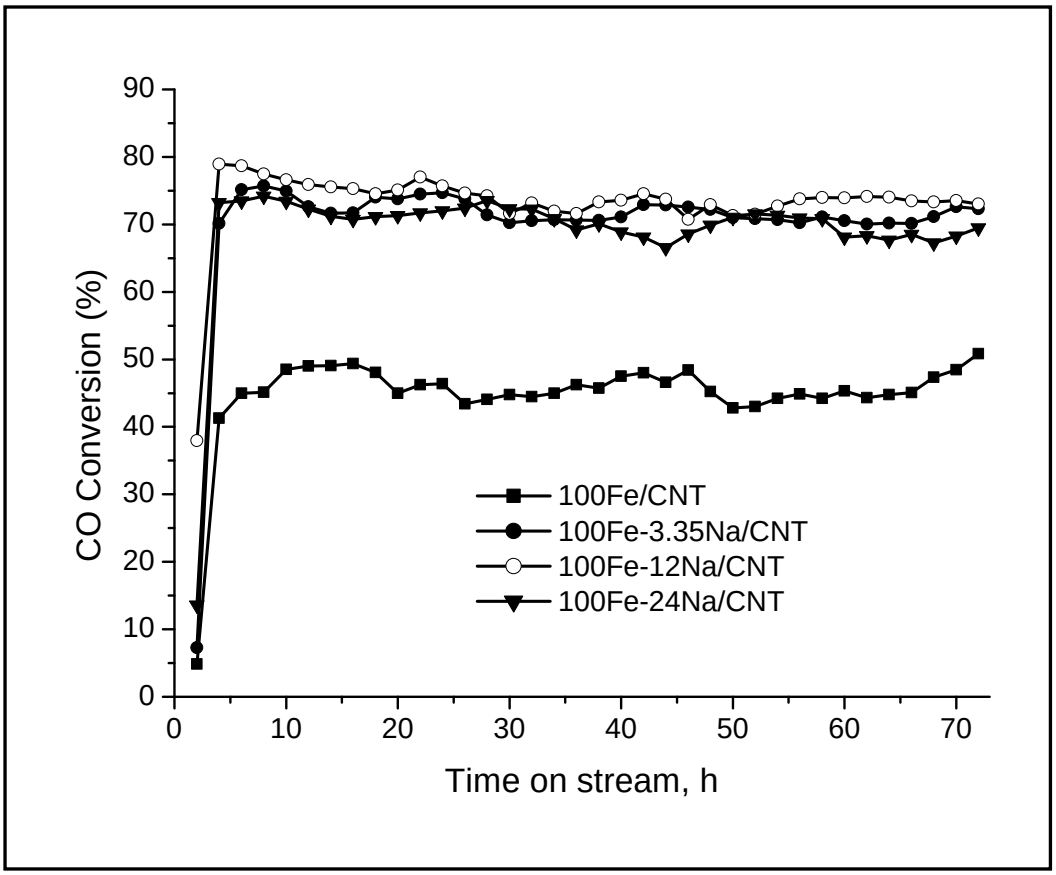


Figure 7.13: CO conversion versus time on stream for unpromoted and sodium promoted Fe/CNTs catalysts.

Table 7.8: Activity and selectivity of sodium promoted iron catalysts supported on CNTs with different sodium loading

Catalyts	100Fe/CNT	100Fe-3.35Na/CNT	100Fe-12Na/CNT	100Fe-24Na/CNT
% CO Conversion	46.4	73.0	74.1	71.0
$10^6 \times$ CO rate[a]	1.79	2.94	3.07	3.06
$10^6 \times CO_2$ rate (WGS)	0.99	1.49	1.55	1.59
$10^6 \times$ FTS rate	0.80	1.45	1.52	1.50
Activity (μmol/s.gFe)	35.8	58.8	61.4	61.2
Alpha (α)	0.53	0.63	0.66	0.74
Selectivity (mol % C)				
C_1	29.1	12.0	9.3	6.6
C_2-C_4	13.5	25.1	27.7	21.6
C_{5+}	57.4	63.0	63.0	71.8
O/O+P (weight ratio)[b]				
$C_2^=/(C_2^=+C_2)$	-[c]	0.068	0.27	0.35
$C_3^=/(C_3^=+C_3)$	0.023	0.59	0.81	0.78
$C_4^=/(C_4^=+C_4)$	-[c]	0.39	0.84	0.79
$C_5^=/(C_5^=+C_5)$	-[c]	0.13	0.15	0.16
CO_2 (% produced)	9.36	14.01	14.07	14.24

Conditions: 8 bar, 275 ^oC, $CO:H_2 = 1:2$, GHSV = 2400 h^{-1}.
[a] Rates are expressed in mol/s.
[b] $C_x^=/(C_x^=+C_x)$.
[c] not detected.

7.5 Conclusion

Carbon nanotubes were successfully synthesized and used as a support for Fe-based FT catalysts. For Fe/CNT catalysts, the effect of different alkali promoters on the particle size, surface area, catalyst reducibility, activity and selectivity during FTS was investigated. It was observed that adding the alkali promoter increased the Fe crystallite size and as a result the catalyst surface area decreased relative to that of the unpromoted catalyst. The presence of Na and K promoters slightly hindered catalyst reducibility by increasing the Fe reduction temperature; the potassium promoted catalyst showed the most pronounced effect in this regard. The potassium and sodium promoted catalysts were found to decrease the selectivity toward methane, increase the olefin production and shift the product selectivity to higher molecular weight hydrocarbons during FTS when compared to the unpromoted catalyst. However, K lowered the CO hydrogenation activity whereas Na greatly increased it. Increasing the sodium loading in the catalyst by 3.7 and 7.2 fold was found to have very little impact on the CO hydrogenation rate, but the product selectivity was affected, with 100Fe/24Na/CNT being the more selective catalyst toward higher molecular weight products. This study revealed that Na is a most effective promoter for an Fe/CNT catalyst, followed by K and lastly Li.

7.5 References

[1] C.H. Bartholomew, Studies in Surface Science and Catalysis 64 (1991) 158.

[2] T. Chronis, "A Fischer-Tropsch study of Co/Ru catalysts", PhD thesis, University of the Witwatersrand, Johannesburg, (1999) .

[3] R.A. van Santen, Surface Science 251 (1991) 6.

[4] D.B. Bukur, D. Mukesh, S.A. Patel, Industrial and Engineering Chemistry Research 29 (1990) 194.

[5] W. Ngantsoue-Hoc, Y. Zhang, R.J. O'Brien, M. Luo, B.H. Davis, Applied Catalysis A: General 236 (2002) 77.

[6] M.E. Dry, In: Anderson J.R., Boudart M (Eds.) Catalysis Science and Technology, Vol. 1 Berlin: Springer-Verlag (1981) 159.

[7] Y. Yang, H.W. Xiang, Y.Y. Xu, L. Bai, Y.W. Li, Applied Catalysis A: General 266 (2004) 181.

[8] H. Arakawa, A.T. Bell, Industrial & Engineering Chemistry Process Design and Development 22 (1983) 97.

[9] R.B. Anderson, J. Feldman, H.H. Storch, Industrial & Engineering Chemistry 44 (1952) 2418.

[10] M.E. Dry, T. Shingles, C.S. van H. Botha, Journal of Catalysis 17 (1970) 341.

[11] G.J. Haddad, B. Chen, J.G. Goodwin, Journal of Catalysis 160 (1996) 43.

[12] J.L. Carter, J.A. Cusumano, J.H. Sinfelt, Journal of Physical Chemistry 70 (1966) 2257.

[13] H.H. Storch, N. Golumbic, R.B. Anderson, The Fischer-Tropsch and Related Syntheses, John Wiley & Sons, Inc., New York, 1951.

[14] G.B. McVicker, M.A. Vannice, Journal of Catalysis 63 (1980) 25.

[15] X. An, B. Wu, H.J. Wan, T.Z. Li, Z.C. Tao, H.W. Xiang, Y.W. Li, Catalysis Communications 8 (2007) 1957.

[16] E. van Steen, F.F. Prinsloo, Catalysis Today 71 (2002) 327.

[17] M.C. Bahome, L.L. Jewell, D. Hildebrandt, D. Glasser, N.J. Coville, Applied Catalysis A, General 287 (2005) 60.

[18] M. Trépanier, A. Tavasoli, A.K. Dalai, N. Abatzoglou, Applied Catalysis A: General 353 (2009) 193.

[19] H. Xiong, M. Moyo, M.A.M. Motchelaho, L.L. Jewell, N.J. Coville, Applied Catalysis A: General (2010).

[20] J. Shen, M. Tu, C. Hu, Y. Chen, Langmuir 14 (1998) 2756.

[21] P. Serp, M. Corrias, P. Kalck, Applied Catalysis A, General 253 (2003) 337.

[22] S. Kundu, Y. Wang, W. Xia, M. Muhler, Journal of Physical Chemistry C 112 (2008) 16869.

[23] M.A.M. Motchelaho, H. Xiong, M. Moyo, L.L. Jewell, N.J. Coville, Journal of Molecular Catalysis A. (2010) Accepted.

[24] W. Chen, X. Pan, M.G. Willinger, D.S. Su, X. Bao, Journal of the American. Chemical Society 128 (2006) 3136.

[25] R.M.M. Abbaslou, A. Tavasoli, A.K. Dalai, Applied Catalysis A: General 355 (2009) 33.

[26] J.L. Rankin, C.H. Bartholomew, Journal of Catalysis 100 (1986) 533.

[27] S.D. Mhlanga, "Sysnthesis and study of carbon nanotubes and nanospheres" PhD thesis, University of the Witwatersrand, Johannesburg (2009) .

[28] Y. Yang, H.W. Xiang, Y.Y. Xu, L. Bai, Y.W. Li, Applied Catalysis A: General 266 (2004) 181.

[29] M.E. Dry, G.J. Oosthuizen, Journal of Catalysis 11 (1968) 18.

[30] H.P. Bonzel, H.J. Krebs, Surface Science Letters 109 (1981) L527.

[31] A.N. Pour, M. Zare, Y. Zamani, Journal of Natural Gas Chemistry 19 (2010) 31.

[32] A.N. Pour, S.M.K. Shahri, H.R. Bozorgzadeh, Y. Zamani, A. Tavasoli, M.A. Marvast, Applied Catalysis A: General 348 (2008) 201.

[33] R.B. Anderson (Ed.), Catalysts for Fischer-Tropsch synthesis, in: P.H. Emmett (ed.), Catalysis, Van Nostrand-Reinhold, New York, 1956.

[34] F.J. Williams, R.M. Lambert, Catalysis Letters 70 (2000) 9.

[35] D.O. Uner, Industrial and Engineering Chemistry Research 37 (1998) 2239.

8

Chapter Eight

Iron-based Fischer-Tropsch catalysts supported on Post-doped nitrogen-containing carbon nanotubes

8.1 Introduction

The Fischer-Tropsch (FT) synthesis is a surface catalyzed polymerization reaction that uses CH_2 monomers, generated from the hydrogenation of adsorbed CO over transition metals, to produce hydrocarbons and oxygenates [1]. The FT process is a proven method for the production of fuels and chemicals from a non-petroleum based feedstock [2, 3]. The FT product distribution depends on a catalyst, the type of reactor used and the operating conditions (temperature, pressure, space velocity) [4]. The role of the catalyst is to activate the reactants and to provide a surface where the various reactions can take place. A catalyst usually consists of an active metal (Fe or Co) deposited on a suitable support. The support is not a neutral spectator in the reaction

and the transition metal-support interface influences catalytic activity and typically generates better catalysts than unsupported transition metals [5, 6].

Carbon materials have been used as active metal supports in many reactions, including the Fischer-Tropsch reaction, because carbon has a relatively high surface area, good thermal and mechanical stability, inertness and most importantly tunable surface properties [7]. Numerous studies over the years have focused on activated carbon as a catalyst support; however the recent interest in shaped carbon materials (carbon nanotubes, carbon nanofibers, carbon spheres, carbon nanocoils etc.) has led to much interest in the synthesis of new carbon morphologies [8] having different properties for use as catalyst supports.

Carbon nanotubes (CNTs) have been used as catalyst supports for the Fischer-Tropsch synthesis [9-13]. Because of their inert nature, CNTs have to be functionalized or their surfaces have to be modified to make them chemically active [14]. Generally, acid treatments have been used to functionalize the carbon surface and to create surface functional groups (carboxylic, carbonyl, hydroxyl) that are able to act as anchoring sites for metal particles. These acid treatments, if very harsh conditions are used, can considerably reduce the mechanical performance of carbon due to the introduction of a large number of defects [15]. An alternative to surface functionalisation is surface doping and indeed, doping of a CNT with nitrogen has been used as an alternative to modify surface activity.

There are two methods that are commonly employed to dope CNTs with nitrogen [16]: doping directly during the synthesis of carbon nanotubes (known as the in-situ doping) or post-treatment of pre-synthesized carbon nanotubes with a nitrogen-containing precursor (N_2, NH_3, acetonitrile etc.) which is called post-doping. It has been established that the incorporation of nitrogen in nanotubes results in enhanced conductivity, enhanced surface basicity due to the strong electron donor behaviour of nitrogen [17-19] and also reduced surface hydrophobicity [20]. Nitrogen-doped

carbon nanotubes (N-CNTs) possess chemically active sites for use in catalytic reactions and these sites also allow for anchoring of metal precursors onto the carbon surface [15, 21]. Sidik et al. [22] has reported that N-CNTs exhibit enhanced electrocatalytic activity toward oxygen reduction. Pt has been supported on N-CNTs for use in the proton exchange membrane fuel cell (PEMFC) electrodes and this catalyst showed superior fuel cell performance and high stability when compared to commercial electrodes [23, 24].

The use of N-CNTs as a catalyst support for FT catalysts has not yet been extensively explored. A study by Xiong et al. [15] demonstrated that a Co-based FT catalyst supported on nitrogen doped carbon spheres (N-CSs) can be autoreduced to produce a stable Co/CS catalyst.

In this study, nitrogen doped carbon nanotubes (N-CNTs) were synthesized by the post-doping method using acetonitrile as the nitrogen source and the suitability of N-CNTs as support for Fe-based FT catalysts was investigated. For purposes of comparison, Fe supported on nitric acid functionalized N-CNTs was also prepared, characterized and tested in the Fischer-Tropsch reaction.

8.2 Experimetal

8.2.1 Synthesis of the N-CNTs by the post-doping technique using acetonitrile as the nitrogen source.

The post-doping method of synthesizing nitrogen-doped CNTs involves two steps: in the first step, the CNT is produced and in the second step the pre-synthesized and purified CNT is treated with a nitrogen-containing precursor at elevated temperatures (600-900^{o}C) [22, 25, 26].

Synthesis of carbon nanotubes (CNTs)

CNTs were prepared by the decomposition of acetylene over a 10% Fe-Co/$CaCO_3$ catalyst in a chemical vapour deposition (CVD) unit. Details concerning the catalyst (10% Fe-Co/$CaCO_3$) preparation and the carbon nanotube production are given in Chapters 4 and 5. The as-grown CNTs were purified using a mild acid treatment (30% HNO_3 for 2 h at room temperature) in order to remove residual reagents used in the synthesis. The CNTs were then washed with distilled water and dried in an oven at 120^{o}C for ~ 12 h. This sample was named purified CNT.

Post-doping treatment of CNTs

The set-up used for doping the CNTs with nitrogen is similar to the one used for the synthesis of carbon nanotubes with a slight modification to allow for the introduction of the nitrogen source. In this experiment, the purified CNTs obtained above were spread in a boat and placed in a quartz tube. The quartz tube was then put in a horizontal furnace (see Chapter 3). A bubbler containing acetonitrile was placed before the quartz tube inlet. High purity argon (100 mL/min) was used as a carrier gas and was bubbled through the acetonitrile maintained at 78^{o}C and the vapour was carried through to the reaction zone where the boat containing the purified CNTs was placed. The experiment was carried out at different furnace temperatures (700^{o}C, 750^{o}C, 800^{o}C, 850^{o}C and 900^{o}C). The reaction time and the argon flowrate were kept constant at 2 h and 100 mL/min respectively.

N-CNTs obtained by post-treatment at 750^{o}C for 2 h, were also functionalized by refluxing the material in 55% HNO_3 at 120^{o}C for 2 h. The sample was labeled N-CNT-750-55R2. Table 8.1 below gives an overview of the N-CNTs synthesized.

Table 8.1: Overview of the N-CNTs synthesized

Sample ID	Doping temperature (^oC)	Doping time (h)	Argon flowrate through bubbler (mL/min)	Further post treatment
Purified CNT	—	—	—	—
N-CNT-700	700	2	100	—
N-CNT-750	750	2	100	55R2[a]
N-CNT-800	800	2	100	—
N-CNT-850	850	2	100	—
N-CNT-900	900	2	100	—

[a]Refluxed in 55% HNO_3 at 120^{o}C for 2 h.

8.2.2 Synthesis of Fe supported on N-CNTs catalysts

Fe (10 wt.%) was loaded on the N-CNTs (N-CNT-750 or N-CNT-750-55R2) by the deposition precipitation method using urea as the precipitating agent. Typically, $Fe(NO_3)_3 \cdot 9H_2O$ (1.44 g) and urea (0.322 g; 1.5 mol of urea per mole of iron) were dissolved in de-ionized water (20 mL) and added dropwise to the nitrogen doped carbon nanotubes (2.00 g) initially slurried with de-ionised water (20 ml) and heated to 90^{o}C in an oil bath. The mixture was left to stir at this temperature for at least 2 h to allow for the decomposition of urea. Thereafter, the temperature was decreased to 80^{o}C to allow for the evaporation of the excess solvent. The catalyst was further dried at 100^{o}C for 12 h and heat-treated in N_2 at 250^{o}C for 2 h in order to decompose the nitrate.

8.3 Characterization techniques

8.3.1 Transmission electron microscopy (TEM) analysis

The structure and morphology of purified CNTs, N-CNTs and Fe/N-CNTs catalysts were characterized by TEM. Sample specimens for TEM analyses were prepared by ultrasonic dispersion of the sample in methanol, and the suspensions were dropped onto a SPI-carbon coated copper grid. TEM images were obtained using a FEI Tecnai Spirit G^2 transmission electron microscope operating at 120 kV. For the Fe/N-CNT catalysts several TEM micrographs were recorded for each sample and analyzed for particle size distribution using the ImageJ software. A least 120 metal nanoparticles per sample were analyzed to determine the average catalyst particle size.

8.3.2 Elemental (CNS) analysis

The nitrogen content in the N-CNTs was determined by elemental analysis using a Carlo Erba NA1500 Nitrogen Carbon Sulfur analyzer. Approximately 1.0-1.5 mg of powder sample was used for the analysis and a GC, coupled to a thermal conductivity detector, was used to separate the gases produced. These analyses were conducted at the Institute for Soil, Climate and Water based in Pretoria, South Africa.

8.3.3 BET surface area measurements

The surface area and pore volume of the CNTs as well as the N-CNTs were determined by N_2 physisorption using a Micromeritics TRISTAR 3000 analyzer. A sample of approximately 300 mg was degassed at 150^{o}C for 4 h under a flow of N_2,

and then the surface area and pore volume were determined by the Brunauer-Emmett-Teller (BET) method.

8.3.4 Thermogravimetric analysis (TGA)

TGA analysis was used to determine the thermal stability of N-CNTs as well as the % wt. metal loading. The TGA analysis was done on a Perkin Elmer STA 4000 analyzer. About 5 to 10 mg of sample was placed in a ceramic pan and placed in the instrument's furnace. The temperature of the sample was increased from room temperature to 900^{o}C at 10^{o}C/min under an oxidative atmosphere (air, 20 mL/min). The metal loading was determined using TGA by simply burning off the carbon support in an oxidative environment. The % loading was calculated from the mass of ash that remained assuming that the ash was only made up of fully oxidized iron (Fe_2O_3). The value obtained was corrected for the ash that remained when the carbon support was oxidized.

8.3.5 Raman spectroscopy

Raman spectroscopy (Jobin-Yvon T64000 micro-Raman spectrometer) was employed to evaluate the quality of the CNTs. A grating with 600 grooves/mm was used to disperse the spectrum onto a charge coupled device (CCD) detector.

8.3.6 Temperature programmed reduction (TPR)

The TPR experiment was performed on a Micromeritics AutoChem II Chemisorption analyser to study the reduction behaviour of the catalysts. A sample of the catalyst (100 mg) was loaded into a U-shaped quartz tube reactor, fitted with a thermocouple for continuous temperature measurement. The reactor was placed in a furnace. Prior

to the H_2-TPR analysis, the sample was first degassed in a flow of high purity argon (20 mL/min) at 150^oC for 30 min to remove traces of water, and then cooled to 40^oC. The sample was then reduced in 5%H_2/Ar (30 mL/min) as the temperature was increased from 40^oC to 800^oC at a rate of 10^oC /min. The gas flow through the reactor was controlled by three Brooks mass flow controllers. A thermal conductivity detector (TCD) was used to measure the H_2 consumption. The temperature and H_2 consumption was captured automatically by a PC to give the TPR profiles.

8.3.7 X-ray diffraction

X-ray powder diffraction (XRD) patterns of the purified CNTs and the Fe/N-CNT catalysts were recorded with a Brucker D2 phaser diffractometer using a Cu source (1.5418 Å) and a LynxEye detector. The scan was within a 2θ range of 15-70^o with 0.03^o steps at 25^oC. Crystallite phases were determined by comparing the diffraction patterns with those in the standard powder XRD files (JCPDS).

8.3.8 Catalytic testing

The Fischer-Tropsch synthesis was performed in a fixed-bed micro reactor. Gas cylinders containing H_2/CO/N_2 mixtures (60%H_2, 30%CO and 10% N_2; purity: 99.99%) were used to supply the reactant gas stream to the catalyst. Nitrogen was used as an internal standard in order to ensure an accurate mass balance.

Catalyst (0.5 g) was added to the reactor and reduced in situ at 350 °C for 20 h under a stream of pure hydrogen (2 bar pressure, 20 mL/minute). After reduction, the temperature was decreased to 275°C under the flow of nitrogen, the pressure was increased gradually to 8 bar and a flow of syngas was passed over the catalyst bed with a flowrate of 20 mL/min (GHSV = 2400 h^{-1}). All gas lines after the reactor were

kept at 150°C and the hot trap placed immediately after the reactor was held at 150°C in order to collect wax. A second trap kept at ambient temperature was used to collect the oil and water mixture. The flow of gases was controlled using a needle valve and measured with a bubble meter. The gaseous product stream was analyzed online using two gas chromatographs. An offline GC was used to analyze the oil and wax. The data analysis method used in our study was performed according to standard procedures as described elsewhere [9].

8.4 Results and discussion

8.4.1 Purified carbon nanotubes and nitrogen doped carbon nanotubes

CNS elemental analysis, BET surface area and pore volume measurements

Table 8.2 presents results from the CNS elemental analysis, the BET surface area and pore volume measurements. It is observed that the purified CNTs (no nitrogen post treatment) contain 0.35% nitrogen. This indicates that a small amount of nitrogen used as the inert gas atmosphere in the CVD growth of carbon nanotubes may be incorporated into the CNTs.

An investigation of the effect of reaction temperature on the carbon mass and nitrogen content in N-CNTs was carried out using a reaction time of 2 h. Figure 8.1 shows the effect of reaction temperature on both the % mass increase (amount by which mass of solid CNTs increases) and % nitrogen content of the product. Both mass and % N increase with increasing reaction temperature from 700 to 900^{o}C. Thus, as the reaction temperature is increased from 700 to 900^{o}C, more acetonitrile is decomposed in the reaction zone and as a result more nitrogen and carbon are incorporated/deposited onto the CNTs. As the reaction temperature is increased, the

C/N ratio decreased indicating that more N than C from the decomposition of CH_3CN is being deposited on the CNTs.

Similarly, the effect of the reaction temperature on the surface area and pore volume was studied after a reaction time of 2 h. The graph presented in Figure 8.2 shows the dependence of surface area and N-CNT mass increase on reaction temperature. It is observed that as the reaction temperature is increased from 700 to 900^{o}C, the surface area of the N-CNTs decreases. The decrease in surface area is attributed to the increased in the amount of carbon deposited (probably amorphous material) with increasing temperature. Similar observations (decrease in specific surface area with increasing synthesis temperature) were made by Shalagina et al. [27] when investigating the texture of N-CNFs. The observed decrease in pore volume with increasing reaction time suggested that the carbon nanotubes tips were closed by the carbon deposit; no evidence to support this was found using TEM.

Table 8.2: % mass increase, C/N ratio, surface area and pore volume of purified and N-CNTs as a function of reaction temperature.

Sample	Mass increase (%)	Nitrogen content (%)	C/N ratio	Surface area (m^2/g)[a]	Pore volume (cm^3/g)
Purified CNTs	—	0.35	273	91	0.34
N-CNT-700	0.04	0.70	137	85	0.30
N-CNT-750	7.98	1.75	54	73	0.28
N-CNT-800	23.5	2.59	37	59	0.22
N-CNT-850	57.5	4.21	22	41	0.17
N-CNT-900	174	6.54	14	14	0.06

[a]Error ± 5%.

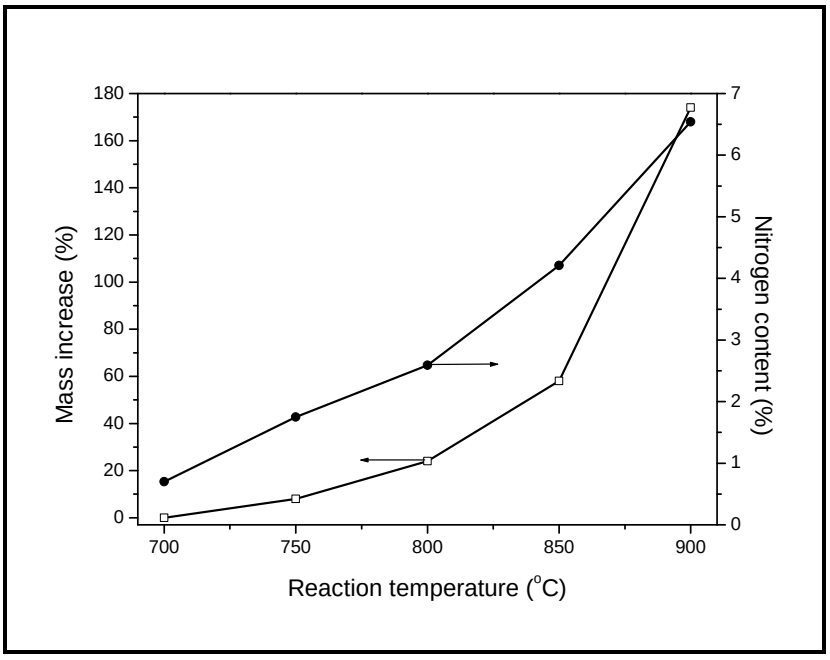


Figure 8.1: Dependence of the % mass increase and nitrogen content in N-CNTs on reaction temperature

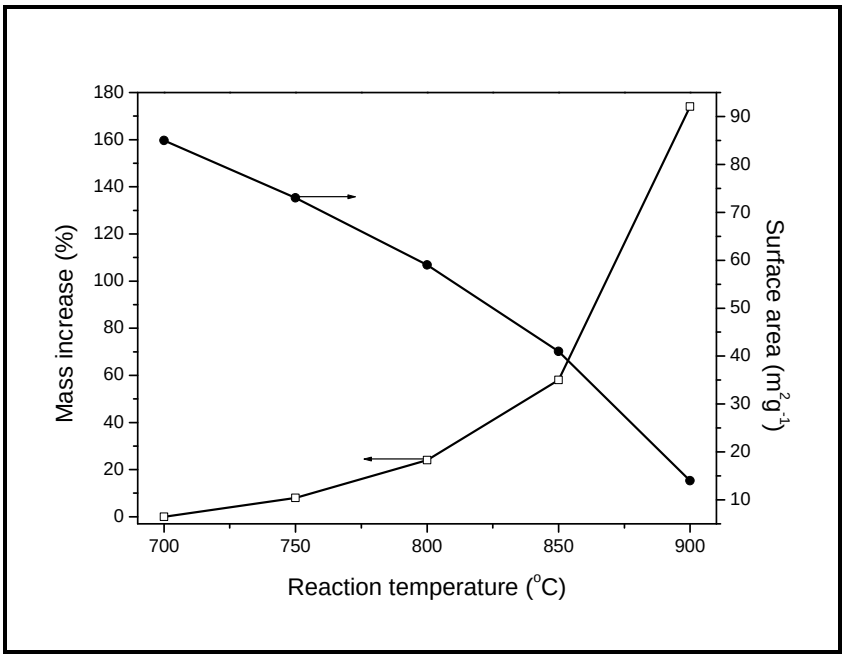


Figure 8.2: Dependence of the % mass increase and surface area in N-CNTs on reaction temperature.

TEM analysis

TEM analysis revealed that nitrogen incorporation via the post doping method did not have a significant impact on the morphology and structure of the CNTs up to about 800^{o}C reaction temperature (Figure 8.3a-d), probably because the concentration of nitrogen incorporated was very low. At temperatures greater that 800^{o}C, there were some obvious changes in the appearance of the N-CNT; amorphous material was clearly being deposited on the surface of the N-CNTs. The material originated from the thermal decomposition of acetonitrile with the N-CNTs produced at 900^{o}C being the most affected (Figure 8.3f). No bamboo structures were observed in these N-CNTs as is in the case of N-CNTs prepared by the in-situ techniques [16, 28]. This means that, the mechanism of N incorporation is different.

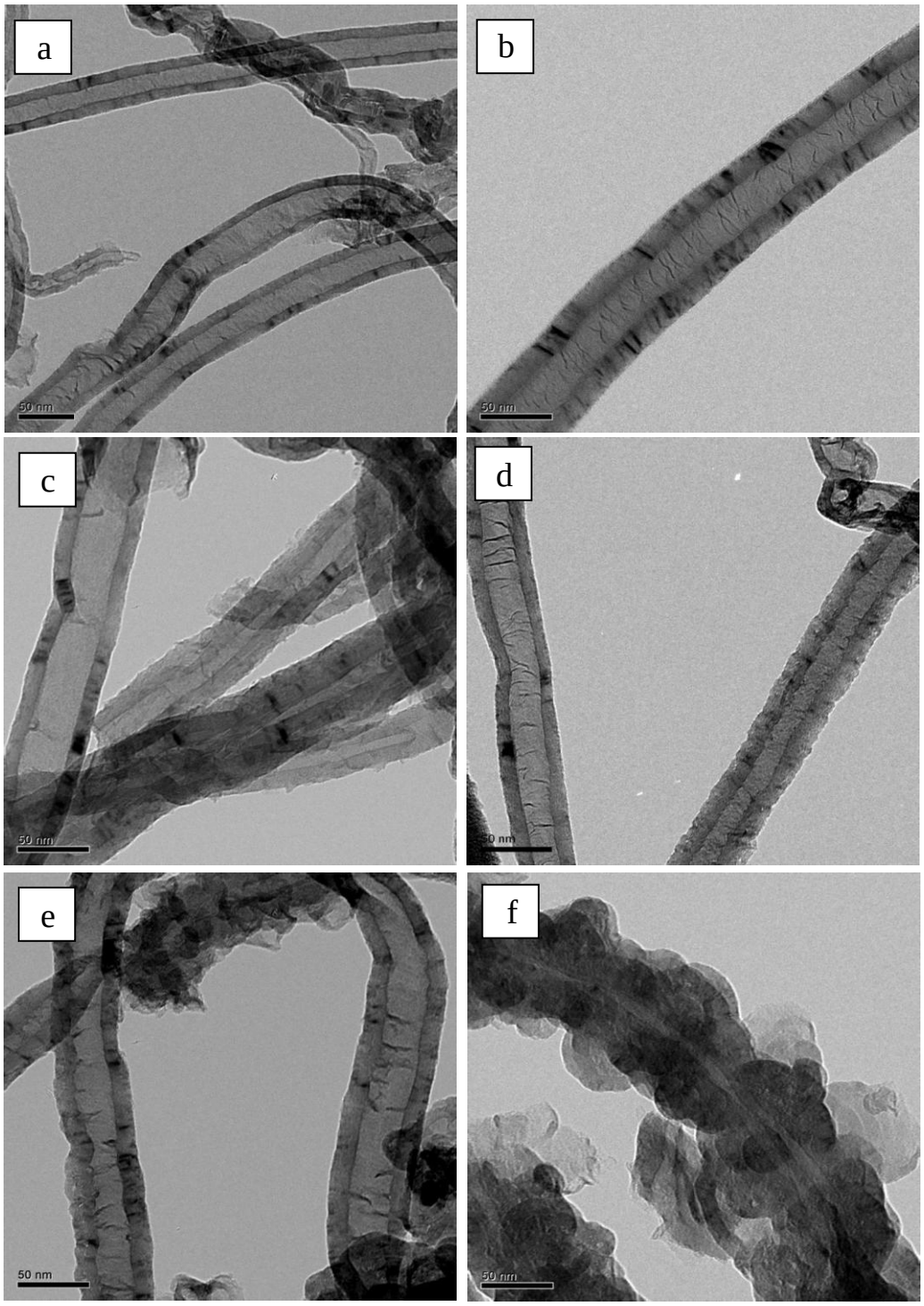


Figure 8.3: TEM images of CNTs and N-CNTs (prepared by post-doping at different temperatures): a) purified CNTs; b) N-CNT-700^{o}C; c) N-CNT-750^{o}C; d) N-CNT-800^{o}C; e) N-CNT-850^{o}C; f) N-CNT-900^{o}C (Duration of deposition in all cases is 2 h)

Thermogravimetric analysis (TGA)

Thermogravimetric analysis (TGA), coupled with derivative curve analysis of the weight loss (DTA) was used to investigate the thermal stability of the purified CNTs and N-CNTs in an air atmosphere. Figures 8.4a-f show the TGA and DTA profiles of the purified CNTs and N-doped CNTs obtained after reaction at different reaction temperatures. Table 8.3 presents the summary of the temperatures at which the carbon material decomposes (half width information) as well as the derivative peak breadth. It is observed that the purified CNTs decomposed at 675^{o}C and they are in general more stable than their doped counterparts. The thermal stability of the N-CNTs shifts to slightly lower temperature as the nitrogen content increases (Figure 8.4, Table 8.3). This is attributed to the presence of nitrogen atoms, creating localized defects that are energetically less stable than the pure carbon lattice [16].

The derivative peak breadth decreases slightly with increasing reaction temperature up to 850^{o}C. This could be due to the formation of a more uniform type of surface material upon heating. For the sample prepared at 900^{o}C, the thermal stability of the N-CNTs increases with a shoulder peak appearing at 717^{o}C, however the derivative peak breadth significantly increases and this is attributed to the deposition of some other form of carbon material on the surface of N-CNT as confirmed by TEM (see figure 8.3 above) that is stable above 600^{o}C.

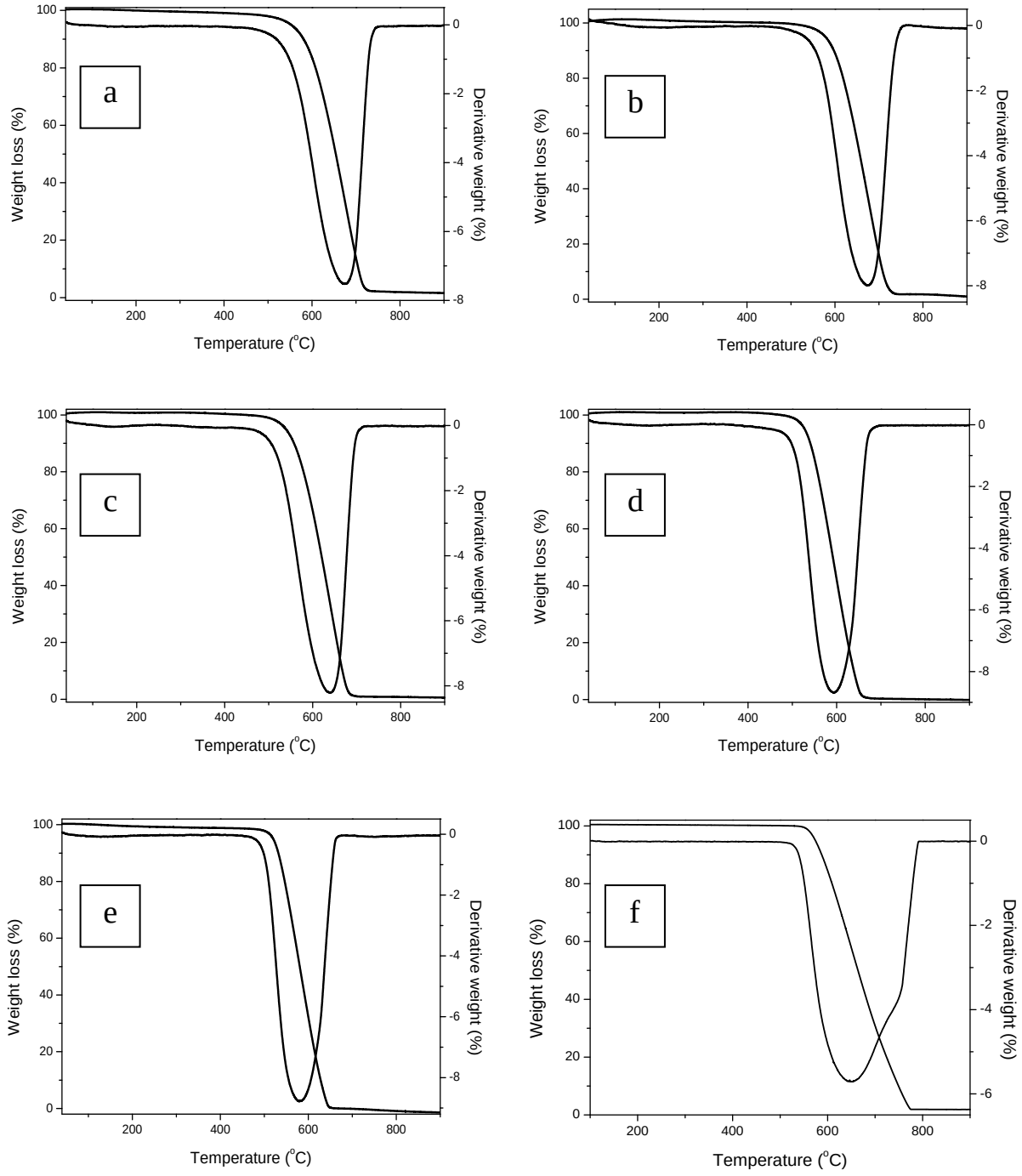


Figure 8.4: TGA and DTA profiles of the purified CNTs and N-CNTs (obtained at different post treatment temperatures): a) purified CNT; b) N-CNT-700°C; c) N-CNT-750°C; d) N-CNT-800°C; e) N-CNT-850°C; f) N-CNT-900°C.

Table 8.3: Decomposition temperature and peak width of purified and N-CNT as a function of reaction temperature.

sample	Post treatment temperature (^{o}C)	Decomposition Temperature (^{o}C)	Peak Breadth (^{o}C)
Purified CNTs	—	675	236
N-CNT-700	700	675	228
N-CNT-750	750	637	224
N-CNT-800	800	595	207
N-CNT-850	850	580	196
N-CNT-900	900	635[a]	262

[a]Shoulder peak at 717^{o}C

Raman analysis

Raman spectroscopy is one of the methods used for determining the degree of structural ordering or the presence of defects in graphitic-like materials [29]. The Raman spectra of the purified and N-CNTs are shown in Figure 8.5 and three peaks can be observed. The first peak at ~ 1350 cm^{-1} corresponds to the disorder-induced band (D-band), the second peak at ~ 1590 cm^{-1} corresponds to the tangential mode (G-band) and the last peak G' occurring at 2D = ~ 2700 cm^{-1} is an overtone mode of the D-band [30] (Figure 8.5). The area ratio of the D and G bands (I_D/I_G) is useful in estimating the defect concentration in the CNTs and N-CNTs. Table 8.4 presents the positions for the most intense components corresponding to the D, G and G' bands, the I_D/I_G area ratios as well as the nitrogen content for the purified and N-CNTs prepared. It is clear from Table 8.4 and Figure 8.6 that the I_D/I_G ratio decreases slightly with increasing nitrogen content up until a reaction temperature of 850^{o}C. At temperature > 850^{o}C, the I_D/I_G ratio was found to increase significantly. These results suggest that increasing the reaction temperature from 700 to 850^{o}C actually reduces the disorder of the carbon material and that the nitrogen incorporation did not

significantly affect the bulk structure of the N-CNTs. This could be due to the low C/N ratio in these temperatures range. Hellgren et al. showed that low concentrations of nitrogen can be incorporated in the graphene layer without changing the graphitic properties too much [31]. However, when the reaction temperature was 900^{o}C, the nitrogen content had increased to about 6.5% and the I_D/I_G ratio was found to increase significantly i.e., there is a loss in ordering in the graphene layers as more nitrogen is incorporated into the CNTs. These results are in agreement with TEM and TGA data.

It is also observed from the Raman data (Table 8.4) that increasing the reaction temperature leads to an up-shift of the D-band. The largest shift (up to 43 cm^{-1} for the N-CNT-900) is characteristic of the D band and indicates the appearance of new types of disorder in N-CNTs relative to that of pure CNTs [29]. Similar observations were also obtained by Jafri et al.[21] and Yang et al.[32]. The position of the G and G' bands is also shifted. However, the G and G' bands are not related to the structural defects and a modification in the electronic structure of CNTs with nitrogen doping could be the reason for the observed shift [29].

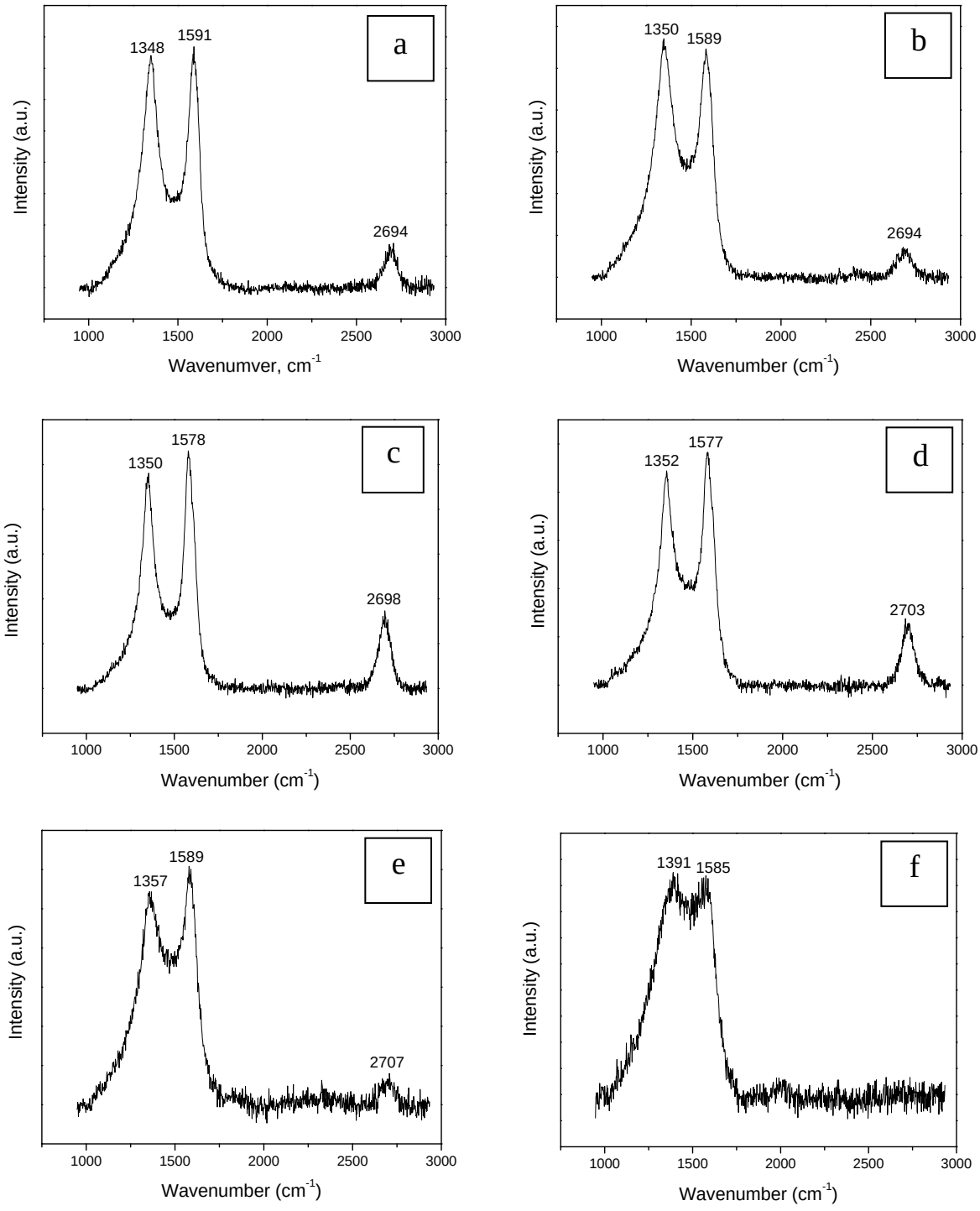


Figure 8.5: Raman spectra of CNTs and N-CNTs (obtained at different post treatment temperatures): a- purified CNT; b- N-CNT-700^{o}C; c- N-CNT-750^{o}C; d- N-CNT-800^{o}C; e- N-CNT-850^{o}C; f- N-CNT-900^{o}C.

Table 8.4: Raman data for the purified and nitrogen-doped CNTs

Sample ID	Nitrogen content (%)	Peak position (cm^{-1})[a]			I_D/I_G
		D-band	G-band	G'-band	
Purified CNT	0.35	1348	1591	2694	1.04
N-CNT-700	0.70	1350	1589	2694	0.99
N-CNT-750	1.75	1350	1578	2698	0.94
N-CNT-800	2.59	1352	1577	2703	0.90
N-CNT-850	4.21	1357	1589	2707	0.87
N-CNT-900	6.54	1391	1585	—	1.28

[a]Error bar ± 2 cm^{-1}

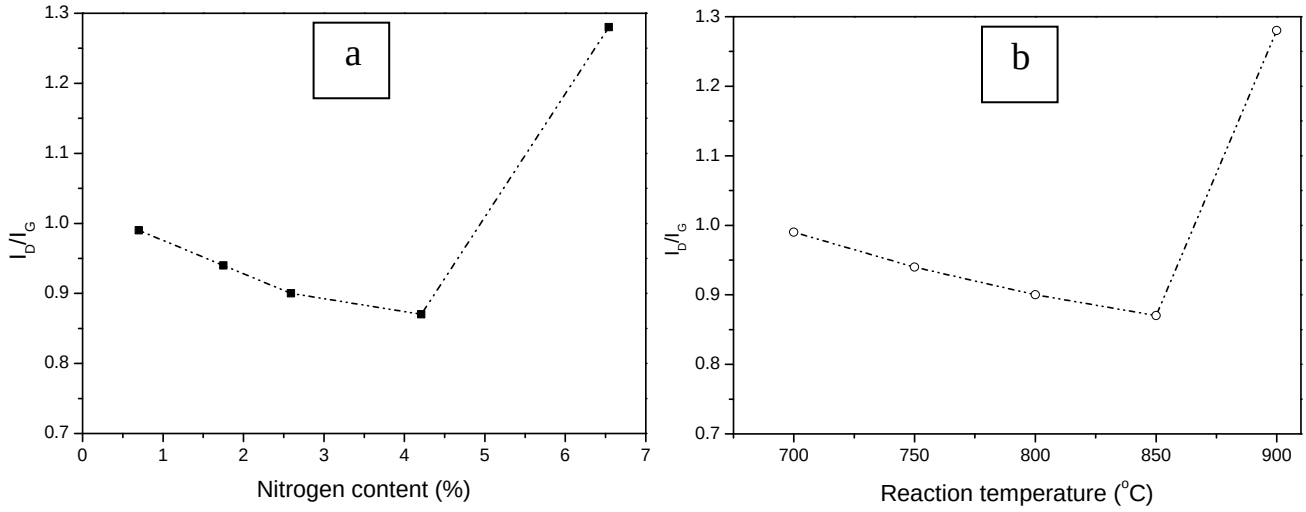


Figure 8.6: I_D/I_G ratio as function of (a) nitrogen content and (b) reaction temperature

8.4.2 Fe catalyst supported on nitrogen-doped carbon nanotubes

N-CNT-750 was chosen as a support for the Fe catalyst as the preliminary characterization studies carried out above suggested that this support had the most desirable characteristics for study (low nitrogen content: 1.75 %, 73 m^2/g surface area, thermally stable up to 500^oC etc.). Fe supported on N-CNT-750 and N-CNT-750-55R2 were used for the studies which were conducted on the prepared catalysts in order to compare the two supports and determine which of the two would provide a better support for Fe based FT catalysts.

CNS elemental analysis and surface area measurements

Results from the CNS elemental analysis and BET surface area measurements are displayed in Table 8.5. The nitrogen content was found to be 1.2 % for the N-CNT supported iron catalyst. The surface area and pore volume did not change significantly when Fe was loaded onto the N-CNT-750. The Fe/N-CNT-750-55R2 had a larger surface area. This could possibly be explained by the increase in the surface area of N-CNT-750-55R2 brought about by the roughened surface formed during acid functionalisation.

Table 8.5: Nitrogen content, surface area and pore volume measurements

Sample ID	Nitrogen content (%)	Surface area m^2/g	Pore volume cm^3/g
N-CNT-750	1.75	73	0.28
Fe/N-CNT-750	1.23	76	0.27
Fe/N-CNT-750-55R2	—[a]	98	0.28

[a]no data available

TEM analysis

The morphology of two the N-CNT supported Fe-catalysts was investigated using TEM. Figures 8.7 and 8.8 are the TEM images and histogram of the Fe particle size of the Fe/N-CNT-750 and Fe/N-CNT-750-55R2 samples respectively. It is clearly seen from the TEM images and histograms that the two catalysts have very different particle sizes and distribution. The Fe particles are smaller and more uniform on the N-CNT-750-55R2. The difference in the Fe particle size is attributed to differences in the amount of functional groups on the support surface. The N-CNT-750 support has localized defects created by the presence of nitrogen (~ 1.7%) as well as surface defects originating from the CNT synthesis as anchoring sites for the metal particle. Catalyst preparation on this type of support would result in particle agglomeration/sintering during heat-treatment because there are not enough surface functional groups to anchor the metal particles. As a result, a broader particle size distribution, and a poorly dispersed catalyst is obtained with an average particle size of 27 nm (Figure 8.7).

Functionalizing the N-CNT-750 support with 55%HNO_3, creates additional surface functional groups that are more evenly spread onto the CNT surface to anchor the metal particle. This helped in the preparation of a narrower size distribution, well dispersed catalyst with an average particle size of 8 nm (Figure 8.8). These results imply that COOH > N in dispersing particles in this study.

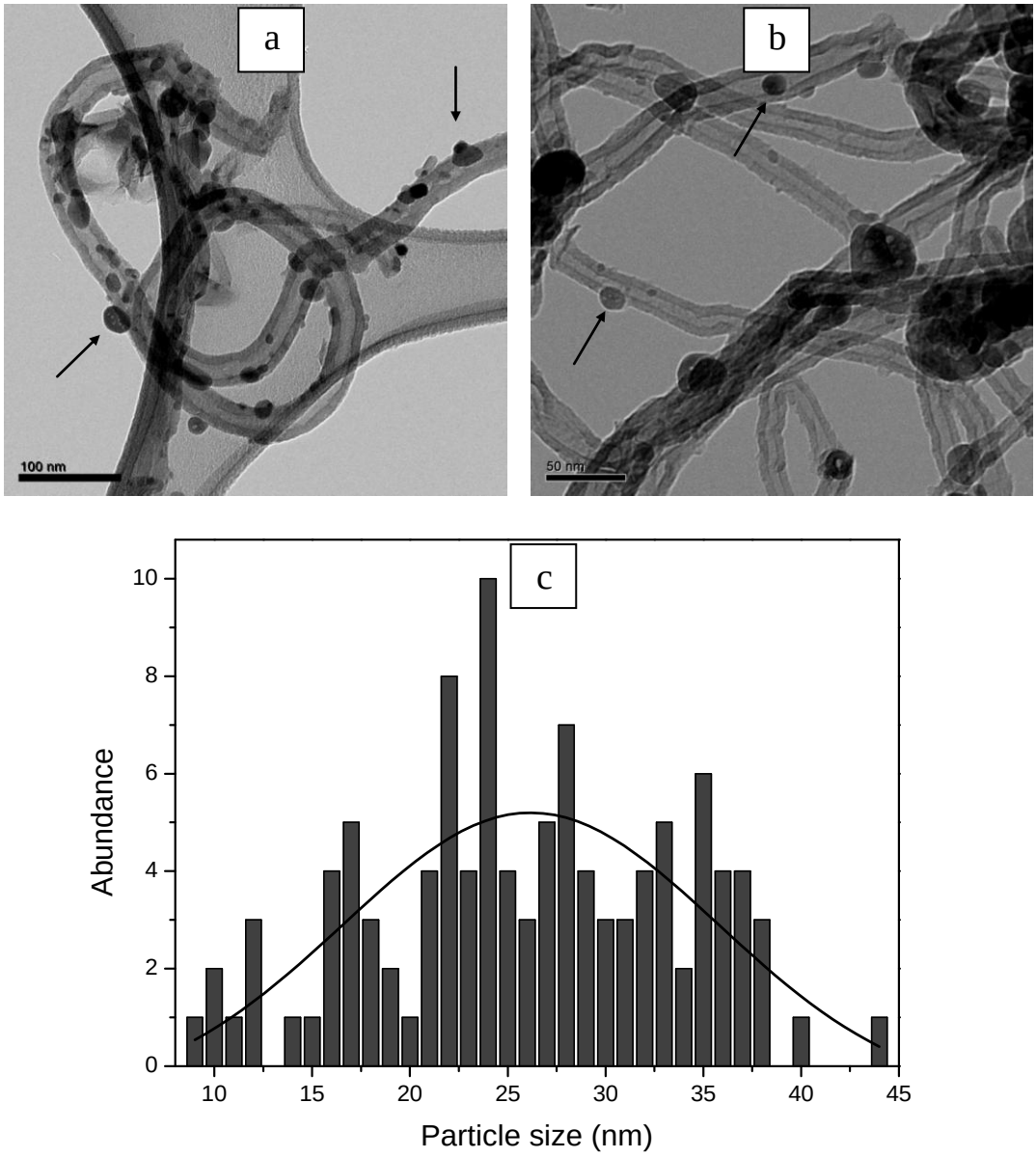


Figure 8.7: (a) and (b) TEM images and (c) Fe particle size histogram of the Fe/N-CNT-750 catalyst, (arrows on the TEM images show iron particles)

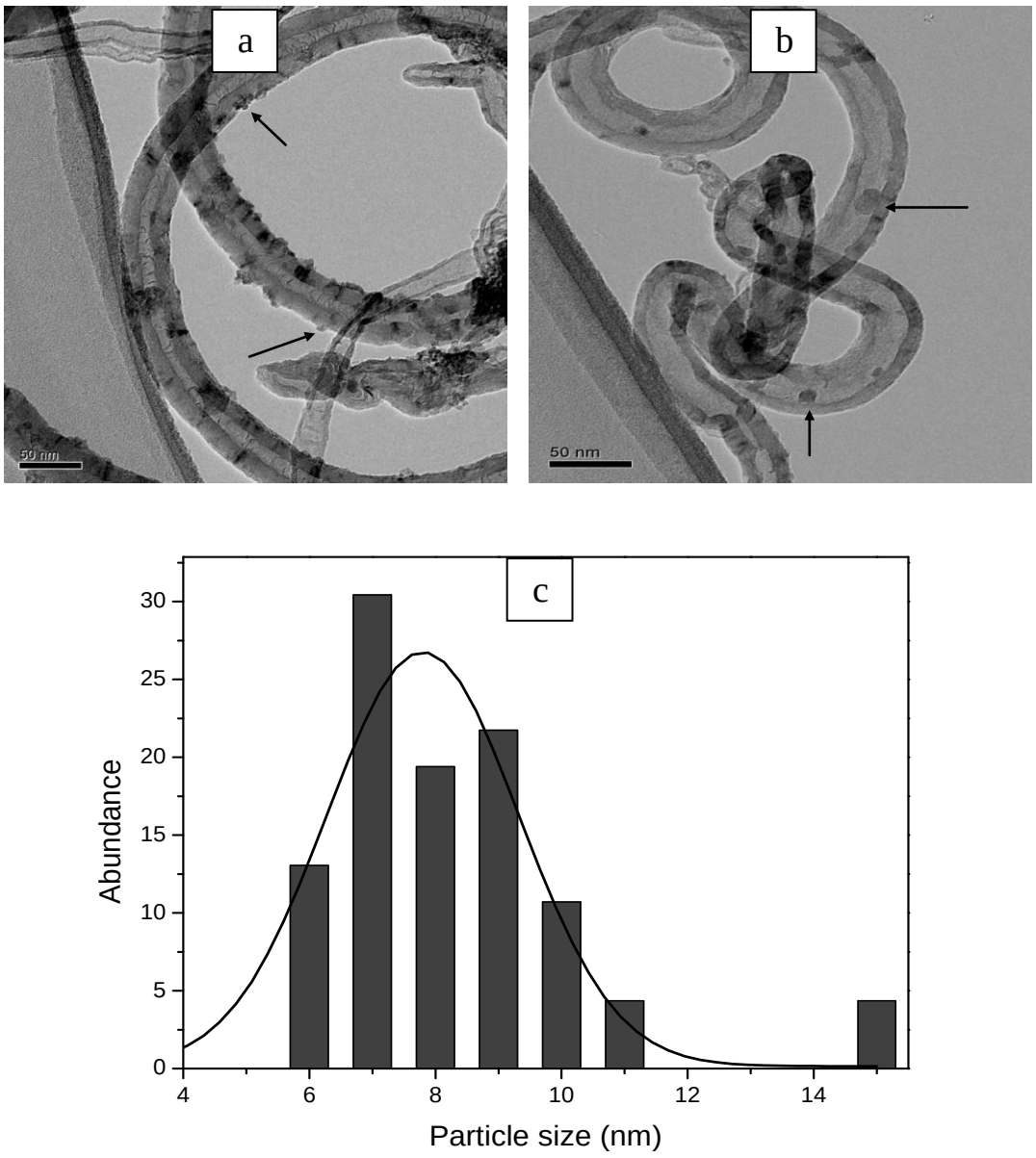


Figure 8.8: (a) and (b) TEM images and (c) Fe particle size histogram of the Fe/N-CNT-750-55R2 catalyst, (arrows on the TEM images show iron particles)

XRD analysis

The XRD patterns of the purified CNTs and the two Fe/N-CNT catalysts are displayed in Figure 8.9. Several diffraction peaks are observed. The peaks appearing at 2θ of 26^o and 45^o are characteristic of the graphitic walls of the CNTs [33]. The broad peak at 2θ = 43^o is attributed to the presence of small amounts of carbides as well as residual catalyst from the CNTs synthesis in the samples (Co-Fe, Fe_3C, Co_3C or Co_2C) [33]. The peaks at 2θ of 30^o and 33^o correspond to the presence of the magnetite (Fe_3O_4) and hematite (Fe_2O_3) phases respectively and the peak at 35.5^o corresponds to the presence of both hematite and magnetite phases. When comparing the XRD patterns of the two catalysts, it is clear that they exhibit different diffraction patterns.

The iron oxide average crystallite size was measured using the line broadening of the peak at 2θ = 33^o and the Scherrer equation. The data are presented in Table 8.6. The Fe/N-CNT-750 has an average particle size of 30 nm whereas the Fe/N-CNT-750-55R2 catalyst has an average iron particle size of 6 nm. This is in good agreement with TEM measured particle size.

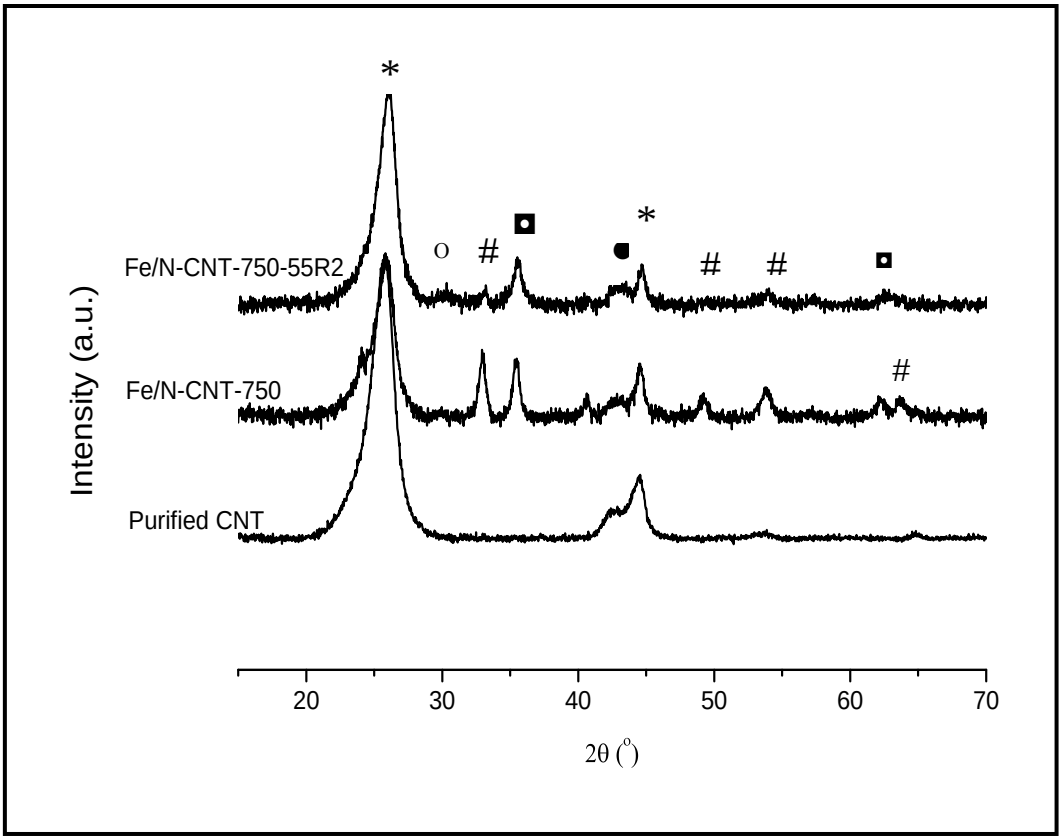


Figure 8.9: XRD patterns of the purified CNTs and Fe supported on N-CNTs: * = graphite; o = Fe_3O_4; # = Fe_2O_3; ◘ = Fe_2O_3 and Fe_3O_4; ● = Co-Fe, Fe_3C, Co_3C or Co_2C [33, 34].

Table 8.6: Metal loading and average particle size of the N-CNT supported Fe catalyst

Catalyst	**Metal loading (%)[a]**	**Fe_2O_3 average particle size, nm**	
		TEM	**XRD**
Fe/N-CNT-750	10.3	27	30
Fe/N-CNT-750-55R2	9.8	8	6

[a]Determined by TGA

Temperature programmed reduction (TPR)

H_2-TPR was used to assess the reducibility of the two N-CNT supported Fe catalysts (Figure 8.10). The profiles are characterized by multiple peaks resulting from the different reduction steps that are taking place. The first significant peak corresponds to the reduction of Fe_2O_3 to Fe_3O_4 (360 – 410^oC) whereas the second peak (460 – 500^oC) is associated with the reduction of Fe_3O_4 to Fe^0 [9, 35]. The reduction peak occurring at 589^oC could be attributed to small particles that are difficult to reduce because of the strong metal-carbon interaction. The peaks appearing at temperatures greater that 600^oC are due to the gasification of the carbon support [12]. The reduction from Fe_2O_3 to Fe_3O_4 occurs at a lower temperature (372^oC) for the Fe/N-CNT-750-55R2 catalyst than the Fe/N-CNT-750 catalyst, however, the reduction from Fe_3O_4 to Fe^0 appears to be more difficult when compared to the Fe/N-CNT-750 TPR data. This is probably due to the difference in particle size as observed by TEM and XRD analysis. It is known that smaller particles tend to interact more strongly with a support and as a result they are more difficult to reduce as compared to larger particles.

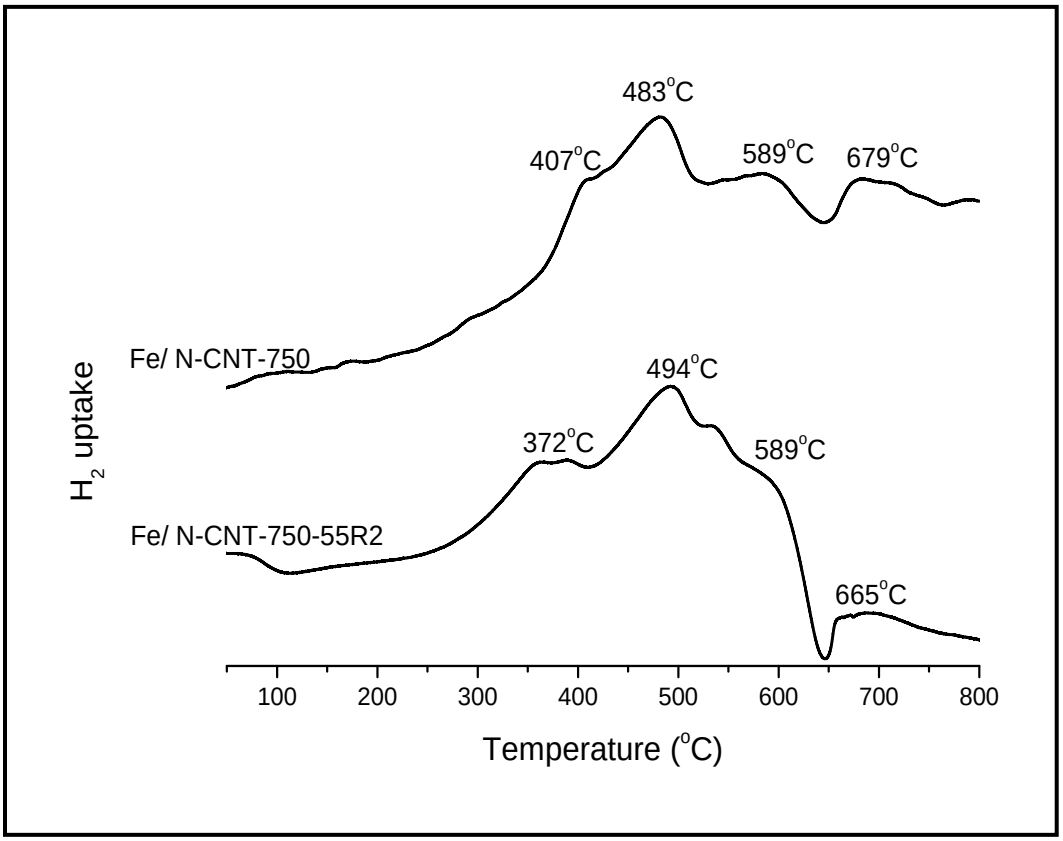


Figure 8.10: H_2-TPR profiles of Fe/N-CNT-750-55R2 and Fe/N-CNT-750 catalysts.

8.4.3 Catalytic evaluation

The performance of the iron catalysts supported on N-CNT in the Fischer-Tropsch synthesis was tested in a fixed bed reactor using the following reaction conditions: T = 275 °C, P = 8 bar, GHSV of 2400 h^{-1} and a H_2:CO ratio of 2. Figure 8.11 shows the % CO conversion as a function of time-on-stream. The catalytic activity and product selectivity data have been calculated after stable conversion was achieved (> 30 h) and results are presented in Table 8.7.

From Figure 8.11, it is observed that the activity of the catalysts was initially low (~ 15%) but increased significantly within 15 h, dropped slightly and become stable

after 30 h for the entire experiment (120 h). The activity drop within the first 10 to 30 h could be due to the restructuring of the catalyst under FT conditions. The catalysts showed limited signs of deactivation after 30 h.

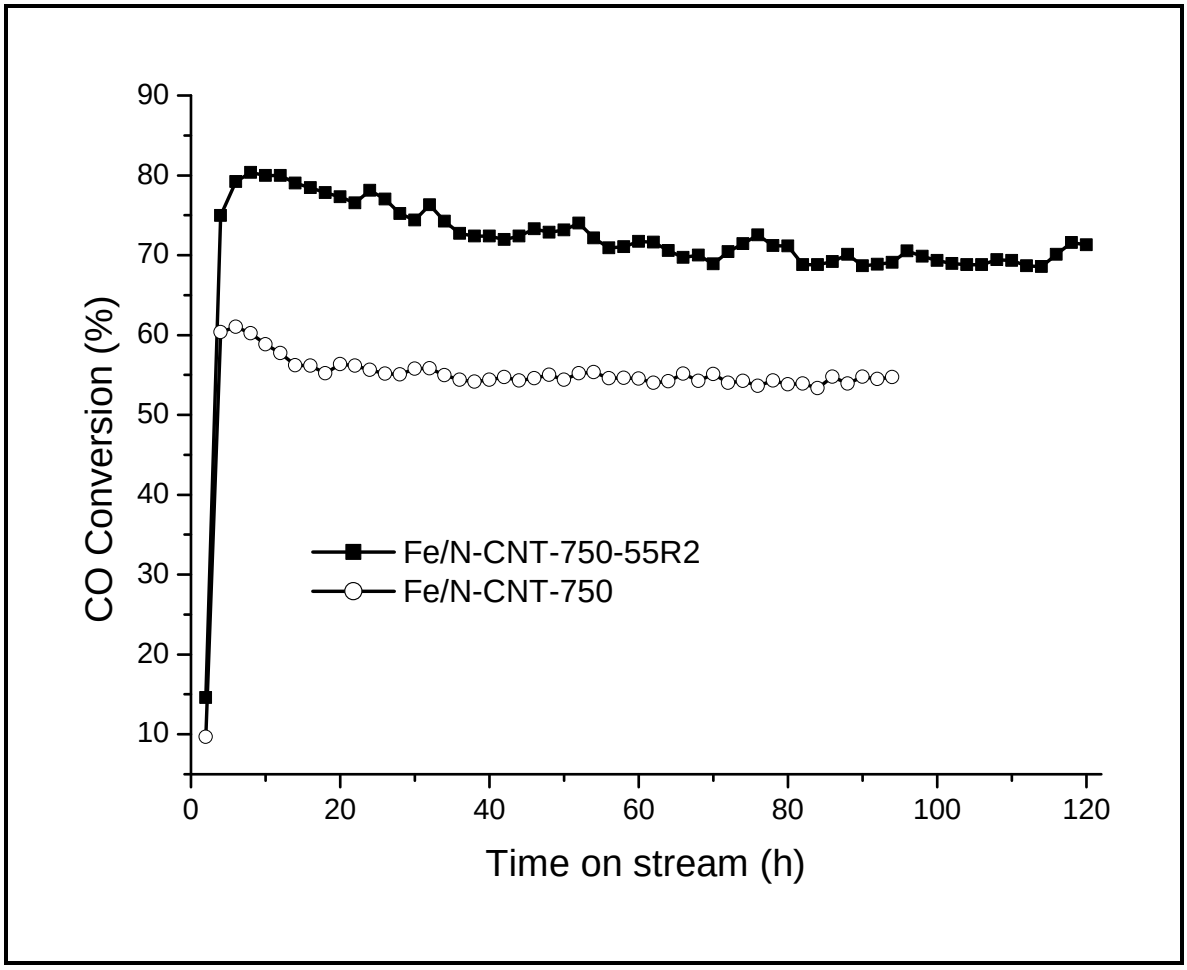


Figure 8.11: CO conversion versus time on stream.

The Fe/N-CNT-750-55R2 catalyst showed a CO conversion of 70% compared to that of Fe/N-CNT-750 catalyst with a conversion of 55%. The difference in CO conversion is related to the number of metal active sites available for the FTS reaction. The lower CO conversion of the Fe/N-CNT-750 catalyst is due to the larger particle size (TEM images-Figure 8.7) which results in poor metal dispersion in the

catalyst and hence a smaller number of active metal sites for the FTS. The Fischer-Tropsch rate as well as the water gas shift rate for the Fe/N-CNT-750 catalyst are also lower than for the Fe/N-CNT-750-55R2.

Comparing the selectivities of the two catalysts revealed that the Fe/N-CNT-750-55R2 catalyst showed lower selectivity to methane and high selectivity to C_{5+} hydrocarbon with an α value of 0.65. Fe/N-CNT-750 catalyst by contrast showed a very high selectivity to lighter hydrocarbons with an α value of 0.29. The Fe/N-CNT-750 catalyst behaves like a methanation catalyst with a methane selectivity of 64%. The mechanism of hydrocarbon synthesis on the Fe catalysts includes three steps namely initiation, propagation and termination reactions [36]. The higher production rate of CH_4 by the Fe/N-CNT-750 catalyst is hence attributed to the faster rate of hydrogenation of the methyl species formed on the surface of the catalyst. No olefin production was observed with the Fe/N-CNT-750 catalyst because of its hydrogenating capabilities.

Clearly, the Fe/N-CNT-750-55R2 catalyst has superior FTS activity compared to the Fe/N-CNT-750 catalyst. The superior behavior relates to the smaller Fe particle size and higher metal dispersion. For comparison, one would need to investigate the FT performance of Fe/CNT-750 without any nitrogen in a further study to determine the role of nitrogen in the catalyst.

Table 8.7: Activity and selectivity of Fe/N-CNT catalysts in FTS.

Catalyts	Fe/N-CNT-750	Fe/N-CNT-750-55R2
Average particle size (nm)[a]	27	8.0
CO Conversion (%)	55.3	70.1
$10^6 \times$ CO rate[b]	1.83	2.75
$10^6 \times CO_2$ rate (WGS)	0.89	1.46
$10^6 \times$ FTS rate	0.94	1.29
Activity (μmol/s.gFe)	36.6	55
Alpha (α)	0.29	0.65
Selectivity (mol C %)		
C_1	63.5	13.5
C_2-C_4	19.6	25.6
C_{5+}	16.9	60.9
O/O+P ratio[c]	—[d]	0.31
CO_2 (% produced)	7.70	13.4

[a]TEM
[b] Rate are expressed in mol/s.
[c] $\sum C_x^{=} / \sum (C_x^{=} + C_x)$, where x = 2,3,4,5.
[d]not detected.

8.5 Conclusion

N-CNTs were synthesized by a post-doping method using acetonitrile as the nitrogen source. There was no significant change in the morphology of the N-CNTs up to 850°C (reaction temperature). The nitrogen content and % mass increase of the N-CNTs increased almost linearly with increasing reaction temperature whereas the surface area was found to decrease. The Raman data showed that the graphite layers of the N-doped CNT are more ordered than the purified CNTs as reflected in the decrease in the I_D/I_G ratio up to 850°C. Two Fe catalysts were prepared using N-CNTs as a support. The Fe/N-CNT-750 catalyst, containing 1.7% nitrogen was found

to have a very broad and large Fe particle size distribution which resulted in a poor FTS catalyst. However, functionalizing the N-CNT before metal loading created more surface functional groups on which to anchor metal particles. The Fe metal deposited on this support has a narrow, smaller Fe particle size and exhibited significantly improved activity during FTS activity. The doping of a CNT with nitrogen is not a necessary condition to generate Fe FT catalysts.

8.7 References

[1] E. Iglesia, Applied Catalysis A: General 161 (1997) 59.

[2] M.J. Gradassi, Studies in Surface Science and Catalysis 119 (1998) 35.

[3] C.H. Bartholomew, Studies in Surface Science and Catalysis 64 (1991) 158.

[4] H.H. Storch, N. Golumbic, R.B. Anderson, The Fischer-Tropsch and Related Syntheses, John Wiley & Sons, Inc., New York, 1951.

[5] S.J. Tauster, S.C. Fung, Journal of Catalysis 55 (1978) 29.

[6] S. Maity, Current Science 80 (2001) 628.

[7] C. Moreno-Castilla, F.J. Maldonado-Hódar, Carbon 43 (2005) 455.

[8] A.A. Deshmukh, R.U. Islam, M.J. Witcomb, W.A.L. van Otterlo, N.J. Coville, ChemCatChem 2 (2009) 51.

[9] M.C. Bahome, L.L. Jewell, D. Hildebrandt, D. Glasser, N.J. Coville, Applied Catalysis A, General 287 (2005) 60.

[10] M.C. Bahome, L.L. Jewell, K. Padayachy, D. Hildebrandt, D. Glasser, A.K. Datye, N.J. Coville, Applied Catalysis A: General 328 (2007) 243.

[11] L. Guczi, G. Stefler, O. Geszti, Z. Koppány, Z. Kónya, É. Molnár, M. Urbán, I. Kiricsi, Journal of Catalysis 244 (2006) 24.

[12] E. van Steen, F.F. Prinsloo, Catalysis Today 71 (2002) 327.

[13] H. Xiong, M.A.M. Motchelaho, M. Moyo, L.L. Jewell, N.J. Coville, Journal of Catalysis (2010) accepted.

[14] P. Ayala, R. Arenal, M. Rümmeli, A. Rubio, T. Pichler, Carbon 48 (2010) 575.

[15] H. Xiong, M. Moyo, M.K. Rayner, L.L. Jewell, D.G. Billing, N.J. Coville, ChemCatChem 2 (2010) 514.

[16] C.P. Ewels, M. Glerup, Journal of Nanoscience and Nanotechnology 5 (2005) 1345.

[17] V.V. Strelko, N.T. Kartel, I.N. Dukhno, V.S. Kuts, R.B. Clarkson, B.M. Odintsov, Surface Science 548 (2004) 281.

[18] R. Czerw, M. Terrones, J.C. Charlier, X. Blase, B. Foley, R. Kamalakaran, N. Grobert, H. Terrones, D. Tekleab, P.M. Ajayan, Nano Letters 1 (2001) 457.

[19] S. Dommele, K.P. Jong, J.H. Bitter, Chemical Communications 2006 (2006) 4859.

[20] S.C. Roy, P.A. Christensen, A. Hamnett, K.M. Thomas, V. Trapp, Journal of the Electrochemical Society 143 (1996) 3073.

[21] R.I. Jafri, N. Rajalakshmi, S. Ramaprabhu, Journal of Power Sources (2010).

[22] R.A. Sidik, A.B. Anderson, N.P. Subramanian, S.P. Kumaraguru, B.N. Popov, Journal of Physical Chemistry B 110 (2006) 1787.

[23] M.S. Saha, R. Li, X. Sun, S. Ye, Electrochemistry Communications 11 (2009) 438.

[24] Y. Chen, J. Wang, H. Liu, R. Li, X. Sun, S. Ye, S. Knights, Electrochemistry Communications 11 (2009) 2071.

[25] L.Q. Jiang, L. Gao, Carbon 41 (2003) 2923.

[26] S.C. Roy, A.W. Harding, A.E. Russell, K.M. Thomas, Journal of the Electrochemical Society 144 (1997) 2323.

[27] A.E. Shalagina, Z.R. Ismagilov, O.Y. Podyacheva, R.I. Kvon, V.A. Ushakov, Carbon 45 (2007) 1808.

[28] S. Van Dommele, A. Romero-Izquirdo, R. Brydson, K.P. De Jong, J.H. Bitter, Carbon 46 (2008) 138.

[29] L.G. Bulusheva, A.V. Okotrub, I.A. Kinloch, I.P. Asanov, A.G. Kurenya, A.G. Kudashov, X. Chen, H. Song, physica status solidi (B) 245 (2008) 1971.

[30] R. Saito, A. Grüneis, G.G. Samsonidze, V.W. Brar, G. Dresselhaus, M.S. Dresselhaus, A. Jorio, L.G. Cançado, C. Fantini, M.A. Pimenta, New Journal of Physics 5 (2003) 157.

[31] N. Hellgren, M.P. Johansson, E. Broitman, L. Hultman, J.E. Sundgren, Physical Review B 59 (1999) 5162.

[32] Q.-. Yang, P.-. Hou, M. Unno, S. Yamauchi, R. Saito, T. Kyotani, Nano Letters 5 (2005) 2465.

[33] S.D. Mhlanga, "Synthesis and study of carbon nanotubes and carbon spheres" PhD thesis, University of the Witwatersrand, Johannesburg (2009).

[34] H. Xiong, M. Moyo, M.A.M. Motchelaho, L.L. Jewell, N.J. Coville, Applied Catalysis A: General (2010).

[35] H. Hayakawa, H. Tanaka, K. Fujimoto, Applied Catalysis A: General 310 (2006) 24.

[36] A. Tavasoli, M. Trépanier, R.M.M. Abbaslou, A.K. Dalai, N. Abatzoglou, Fuel Processing Technology 90 (2009) 1486.

9

Chapter Nine

The effect of Co(nitrate) and Co(acetate) catalysts supported on CNT for use in the Fischer-Tropsch synthesis

9.1 Introduction

The Fischer-Tropsch synthesis, which is the catalytic conversion of syngas (a mixture of CO and H_2) to hydrocarbons, has been shown to be catalyzed by group 8-10 transition metals, with Fe, Co and Ru exhibiting the highest activity [1-8].

Co-based catalysts have been seen as the preferred candidate to catalyse the FT reaction based on natural gas because of their high selectivity to linear hydrocarbons, their high stability towards deactivation by water (a by-product of the FT reaction)

and their low activity for the competing water-gas-shift reaction. Cobalt catalysts are also cheaper than ruthenium and can be used at lower temperatures and pressures than iron catalysts [3, 9-13]. Cobalt precursors are usually placed on a support in order to obtain well dispersed, high density surface active sites. Previous research on Co-based FT catalysts has been mostly conducted on cobalt metal supported on an oxidic support such as SiO_2, Al_2O_3 and to a lesser extent TiO_2 [10, 11, 13]. One disadvantage of these support materials is that they are very reactive toward cobalt and they form mixed compounds with the metal that are only reducible at high temperatures [5, 10, 11, 14]. More recent studies have reported on the use of carbon materials such as carbon nanotubes (CNTs) [15-18], carbon nanofibers (CNFs) [19, 20], [21] and carbon spheres (CSs) [22, 23] as a support material. Bezemer et al. [5] have shown that carbon nanofibers may be a promising support for Co-based FTS catalysts, exhibiting good activity and selectivity towards high molecular weight hydrocarbons. De Jong and co-workers [19, 24] have used fishbone-like CNFs as a support to study Co-based FTS catalysts. They reported that the turn over frequency (TOF) for CO hydrogenation was lower for small Co particles (< 6-8 nm); and that with Co particles with sizes larger than 6-8 nm, the TOF was not dependent on the cobalt particle size [19]. Studies on the effects of cobalt precursors reported in the literature have focussed on cobalt supported on oxidic supports [25, 26].

Conventional cobalt FT catalysts are usually prepared using cobalt nitrate as the precursor. However the desire to control parameters affecting the catalyst behaviour such as cobalt dispersion has prompted researchers to study the effect of other sources of cobalt. Some early studies have shown that cobalt acetate can be used to prepare highly dispersed cobalt metal catalysts supported on silica [27], titania [25] or SBA-15 [13]. The resulting catalysts were found to be poorly reduced in a hydrogen stream and as a result these catalysts were much less active for CO hydrogenation compared to catalysts prepared using cobalt nitrate as precursor.

This work presents a preliminary study on the effect of catalyst precursors on the properties of carbon nanotube supported Co-based FTS catalysts. The catalysts were prepared by a deposition precipitation method using either $Co(NO_3)_2 \cdot 6H_2O$ or $Co(OOCCH_3)_2$ as precursors. The resulting materials were characterized using transmission electron microscopy (TEM), temperature programmed reduction (TPR), N_2-physisorption, thermogravimetric analysis (TGA), and X-ray diffraction. The catalytic testing was carried out in a fixed-bed micro reactor at 8 bar, 2400 h^{-1}, 220^oC, and at a H_2: CO ratio of 2.

9.2 Experimental

9.2.1 Carbon nanotube synthesis

Carbon nanotubes were grown from the catalytic decomposition of acetylene at 700^oC over a 10% Fe-Co/$CaCO_3$ catalyst. Detailed synthetic procedures can be found elsewhere [28]. The as-grown CNTs were purified and functionalized by refluxing the material in 55% HNO_3 at 120^oC for 2 h. After washing and drying at 120^oC for approximately 12 h, CNTs with a BET surface area of 101 m^2/g and pore volume of 0.32 cm^3/g were obtained.

9.2.2 Catalyst preparation

Cobalt (10 wt. %) was loaded onto the CNTs obtained above using a deposition precipitation method with urea as the precipitating agent. In brief, $Co(NO_3)_2 \cdot 6H_2O$ (0.987 g) and urea (0.306 g; 1.5 mol of urea per mole of cobalt) were dissolved in deionized water (20 mL) and added to the functionalized carbon nanotubes (2.00 g). The temperature was subsequently raised to 90^oC. After allowing sufficient time (at least 2 h) for the hydrolysis of urea, the excess solvent was evaporated, followed by

drying in a static air oven at 100°C for 12 h. The catalyst obtained was heat-treated in N_2 at 250°C for 2 h in order to decompose the nitrate; this catalyst was denoted Co-N/CNT (N = nitrate). The same preparation procedure was followed for the preparation of Co-A/CNT catalyst (A = acetate) using $Co(OOCCH_3)_2$ as the precursor.

9.2.3 Catalyst characterization

The structures and morphologies of the CNT support and the Co/CNT catalysts were characterized by TEM. Sample specimens for TEM studies were prepared by ultrasonic dispersion of the sample in methanol, and the suspensions were dropped onto a SPI-carbon coated copper grid. TEM investigations were carried out using a FEI Tecnai Spirit G^2 transmission electron microscope operating at 120 kV. Several TEM micrographs were recorded for each sample and analyzed for particle size distribution using the ImageJ software. A least 120 metal nanoparticles per sample were analyzed to determine the average catalyst particle size.

The surface area and pore volume of the catalysts were determined by N_2 physisorption using a Micromeritics TRISTAR 3000 analyzer. A sample of approximately 300 mg was degassed at 150°C for 4 h under a flow of N_2, and then the surface area and pore volume were determined by the Brunauer-Emmett-Teller (BET) method.

The TGA analysis was done on a Perkin Elmer STA 4000 analyzer. About 5-10 mg of sample was placed in a ceramic pan and placed in the instrument's furnace. The temperature of the sample was increased from room temperature to 900°C at 10°C/min under an oxidative atmosphere (air, 20 mL/min). The percentage Co loading in the catalyst was determined using the % residual ash that remained after

burning the carbon from the catalyst and assuming that the ash consists only of Co_3O_4.

The TPR experiment was performed on a Micromeritics AutoChem II Chemisorption analyser to study the reduction behaviour of the catalysts. A sample of the catalyst (100 mg) was loaded into a U-shaped quartz tube reactor, fitted with a thermocouple for continuous temperature measurement. The reactor was placed in a furnace. Prior to the H_2-TPR analysis, the sample was first degassed in a flow of high purity argon (20 mL/min) at 150^{o}C for 30 min to remove traces of water, and then cooled to 40^{o}C. The sample was then reduced in 5%H_2/Ar (50 mL/min) as the temperature was increased from 40^{o}C to 800^{o}C at a rate of 10^{o}C /min. The gas flow through the reactor was controlled by three Brooks mass flow controllers. A thermal conductivity detector (TCD) was used to measure the H_2 consumption. The temperature and H_2 consumption was captured automatically by a PC to give the TPR profiles.

X-ray powder diffraction (XRD) patterns for the support and the Co/CNT catalysts were recorded with a Brucker D2 phaser diffractometer using a Cu source (1.5418 Å) and a LynxEye detector. The scan was within a 2θ range of 15-70^o with 0.03^o steps at 25^{o}C. Crystallite phases were determined by comparing the diffraction patterns with those in the standard powder XRD files (JCPDS).

9.2.4 Catalyst testing

Catalyst (0.5 g) was added to the fixed-bed reactor and reduced in-situ at 350^{o}C for 20 h under a stream of pure hydrogen (2 bar, 20 mL/minute). After reduction the temperature was decreased to 220^{o}C under the flow of H_2, the pressure was gradually increased to 8 bar and a flow of syngas was passed over the catalyst bed at a flowrate of 20 mL/min. All gas lines after the reactor were kept at 150^{o}C, and a hot trap placed immediately after the reactor was held at 150^{o}C in order to collect wax. A second

trap, kept at ambient temperature was used to collect the oil and water mixture. The flow of gases was controlled using a metering valve and measured with a bubble meter. The gaseous product stream was analyzed online using two gas chromatographs. A thermal conductivity detector (TCD), equipped with a Poropak Q packed column, used to analyze N_2, CO, CO_2 and H_2, and a flame ionization detector (FID), used to analyze the hydrocarbon products. An offline GC was used to analyze the oil and wax products.

9.3 Results and discussion

9.3.1 Surface Area and pore volume measurements

Results of surface area and pore volume measurements of the as-grown CNTs, functionalized CNTs and Co/CNTs catalysts are presented in Table 9.1. As observed in Table 9.1, the BET surface area increased from 70 to 101 m^2/g after purification due to the removal of residual catalyst and CaO support as well as the opening of some carbon nanotube caps. Upon loading the purified carbon nanotubes with cobalt nitrate or cobalt acetate, the BET surface area of the resultant catalysts decreased from 101 to 86 and 71 m^2/g respectively. The pore volume also decreased upon adding the Co metal from 0.32 to 0.22 and 0.24 cm^3/g. Loading of the cobalt metal onto the CNT support led to a decrease in both the surface areas and pore volumes and these are attributed to pore blockage. Similar observations were made by Tavasoli et al. [29] and Martinez et al. [13].

Table 9.1: Metal loading, BET surface area and pore volume results of CNT and Co/CNT

Samples	Cobalt Precursor	Surface Area (m^2/g)[a]	Pore Volume (cm^3/g)
As-grown CNTs	–	70	0.28
Purified CNTs	–	101	0.32
Co-N/CNT	nitrate	86	0.22
Co-A/CNT	acetate	71	0.24

[a]Error ± 5%

9.3.2 TEM analysis of carbon nanotubes

CNTs were produced by the catalytic chemical vapour deposition method where acetylene was decomposed over a 10%Fe-Co/$CaCO_3$ at 700^oC. TEM images of the as-grown and the purified CNTs are shown in Figure 9.1. The morphology and structure of the CNTs are clearly visible (Figure 9.1a) which were found to be multi-walled (Figure 9.1b: HRTEM inset) with internal diameters ranging from 8-18 nm, and outer diameters ranging from 20-35 nm. The as-grown CNTs (Figure 9.1a) contain some non-CNT material such as the residual growth catalyst and the catalyst support. Purification is therefore an essential step to remove the non-carbon materials and at the same time, add functional groups that render the CNTs less hydrophobic. Figure 9.1c shows the TEM image of the purified CNTs. Upon purification, the CNT surface is roughened and this roughness is required for the preparation of stable catalysts since it provides additional anchoring sites for the catalyst nanoparticles [2, 30].

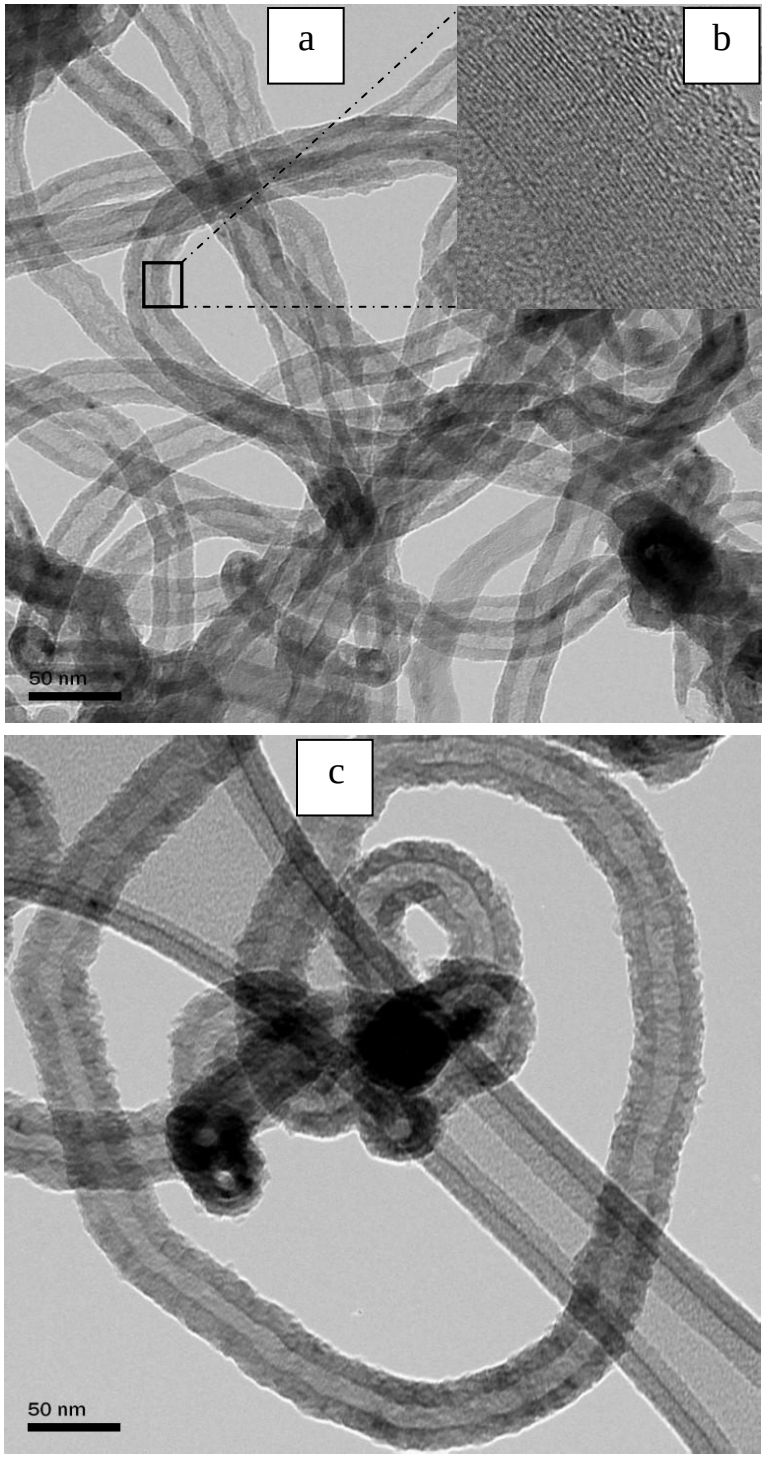


Figure 9.1: (a) TEM image of as-grown CNTs; (b) HRTEM of CNTs showing multi-walls and (c) TEM image of purified CNTs

9.3.3 TEM analysis of Co/CNT catalysts

Co-based FTS catalysts were prepared by a deposition precipitation method using $Co(NO_3)_2 \cdot 6H_2O$ and $Co(OOCCH_3)_2$ as cobalt precursors. Figures 9.2 and 9.3 show the TEM images and particle size histograms of the Co-N/CNT and Co-A/CNT respectively. The CNT structure was clearly preserved after cobalt loading and thermal treatment. It can be seen that the majority of the cobalt particles were distributed on the outer surface on the CNTs with very few found on the inside. This differs from the results obtained by Trépanier et al. [31] who prepared 10%Co/CNT and found that the majority of the cobalt particles were distributed inside the tubes. However, their catalysts were prepared using the incipient wetness impregnation method and that could explain the observed difference. TEM analysis of the catalysts revealed that the average cobalt particle size is dependent on the precursor used with Co-A/CNT having the smaller average particle size of ~ 9 nm. The Co-N/CNT catalyst has a broader range of particle sizes (5-15 nm) with an average particle size centered at ~ 12 nm. The difference in the catalysts' average particle size could be due to the way the precursors interact with the solvent and the support surface.

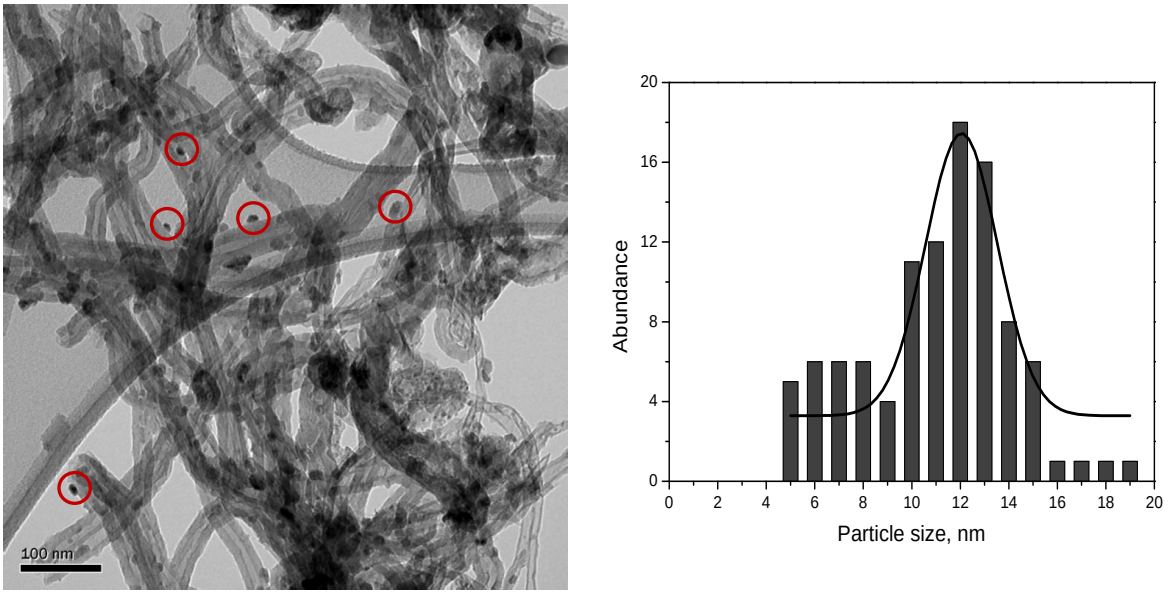


Figure 9.2: TEM image and cobalt particle size histogram for Co-N/CNT (average cobalt particle size = 12 nm): some Fe particles are indicated by the circles

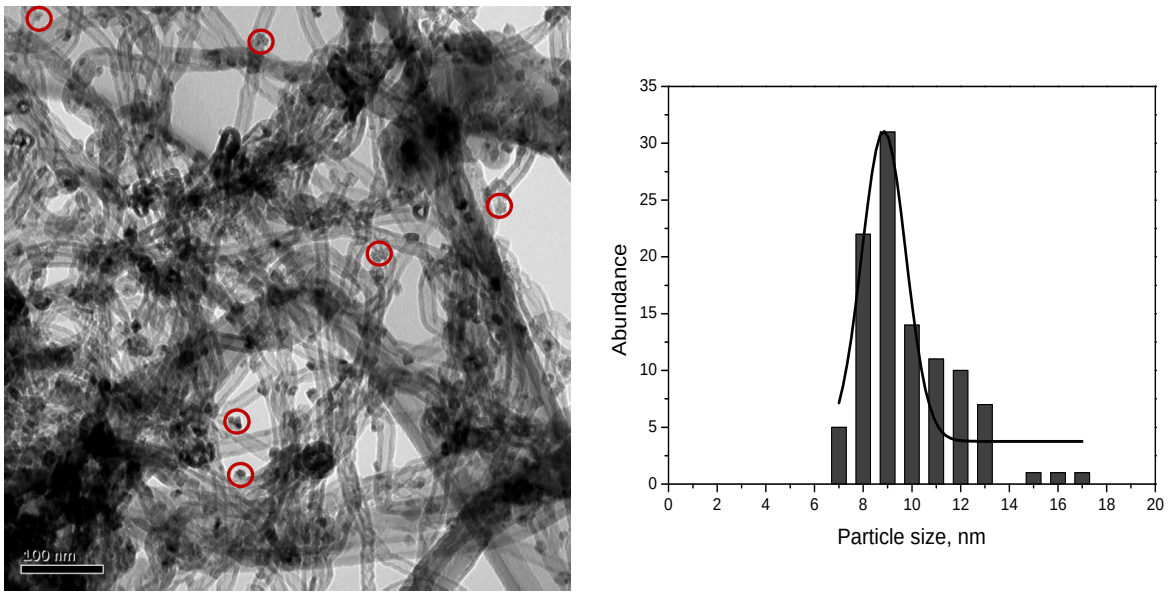


Figure 9.3: TEM image and cobalt particle size histogram for Co-A/CNT (average cobalt particle size = 8.9 nm): some Fe particles are indicated by the circles

9.3.4 XRD analysis

The XRD patterns of CNT, Co-N/CNT and Co-A/CNT catalysts are displayed in Figure 9.4 with the most pronounced diffraction lines indicated. The peaks at 2θ values of 25^o and 44.6^o are present in all three XRD patterns and are characteristic of the graphitic walls of the CNTs [31, 32]. The XRD pattern of Co-N/CNT shows several diffraction peaks at 2θ values of 31.3^o, 36.8^o, 59.4^o and 65.2^o whereas that of the Co-A/CNT catalyst shows one diffraction peak at a 2θ values of 36.8^o. All of these peaks are related to the diffraction of different crystal planes of the Co_3O_4 phase. The peak at 2θ = 36.8^o is the most intense peak of Co_3O_4 in the XRD spectrum of the catalysts. However, the intensity of Co_3O_4 in Co-A/CNT was much lower than that of the catalyst prepared from cobalt nitrate, suggesting that most of the cobalt crystals in the acetate sample are small and are highly dispersed on the CNT surface. It is clear from the XRD patterns that the precursor used in the preparation of the cobalt catalysts has a major impact on the fraction of different cobalt phases present. Using the Scherrer equation, the average crystallites size of the Co_3O_4 in the catalysts was estimated from the line broadening of a Co_3O_4 at 2θ values of 36.8^o. Table 9.2 presents the result of the average crystallite size obtained by XRD and the data are in good agreement with cobalt particle sizes determined by TEM for the Co-N/CNT samples. The average crystallite size for the Co-A/CNT catalyst could not be measured using XRD possibly because the crystallite size in this catalyst is below the detection limit of the XRD.

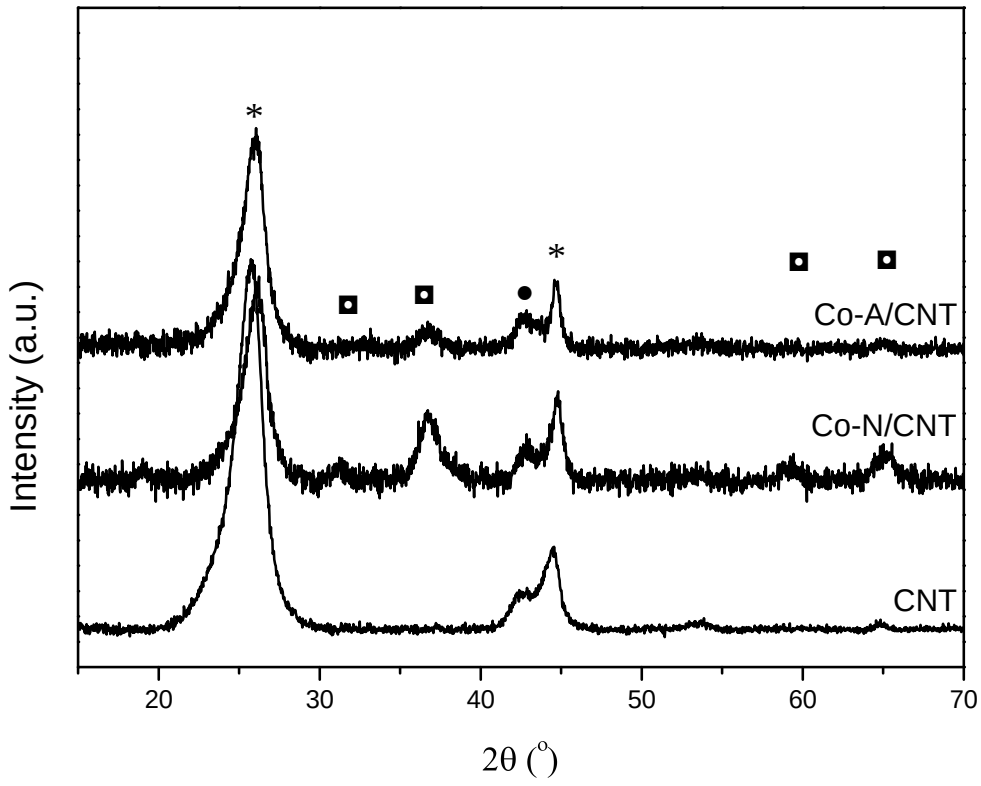


Figure 9.4: XRD patterns of the CNT support and Co/CNT catalysts: * = CNT; ◘ = Co_3O_4; ● = Co-Fe, Co_3C, Co_2C or Fe_3C.

Table 9.2: Metal loading and particle size for Co-N/CNT and Co-A/CNT

Catalyst	Metal loading (%)[a]	Cobalt Particle size, nm	
		TEM	XRD
Co-N/CNT	10.3	5-15	7.0
Co-A/CNT	9.5	8-10	—[b]

[a]Determined by TGA.

[b]could not be measured.

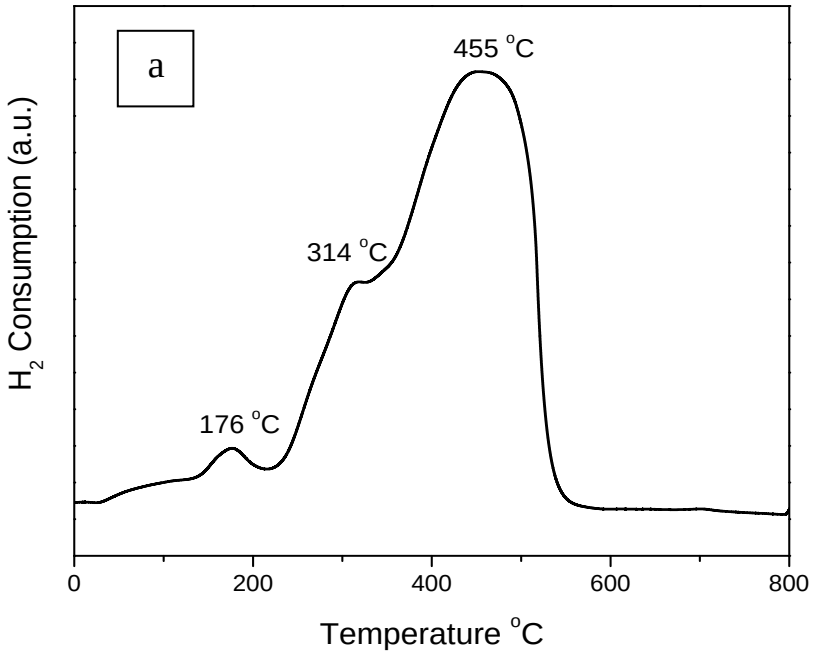
9.3.5 Temperature programmed reduction (TPR)

TPR is a powerful tool for studying the reduction behaviour of oxidized catalysts. It is sometimes possible to obtain useful information about the degree of interaction between the active metal and the support from the reduction profiles of supported catalysts [13]. The reduction of Co_3O_4 takes place in two steps [33]:

$$Co_3O_4 + H_2 \rightarrow 3CoO + H_2O$$
$$CoO + H_2 \rightarrow Co^0 + H_2O$$

Figure 9.5a presents the TPR profile of cobalt oxide obtained by calcining $Co(NO_3)_2{\cdot}6H_2O$ at 250^{o}C for 150 min and Figure 9.5b the TPR profiles of Co-N/CNT and Co-A/CNT. From Figure 9.5a, (unsupported cobalt nitrate used as reference), there are three peaks present. The low temperature TPR peak appearing at T = 176^{o}C is commonly assigned to either the partial reduction of Co_3O_4 ($Co_3O_4 \rightarrow$ CoO) or the reduction or decomposition in hydrogen of residual cobalt nitrate [14]. The second reduction peak, which corresponds to the reduction of Co^{3+} to Co^{2+} [34], occurs at 314^{o}C and the third reduction step from Co^{2+} to Co^0 [34] occurs at 455^{o}C. The TPR profiles of the Co/CNT catalyst (Figure 9.5b), show three reduction peaks and the temperature at which each peak occurs is presented in Table 9.3. As revealed by XRD in Figure 9.4, Co_3O_4 is the main cobalt phase in the Co-N/CNT and Co-A/CNT catalysts after thermal treatment in N_2. Thus the 1st and 2nd peaks are ascribed to the stepwise reduction of $Co_3O_4 \rightarrow CoO \rightarrow Co^0$ and the 3rd peak corresponds to the hydrogenation of the CNT to produce methane [1, 34]. The reduction of CNT supported Co catalysts (Co/CNTs) (Figure 9.5b) occurs at a slightly lower temperature and the peak intensities are also smaller relative to those of the unsupported Co_3O_4 (Figure 9.5a). The presence of the CNT support enhances the reducibility of the Co catalyst. The first reduction peak (T = 333^{o}C) of Co-A/CNT catalyst is very small compared to that of Co-N/CNT (T = 303^{o}C), this suggests that there is a rapid conversion from Co_3O_4 to CoO in the case of the Co-A/CNT

catalysts; and the second reduction peak (T = 433°C) for the Co-A/CNT catalyst is broader and occurs at higher temperature than that of the Co-N/CNT catalyst (T = 376°C), suggesting a hindered reduction of CoO to Co^0 for the Co-A/CNT catalyst (Figure 9.5b). It is suggested that the kinetics of the CoO reduction to metallic cobalt strongly depend on the initial Co_3O_4 particle size [10, 35]. Smaller particles reduce slowly due to their interaction with the support. We can therefore say that the difference in the reduction behaviour of the Co-N/CNT (TEM average particle size = 12 nm) and Co-A/CNT (TEM average particle size = 8.9 nm) catalysts is related to the difference in particle size of the two catalysts.



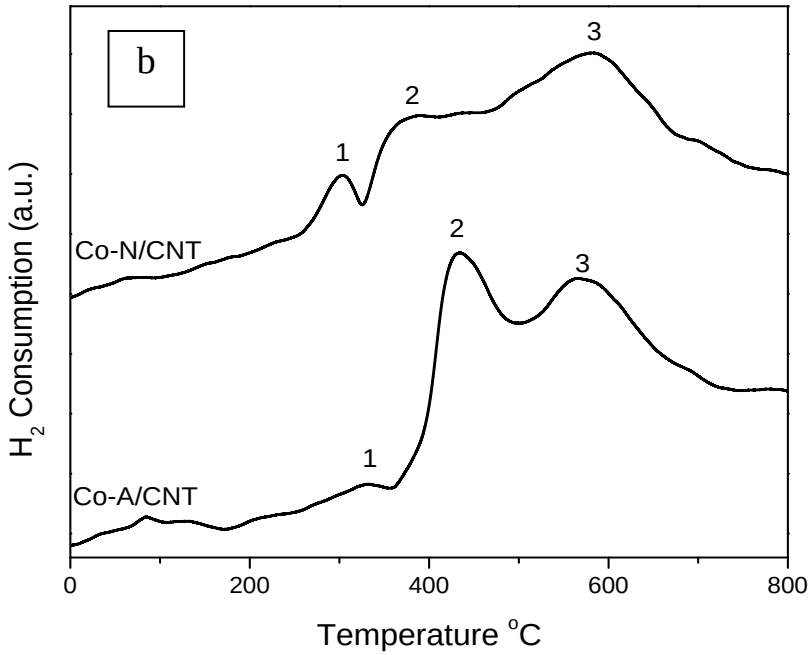


Figure 9.5: TPR profiles of (a) $Co(NO_3)_2 \cdot 6H_2O$ calcined at 250°C for 2 h and (b) 10 wt% Co/CNT prepared using cobalt nitrate and cobalt acetate precursors.

Table 9.3: Temperature of the peak maxima at which each reduction steps occured during the H_2-TPR

Catalyst	Reduction temperature (°C)		
	peak 1 $Co_3O_4 \rightarrow CoO$	peak 2 $CoO \rightarrow Co$	peak 3 $CNT \rightarrow CH_4$
Co_3O_4[a]	314	455	–
Co-N/CNT	303	376	581
Co-A/CNT	333	433	575

[a]Co_3O_4 was obtained by calcining $Co(NO_3)_2 \cdot 6H_2O$ at 250°C for 150 min.

9.3.6 Thermogravimetric analysis (TGA)

TGA was employed to determine the catalyst composition, thermal stability and the wt. % metal loading of the Co catalysts (Figure 9.6). TGA/DTG of the as-grown CNTs shows that the sample consists of 82% carbonaceous material and is stable up to 642^{o}C in an oxidative atmosphere. The small weight gain at 440^{o}C is due to the oxidation of residual catalyst used in the preparation of the CNTs (Figure 9.6a). After purification the thermal stability of the CNT slightly decreases to 631^{o}C due to the introduction of defects (surface roughness; see TEM image, Figure 9.1c) and the level of purity increases (~ 1% non carbonaceous material present) (Figure 9.6b).

Loading cobalt from cobalt nitrate and cobalt acetate onto the purified CNTs decreased its thermal stability with Co-A/CNT being the most affected (Figure 9.6c and d). The presence of Co metal catalyzes the oxidation of CNT. Co-A/CNT has the smaller average particle size as confirmed by TEM and XRD therefore the particles are in close contact with the CNTs. This could explain why Co-A/CNT is slightly less stable than Co-N/CNT in the oxidation reaction. Table 9.4 summarises the results.

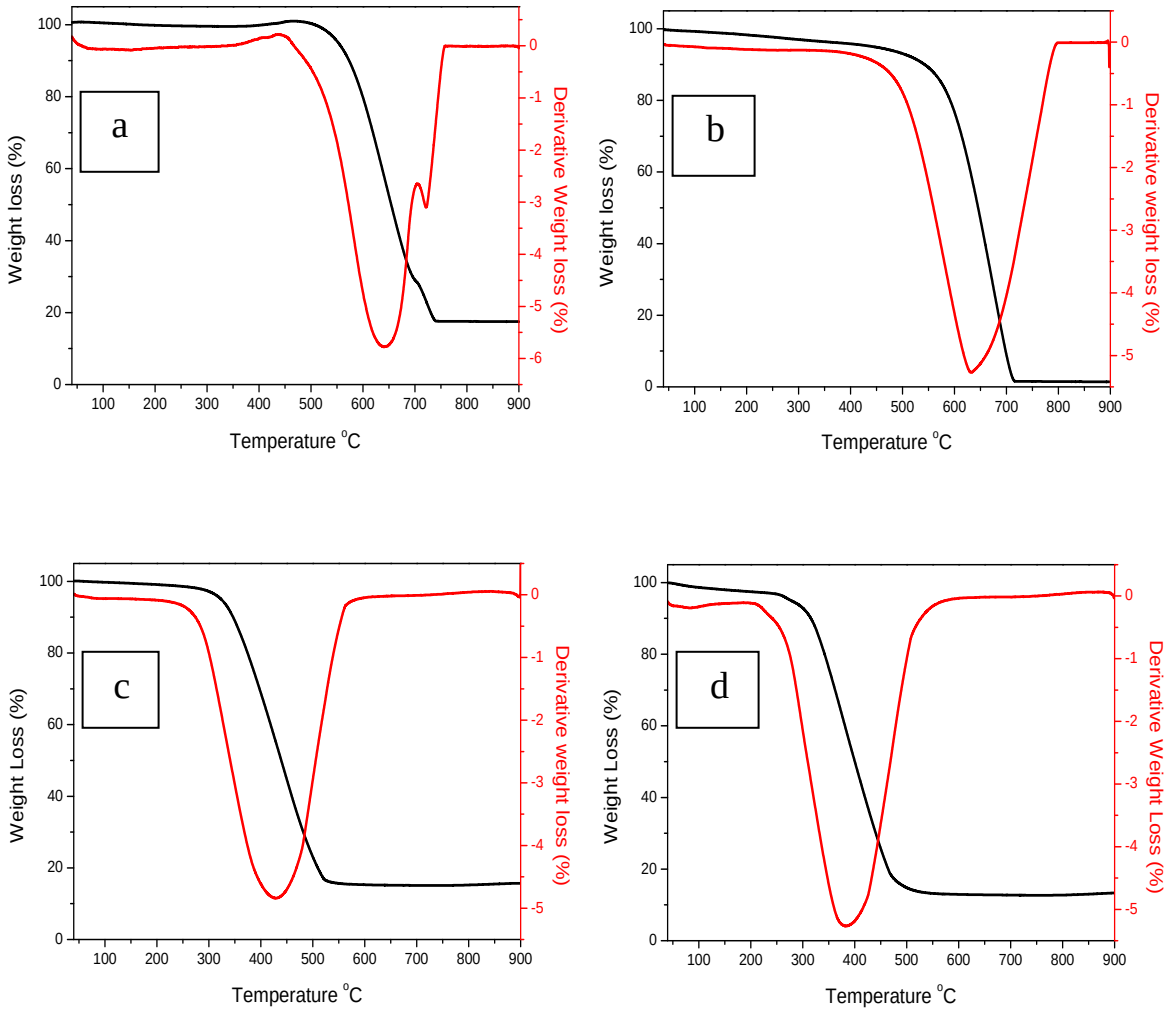


Figure 9.6: TGA curves of as-grown and purified carbon nanotubes and cobalt catalysts under air: (a) As-grown CNTs; (b) purified CNTs; (c) Co-N/CNT; and (d) Co-A/CNT.

Table 9.4: TGA peak position of weight loss/gain for different samples

Samples	Atmosphere	Peak position ^{o}C			Residual mass (%)	
		I	II	III	Co_3O_4	Co
As-grown CNT	Air	440	642	712	18[a]	—
Purified CNTs	Air	—	631	—	1.0	—
Co-N/CNT	Air	—	429	—	15	10.3
Co-A/CNT	Air	—	385	—	14	9.5

[a]Total amount of non-carbon material left behind after burning the carbon

9.4 Catalytic results for the FTS process

Fischer-Tropsch activity and selectivity of the Co-N/CNT and Co-A/CNT catalysts were studied in a fixed-bed reactor under similar operating conditions (220^{o}C, 8 bar, 20 mL/min and CO:H_2 ratio equal 2). Prior to catalytic testing, a blank FT reaction was performed on the purified CNTs (no metal loaded), under the same operating conditions as for the actual runs. Results showed that the % CO conversion was very low and the only product formed was methane. Similar results were obtained by Guczi et al. [36] and Bahome et al. [16]. These data suggest that the residual Fe and Co encapsulated inside the tubes were not accessible to the syngas.

Figure 9.7 shows the CO conversion versus time on stream of the Co-N/CNT and Co-A/CNT catalysts, and Table 9.5 summarises the catalytic results calculated at steady state (steady state was reached after approximately 24 h).

It is observed from Figure 9.7 and Table 9.5 that on average, the % CO conversion/activity is not dependent on the cobalt precursor used to prepare the catalyst although the two catalysts had different average particle size. It is known that in principle the activity of reduced Co catalysts should be proportional to the

concentration of surface Co^0 sites [13] which implies that both catalysts have a similar concentration of surface Co^0 sites. These findings are different from those reported by Martinez et al. [13]. They studied the effect of Co precursor in the FTS synthesis of hydrocarbons and found that the catalyst prepared from a cobalt acetate precursor was much less active than that prepared from cobalt nitrate. Their catalysts were prepared by impregnation on a SBA-15 support and the cobalt acetate catalyst had a much better dispersion and a stronger cobalt-support interaction compared to the cobalt nitrate catalyst that led to the formation of low reducible cobalt species and hence low FTS activity. However with CNT supported cobalt nitrate and cobalt acetate, although the cobalt acetate was found to have smaller average particle size compared to cobalt nitrate, the average activity of both catalysts was found to be similar.

The selectivity to methane was also observed to be similar for both catalysts and this could indicate that both Co-N/CNT and Co-A/CNT have the same concentration of active sites for methane formation. The selectivity towards C_{5+} product was slightly different with Co-N/CNT being more selective towards longer chain hydrocarbons (α = 0.76). Co-N/CNT and Co-A/CNT were both not active for the water gas shift reaction at this low conversion, which is expected for a cobalt-based FTS catalyst. Co-A/CNT yields more olefins compared to Co-N/CNT.

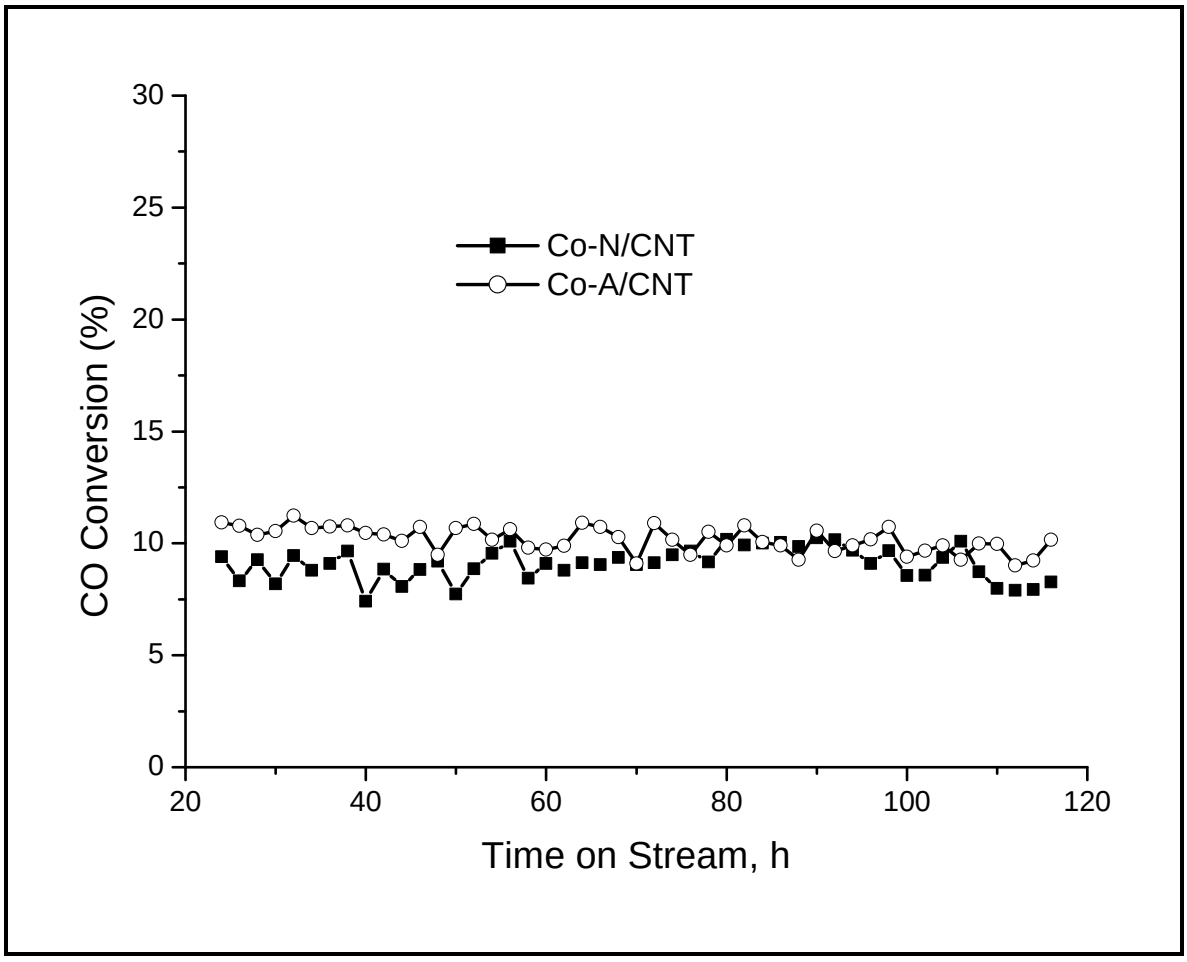


Figure 9.7: CO conversion versus time on stream (reaction conditions: T = 220^{o}C, P = 8 bar, H_2 : CO = 2, GHSV = 2400 h^{-1})

Table 9.5 FTS catalytic performance of Co/CNT catalysts

Catalyts	Co-N/CNT	Co-A/CNT
TOS (h)	120	120
Particle size range[a]	5-15	8-10
% CO Conversion	9.13	10.02
Activity (μmol/s.gCo)	6.62	6.34
Alpha (α)	0.74	0.76
Selectivity (mol % C)		
C_1	31.8	30.5
C_2-C_4	11.2	10.34
C_{5+}	57.0	59.2
$C_2^{=}/(C_2^{=} + C_2)$	0.031	0.034
CO_2	0.0	0.0

[a]TEM analysis.

9.5 Conclusion

Carbon nanotubes with outer diameters ranging between 20 and 35 nm were synthesized by the CVD of acetylene over a $CaCO_3$ supported Fe-Co bimetallic catalyst and used as the support for cobalt catalysts. Co-N/CNTs and Co-A/CNTs catalysts were prepared by the deposition precipitation method using $Co(NO_3)_2 \cdot 6H_2O$ and $Co(OOCCH_3)_2$ respectively as the metal precursors. The catalysts were characterized by TEM, XRD, BET surface area, TPR and TGA and tested in the Fischer-Tropsch synthesis using a fixed bed reactor. TEM analysis revealed that Co-A/CNT has smaller average particle size (8.9 nm) compared to Fe-N/CNT (12 nm). The TPR measurements showed the easy reducibility of the Co-N/CNT catalysts.

The Fischer-Tropsch performance testing of the two catalysts under similar operating conditions showed that the catalysts were stable and that there was no significant difference in their Fischer-Trospch activity despite the observed differences in cobalt particle size and in surface area. Thus the precursor used in the preparation the Co/CNT catalyst did not have a significant influence on the FTS performance of the resulting catalyst.

9.6 References

[1] E. van Steen, F.F. Prinsloo, Catalysis Today 71 (2002) 327.

[2] P. Serp, M. Corrias, P. Kalck, Applied Catalysis A, General 253 (2003) 337.

[3] E. Iglesia, Applied Catalysis A: General 161 (1997) 59.

[4] L. Guczi, G. Stefler, O. Geszti, Z. Koppány, Z. Kónya, É. Molnár, M. Urbán, I. Kiricsi, Journal of Catalysis 244 (2006) 24.

[5] G.L. Bezemer, A. Van Laak, A.J. Van Dillen, K.P. De Jong, Studies in Surface Science and Catalysis 147 (2004) 259.

[6] R.C. Reuel, C.H. Bartholomew, Journal of Catalysis 85 (1984) 78.

[7] R. Oukaci, 2nd Annual Global GTL Summit Executive Briefing, London, UK (2002).

[8] M.A. Vannice, Journal of Catalysis 50 (1977) 228.

[9] R.B. Anderson, The Fischer-Tropsch Synthesis, Academic Press Inc., New York, 1984, p. 295.

[10] G. Jacobs, T.K. Das, Y. Zhang, J. Li, G. Racoillet, B.H. Davis, Applied Catalysis A: General 233 (2002) 263.

[11] P.J. Van Berge, J. Van de Loosdrecht, S. Barradas, A.M. Van der Kraan, Catalysis Today 58 (2000) 321.

[12] R. Bechara, D. Balloy, D. Vanhove, Applied Catalysis A: General 207 (2001) 343.

[13] A. Martínez, C. López, F. Marquez, I. Diaz, Journal of Catalysis 220 (2003) 486.

[14] A.Y. Khodakov, W. Chu, P. Fongarland, Chemical Reviews 107 (2007) 1692.

[15] M.C. Bahome,"Synthesis and use of carbon nanotubes as a support for the Fischer-Tropsch synthesis" PhD thesis, University of the Witwatersrand, Johannesburg (2008).

[16] M.C. Bahome, L.L. Jewell, D. Hildebrandt, D. Glasser, N.J. Coville, Applied Catalysis A, General 287 (2005) 60.

[17] M.C. Bahome, L.L. Jewell, K. Padayachy, D. Hildebrandt, D. Glasser, A.K. Datye, N.J. Coville, Applied Catalysis A: General 328 (2007) 243.

[18] J. Kang, S. Zhang, Q. Zhang, Y. Wang, Angewandte Chemie International Edition English 48 (2009) 2565.

[19] G.L. Bezemer, J.H. Bitter, H.P.C.E. Kuipers, H. Oosterbeek, J.E. Holewijn, X. Xu, F. Kapteijn, A.J. van Dillen, K.P. de Jong, Journal of the American Chemial Society 128 (2006) 3956.

[20] J.P. den Breejen, P.B. Radstake, G.L. Bezemer, J.H. Bitter, V. Frøseth, A. Holmen, K.P. Jong, Journal of the American Chemial Society 131 (2009) 7197.

[21] G.L. Bezemer, P.B. Radstake, V. Koot, A.J. van Dillen, J.W. Geus, K.P. de Jong, Journal of Catalysis 237 (2006) 291.

[22] H. Xiong, M. Moyo, M.K. Rayner, L.L. Jewell, D.G. Billing, N.J. Coville, ChemCatChem 2 (2010) 514.

[23] H. Xiong, M.A.M. Motchelaho, M. Moyo, L.L. Jewell, N.J. Coville, Journal of catalysis (2010).

[24] J.P. den Breejen, P.B. Radstake, G.L. Bezemer, J.H. Bitter, V. Froseth, A. Holmen, K.P. de Jong, Journal of the American Chemical Society 131 (2009) 7197.

[25] M. Kraum, M. Baerns, Applied Catalysis A: General 186 (1999) 189.

[26] K. Jalama, " Fischer Tropsch synthesis over supported cobalt catalysts: effect of ethanol addition, precursors and gold doping " PhD thesis, University of the Witwatersrand, Johannesburg (2008).

[27] T. Matsuzaki, K. Takeuchi, T. Hanaoka, H. Arawaka, Y. Sugi, Applied Catalysis A: General 105 (1993) 159.

[28] M.A.M. Motchelaho, H. Xiong, M. Moyo, L.L. Jewell, N.J. Coville, Journal of Molecular Catalysis A: Chemical 335 (2011) 189.

[29] A. Tavasoli, M. Trépanier, R.M.M. Abbaslou, A.K. Dalai, N. Abatzoglou, Fuel Processing Technology 90 (2009) 1486.

[30] S. Kundu, Y. Wang, W. Xia, M. Muhler, Journal of Physical Chemistry C 112 (2008) 16869.

[31] M. Trépanier, A. Tavasoli, A.K. Dalai, N. Abatzoglou, Fuel Processing Technology 90 (2009) 367.

[32] S.D. Mhlanga, "Synthesis and study of carbon nanotubes and carbon spheres" PhD thesis, University of the Witwatersrand, Johannesburg (2009).

[33] F. Morales, F.M.F. de Groot, P. Glatzel, E. Kleimenov, H. Bluhm, M. Haevecker, A. Knop-Gericke, B.M. Weckhuysen, Journal of Physical Chemistry B 108 (2004) 16201.

[34] A. Tavasoli, K. Sadagiani, F. Khorashe, A.A. Seifkordi, A.A. Rohani, A. Nakhaei Pour, Fuel Processing Technology 89 (2008) 491.

[35] L. Leite, V. Stonkus, K. Edolfa, L. Ilieva, D. Andreeva, L. Plyasova, J.W. Sobczak, S. Ionescu, G. Munteanu, Journal of Molecular Catalysis A: Chemical 215 (2004) 95.

[36] L. Guczi, G. Stefler, O. Geszti, Z. Koppány, Z. Kónya, É. Molnár, M. Urbán, I. Kiricsi, Journal of Catalysis 244 (2006) 24.

10

Chapter Ten

General Conclusions

The aims of this study were to synthesize carbon nanotubes (CNTs) and nitrogen-doped carbon nanotubes (N-CNTs) using the chemical vapour deposition method and the post-doping method respectively. These carbon materials were then used as supports for iron and cobalt based Fischer-Tropsch catalysts. Issues such as the effect of support pre-treatment, catalyst precursor salts and solvent, alkali (Li, Na, K) promoters on the catalyst properties and performance during the Fischer-Tropsch reaction were explored.

Carbon nanotubes were successfully synthesized by the catalytic decomposition of acetylene (C_2H_2) at 700^{o}C over a 10% Fe-Co supported on calcium carbonate ($CaCO_3$) catalyst. Previous studies in our research group have focused on the optimization of this process. Under optimum conditions (synthesis time: 1 h, reaction temperature: 700^{o}C, acetylene to nitrogen flowrate ratio of 1: 2.67), high yields and high quality carbon nanotubes were obtained. TEM analysis revealed that the CNTs

produced were multiwalled, with outer diameters ranging from 20 to 35 nm and the distance between the graphene layers was found to be 0.34 nm. The as-grown CNTs were purified/functionalized by refluxing the obtained product in nitric acid at different concentrations (30% and 55%) and different times (2 h and 6 h). Purification not only removed the residual growth reagents, but also introduced surface functional groups onto the CNTs. The presence of those groups altered the surface chemistry of CNTs; for example, they rendered the CNTs surface less hydrophobic. The surface functional groups were identified and quantified using FTIR spectroscopy, Raman spectroscopy, TGA and zeta potential measurements (Chapter 5). The BET surface area measurements showed that the surface area increased with acid treatment due to the removal of the residual growth reagents and possibly the opening of the ends of the tubes. Moderate acid treatment of CNTs produced from Fe-Co supported on $CaCO_3$ can readily generate roughened CNT surfaces and these carbons can be used as stable supports for Fischer-Tropsch catalysts. Fe catalysts supported on differently functionalized CNTs have exhibited different catalytic behavior and the activity during FT was shown to correlate with the degree of acid functionalisation of the carbon support, indicating that the surface groups introduced during the acid treatment are linked to the active sites.

The dependence of the activity and selectivity of Fe/CNT catalysts on the type of iron precursor and solvent used in the catalysts' preparation was investigated. The precursors used were $Fe(C_5H_8O_2)_3$, $Fe(OOCCH_3)_2$, $Fe(NO_3)_3{\cdot}9H_2O$ and $Fe(C_2O_4){\cdot}2H_2O$ and the solvent used to dissolve the precursors was either de-ionised water or acetone. The catalysts were prepared by a deposition precipitation method using urea and were characterized by TEM, HRTEM, TGA, TPR, XRD and N_2-physisorption analysis. The Fe/CNT catalysts were tested for CO hydrogenation activity in a fixed-bed micro reactor. The XRD results showed that the precursor and the solvent used in the preparation of the Fe catalysts has an impact on the fraction of different iron phases present and TEM analysis revealed a slight difference in the average iron particle sizes. The average Fe particle sizes affects the interaction

between the precursor and the support (smaller particles interact more strongly with the support). For the catalysts prepared by dissolving the precursors in de-ionised water, the activity increased in the order Fe-acet ≤ Fe-oxal < Fe-nitr. The precursor salt used in the preparation of the catalyst had an influence on the catalyst performance. The counter-ions probably play a role in the way the active metal interacts with the support thereby affecting the metal particle size, the reducibility and the dispersion, which in turn affects the catalyst performance in the FTS. The choice of solvent (de-ionised water versus acetone) was found to have a marked effect on the CO hydrogenation activity and hydrocarbon selectivity of the catalysts tested under fixed FT conditions. The use of acetone as the solvent was found to result in catalysts that were significantly more active than those prepared using de-ionised water. The solvent did influence the metal dispersion and the reducibility of the catalysts. Improvements in metal dispersion created more active metal sites available for FTS reaction and as a result enhanced the catalyst activity.

The effect of alkali (Li, Na and K) promoters on the particle size, surface area, catalyst reducibility, activity and selectivity during FTS for Fe/CNT catalysts was investigated. The catalysts were prepared in such a way that the molar ratio was kept constant at a ratio of 100: 3.4 moles of Fe/promoter. It was observed that adding the promoter increased the Fe crystallite size and as a result the catalyst surface area decreased relative to that of the unpromoted catalyst. The presence of Na and K promoters slightly hindered catalyst reducibility by increasing the Fe reduction temperature with the potassium promoted catalyst showing the most pronounced effect. Potassium and sodium promoted catalysts were found to decrease the selectivity toward methane, increase the olefin production and shift the product selectivity to higher molecular weight hydrocarbons during FTS when compared to the unpromoted catalyst. However, K lowered the CO hydrogenation activity whereas Na greatly increased it. The Na promoted Fe catalyst was also more active for the water gas shift reaction compared to the other promoted and unpromoted catalysts. Increasing the sodium loading in the catalyst 3.7 and 7.2 fold was found to have very

little impact on the CO hydrogenation rate, but the product selectivity was affected, with 100Fe/24Na/CNT being the more selective catalyst toward higher molecular weight products. The selectivity to methane was found to decrease on increasing sodium loading in the catalyst. This study revealed that Na is a most effective promoter for an Fe/CNT catalyst, followed by K and lastly Li.

The suitability of nitrogen-doped CNTs as a Fe-catalyst support was investigated. The N-CNTs were synthesized by a post-doping method using acetonitrile as the nitrogen source, 2 h synthesis time and reaction temperature ranging from 700 to 900^{o}C. There was no significant change in the morphology of the N-CNTs up to 850^{o}C. The nitrogen content and % mass increase of the N-CNTs increased almost linearly with increasing reaction temperature whereas the surface area was found to decrease. Two iron catalysts were prepared using N-CNTs as a support. The Fe/N-CNT-750 catalyst, containing 1.7% nitrogen was found to have a very broad particle size distribution ranging from 26 to 35 nm. However, functionalizing the N-CNT before metal loading created more surface functional groups on which to anchor metal particles and as a result Fe metal deposited on this support has a narrow particle size distribution. Fischer-Tropsch activity testing on these two catalysts showed that the Fe/N-CNT-750 without functionalisation is not a suitable catalyst for the Fischer-Tropsch synthesis as the major product formed is methane.

A preliminary study on the effect Co-N/CNTs (N = nitrate) and Co-A/CNTs (A = acetate) catalysts in the FT synthesis was undertaken. The catalysts were prepared by the deposition precipitation method using $Co(NO_3)_2{\cdot}6H_2O$ and $Co(OOCCH_3)_2$ respectively as the metal precursors. TEM analysis revealed that Co-A/CNT has smaller average particle size (8.9 nm) compared to Fe-N/CNT (12 nm) and this was in agreement with XRD data. The TPR measurements showed an easy reducibility of the Co-N/CNT catalysts. The Fischer-Tropsch performance testing of the two catalysts under similar operating conditions showed that the precursor used in the

preparation of the Co/CNT catalyst did not have a significant influence on the FTS performance of the resulting catalyst.

Future studies may entail:

1- Elucidating the mechanism by which different metal precursors interact with the support and the metal-solvent-support interaction. This may require EXAFS study of suitable CNT supported catalysts.
2- Investigating the effect of alkali promoted Fe/CNT catalysts at the same conversion in order to effectively compare their selectivity toward the different products.
3- Undertaking a systematic study of the Na-promoted Fe/CNTs catalyst in order to determine the optimum Na loading if any for the best FT performance. In FT catalysis K is normally a better promoter than sodium. This peculiar finding may reveal a better understanding to how alkali metals perform in FTS.
4- Determining the optimum nitrogen content in the nitrogen-doped carbon nanotubes that can give maximum activity in the FT reaction. In this study only a 1.7 % N-doped CNT was used. The remarkable finding that the Fe/N-CNT gave superior activity when compare to Fe/CNT catalyst needs to systematically investigated.